

The Role of Dynamins in the Fusion of Synaptic Vesicles and their Subsequent Recycling

by

Adam Rostron (B.Sc.)

A thesis submitted in partial fulfilment for the requirements
for the degree of Doctor of Philosophy at the University of Central Lancashire.

October, 2019

This thesis is dedicated to my mum and dad,
before day one you were there for me.

STUDENT DECLARATION FORM

Concurrent registration for two or more academic awards

I declare that while registered as a candidate for the research degree, I have not been a registered candidate or enrolled student for another award of the University or other academic or professional institution.

Material submitted for another award

I declare that no material contained in the thesis has been used in any other submission for an academic award and is solely my own work.

Signature of Candidate

Adam Paul Rostron (B.Sc.)

Type of award

Doctorate of Philosophy, PhD

School

School of Pharmacy and Biomedical Sciences,
University of Central Lancashire

Abstract

Kiss and run (KR) is a highly debated mode of synaptic vesicle (SV) recycling in neurons, and limited research has investigated the protein pathways that regulate it. This thesis demonstrates that protein kinase A (PKA) activation can specifically switch the reserve pool (RP) of SVs to KR, whilst PKA inhibition switches the readily releasable pool (RRP) of SVs to full fusion (FF) for some stimuli. This thesis also demonstrated that cytosolic Dynamin-I (Dyn-I) is not required to mediate the basal KR observed during exocytosis, but a membrane bound sub-pool of Dyn-I is. KR can only occur when actin filaments are polymerised or able to polymerise, and actin polymerisation is also required to mobilise the RP to fuse at the active zone (AZ). Activation of adenylyl cyclase (AC) can block release of the RP by lowering intracellular Ca^{2+} ($[\text{Ca}^{2+}]_i$) levels via activation of exchange-proteins activated by cyclic-AMP (EPACs), but activation of AC can also switch the RRP to a KR mode of exocytosis by increasing $[\text{Ca}^{2+}]_i$ during certain stimulation paradigms. This thesis also validates that Serine (Ser-795) is an *in vivo* phosphorylation site, and a confirmed target of protein kinase C (PKCs) and protein phosphatase 1 or 2A (PP1 or PP2A). Activation of PKA significantly decreases the basal phosphorylated state of Ser-795, A conditions which increases the prevalence of KR. These results reveal significant new roles for PKA and AC in regulation of SV exocytosis, for distinct pools, and highlight the sub-pool of membrane bound Dyn-I and the vital role of actin during exocytosis. Certainly future research may reveal the overall importance of dysfunction in these processes and the roles they could play in understanding neuronal disorders and disease states as dysfunctional communication has been associated with many of these. The understanding of how distinct modes of recycling are regulated by protein pathways is vital to this research.

Contents

Dedication	i
Declaration	ii
Abstract	iii
Contents	iv
List of Tables	x
List of Figures	xi
List of Abbreviations and Acronyms	xv
Acknowledgements	xvii
Chapter 1: Introduction	1
1.1 Synaptic Transmission	2
1.2 Synaptic Vesicles	3
1.3 SV Pools	6
1.4 SV Recycling	11
1.5 KR	15
1.6 Dyn-I in KR	17
1.7 Dyns	19
1.8 Phosphorylation of Dyns	24
1.9 Review of Previous Research	31
1.9.1 Maximal Glu Release	31
1.9.2 A Single Round of Exocytosis	35
1.9.3 Maximal Labelling of SVs with FM 2-10 Dye	37

1.9.4 The Mode of Exocytosis is Stimulation Dependent.....	38
1.9.5 Presynaptic Proteins Regulating Exocytosis	42
1.9.6 Phosphorylation of Dyn-I Ser-795 <i>in vivo</i>	48
1.9.7 Conclusion	52
1.10 Research Aims	53
1.10.1 Specific Aims	53
Chapter 2: Materials and Methods.....	54
2.1 Materials.....	55
2.1.1 Buffering Reagents	55
2.1.2 Stimulation Solutions	55
2.1.3 Drugs and Final Concentrations (Dissolved in DMSO)	58
2.1.4 Various Chemicals Employed	59
2.1.5 Equipment	60
2.1.6 Specific Antibodies Employed	61
2.2 Preparing Synaptosomes	62
2.3 Glutamate Release Assay.....	63
2.4 FM 2-10 Styryl Dye Release Assay	69
2.4.1 Background/Rationale	69
2.4.2 Method	70
2.5 Intracellular Ca ²⁺ Assay	72
2.5.1 Background/Rationale	72
2.5.2 Method	74
2.6 Western Blotting	77

2.6.1 Introduction	77
2.6.2 Sample Preparation	77
2.6.3 Electrophoresis and Transfer	78
2.6.4 Probing and Chemiluminescence.....	79
2.6.5 Quantification of Bands from PVDF Membranes.....	79
2.7 Bioenergetics Assay	81
2.7.1 Background/Rationale	81
2.7.2 Method	83

Chapter 3: The Role of PKA, Dyn-I and the Actin Cytoskeleton in Regulating

the Mode of exocytosis for SV Pools.....	86
3.1 The Effect of Protein Kinase A Regulation on Evoked Glu Release	87
3.1.1 The Effect of PKA Inhibition on Evoked Glu Release	88
3.1.2 The Effect of PKA Activation on Evoked Glu Release	90
3.2 The Effect of Dyn-I Inhibition on Evoked Glu Release	92
3.3 The Effect of Actin Disruption on Evoked Glu Release	95
3.4 The Effect of PKA Regulation on Evoked FM 2-10 Dye Release.....	97
3.4.1 The Effect of PKA Inhibition on Evoked FM 2-10 Dye Release	97
3.4.2 The Effect of PKA Activation on Evoked FM 2-10 Dye Release	100
3.4.3 The Specificity of cBIMPS Action on Evoked FM 2-10 Dye Release	103
3.5 The Effect of Dyn-I Inhibition on Evoked FM 2-10 Dye Release	105
3.6 The Effect of Actin Disruption on Evoked FM 2-10 Dye Release	107
3.7 Intracellular Ca ²⁺ Levels.....	113
3.7.1 The Effect of PKA Inhibition on Evoked Changes in [Ca ²⁺] _i	113

3.7.2 The Effect of PKA Activation on Evoked Changes in $[Ca^{2+}]_i$	115
3.8 Nerve Terminal Bioenergetics.....	117
3.8.1 The Effect of PKA Inhibition on Nerve Terminal Bioenergetics	118
3.8.2 The Effect of PKA Activation on Nerve Terminal Bioenergetics	121
3.8.3 The Effect of Dyn-I Inhibition on Nerve Terminal Bioenergetics	124
3.8.4 The Effect of Actin Disruption on Nerve Terminal Bioenergetics	127
3.9 Discussion	130
3.9.1 Evoked Glu Release	131
3.9.2 Evoked FM 2-10 Dye Release	133
3.9.3 Dual Treatments	136
3.9.4 Effect of Dyn-I and Actin Modulation on Evoked FM 2-10 Dye Release.....	137
3.9.5 Evoked $[Ca^{2+}]_i$ Levels	139
3.9.6 Bioenergetics of Synaptosomes.....	140
3.10 Conclusion	143

Chapter 4: The Role of AC in Modulating the Mode of Exocytosis and SV Pool

Release via PKA and EPAC Regulation	144
4.1 Introduction.....	145
4.2 The Effect of Adenylyl Cyclase Regulation on Evoked Glu Release	145
4.2.1 The Effect of AC Inhibition on Evoked Glu Release	146
4.2.2 The Effect of AC Activation on Evoked Glu Release	148
4.2.3 The Effect of EPAC Inhibition on Evoked Glu Release	152
4.3 The Effect of AC Regulation on Evoked FM 2-10 Dye Release	155
4.3.1 The Effect of AC Inhibition on Evoked FM 2-10 Dye Release	155

4.3.2 The Effect of AC Activation on Evoked FM 2-10 Dye Release	157
4.4 The Effect of AC Regulation on Evoked Changes in $[Ca^{2+}]_i$	163
4.4.1 The Effect of AC Inhibition on Evoked Changes in $[Ca^{2+}]_i$	163
4.4.2 The Effect of AC Activation on Evoked Changes in $[Ca^{2+}]_i$	165
4.4.3 The Effect of EPAC Inhibition on Evoked Changes in $[Ca^{2+}]_i$	168
4.5 The Effect of the Regulation of AC on Nerve Terminal Bioenergetics.....	172
4.5.1 The Effect of AC Inhibition on Nerve Terminal Bioenergetics	172
4.5.2 The Effect of AC Activation on Nerve Terminal Bioenergetics.....	174
4.5.3 The Effect of EPAC Inhibition on Nerve Terminal Bioenergetics	177
4.6 Discussion	181
4.6.1 Evoked Glu Release	182
4.6.2 Evoked FM 2-10 Dye Release	184
4.6.3 Evoked $[Ca^{2+}]_i$ Levels	186
4.6.4 Bioenergetics of Synaptosomes	189
4.7 Conclusion	190
Chapter 5: Studies of Dyn-I Phosphorylation during Exocytosis	191
5.1 Introduction.....	192
5.2 Results.....	196
5.2.1 Phosphorylation of Dyn-I Ser-795 <i>in vivo</i>	197
5.2.2 The Effect of 0.8 μ M OA upon Dyn-I Phosphorylation in the RRP.....	200
5.2.3 The Effect of 2 μ M KT5720 upon Dyn-I Phosphorylation in the RRP.....	209
5.2.4 The Effect of 50 μ M cBIMPS upon Dyn-I Phosphorylation	213
5.3 Discussion	220

5.3.1 Phosphorylation of Dyn-I Ser-795 <i>in vivo</i>	221
5.3.2 The Effect of 0.8 μ M OA upon Dyn-I during 4AP5C Stimulation.....	222
5.3.3 The Effect of PKA Inhibition upon Dyn-I during 4AP5C Stimulation.....	223
5.3.4 The Effect of PKA Activation upon Dyn-I Phosphorylation.....	225
5.4 Conclusion	225
Chapter 6: General Discussion	227
6.1 Results.....	228
6.1.1 The Role of PKA, Dyn-I and Actin in Neurotransmission.....	229
6.1.2 The Role of cAMP and EPACs in Neurotransmission.....	231
6.1.3 The Role of Dyn-I Ser-795 in Mode Regulation	233
6.2 Future Studies.....	236
Chapter 7: References and Appendix	239
7.1 Appendix A	290
7.2 Appendix B.....	294

List of Tables

Table 1.1: Overview of the Four Major Recycling Modes.....	16
Table 1.2: Known Dyn-I Phosphorylation Sites.....	29
Table 2.1: Antibodies for Western Blotting.....	61

List of Figures

Figure 1.1: Vesicle Pools and Sizes.....	10
Figure 1.2: Overview of CME and ADBE	11
Figure 1.3: Overview of CME, UE and KR	12
Figure 1.4: The Crystal Structure of Dyn.....	22
Figure 1.5: Dyn Tetramers form a Helix.....	23
Figure 1.6: Domains and Established Phosphorylation Sites Present on Dyn-I.....	25
Figure 1.7: Effect of a Range of $[Ca^{2+}]_e$ upon Evoked Glu Release.....	32
Figure 1.8: Effect of Stimuli upon Cytosolic free Calcium $[Ca^{2+}]_i$	34
Figure 1.9: Effect of 1 μ M Bafilomycin A1 upon Evoked Glu release.....	36
Figure 1.10: Difference between SVs Loaded with 1 mM or 100 μ M FM 2-10 Dye.....	38
Figure 1.11: Mode of RRP Release during Control and 0.8 μ M OA Treatment.....	40
Figure 1.12: Mode of RRP Release.....	41
Figure 1.13: Effect of 160 μ M Dynasore vs Control upon Evoked Glu and.....	42
FM 2-10 Dye Release	
Figure 1.14: Effect of 50 μ M Blebb upon Evoked Glu Release.....	44
Figure 1.15: Effect of 50 μ M Blebb upon Evoked FM 2-10 Dye Release.....	45
Figure 1.16: Effect of 1 μ M Cys A upon Evoked Glu and FM 2-10 Dye Release.....	47
Figure 1.17: Phosphorylation of Dyn-I Ser-795 across a range of Treatments.....	49
Figure 1.18: Phosphorylation of Dyn-I Ser-778.....	50
Figure 1.19: Phosphorylation of Dyn-I Ser-774.....	51
Figure 2.1: Glu Assay Time Course.....	63
Figure 2.2: Average Size of Maximum Glu Release with HK5C and ION5C	67
Stimulation	

Figure 2.3: Evoked Glu Release Equivalency of Approach.....	68
Figure 2.4: FM 2-10 Assay Time Course.....	70
Figure 2.5: Fura-2 Assay Time Course.....	74
Figure 3.1: Effect of 2 μ M KT5720 vs Control upon Evoked Glu Release.....	89
Figure 3.2: Effect of 50 μ M cBIMPS vs Control upon Evoked Glu Release.....	91
Figure 3.3: Effect of 30 μ M MITMAB vs Control upon Evoked Glu Release.....	94
Figure 3.4: Effect of 15 μ M Latrunculin vs Control upon Evoked Glu Release.....	96
Figure 3.5: Effect of 2 μ M KT5720 vs Control upon Evoked FM 2-10 Dye Release.....	99
Figure 3.6: Effect of 50 μ M cBIMPS vs Control upon Evoked FM 2-10 Dye Release....	101
Figure 3.7: Effect of 2 μ M KT5720 plus 50 μ M cBIMPS Treatment upon.....	104
Evoked FM 2-10 Dye Release	
Figure 3.8: Effect of 30 μ M MITMAB vs Control upon Evoked FM 2-10 Dye.....	106
Release	
Figure 3.9: Effect of 15 μ M Latrunculin vs Control upon Evoked FM.....	109
2-10 Dye Release	
Figure 3.10: Comparison of Latrunculin plus Control upon Evoked FM 2-10.....	112
Dye Release	
Figure 3.11: Effect of 2 μ M KT5720 vs Control upon Evoked $[Ca^{2+}]_i$ Levels.....	114
Figure 3.12: Effect of 50 μ M cBIMPS vs Control upon Evoked $[Ca^{2+}]_i$ Levels.....	116
Figure 3.13: Effect of 2 μ M KT5720 upon Synaptosomal Bioenergetics.....	119
Figure 3.14: Effect of 2 μ M KT5720 upon Mitochondrial Function.....	120
Figure 3.15: Effect of 50 μ M cBIMPS upon Synaptosomal Bioenergetics.....	121
Figure 3.16: Effect of 50 μ M cBIMPS upon Mitochondrial Function.....	122
Figure 3.17: Effect of 30 μ M MITMAB upon Synaptosomal Bioenergetics.....	125
Figure 3.18: Effect of 30 μ M MITMAB upon Mitochondrial Function.....	126

Figure 3.19: Effect of 15 μM Latrunculin upon Synaptosomal Bioenergetics.....	128
Figure 3.20: Effect of 15 μM Latrunculin upon Mitochondrial Function.....	129
Figure 4.1: Effect of 100 μM 9-cp-ade vs Control upon Evoked Glu Release.....	147
Figure 4.2: Effect of 100 μM Forskolin vs Control upon Evoked Glu Release.....	150
Figure 4.3: Effect of 100 μM 1,9-dideoxyforskolin and 100 μM 9-cp-ade plus.....	151
100 μM Forskolin Treatment upon Evoked Glu Release	
Figure 4.4: Effect of 100 μM ESI-09 and 100 μM ESI-09 plus 100 μM	154
Forskolin upon Evoked Glu Release	
Figure 4.5: Effect of 100 μM 9-cp-ade vs Control upon Evoked FM 2-10.....	156
Dye Release	
Figure 4.6: Effect of 100 μM Forskolin; 100 μM 9-cp-ade plus 100 μM	159
Forskolin upon 4AP5C Evoked FM 2-10 Dye Release	
Figure 4.7: Effect of 2 μM KT5720 Pre-treatment and 100 μM Forskolin.....	160
upon 4AP5C Evoked FM 2-10 Dye Release	
Figure 4.8: Effect of 0.8 μM OA; 0.8 μM OA plus 100 μM Forskolin upon.....	162
4AP5C Evoked FM 2-10 Dye Release	
Figure 4.9: Effect of 100 μM 9-cp-ade vs Control upon Evoked $[\text{Ca}^{2+}]_i$ Levels.....	164
Figure 4.10: Effect of 100 μM Forskolin vs Control upon Evoked $[\text{Ca}^{2+}]_i$ Levels.....	167
Figure 4.11: Effect of 100 μM ESI-09 vs Control upon Evoked $[\text{Ca}^{2+}]_i$ Levels.....	169
Figure 4.12: Effect of 100 μM ESI-09 plus 100 μM Forskolin upon.....	171
Evoked $[\text{Ca}^{2+}]_i$ Levels	
Figure 4.13: Effect of 100 μM 9-cp-ade upon Synaptosomal Bioenergetics.....	173
Figure 4.14: Effect of 100 μM 9-cp-ade upon Mitochondrial Function.....	174
Figure 4.15: Effect of 100 μM Forskolin upon Synaptosomal Bioenergetics.....	175

Figure 4.16: Effect of 100 μ M Forskolin upon Mitochondrial Function.....	176
Figure 4.17: Effect of 100 μ M ESI-09 upon Synaptosomal Bioenergetics.....	178
Figure 4.18: Effect of 100 μ M ESI-09 upon Mitochondrial Function.....	179
Figure 5.1: Effect of 40 nM or 1 μ M PMA upon Dyn-I Ser-795 over 120 sec.....	199
Figure 5.2: Effect of OA or KT5720 upon Dyn-I Ser Sites 2-15 sec.....	202
Figure 5.3: Effect of OA or KT5720 upon Dyn-I Ser Sites 30-120 sec.....	203
Figure 5.4: Effect of 0.8 μ M OA upon Dyn-I Ser-795 over 120 sec.....	205
Figure 5.5: Effect of 0.8 μ M OA upon Dyn-I Ser-774 over 120 sec.....	206
Figure 5.6: Effect of 0.8 μ M OA upon Dyn-I Ser-778 over 120 sec.....	208
Figure 5.7: Effect of 2 μ M KT5720 upon Dyn-I Ser-795 over 120 sec.....	210
Figure 5.8: Effect of 2 μ M KT5720 upon Dyn-I Ser-774 over 120 sec.....	211
Figure 5.9: Effect of 2 μ M KT5720 upon Dyn-I Ser-778 over 120 sec.....	212
Figure 5.10: Effect of 50 μ M cBIMPS upon Dyn-I Ser sites 2-15 sec.....	214
Figure 5.11: Effect of 50 μ M cBIMPS upon Dyn-I Ser-795 over 15 sec.....	216
Figure 5.12: Effect of 50 μ M cBIMPS upon Dyn-I Ser-774 over 15 sec.....	218
Figure 5.13: Effect of 50 μ M cBIMPS upon Dyn-I Ser-778 over 15 sec.....	219

List of Abbreviations and Acronyms

[Ca²⁺]_e – Extracellular Ca²⁺
[Ca²⁺]_i – Intracellular Ca²⁺
9-cp-ade – 9-cyclopentyladenine mesylate
AC – Adenylyl cyclase
ADBE – Activity dependent bulk endocytosis
AP – Action potential
ATP – Adenosine triphosphate
AZ – Active zone
BSE – Bundle signalling element
cAMP – Cyclic adenosine monophosphate
CAZ – Cytomatrix at the active zone
CBD – cAMP binding domain
cBIMPS – Sp-5,6-dichloro-cBIMPS
CDK5 – Cyclin-dependent kinase 5
CME – Clathrin mediated endocytosis
CNS – Central nervous system
Cys A – Cyclosporine A
DAG – Diacylglycerol
DTT – Dithiothreitol
Dyn – Dynamin
EM – Electron microscopy
EPAC – Exchange protein activated by cAMP
ETC – Electron transport chain
F-actin – Filamentous actin
FF – Full fusion
FP – Fusion pore
Fura-2-AM – Fura-2-acetoxymethyl ester
GDH – Glutamate dehydrogenase type-II
GED – GTPase effector domain
GEF – Guanine-nucleotide exchange factor
Glu – Glutamate
Gs α – G-protein α -subunit
GSK3 – Glycogen synthase kinase 3
GTP – Guanosine triphosphate
HCN – Hyperpolarisation-activated cyclic nucleotide-modulated
KO – Knockout
KR – Kiss and run
LDS – Lithium dodecyl sulphate
LTD – Long-term depression
LTP – Long-term potentiation
MD – Middle domain
MITMAB – Myristyl trimethyl ammonium bromide
Mito-Stress – Mitochondrial stress
mUnits – Milli-Units
NM-II – Non-muscle myosin-II

NMJ – Neuromuscular junction
NT – Neurotransmitter
OA – Okadaic acid
OCR – Oxygen consumption rate
PAA – Phosphoamino acid analysis
PAZ – Peri-active zone
PEA – Polyethyleneamine
PH – Pleckstrin-homology
PIP2 – Phosphatidylinositol 4, 5-bisphosphate
PKA – Protein kinase A
PKC – Protein kinase C
PM – Plasma membrane
PMA – Phorbol 12-myristate 13-acetate
PP1 – Protein phosphatase 1
PP2A – Protein phosphatase 2A
PP2B – Protein phosphatase 2B
PRD – Proline rich domain
PVDF – Polyvinylidene fluoride
RP – Reserve pool
RRP – Readily releasable pool
RT – Room temperature
S.E.M. – Standard error of mean
Ser – Serine
SP – Silent pool
SVs – Synaptic vesicles
TBS – Tris buffered saline
UE – Ultrafast endocytosis

Acknowledgements

Without the commitment, love and support from a myriad of individuals this thesis would never have been a possibility. Special thanks go to my supervisor and mentor, Dr. Anthony Ashton for his tireless guidance and many hours of tutoring, support and training. Without his support and good practice at scientific accuracy, this thesis would have never seen the light of day. Many thanks go to Deeba Singh who trained me well, and wasn't afraid to correct my laziness and bad practices. A special mention goes to Stephen Gilbody, who made the long car journeys into Preston so much more bearable, and who constantly challenges me with his in-depth knowledge of chemistry and biology. I would also like to thank Tae Guan Kuan and Dan, who brought levity to sometimes dull working days, and joy to my life through friendship over the years.

I am thankful to all the staff at UCLan who have put up with me, advised me and asked me questions which have enriched my time here. Many thanks should also go to the unsung heroes of UCLan who work to help, guide and support students to realise their full potential.

A very special mention is also due to mum and dad, who put up with me at home for all these long uni years, and who have also provided me with everything I could ever need to establish myself in the world. No better parents could exist. Thanks also to Nannan and Grandad who have believed in me before I knew what I was capable of, who have prayed for me and looked after me since before I was born. I must also say a special thanks to Naomi, my incredible wife, who joined me partway through this thesis, but who has given up evenings and weekends to look over chapters, offer support and guidance when my determination was fading.

It has been a long road, but I like to think this is still the start of my journey, I have no idea what the future holds, but I know my future is in God's hands, and I know what a good and gracious God he is. I leave you with a few stats from my time as a PhD student: serious headaches – 4, sleepless nights – 0, litres of tea drunk – 2,741, and still counting...

Chapter 1:

Introduction

1.1 Synaptic Transmission

Neurons communicate with other neurons and target cells by synaptic transmission. Action potentials (APs) travel along axons and this leads to the depolarisation of the presynaptic nerve terminals, the opening of voltage-gated Ca^{2+} channels, and as a consequence an increase in intracellular Ca^{2+} ($[\text{Ca}^{2+}]_i$). This $[\text{Ca}^{2+}]_i$ increase stimulates fusion between the membranes of synaptic vesicles (SV) and the presynaptic plasma membrane (PM), creating fusion pores (FPs). Following the formation of FPs SVs undergo exocytosis and release neurotransmitters (NT) which diffuse across the synapse, and stimulate postsynaptic receptors to excite or inhibit the postsynaptic neuron. The exocytosed SV proteins and lipids are then recovered from the PM in a process termed endocytosis. Competent SVs are then reformed, re-acidified and filled with NT such that they are subsequently ready for further rounds of release. This whole process is termed SV recycling (Heuser and Reese, 1973; Saheki and De Camilli, 2012; Südhof, 2004).

Neurons contain a finite number of small, clear SVs, therefore it is vital that recycling occurs quickly and efficiently to maintain neurotransmission during different stimulation intensities (Schikorski and Stevens, 1997; Rizzoli, 2014). Any imbalance between the rate of exocytosis and endocytosis may have a detrimental impact upon the surface area of the presynaptic neuron, and could also impact signal intensity and frequency leading to erroneous communications with lethal consequences (Bittner and Kennedy, 1970; Alabi and Tsien, 2013; Maritzen and Haucke, 2018; Milosevic, 2018). Indeed defects in the presynaptic protein machinery have been linked to various disease states, including disruption in short and long-term memory, deficits in behaviour, types of dementia (Li and Kavalali, 2017), and neurological disorders

(Cortès-Saladelafont, *et al.*, 2018). In order to maintain healthy neurotransmission during different stimulation intensities, neurons have developed multiple modes of SV recycling, regulated by many complex protein pathways (Soykan, *et al.*, 2016), to elegantly match release of NT with demand (Kavalali, 2007).

It is imperative to understand the molecular, morphological and functional features of SV recycling in healthy models, in order to understand what detrimental changes may have occurred in various disease states and chronic conditions, e.g. diabetes, Alzheimer's and so forth (Waites and Garner, 2011; Esposito, *et al.*, 2012).

1.2 Synaptic Vesicles

In the early 1950's Bernard Katz performing research with Paul Fatt and José del Castillo, discovered that the release of acetylcholine at frog neuromuscular junctions (NMJs) occurs in discrete parcels of uniform volume (Fatt and Katz, 1952; Del Castillo and Katz, 1954). From this research, Katz developed his quantal theory which suggested that distinct uniform packets of NT 'quanta' were released from the presynaptic terminal. It was not clear at this time if the NT was released from a single pool within the cytoplasm, or if it was stored in discrete organelles.

Following this theory, electron microscopy (EM) studies noted granular components present in presynaptic terminals from a range of synapses (De Robertis and Bennett, 1955; Palade and Palay, 1954; Palay, 1956). These granules ranged between 40-60 nm in diameter, had a uniform appearance, limited spatial organisation and were named small, clear-cored synaptic vesicles by De Robertis and Bennett (De Robertis and Bennett, 1955). The number of vesicles present in a terminal could vary from dozens to

hundreds, leading Palay to theorise that the SVs may play a direct role in neurotransmission, either containing small units of NT or a precursor molecule (Palay, 1956).

Further evidence for NTs being stored in SVs came in 1962 when Gray and Whittaker performed EM studies on a particulate fraction which Whittaker had obtained through the differential centrifugation and density gradient separation from sucrose homogenates of the fore-brains of rabbit, guinea-pig and other species (Whittaker, 1959; Gray and Whittaker, 1962). This fraction was distinct from nuclei, mitochondria and microsomes and contained the highest fraction of bound acetylcholine. It was discovered that this fraction (fraction B) was composed mainly of particles derived from nerve endings, which had been created by being pinched or torn-off from axons. Interestingly, the nerve endings retaining their structural integrity and even resealed at the point of rupture to form a continuous structure surrounding the nerve terminal contents. These pinched-off terminals were found to be packed with SVs and were named 'synaptosomes' the following year and have since become a vital tool in studying synapses and neurotransmission (Whittaker, *et al.*, 1964; Evans, 2015).

The final evidence proving that SVs contained and released NTs at the PM, instead of simply a pool of NT in the cytoplasm, came when Heuser and colleagues correlated quantal release of NTs with SVs undergoing exocytosis (Heuser, *et al.*, 1979). Heuser and colleagues performed quick-freezing of frog NMJs milliseconds after they were stimulated for release. They found a strong correlation between SVs undergoing exocytosis, and the release time of NTs. Through statistical analysis they also noted

that each vesicle released a similar volume of transmitter (a quanta), proving Katz's quantal theory.

Within the central nervous system (CNS), co-secretion of NTs and neuropeptides has been shown to occur at a variety of synapses (Van Den Pol, 2012). These molecules are stored and released from two different types of secretory vesicle. Classical NTs are stored in small synaptic vesicles (SVs) which have an average diameter of 40-60 nm (Südhof, 2004), whilst neuropeptides are stored in larger organelles, 80-120 nm in diameter, and feature a dense core, termed large dense-core vesicles (LDCVs) (Matteoli, *et al.*, 1988). Though exocytosis of both SSVs and LDCVs occurs at the AZ of CNS terminals (Jung, *et al.*, 2018), and is mediated following Ca^{2+} entry, both organelles have distinct release and molecular properties (Laurent, *et al.*, 2018). After exocytosis SVs can be locally rescued from the PM, but LDCVs can only be replenished via *de novo* synthesis at the endoplasmic reticulum (ER) (Zupanc, 1996; Moghadam and Jackson, 2013).

Secretory vesicles are composed entirely of phospholipids and proteins, with the latter being in greater proportion. This is contrary to many other membrane bound organelles and the PM, where proteins are described as 'icebergs floating in a sea of lipids'. In a landmark study, Takamori and colleagues found over 400 proteins present in purified SVs, and while a great majority were loosely associated or interaction partners, more than 80 were integral proteins vital to trafficking and transport, with their number being bolstered by multiple copies (Takamori, *et al.*, 2006). This highlights the complexity of the molecular mechanisms in vesicular trafficking and recycling, to ensure synaptic transmission is not perturbed.

Between types of organisms and synapses the number of vesicles found in the presynaptic terminal can vary greatly between a few dozen to several thousand (Alabi and Tsien, 2012; Chamberland and Tóth, 2016). There is also a great difference between the pool sizes of SVs and LDCVs. Indeed multiple research groups have calculated the total pool size of SVs present in CNS terminals to be ~100-200, and recently the total pool size of LDCVs was calculated at two to three per synapse (Neher, 2015; Persoon, *et al.*, 2018). However, synaptic transmission has a vesicular requirement which would rapidly exhaust the finite pool of available SVs over several stimulation events (Schikorski and Stevens, 1997; Schweizer and Ryan, 2006; Maeno-Hikichi, *et al.*, 2011; Ikeda and Bekkers, 2009; Alabi and Tsien, 2012). Therefore, the rapid and efficient recycling of SVs is vital to maintain neurotransmission for stable and coherent communication.

1.3 SV Pools

There has been much discussion and debate over the last 40 years as to how exactly SVs should be quantified and organised. At the visual level, EM studies demonstrate that SVs found in CNS synapses look homogenous, with the only distinction being a small number of vesicles attached to the PM, while the remaining vesicles are located in an adjacent group (Rizzoli and Betz, 2005; Denker and Rizzoli, 2010; Alabi and Tsien, 2012).

On the molecular level Synapsin I has been found to be a tag which distinguishes the reserve pool of SVs (here termed the silent pool), from vesicles which undergo recycling. Synapsin I is able to achieve this by reversibly cross-linking SVs to each other and binding them to the actin cytoskeleton (Cesca, *et al.*, 2010; Guarnieri, 2017).

Numerous studies have demonstrated this role for Synapsin I, as a decrease in pool size was observed during Synapsin I knockout (KO) or inhibition (Rizzoli and Betz, 2005; Guarnieri, 2017). Research has also indicated that Synapsin I may work as part of a ternary complex with Tomosyn I and Rab3A to secure vesicles, as Synapsin I deletions still displayed filaments tethering SVs together (Siksou, *et al.*, 2007; Cazares, *et al.*, 2016).

As the majority of vesicles do not arrange into distinct groups, SVs have tended to be pooled in accordance to their physiological responses to stimulation. Currently SVs are arranged into three pools based on speed and ease of release, though more recent advances in research may divide these into a number of sub-pools (Doussau, *et al.*, 2017). The three pools in the pre-synaptic terminal are:

- (i) The readily releasable pool (RRP) which undergoes release at the active zone (AZ) immediately upon depolarisation.
- (ii) The reserve pool (RP), also termed the recycling pool, which begins to mobilise toward the AZ upon terminal depolarisation and only releases once the RRP is exhausted.
- (iii) The silent pool (SP), which has also been termed the resting pool or the reluctant pool, which does not release under normal physiological stimulation conditions (Alabi and Tsien, 2012). Figure 1.1 outlines how these pools are positioned in presynaptic terminals.

Under physiological conditions, all exocytosis in the neuron occurs at the AZ. Indeed the AZ is the only place that SVs can undergo exocytosis due to the protein-rich cytomatrix at the AZ (CAZ), making SV targeting to this area vital (Michel, *et al.*, 2015). AZs contain enrichments of complexes containing RIM, Munc13, RIM-BP, α -liprin, and ELKS proteins, which work to 'dock' and prime the SV at the PM ready for release (Südhof, 2013). During exocytosis the AZ can potentially undergo much structural change with the addition of protein and lipids into the PM. In order to maintain release an AZ must have several mechanisms in place to maintain stability (Byczkowicz, *et al.*, 2017). The mechanism of release at the AZ is mediated by vesicular SNAREs and PM SNAREs which interact and are vital to open and maintain FPs for NT release during exocytosis (Rizo and Rosenmund, 2008; Shi, *et al.*, 2012; Zhou, *et al.*, 2015). A FP is a direct channel between the SV lumen and the extracellular space. In neurons FPs are ≤ 20 nm in diameter and allow rapid (≤ 100 μ s) conduct of small neurotransmitters from the SVs (Lindau and Alvarez de Toledo, 2003; Jackson and Chapman, 2006; Chang, *et al.*, 2017).

In a resting neuron under physiological conditions, the RRP is already docked at the AZ awaiting an increase in local Ca^{2+} concentration to exocytose. During terminal depolarisation and Ca^{2+} influx, the RRP rapidly forms FPs with the PM and releases NTs into the synaptic cleft (Katz, 1969; Barclay, *et al.*, 2005; Rizzo and Rosenmund, 2008; Hosoi, *et al.*, 2009; Kaeser and Regehr, 2017). Research indicates that the RRP can be recycled independently of the RP under certain stimulation conditions, increasing efficiency through placing a low demand on the terminal to recycle (Rizzoli and Betz, 2004; Ashton and Ushkaryov, 2005; Schikorski, 2014). The RP begins to migrate toward the AZ and undergoes docking and fusion once the RRP is exhausted. This occurs when

the stimulation intensity is higher, or more frequent, leading to a greater demand for neurotransmission. Finally, the SP is release incompetent under physiological conditions, but can be released under intense non-physiological stimulation, or pharmacological treatment.

Considering there are ~100-200 SVs in every nerve terminal, it would make sense to assume that the majority of these are found in either the RRP or RP. However, this is not the case. In most terminals studied, the SP contains the largest number of vesicles $\leq 80\%$, while the RRP may contain $\leq 5\%$ of vesicles present (Figure 1.1) (Rizzoli and Betz, 2005; Denker, *et al.*, 2011; Fowler and Staras, 2015). It is debated if this large variation in SP size is due to individual neuronal activity or plasticity, specific function tied to the location of the neuron, or methodology of measurement (Harata, *et al.*, 2001; Rizzoli and Betz, 2005; Ikeda and Bekkers, 2009; Denker and Rizzoli, 2010; Guarnieri, 2017). Recently Kavalali has suggested that the size of the SP may have a specific role in neurotransmission, and this could be linked to spontaneous release (Kavalali, 2015; Cousin, 2017).

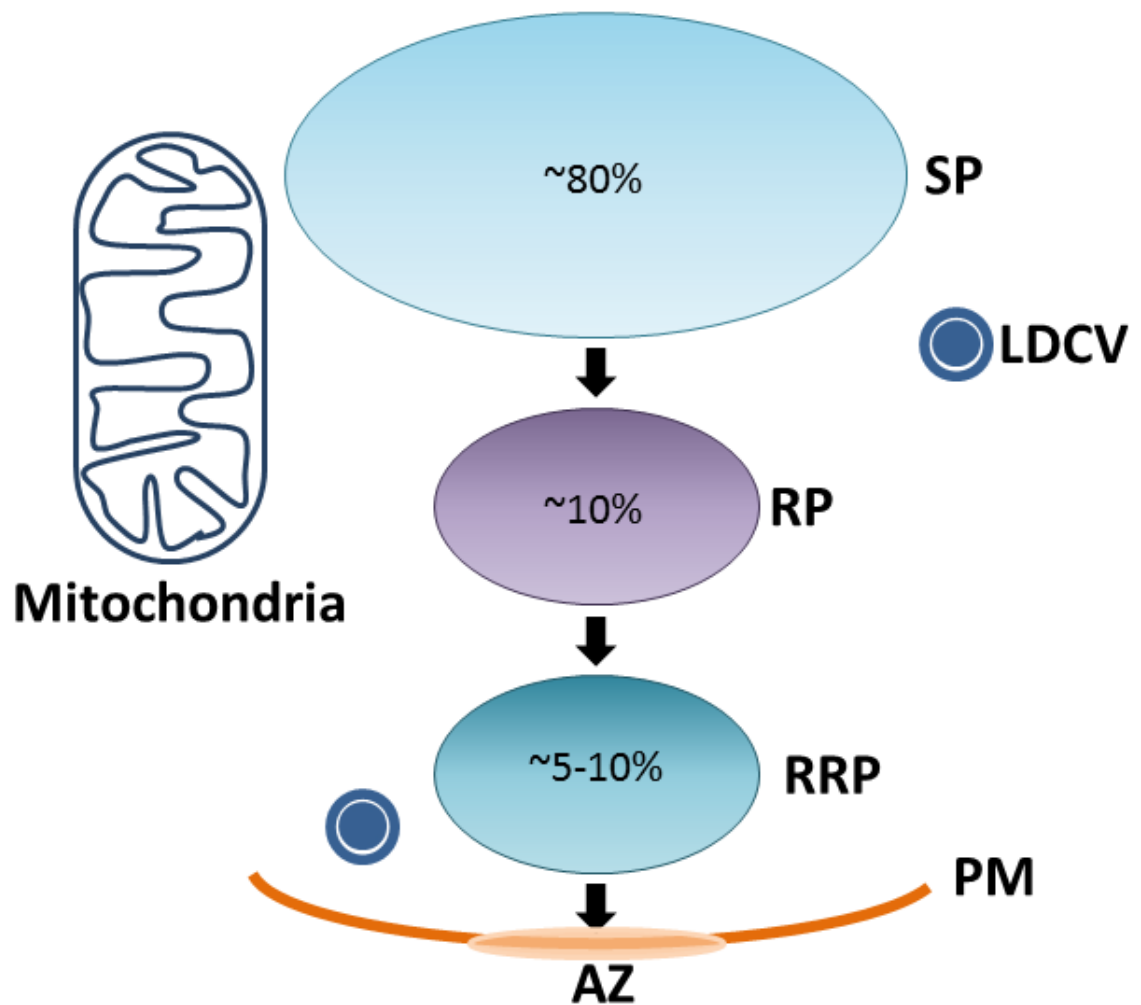


Figure 1.1: Vesicle Pools and Sizes

The RRP is docked at the AZ ready to release upon Ca^{2+} influx. The RP docks upon RRP exhaustion and is roughly the same size as the RRP. The SP contains the majority of vesicles in the terminal, which cannot be released during physiological stimulation. Though these percentages may vary between species and neurons, they are a good representation of the average size of each pool. Note the presence of a mitochondrion and two LDCVs, which is a typical representation of a synaptosome.

1.4 SV Recycling

As previously mentioned, recycling has two major stages: exocytosis and endocytosis, both of which have a number of alternate forms. There are four prevalent theories as to the modes of SV recycling; clathrin-mediated endocytosis (CME), activity dependent bulk endocytosis (ADBE), ultrafast endocytosis (UE) and kiss and run (KR), evidence for which has been found in a range of model systems including neurons (Gan and Watanabe, 2018). Figures 1.2 & 1.3 provide a basic overview of these recycling modes and the molecular mechanisms involved.

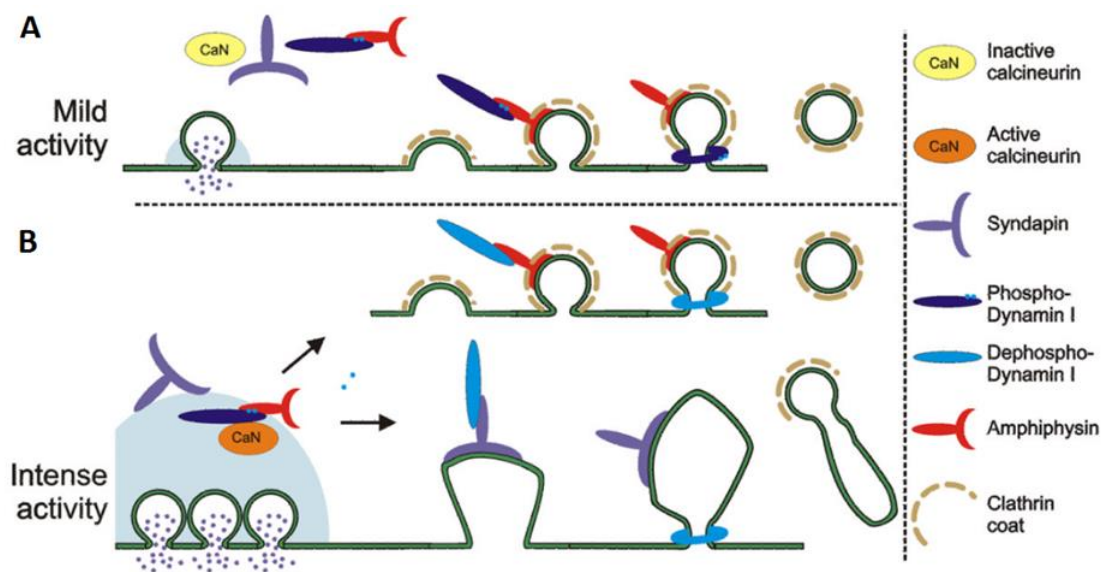


Figure 1.2: Overview of CME and ADBE

(A) CME – SVs fully collapse into the PM (left) and clathrin is recruited to rescue SVs from the PM (right). (B) ADBE – Large invaginations of the PM are recaptured during intense neuronal activity to reform large numbers of SVs (from Clayton and Cousin, 2009).

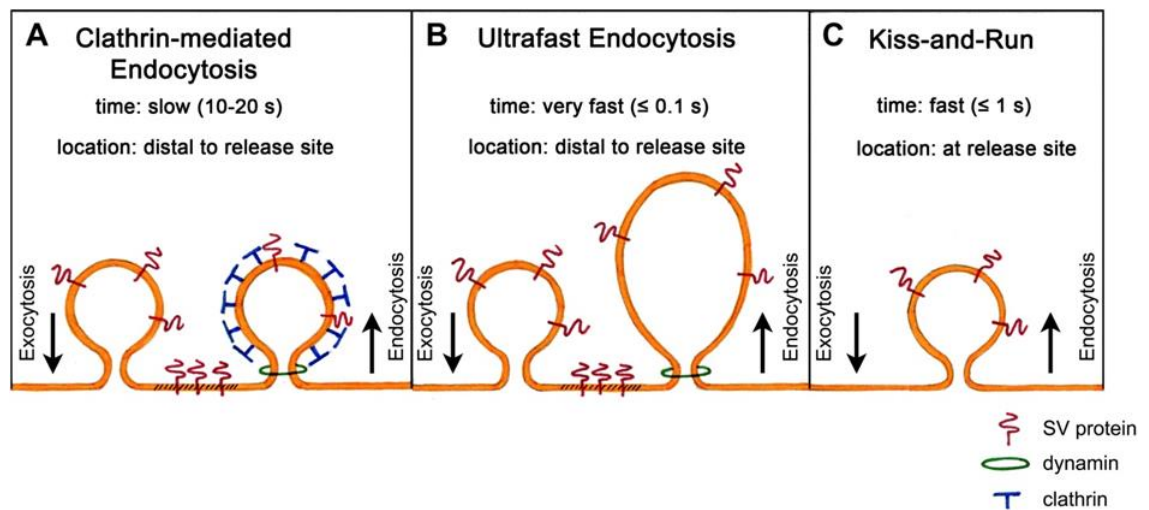


Figure 1.3: Overview of CME, UE and KR

(A) CME has a long recycling duration and SVs are recovered at a distance by clathrin and dynamin-dependent mechanisms. (B) UE invaginates a large area of the PM rapidly, which is then transferred to a large endosome, from which SVs are later generated. Here the time to occur is described as ≤ 0.1 sec, but when taking endosomal sorting and clathrin-dependent SV generation into account takes ~ 5 -10 sec. (C) In KR a FP is created and restricted from expansion, which would collapse the SVs into the PM. Instead, protein mechanisms rapidly work to close the FP so the SVs can recycle rapidly within local proximity to the AZ (from Kononenko, *et al.*, 2013).

Each form of recycling utilises a different method to retrieve SVs from the PM, and each has its own benefits and disadvantages (He, *et al.*, 2006; Granseth, *et al.*, 2007; Watanabe, *et al.*, 2013; Watanabe, *et al.*, 2014). It is debated which mode of recycling is most prevalent in neuronal signalling, though this is dependent upon many factors such as stimulation intensity and duration, neuronal plasticity and depression of signal (Granseth, *et al.*, 2006; Harata, *et al.*, 2006; Wu and Wu, 2007; Mellander, *et al.*, 2012; Nicholson-Fish, *et al.*, 2015; Morton, *et al.*, 2015).

Of these, CME, ADBE and UE all employ classical exocytosis, where during fusion, the FP expands and the SV, unable to retain its shape, fully collapses into the PM, here termed full fusion (FF) (Rizzoli and Jahn, 2007; Rizo and Rosenmund, 2008). Upon collapse the SV protein complex and lipid arrangement migrate from the AZ to the peri-active zone (PAZ) (immediate area surrounding the AZ) where endocytosis can occur via clathrin and/or dynamin-dependent means (Sone, *et al.*, 2000; Cano and Tabares, 2016). Either individual SVs are retrieved from the PM, as in CME; or a large portion of the PM is retrieved to form an endosome, from which SVs are later generated as in ADBE. UE utilises a combination of the two as it retrieves sections of the PM roughly equal in surface area to four SVs, which then proceed to join with a large endosome from which SVs are later generated, via a clathrin-dependent pathway (Watanabe, *et al.*, 2014).

The mechanism of generating SVs from either the PM or an endosome requires clathrin, a triskeletal scaffold protein. Through interactions with adaptor proteins, clathrin invaginates the membrane into clathrin-coated pits (Von Kleist, *et al.*, 2011; Rizzoli, 2014). For a short duration 1-2 sec these coated pits are attached to the plasma or endosomal membrane via a narrow neck consisting of lipids and/or proteins. In order for a coated pit to detach from membrane and become a vesicle, the neck must be severed.

Scission is performed by the protein dynamin (Dyn), which is a 100-KDa lipid-binding GTPase which is recruited and oligomerises into a spiral around the neck of budding pits (Urrutia, *et al.*, 1997; Ferguson and De Camilli, 2012; Cocucci, *et al.*, 2014). Dyn is a mechanoenzyme and through guanosine triphosphate (GTP) hydrolysis it undergoes a

structural change, which may place tension and or torsion on the vesicle neck, leading to destabilisation of the structure and eventually scission (Stowell, *et al.*, 1999; Hinshaw, 2000; Yamashita, *et al.*, 2005; Heymann and Hinshaw, 2009). The vesicle is then able to migrate away from the PM, dissociate from clathrin and other scaffold proteins and re-acidify ready for NT filling.

Dyn inhibition and knockout (KO) models highlight the dependence of classical endocytic modes upon Dyn, especially during high or prolonged stimulation where presynaptic terminals are depleted of SVs (Harata, *et al.*, 2006; Chang, *et al.*, 2010; Chung, *et al.*, 2010; Douthitt, *et al.*, 2011). Research has also demonstrated that blockade of Dyn using anti-dynamin IgGs, and a non-hydrolysable form of GTP (GTP γ S) describe a role regulating the FP during exocytosis, including fast recycling and KR (Graham, *et al.*, 2002; Holroyd, *et al.*, 2002; Harata, *et al.*, 2006; Chan, *et al.*, 2010; Chanaday and Kavalali, 2017). This indicates that Dyn has a distinct role separate from endocytosis to regulate synaptic transmission through the exocytotic pathway.

CME, UE and ADBE all have dependencies upon clathrin and Dyn in order to endocytose SV for further rounds of release, especially in ADBE where clathrin-dependent endocytosis buds SVs from bulk endosomes (Clayton, *et al.*, 2007). This Dyn-dependence can be observed in the *shibire* gene mutant, found in *Drosophila*. Here an increase in environmental temperature to 30°C causes the flies to exhibit complete muscular paralysis, caused by a blockade in the ability of the mutated Dyns to cut the neck of endocytosing vesicles. EM studies have highlighted electron dense collars which surround the endocytosing pits and large membrane in-folds, and these collars have been identified as Dyns unable to perform scission (Hinshaw, 2000).

1.5 KR

SVs which release via KR have a unique and more distinct recycling mode. Ca^{2+} influx activates synaptotagmins which modulate SNAREs complexes to form a FP (Jackman, *et al.*, 2016; Bao, *et al.*, 2018; Sharma and Lindau, 2018). The FP then can be stabilised, restricted from expanding and rapidly closed through the actions of Dyn-I or Non-muscle myosin-II (NM-II), though this may depend upon the stimulation utilised (see Section 1.9), and interactions with the actin cytoskeleton (Fesce, *et al.*, 1994; Harata, *et al.*, 2006; Chan, *et al.*, 2010; Chang, *et al.*, 2017; Lasič, *et al.*, 2017; Soykan, *et al.*, 2017). This allows the full content of NT to be released from the SV in $\leq 1\text{sec}$, creating an empty SV which requires no vesicular processing steps or endocytosis and is immediately ready for re-acidification and refilling with NT (Zhang, *et al.*, 2007; Zhang, *et al.*, 2009; Alabi and Tsien, 2013).

As a KR SV does not collapse into the PM and does not require rescuing, it has no clathrin dependency and can migrate directly into the terminal from the AZ upon FP closure and scission. This leads to a much shorter 'recycling' duration of $\leq 1\text{sec}$ for KR making it a much more efficient method of vesicular replenishing. This mode of recycling allows conservation of scarce resource within nerve terminals and rapid turnover of NT release during moderate stimulation. Table 1.1 compares the major aspects of each of the four recycling pathways.

Pathway	Time before SV is available to release (s)	Stimulation Intensity	Clathrin Requirement	Dyn Requirement
CME	10-20	Low	Yes	Yes
ADBE	10-15	High	Yes	Yes
UE	5-10	Low/Moderate	Yes	Yes
KR	≤ 1	Moderate	None	Not Always*

Table 1.1: Overview of the Four Major Recycling Modes

*Dyn-I and NM-II have been implicated in different forms of FP closure.

CME, ADBE and UE all have large durations before SVs are ready for re-release because of the necessary FF, the migration of vesicular components to the PAZ, the dwelling time of SV cargo on the PM and endosomal sorting and SV generation (Südhof, 2004). The estimated dwelling time of proteins on the PM between FF and before endocytosis is 5-15 sec for CME, which can create a rate limiting step during intense neuronal stimulation (Balaji and Ryan, 2007; Zhu, *et al.*, 2009; Armbruster and Ryan, 2011). This restricts the firing rate of the neuron, leading to a depression in the rate of NT release, making these FF recycling pathways impractical during prolonged or high demand stimulation. KR on the other hand does not require migration to the PAZ or classical endocytosis, as the vesicle never collapses into the PM. The KR vesicle can be instantly retrieved directly from the AZ, re-acidified and refilled with NT, being ready for re-release in ≤3 seconds, making KR faster and more energy efficient than conventional clathrin-dependent recycling (Alabi and Tsien, 2013; Chanaday and Kavalali, 2017).

1.6 Dyn-I in KR

As well as having a role in membrane fission during endocytosis (Herskovits, 1993; van der Blied, 1993; Artalejo, 1995), Dyn-I has also been implicated in exocytosis and the regulation of the FP (Min, *et al.*, 2007; Fulop, *et al.*, 2008; Chan, *et al.*, 2010; Chang, *et al.*, 2017; Chanaday and Kavalali, 2017). It is theorised that under certain stimulation conditions the regulation of the FP during KR can be mediated by Dyn-I which is recruited to the FP (Artalejo, *et al.*, 2002; Graham, *et al.*, 2002; Chan, *et al.*, 2010; Anantharam, *et al.*, 2012; Zhao, *et al.*, 2016), and indeed a population of Dyn-I has been found highly enriched around the AZ in some models (Wahl, *et al.*, 2013).

Just as Dyns have been proved to have a vital role in endocytic neck scission, evidence suggests they are recruited during exocytosis to close the newly formed FP, mediating the KR mode of recycling (Chan, *et al.*, 2010; Anantharam, *et al.*, 2011; Zhao, *et al.*, 2016). In this role Dyn-I may interact and work with the actin cytoskeleton in order to regulate neurotransmitter exocytosis, by mediating pore constriction (Gu, *et al.*, 2010; Trouillon and Ewing, 2013). Filamentous actin (F-actin) is enriched at AZs and sites of endocytosis (Dunaevsky and Connor, 2000; Lou, 2018), and F-actin disruption inhibits several forms of endocytosis, SV replenishment and SV fusion in nerve terminals, highlighting a dual-role during exocytosis and endocytosis (Cingolani and Goda, 2008; Wu, *et al.*, 2016; Lou, 2018).

NM-II in conjunction with F-actin, has also been implicated in regulating FP kinetics and facilitation of transmitter release during KR, mainly in chromaffin cells (Doreian, *et al.*, 2008; Berberian, *et al.*, 2009; Gutiérrez and Villanueva, 2018). NM-II is able to expand the KR fusion pore in chromaffin cells by remodelling the nanoscale, cortical F-actin

network during high frequency stimulation conditions, while NM-II inhibition prevents FP dilation and retains an extended KR mode (Doreian, *et al.*, 2008). Though the exact mechanisms of NM-II and F-actin on SV regulation in KR are not well established, the presence of NM-II in the neuronal presynaptic terminal, and a role during ADBE may indicate a place for NM-II during KR (Papadopoulos, *et al.*, 2013; Kokotos and Low, 2015; Miki, *et al.*, 2016).

It has been theorised that Dyn dephosphorylation can recruit NM-II to work with actin, mediating FP closure during exocytosis (Chan, *et al.*, 2010), and a similar mechanism has recently been described during SV endocytosis (Soykan, *et al.*, 2017); however this may conflict with recent studies performed by Ashton and colleagues (Ashton, unpublished).

KR has been well established in many non-neuronal tissues such as adrenal chromaffin cells (Albillos, *et al.*, 1997; Elhamdani, *et al.*, 2006; Doreian, *et al.*, 2008), and evidence from FM dye studies has suggested KR occurs in hippocampal neurons (Stevens and Williams, 2000; Zhang, *et al.*, 2007), but the existence of KR in synaptic communication is controversial partially due to the speed at which KR occurs (Henkel, *et al.*, 2001; He and Wu, 2007; Aravanis, *et al.*, 2003; Chanaday and Kavalali, 2017). This makes the study of the role of Dyn-I in nerve terminals vital to the research of the KR mechanism.

1.7 Dyns

Mammals have three Dyn genes, which code for three isoforms of Dyn (Dyn I, II & III) (Cao, Garcia and McNiven, 1998). Dyn-I is expressed at high levels specifically in the brain, Dyn-II is expressed at a low level ubiquitously in all tissues, and Dyn-III is expressed at a high level in testis with lower levels of expression in the brain, heart and lung (Sontag, *et al.*, 1994; Cook, Urrutia and McNiven, 1994; Cook, Mesa and Urruita, 1996; Cao, Garcia and McNiven, 1998). Though all three proteins are present in the presynaptic terminal, the expression rate of Dyn-I is 100-fold that of both Dyn II and Dyn III, demonstrating the importance of Dyn I in the terminal (Anggono and Robinson, 2009). To date 25 splice variants of Dyns have been identified; Dyn I, II and III having 8, 4 and 13 splice variants respectively (Cao, Garcia and McNiven, 1998). Though individual functions for each splice variant have yet to be discovered, their specific tissue expression and concentration gives each Dyn variant specific functions with some redundancy, which can be seen especially well in single KO studies.

Mice generated with Dyn I KO were able to form synapses, but such animals die within two weeks of birth suggesting a Dyn I requirement for healthy postnatal development, and a Dyn II and Dyn III role for embryonic development and synaptic formation (Ferguson, *et al.*, 2007). Though Dyn I is not essential for neurotransmission, as Dyn II and Dyn III can mediate slow endocytosis (Liu, *et al.*, 2011), it is vital for efficient and sustained recycling, with synaptic fatigue occurring much faster and a depression in both long-term potentiation (LTP) and neurotransmission seen with repeated stimulation (Fà, *et al.*, 2014). This is due to the deficit in CME leading to the accumulation of clathrin-coated pits on the PM, and a depletion of SVs in the nerve terminal as Dyn is unable to perform fission during endocytosis (Ferguson, *et al.*, 2007;

Ritter, *et al.*, 2013). The KO of Dyn II led to early embryonic lethality, describing a vital role for perinatal development, due to the ubiquitous expression of Dyn II and its role in all cell types (Liu, *et al.*, 2008; Ferguson, *et al.*, 2009). Double KO of Dyn I and Dyn II enhanced the Dyn I KO phenotype, with severe defects in CMS, and also described a relationship between Dyns and actin to regulation the fission pore (Ferguson, *et al.*, 2009).

The KO of Dyn III displayed no overt phenotype, but also enhanced the phenotype of Dyn I KO in double KO studies, leading to perinatal lethality and greater deficits in endocytosis (Raimondi, *et al.*, 2011). However in cultured cells from this model, Dyn II was able to mediate much reduced synaptic transmission in cells, highlighting the redundancies of these proteins. The generation of a triple Dyn KO fibroblast cell line (where Dyn II is reducing using anti-sense RNA) did not reveal any new information beyond what was observed in double KO studies (Park, *et al.*, 2013).

Dyns have 5 well-characterised domains (Figure 1.4 A) providing a range of functions, vital to their roles as enzymes, protein recruiters and mechanoproteins. These domains consist of:

- (i) A GTPase head (G domain) which undergoes structural change when GTP is bound and hydrolysed.
- (ii) A middle domain (MD) which contains the majority of the stalk of the Dyn and contains multiple sites important for cross linking to form dimers and further oligomerisation.
- (iii) A pleckstrin-homology (PH) domain which binds to phospholipids present in the PM most notably Phosphatidylinositol 4, 5-bisphosphate (PIP₂).

- (iv) A GTPase effector domain (GED) which is also important for self-assembly and when phosphorylated inhibits GTPase activity of the G domain through direct association.
- (v) A proline rich domain (PRD) which contains multiple binding sites for SH3 domain proteins, but is also the region of Dyn with the highest variation in sequence homology, which is theorised to play a role in tissue specificity and selective protein binding (Niemann, *et al.*, 2001; Ford, *et al.*, 2011; Faelber, *et al.*, 2011; Reubold, *et al.*, 2015).

Figure 1.4 B demonstrates the overall crystal structure of a single Dyn molecule, lacking the PRD which has not yet been resolved. Dyn dimerization is mediated by interface 2 upon the stalk in the MD to form an X shape; interactions between interfaces 1 and 3 facilitate assembly into tetramers followed by helical polymers where the PH domains face inward toward the membrane (Figure 1.4 C) (Antonny, *et al.*, 2016). Figure 1.5 outlines how multiple Dyn dimers interact to form a helix.

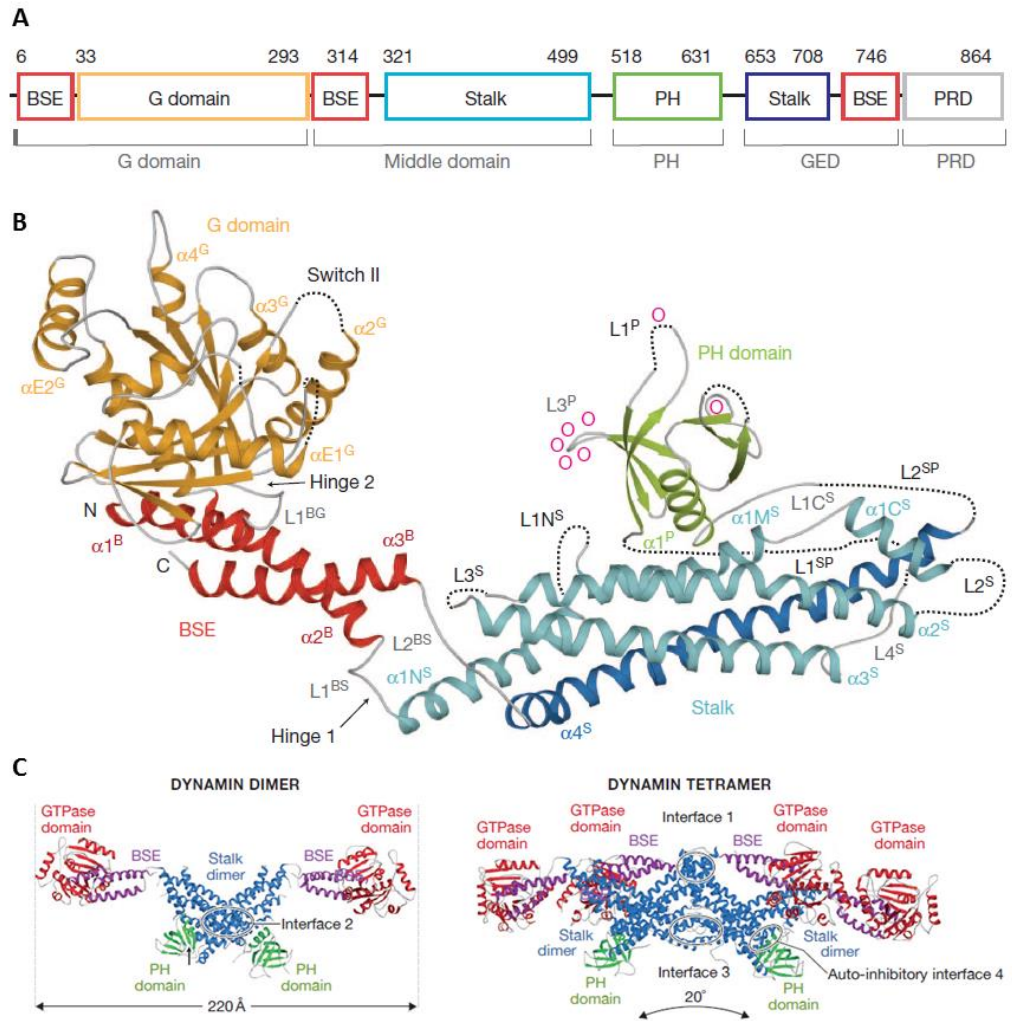


Figure 1.4: The Crystal Structure of Dyn

(A) The sequence of the 5 major domains in Dyns. The numbers indicate where domains start and end. (B) The crystal structure of a single Dyn-I protein. Note how the GED folds back to interact with the GTPase domain (Dark blue and red), and how multiple hinges can inhibit protein binding during phosphorylation. The bundle signalling element (BSE) forms a neck between the G domain and the MD. (C) The crystal structures of a Dyn dimer and tetramer with the interfaces required for assembly (modified from Faelber, *et al.*, 2011; Antonny, *et al.*, 2016).

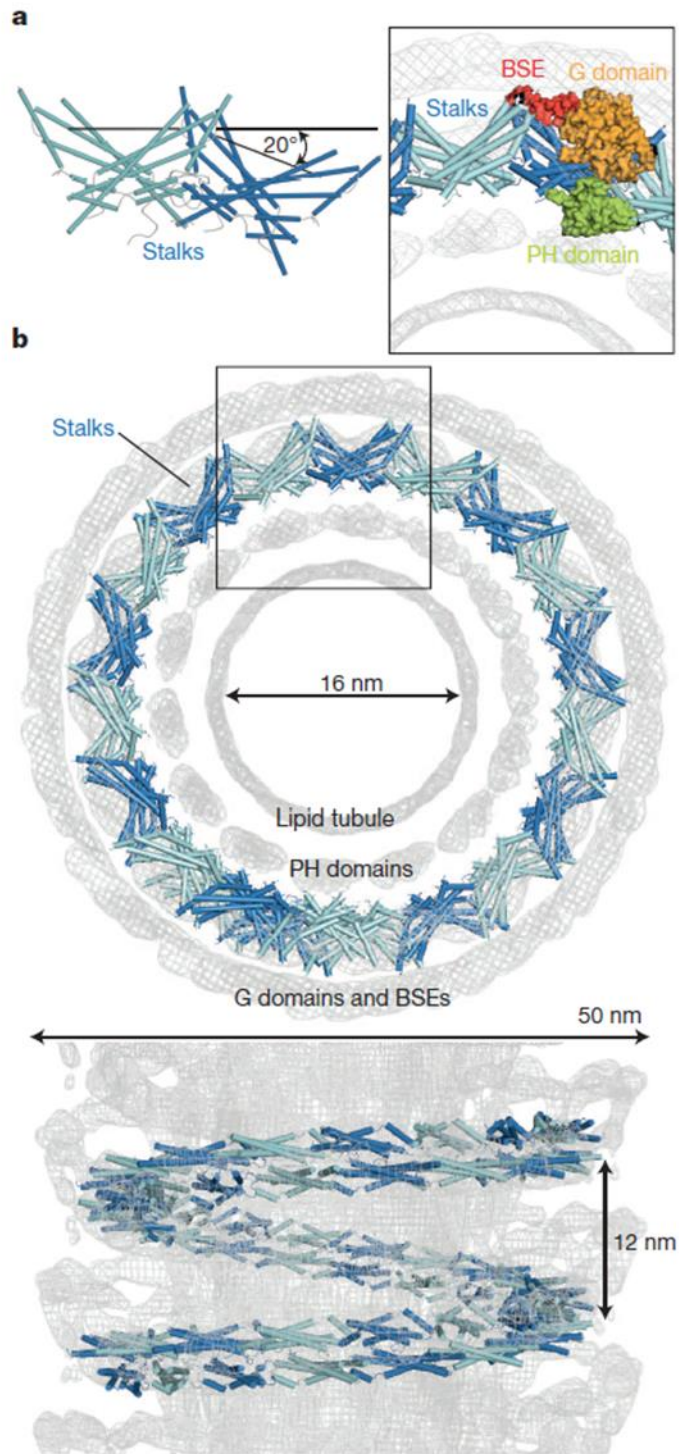


Figure 1.5: Dyn Tetramers Form a Helix

(A) Dyn tetramer (in this case a pair of dimers) goes through a 20° turn upon cross-linking and assembly. (B) Assembly of multiple tetramers forms a right-handed helix, which has an internal diameter large enough to incorporate a FP (from Reubold, *et al.*, 2015).

1.8 Phosphorylation of Dyns

As in any cell, phosphorylation plays a vital role in regulating the activity, subcellular location and stability of proteins. In neurons however, the phosphorylated state of proteins can be regulated by neuronal activity as well as physiological pathways, creating unique phosphorylation expression. During nerve terminal depolarisation the large influx of Ca^{2+} activates the phosphatase calcineurin, which dephosphorylates, and activates, a group of proteins termed the dephosphins, these proteins play vital roles in triggering synaptic vesicle recycling (Robinson, *et al.*, 1994; Cousin and Robinson, 2001).

Dyn is one of these dephosphins and regulation of Dyn activity through phosphorylation and dephosphorylation is essential for endocytosis and exocytosis of vesicles (Robinson, *et al.*, 1994; Smillie and Cousin, 2005). After terminal depolarisation, Dyn remains dephosphorylated during endocytosis and is rephosphorylated while endocytosis is completing (Robinson, 1991).

Following classical endocytosis the specific phosphorylation of Dyn-I works to reverse oligomerisation, protein binding, phospholipid binding on membranes and GTP hydrolysis, stopping any Dyn-I activity within the neuron and leaving a majority of the Dyns residing in the cytosol, waiting for dephosphorylation (Robinson, 1991; Smillie and Cousin, 2005). This is the situation observed in resting nerve terminals, where a fraction of Dyns reside in the cytosol in a heavily phosphorylated state, while a portion reside on membrane sites that become saturated, with almost no phosphorylation (Robinson, 1991; Liu, *et al.*, 1994).

Since Dyn-I was first discovered as a 'dephosphin', research focused upon which kinases and phosphatases regulate its phosphorylated state, and at which sites this phosphorylation occurs. Early on it was established that Dyns were specifically dephosphorylated both *in vitro* and *in vivo* by the Ca^{2+} /calmodulin-dependent phosphatase calcineurin in a Ca^{2+} -dependent manner. The use of pharmacological calcineurin antagonists abolishes Dyn-I dephosphorylation in nerve terminals (Liu, *et al.*, 1994; Bauerfeind, *et al.*, 1997; Marks and McMahon, 1998; Smillie and Cousin, 2005). To date no other phosphatases specific to Dyn-I have been discovered, suggesting this exclusive interaction is in part due to the role of Dyn-I as a dephosphin.

Regarding sites of phosphorylation, Dyn-I phosphorylation occurs exclusively on serine (Ser) sites in intact models (Robinson, 1991; Liu, *et al.*, 1994; Graham, *et al.*, 2007), and 8 major Ser sites have been established to date (Powell, *et al.*, 2000; Graham, *et al.*, 2007) (Figure 1.6). Of these sites only four have currently been studied to determine the effect upon Dyn-I regulation (see Table 1.2).

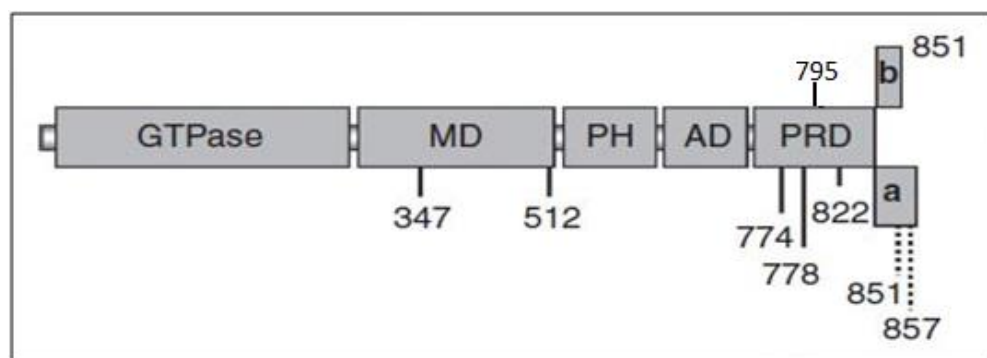


Figure 1.6: Domains and Established Phosphorylation Sites Present on Dyn-I

All known Ser sites present on Dyn-I. Note both a/b splice variants of the PRD tail and how these modulate expression of Ser-851 and Ser-857 (modified from Chan, *et al.*, 2010).

The roles of Ser-774 and Ser-778 have been well established. Upon terminal depolarisation and Ca^{2+} influx, calcineurin is activated which rapidly dephosphorylates Dyn-I (Liu, *et al.*, 1994; Smillie and Cousin, 2005), mainly at these sites. This mobilises Dyn-I to mediate SV endocytosis, bringing about scission at the fission pore via GTP hydrolysis, and completing SV recycling. After vesicular scission has occurred, Dyn-I Ser-778 is phosphorylated by CDK5 (Graham, *et al.*, 2007), and Ser-774 is phosphorylated by glycogen synthase kinase 3 (GSK3) (Clayton, *et al.*, 2010; Srinivasan, *et al.*, 2018), which in tandem with GTP hydrolysis causes Dyn-I to dissociate from the endocytotic machinery, disassemble into monomers and migrate back to the cytosol (Graham, *et al.*, 2007; Saheki and De Camilli, 2012). Ser-774 and Ser-778 were highlighted as the main sites that underwent changes in phosphorylation during terminal depolarisation with ~69% of the total sample phosphorylation associated with these sites (Graham, *et al.*, 2007).

Initially it was suggested that these two sites mediated CME, but Cousin and colleagues provided data which suggested that Ser-774 and Ser-778 mediate ADBE but not CME (Clayton, *et al.*, 2010), however this is controversial. Cousin originally discussed phosphorylation changes at these two sites to be the main regulator of CME (Cousin and Robinson, 2001; Tan, *et al.*, 2003; Clayton, *et al.*, 2007; Mettlen, *et al.*, 2009), but later they suggested perturbation of these two sites arrests ADBE but this had no effect upon CME (Clayton, *et al.*, 2009). However, primary neuron cultures with Dyn-I and Dyn-II double KO's did not see perturbation of ADBE (Wu, *et al.*, 2014); and recently Dyn phosphomimetic 774 and 778 knock-in models have not been found to affect ADBE (Armbruster, *et al.*, 2013). Clearly the roles of Ser-774 and Ser-778 are not

yet clear-cut and further research needs to be undertaken before they are fully understood.

Ser-857 also undergoes Ca^{2+} -dependent dephosphorylation during terminal depolarisation, and rephosphorylation is mediated by dual-specificity tyrosine phosphorylation-regulated kinase 1A (DYRK1A) (Xie, *et al.*, 2012). This dissociates Dyn-I from amphiphysins, which induce membrane curvature and are thought to recruit Dyns to the neck region of endocytosing vesicles, especially during CME (Huang, *et al.*, 2004; Meinecke, *et al.*, 2013).

Intriguingly another site Ser-795 – which was not reported by Graham *et al.*, 2007 – was found in non-stimulated tissues on Dyn-I, though there is some confusion if it is an *in vitro* artefact or an *in vivo* site (Powell, *et al.*, 2000). Purified Dyn-I was found to have the highest affinity for protein kinase C (PKC) of any known substrate, and *in vivo* PKC was found to regulate Dyn-I phosphorylation and endocytosis (Robinson, *et al.*, 1993; Robinson, *et al.*, 1994). This PKC phosphorylation site was theorised to reside in the PRD where protein fragment studies had found increases in phosphorylation, suggesting a role for PKC in intact terminals (Robinson, 1992; Liu, *et al.*, 1994; Robinson, *et al.*, 1994).

Ser-795, in the PRD, was then discovered as a strong phosphorylation target of PKC *in vitro*, and was thought to be the most likely candidate to be phosphorylated by PKC *in vivo* (Powell, *et al.*, 2000). This study found that Dyn-I Ser-795 underwent phosphorylation by PKC *in vitro* and this prevented phospholipid association, localising Dyn-I to the cytosol, which may regulate the recruitment of Dyn-I to the fission or

fusion pores *in vivo* (Powell, *et al.*, 2000). However this was later dismissed and Ser-795 was described as an *in vitro* site only – even though some authors had apparently observed it *in vivo* previously – explaining why it was not responsible for regulating endocytosis and the lack of Ser-795 observed in isolated Dyn-I studies (Smillie and Cousin, 2005; Graham, *et al.*, 2007).

Recent evidence has shown that Dyn-I Ser-795 is actually an *in vivo* site that has a distinct role from what originally thought as phosphorylation levels can be dramatically increased through the inhibition of PP2A with OA or PMA (Bhuva, 2015, p. 149), and Ser-795 could regulate NT release during Ca²⁺-dependent exocytosis (Singh, 2017, p. 234).

Though the phospho-regulation of Dyn-I activity has been well established during endocytosis, little research has been done investigating the phosphorylated state of Dyn-I during exocytosis, and in particular KR. As Dyn-I must be dephosphorylated to become active, it is theorised that during exocytosis, where Dyn-I undergoes dephosphorylation, it can regulate FP closure, switching the mode of exocytosis to KR. Ser-774 and Ser-778 are both well known to regulate the scission activity of Dyn-I during endocytosis, but no correlation has been discovered between these sites and KR (Bhuva, 2015). Furthermore, Ser-795 has been shown to block the association of Dyn-I with phospholipids *in vitro* (Powell, *et al.*, 2000), and the recent discovery that Ser-795 may be an *in vivo* site (Bhuva, 2015) highlight this site, and the kinases that regulate it as a potential regulator of KR during exocytosis.

Not much Ser-795 phosphorylation is observed during basal conditions, and this site can clearly be dephosphorylated very easily. Therefore it is possible that due to methodological differences, no *in vivo* Ser-795 could be detected (Graham, *et al.*, 2007). Further if the normal physiologically relevant Ser-795 only occurs on a sub-pool of Dyn-I already membrane bound (Wahl, *et al.*, 2013), then this may not have been purified, or may have undergone dephosphorylation due to stimulation in the method used by Graham, *et al.*, (2007) (Table 1.2).

Serine	Kinase	Effect on Dyn	Phosphatase
347	Unknown	-	Calcineurin dephosphorylates all sites (Liu, <i>et al.</i> , 1994; Xie, 2012).
512	Unknown	-	
774	GSK3	Phosphorylation mediates ADBE, but not CME (Clayton, <i>et al.</i> , 2010).	
778	CDK5	Phosphorylation primes Ser-774 for phosphorylation (Graham, <i>et al.</i> , 2007)	
795	PKC (<i>in vitro</i>)	Phosphorylation prevents phospholipid binding <i>in vitro</i> (Powell, <i>et al.</i> , 2000). Unknown <i>in vivo</i> effects (Bhuva, 2015).	
822	Unknown	-	
851	Unknown	-	
857	DYRK1A	Phosphorylation prevents amphiphysin binding <i>in vitro</i> (Xie, <i>et al.</i> , 2012).	

Table 1.2: Known Dyn-I Phosphorylation Sites

Established phosphorylation sites on Dyn-I, their kinases and the effects of phospho-regulation during recycling.

Recently PKC has been shown to regulate the mode of exocytosis in neurons (Sun and Alkon, 2012; Petrov, *et al.*, 2015), although no direct correlation between PKC mediated Dyn-I phosphorylation and the mode of release could be established (Singh, 2017). Alternatively protein kinase A (PKA) could be a strong candidate for regulating nerve terminal exocytosis (Seino and Shibasaki, 2005). PKA is expressed in presynaptic nerve terminals (Leenders and Sheng, 2005), becomes active when cyclic-AMP (cAMP) levels increase and phosphorylates serine and threonine residues (Nguyen and Woo, 2003; Park, *et al.*, 2014). Activation of PKA has been implicated in LTP and memory (Chavez-Noriega and Stevens, 1994; Hilfiker, *et al.*, 2001; Leenders and Sheng, 2005; Zhang, *et al.*, 2018), and has been shown to increase the instance of fast exocytosis, potentially by enhancing presynaptic Ca^{2+} influx, and modulating synaptic plasticity and memory through regulation of the RRP (Yoshihara, *et al.*, 2000; Seino and Shibasaki, 2005; Park, *et al.*, 2014).

PKA is a vital kinase to presynaptic function, phosphorylation of RIM1 has been shown to control exocytosis (Gao, *et al.*, 2016), while phosphorylation of synapsin I enhances exocytosis (Menegon, *et al.*, 2006), and phospho-regulation of syntaphilin regulates the availability of Dyn-I in terminals (Boczan, *et al.*, 2004) which may affect the ability of Dyn-I to regulate the mode of exocytosis, making it a viable candidate to study during release.

1.9 Review of Previous Research

Results in this section reflect previous research carried out by Ashton group. These results were created whilst establishing optimal experimental conditions for use with the synaptosomes model, and are displayed here to aid understanding of new and original data presented and discussed later in this thesis.

1.9.1 Maximal Glu Release

For a direct comparison between FM 2-10 dye and glutamate (Glu) release assays it was necessary that the stimuli employed in this thesis produced a maximal level of Glu release. In order to determine this, synaptosomes were treated with the three stimuli (HK, ION and 4AP) – see material and methods for further details – in the presence of a range of extracellular Ca^{2+} concentrations ($[\text{Ca}^{2+}]_e$) (Figure 1.7). It can be observed that 5 mM $[\text{Ca}^{2+}]_e$ produced maximal Glu release for all stimuli, and a further increase in $[\text{Ca}^{2+}]_e$ to 10 mM had no effect on HK evoked Glu release (Figure 1.7 A), and possibly decreased Glu release with ION and 4AP (Figure 1.7 B-C). For all experiments in this study a concentration of 5 mM $[\text{Ca}^{2+}]_e$ was therefore used with each of the three stimuli to maximally release Glu from synaptosomes.

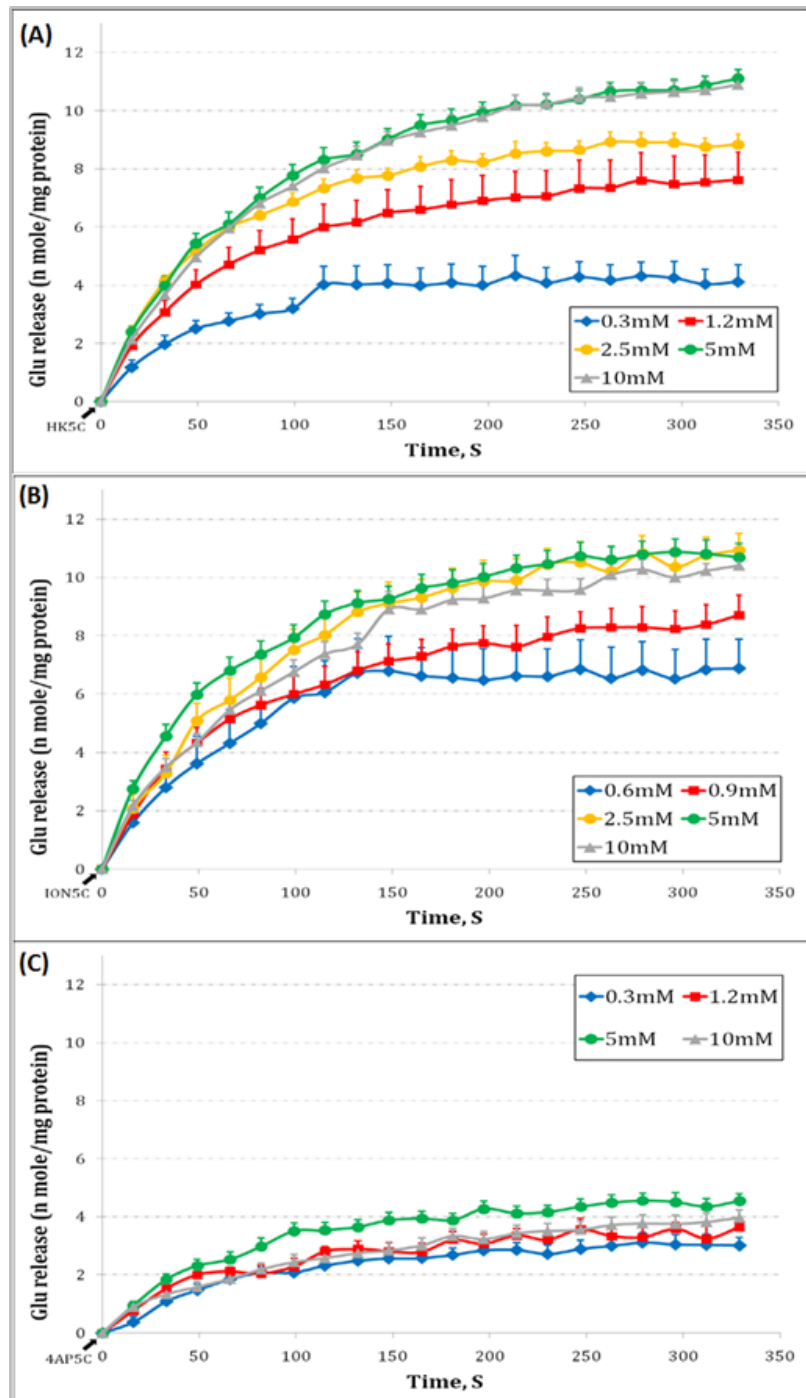


Figure 1.7: Effect of a Range of $[Ca^{2+}]_e$ upon Evoked Glu Release

Stimulation in the presence of 5 mM $[Ca^{2+}]_e$ induces maximal Glu release for HK (A), ION (B) and 4AP (C). Values represented are the mean plus S.E.M. from 4 independent experiments.

Stimulation with 4AP5C produced a lower maximal Glu release (4.5 moles/mg of protein) (Figure 1.7 C) compared to HK5C (10.8 moles/mg of protein) ($p < 0.05$) (Figure 1.7 A) or ION5C (11 moles/mg of protein) ($p < 0.05$) (Figure 1.7 B) with 5 mM $[Ca^{2+}]_e$. An explanation for this can be found when looking at the different changes in $[Ca^{2+}]_i$ produced by each stimuli (Figure 1.8). 4AP5C produces a lower, more gradual change in $[Ca^{2+}]_i$ (180 ± 20 nM Ca^{2+}) than either HK5C or ION5C (370 ± 25 nM Ca^{2+}) ($p < 0.05$), which is interpreted as 4AP5C only being able to release the RRP of SVs whilst HK5C and ION5C can release both the RRP and the RP of SVs.

Though HK5C and ION5C achieved an equivalent level of $[Ca^{2+}]_i$, this is mediated by different kinetics (Figure 1.8). HK5C produced much of the $[Ca^{2+}]_i$ increase upon the application of stimulation, plateauing rapidly (< 10 sec), potentially due to VGCC desensitisation (Bähring & Covarrubias, 2011); whilst ION5C produced a more gradual increase in $[Ca^{2+}]_i$ which plateaus later (~ 40 sec) (Figure 1.8). This speed of achieving maximum increase in $[Ca^{2+}]_i$ occurred in every experiment performed in this thesis and over 10 years of research. However, it would appear that distinct batches of ionomycin may achieve higher maximum $[Ca^{2+}]_i$ although maximum release is not altered (Ashton, manuscript in preparation).

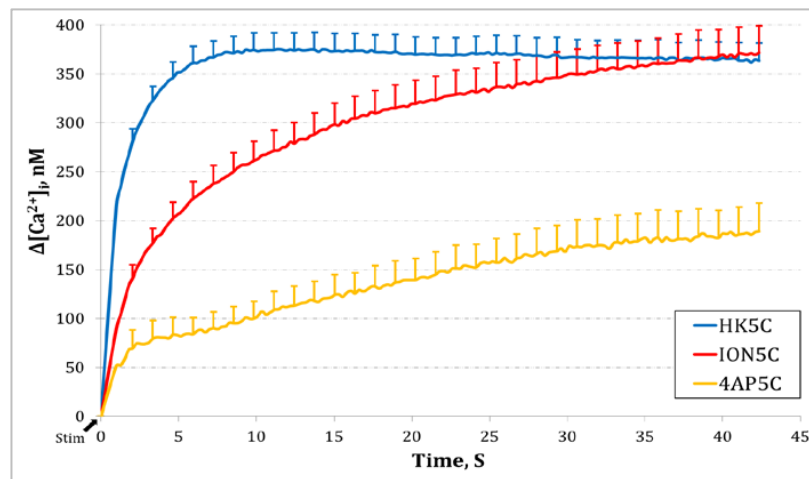


Figure 1.8: Effect of Stimuli upon Cytosolic free Calcium $[Ca^{2+}]_i$

All three stimuli employed in this study produce a change in $[Ca^{2+}]_i$ via different kinetics. 4AP5C evokes a significantly lower $[Ca^{2+}]_i$ change than HK5C or ION5C ($p < 0.05$). No significant difference was observed between HK5C and ION5C ($p > 0.05$) in this set of experiments. Values represented are the mean plus S.E.M. from 3 independent experiments.

1.9.2 A Single Round of Exocytosis

Due to the kinetics of the FM 2-10 dye and Glu release assays, synaptosomes in this study are subject to long stimulation periods (between 60-300 sec). Due to this long duration of stimulation there is a possibility that SVs could undergo multiple rounds of recycling, refilling with and re-release Glu, leading to an erroneous interpretation of Glu release. Further, it is possible that a SV releasing via KR could retain its FM 2-10 dye label while undergoing several round of KR recycling, or SV could lose its FM 2-10 dye and release additional Glu without a link to dye fluorescence. In order to accurately compare Glu and FM 2-10 dye release, it is essential to establish that SVs are only undergoing one round of release during the stimulation and measurement period.

In order to ensure recycling was not occurring during stimulation and measurement, synaptosomes were acutely treated with 1 μM of the selective vacuolar H^+ ATPase (V-ATPase) inhibitor Bafilomycin A1. The V-ATPase pump is a complex found on SVs that is responsible for re-acidification of the vesicular lumen after endocytosis, which is vital in order for SVs to be re-filled with Glu (Cotter, *et al.*, 2015). Such acute bafilomycin A1 treatment has no effect upon the Glu content of non-exocytosed SVs, and does not impede their release upon stimulation (Ikeda and Bekkers, 2008). An acute treatment of 1 μM Bafilomycin A1 did not significantly affect Glu release compared with untreated controls, regardless of stimulation (Figure 1.9) ($p>0.05$). If SVs were undergoing multiple rounds of recycling, the level of Glu release would be expected to decrease with the Bafilomycin A1 treatment.

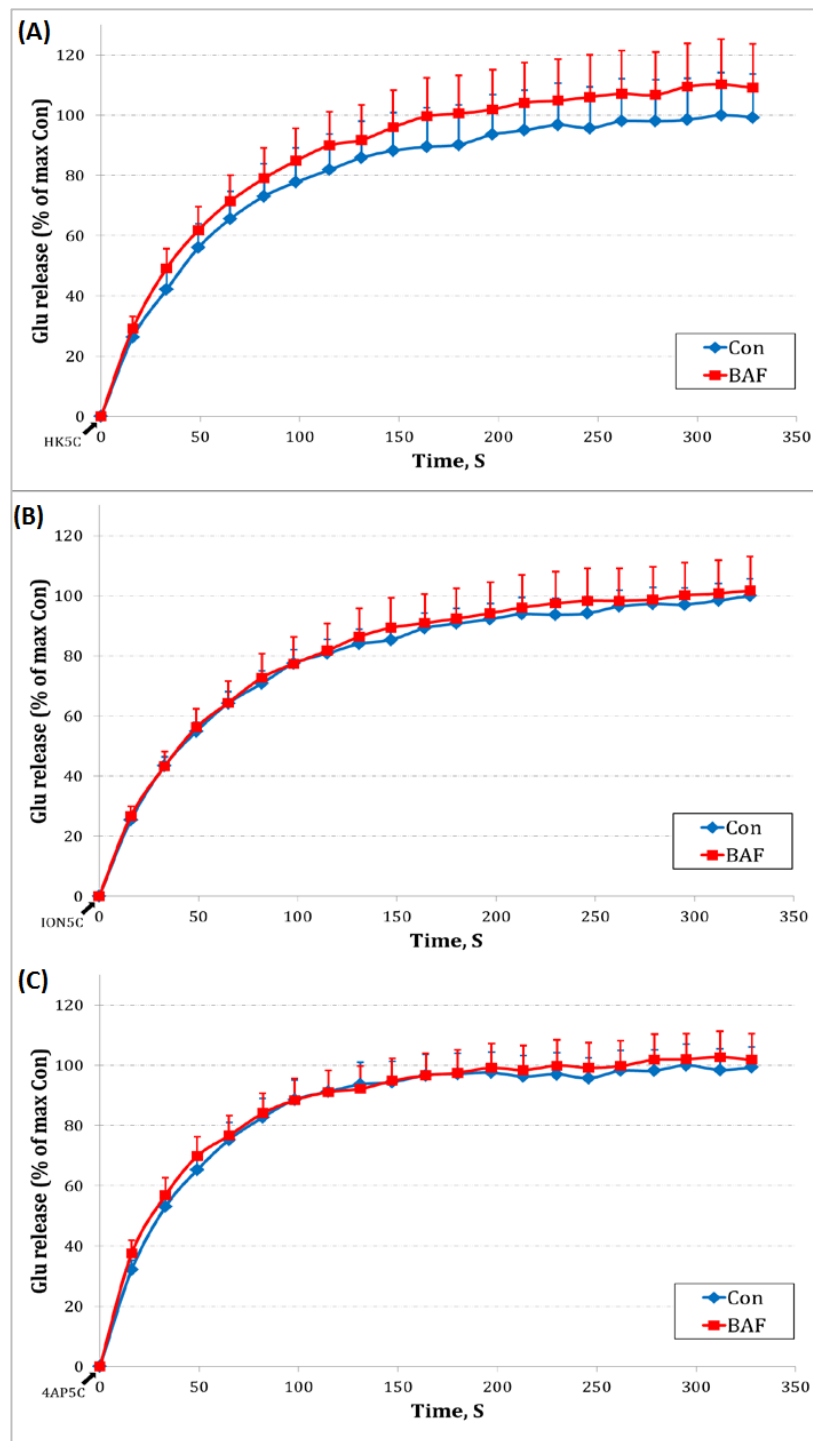


Figure 1.9: Effect of 1 μ M Bafilomycin A1 upon Evoked Glu release

Treatment with 1 μ M Bafilomycin A1 does not significantly affect Glu release when stimulated with HK5C (A), ION5C (B) or 4AP5C (C) compared to untreated controls ($p > 0.05$ for all). Values represented are the mean plus S.E.M. from 4 independent experiments.

1.9.3 Maximal Labelling of SVs with FM 2-10 Dye

Styryl dyes, such as FM 2-10, have been used extensively to label lipid membranes and in particular vesicular trafficking and recycling (see Chapter 4.1). In all experiments a concentration of 100 μM FM 2-10 dye was utilised, as many researchers have employed the same concentration (Baldwin, *et al.*, 2003; Cheung, *et al.*, 2010). Clayton and Cousin (2008) however, have previously suggested that the labelling of SVs, especially via bulk endocytosis, is dependent upon the concentration of FM 2-10 dye, and 1 mM but not 100 μM will fully label all SVs (Clayton and Cousin, 2008).

In order to ensure that all SVs are fully labelled with FM 2-10 dye, synaptosomes were incubated with 1 mM or 100 μM and evoke to release during a drug treatment (160 μM dynasore (DYN)) which has been observed to increase exocytosis via FF (Figure 1.10). In this model system there was no significant difference in FM 2-10 dye release seen between synaptosomes loaded with 1 mM or 100 μM ($p>0.05$), and drug treatment had no significant impact upon labelling or release of SVs ($p>0.05$). If 100 μM FM 2-10 dye had been failing to label all releasable SVs, then a reduced amount of dye would be released.

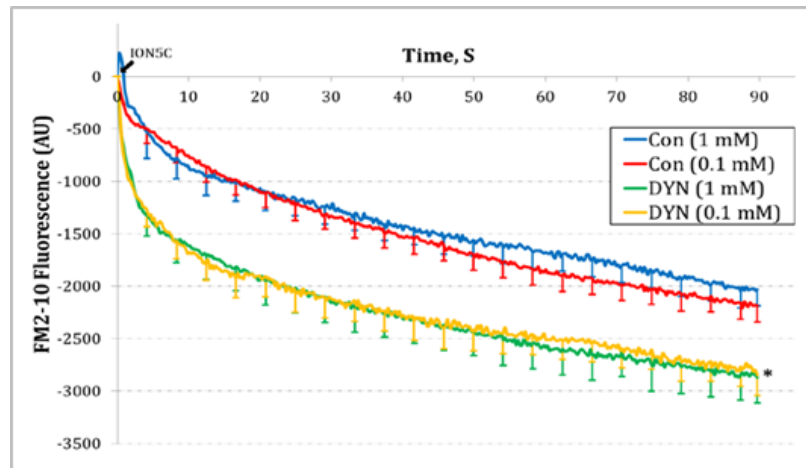


Figure 1.10: Difference between SVs Loaded with 1 mM or 100 μ M FM 2-10 Dye

SVs loaded with 1 mM (Blue) or 100 μ M (Red) release equivalent levels of FM 2-10 dye following stimulation ($p>0.05$). Drug treatment, 160 μ M dynasore, increases FM 2-10 dye release by a corresponding amount, regardless of amount of FM 2-10 dye loaded, following stimulation (Green vs Yellow) ($p>0.05$). Values represented are the mean minus S.E.M from 4 independent experiments.

1.9.4 The Mode of Exocytosis is Stimulation Dependent

Each of the stimuli used in this thesis have been shown to evoke release through distinct $[Ca^{2+}]_i$ kinetics (Figure 1.8), and changes in $[Ca^{2+}]_i$ have been linked to regulating the mode of exocytosis of distinct pools (Alés, *et al.*, 1999), therefore each stimuli could evoke release of SVs pools via unique modes. As the RRP is suggested to be released within 2 sec of stimulation (Rizzoli and Betz, 2005), this time period was studied during FM 2-10 dye release for all stimuli (Figure 1.11 A).

Interestingly HK5C and ION5C did not cause any significantly release of FM 2-10 dye in this period ($p>0.05$), unlike 4AP5C (Figure 1.11 A) ($p<0.05$). It could be argued that this indicates no SVs are being release during this time period, however when the experiment was repeated with a pre-treatment of 0.8 μ M OA (Figure 1.11 B), an inhibitor of protein phosphatase 1 and 2A which is known to convert all RRP SVs to FF (Ashton, *et al.*, 2011), an increase in FM 2-10 dye release was noted for all stimuli, that was not significantly different between stimuli at 2 sec ($p>0.05$). Comparison of these results are interpreted as HK5C and ION5C releasing the RRP via KR under control conditions, while 4AP5C releases roughly half the RRP via KR and half by FF. All three stimuli release an equivalent amount of FM 2-10 dye during this period (2 sec), suggesting it is the RRP being released.

In order to determine the exocytic mode of the RRP and RP, the fluorescence value of FM 2-10 dye release during control conditions was subtracted from the fluorescence value achieved during OA treatment (Figure 1.12). HK5C stimulation caused all RRP SVs to undergo KR in the first 2 sec (Figure 1.12 A), and all RP SVs to release via FF (after 2 sec; Figure 1.12 B). Stimulation with 4AP5C releases all RRP SVs some via KR and some by FF, with fluorescence subtraction demonstrating that both modes contribute equally (Figure 1.12 C). RP SVs do not release when synaptosomes are stimulated with 4AP5C, as this stimuli induced a lower average $[Ca^{2+}]_i$ compared to HK5C and ION5C, and this is unable to drive RP fusion (see Figure 1.7 C and Figure 1.8).

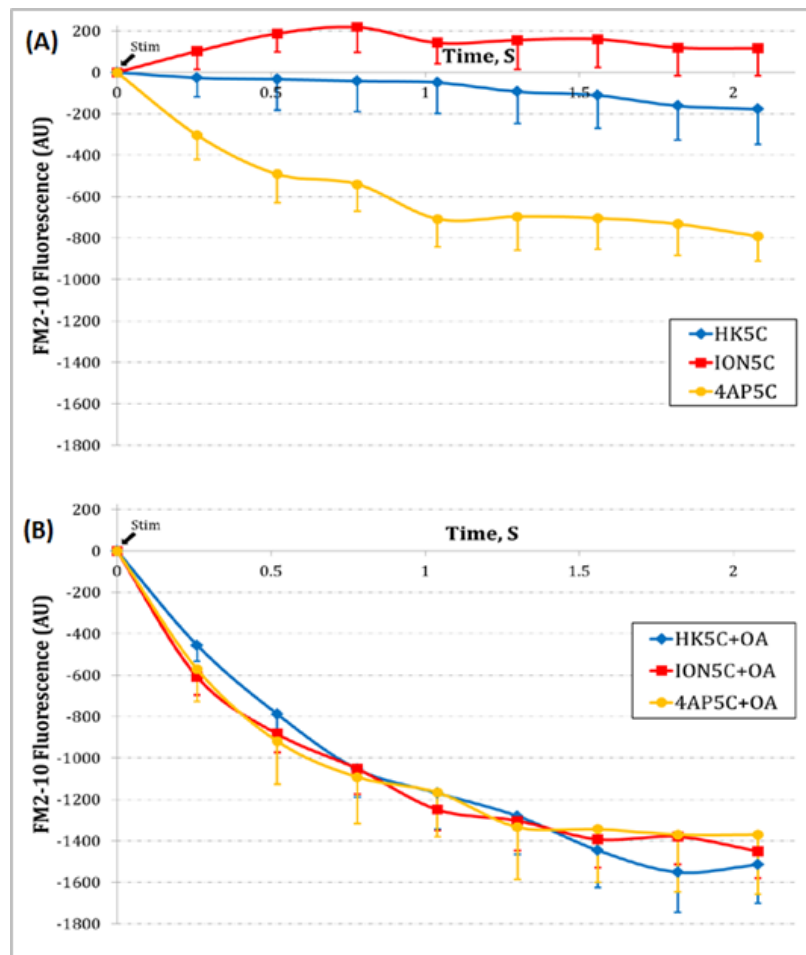


Figure 1.11: Mode of RRP Release during Control and 0.8 μM OA Treatment

(A) Measurement of control levels of FM 2-10 dye release after stimulation during first 2 sec. Only 4AP5C releases a significant amount of dye ($p < 0.05$). (B) Treatment with OA induces equivalent release of FM 2-10 dye regardless of stimulation over first 2 sec ($p > 0.05$). Values represented are the mean plus S.E.M. from 3 independent experiments.

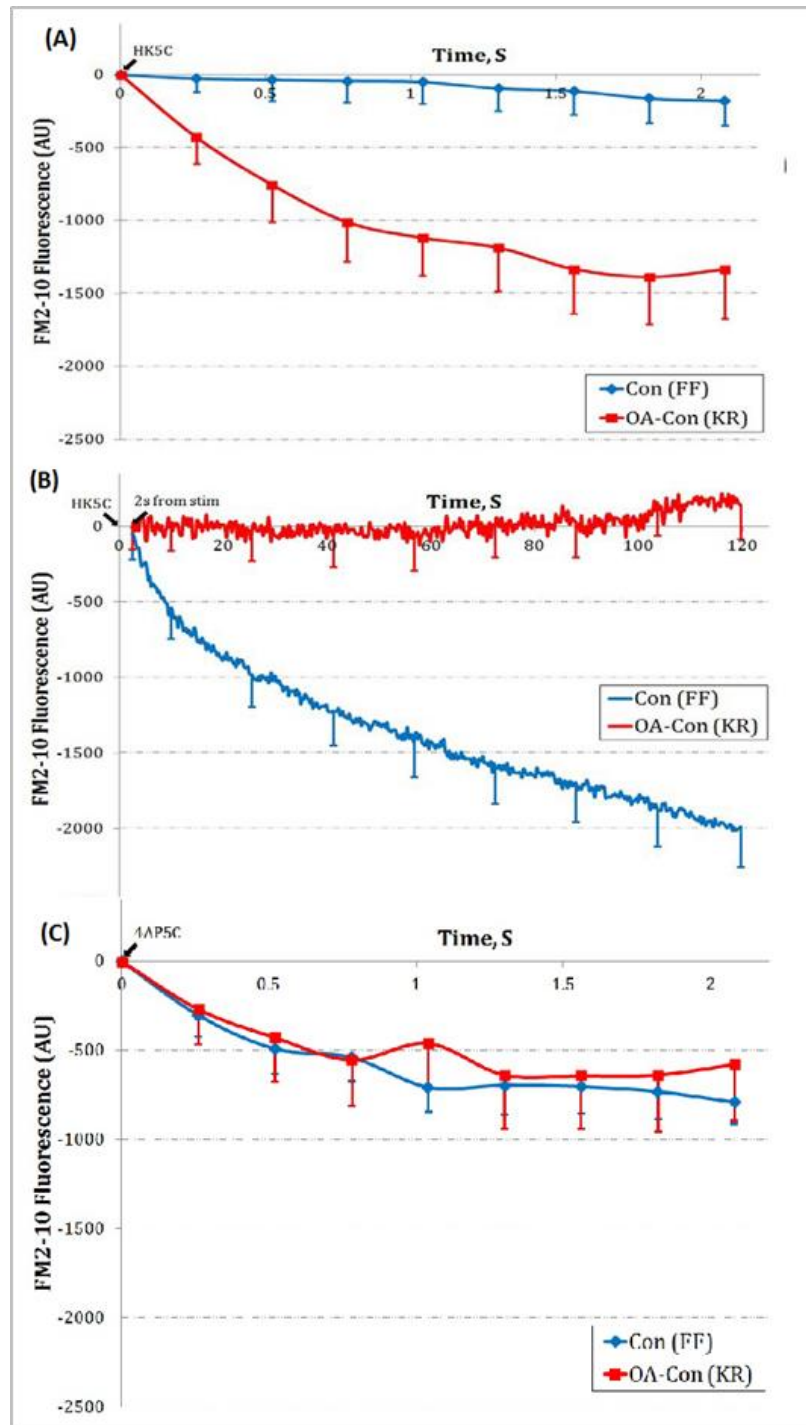


Figure 1.12: Mode of RRP and RP Release during Control and 0.8 μ M OA Treatment

When FM 2-10 dye fluorescence of control was subtracted from OA conditions, it was found that all SVs release via KR during initial 2 sec of HK5C stimulation (A), and remaining SVs are released via FF after 2 sec (B). During 4AP5C stimulation (C), all SVs are released by a combination of KR and FF for initial 2 sec. Values are average of 3 experiments plus S.E.M, taken from (Bhuva, 2015, p. 62) with permission.

1.9.5 Presynaptic Proteins Regulating Exocytosis

Dyn-I could have a role in modulating the mode of exocytosis at the FP. Previous research undertaken by Ashton group has demonstrated that inhibition of Dyn-I GTPase activity with 160 μM DYN did not perturb Glu release with any stimuli (Figure 1.13 A-C) ($p>0.05$), but significantly increased FM 2-10 dye release with ION5C and 4AP5C (Figure 1.13 E-F) ($p<0.05$). These results were interpreted as ION5C and 4AP5C having a Dyn-I dependence to release the RRP via KR, while HK5C was able to release the RRP independent of Dyn-I.

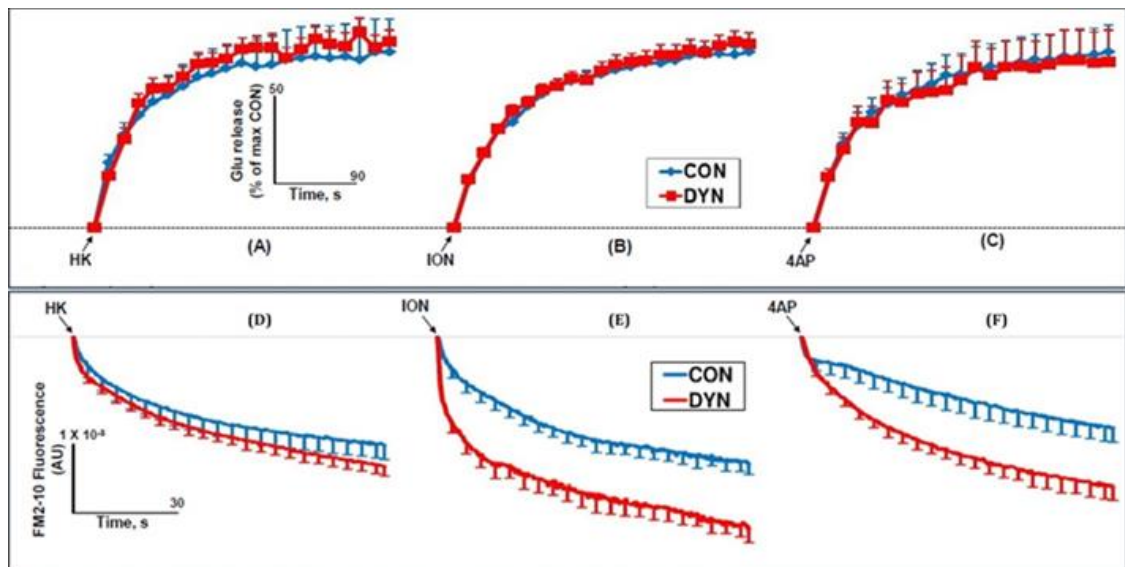


Figure 1.13: Effect of 160 μM Dynasore vs Control upon Evoked Glu and FM 2-10 Dye Release

Treatment with 160 μM dynasore does not perturb Glu release evoked by HK5C (A), ION5C (B) or 4AP5C (C) ($p>0.05$). 160 μM dynasore had no significant effect of HK5C evoked FM dye release (D) ($p=0.508$), but increased ION5C (E) ($p=0.014$) and 4AP5C evoked FM dye release (F) ($p=0.034$). Values are mean plus SEM from 4 experiments.

Figure taken with permission from a manuscript prepared by A. Ashton.

NM-II has also been implicated in regulating the mode of exocytosis at the FP (Chan, *et al.*, 2010; Berberian, *et al.*, 2009; Neco, *et al.*, 2008). Since no change in FM 2-10 dye release was observed when Dyn-I was inhibited with DYN during HK5C stimulation (Figure 1.13 D), it was theorised NM-II could be responsible for regulating the FP during this mode of exocytosis. Thus NM-II was blocked with 50 μ M blebbistatin (Blebb), a selective, high affinity small molecule which blocks NM-II by inhibiting ATPase activity (Shu, *et al.*, 2005; Kovacs, *et al.*, 2004).

A treatment of 50 μ M Blebb did not perturb Glu release with any stimuli ($p>0.05$) (Figure 1.14), but did significantly increase FM 2-10 dye release with HK5C stimulation only ($p<0.05$) (Figure 1.15 A). These data may suggest that NM-II is able to close the FP during HK5C stimulation, when the $[Ca^{2+}]_i$ level at the AZ is high (Figure 1.8), as Ca^{2+} is required to regulate NM-II phosphorylation and activation (Martinsen, *et al.*, 2014). These data may also suggest that the $[Ca^{2+}]_i$ level achieved at the AZ during ION5C and 4AP5C stimulation may not be high enough to activate NM-II, but satisfactory to activate Dyn-I to regulate the exocytosing FP (Figure 1.13 E-F).

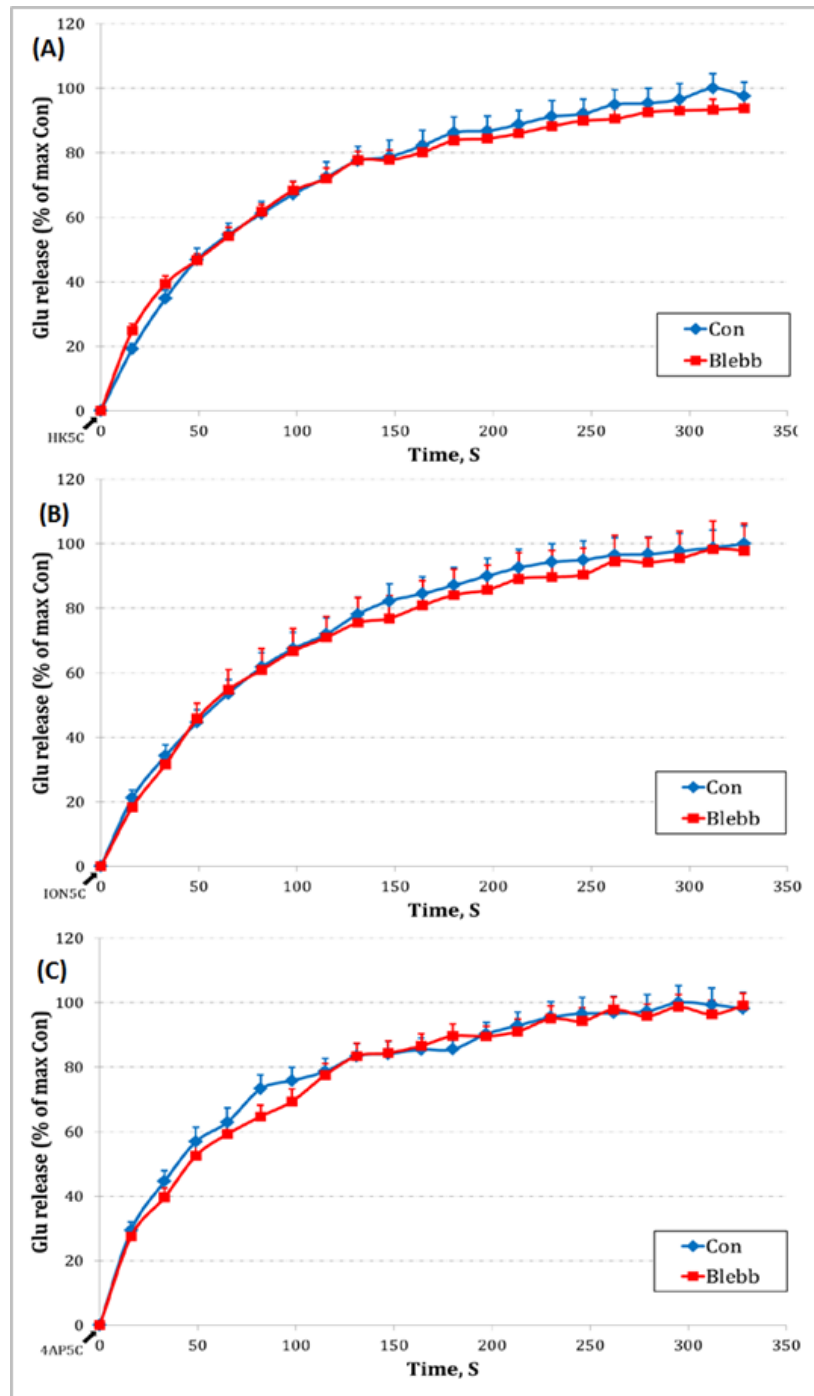


Figure 1.14: Effect of 50 μM Blebb upon Evoked Glu Release

Treatment with 50 μM Blebb did not significantly affect Glu release when stimulated with HK5C (A), ION5C (B) or 4AP5C (C) ($p > 0.05$). Values represented are the mean plus S.E.M. from 4 independent experiments.

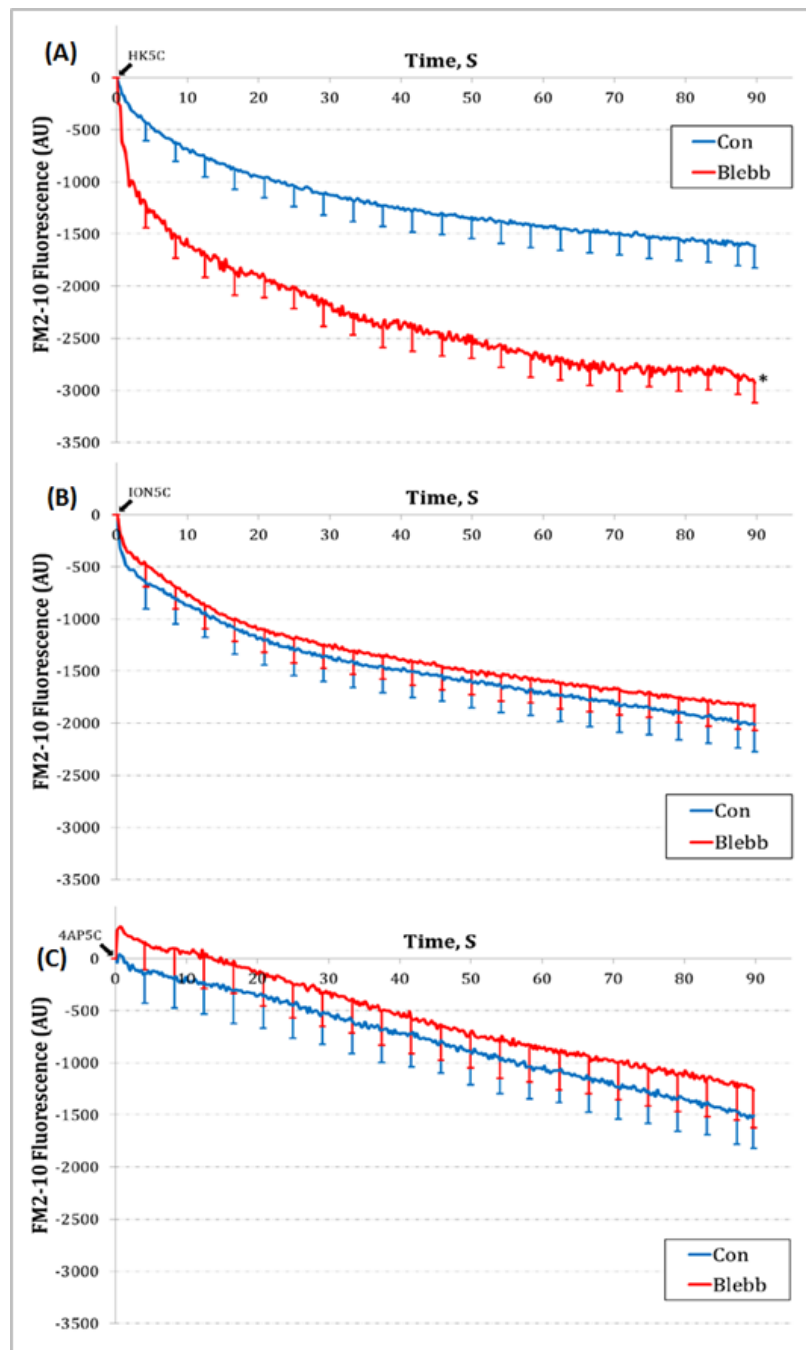


Figure 1.15: Effect of 50 μ M Blebb upon Evoked FM 2-10 Dye Release

Treatment with 50 μ M Blebb significantly increased FM 2-10 dye release when stimulated with HK5C (A) ($p < 0.05$), but had no effect when stimulated with ION5C (B) ($p = 0.716$) or 4AP5C (C) ($p = 0.642$). Values represented are the mean plus S.E.M. from 3 independent experiments.

The Ca^{2+} -dependent phosphatase calcineurin may also have a role in regulating proteins which participate in exocytosis, as calcineurin rapidly dephosphorylates many presynaptic proteins upon terminal depolarisation (Robinson, *et al.*, 1994). Inhibition of calcineurin with 1 μM Cyclosporine A (Cys A) did not significantly affect Glu release (Figure 1.16 A-C) ($p > 0.05$), but significantly decreased FM 2-10 dye release when stimulated with HK5C and ION5C (Figure 1.16 D-E, respectively) ($p < 0.05$). This differs with some studies that have shown Cys A treatment increases Glu release (Gaydukov, *et al.*, 2013), but in the context of this model this further indicates maximal Glu release is being observed under these conditions already (i.e. with 5 mM $[\text{Ca}^{2+}]_e$ Figure 1.7).

When the effects of calcineurin inhibition with 1 μM Cys A were investigated upon $[\text{Ca}^{2+}]_i$ levels, a significant increase was noted with all three stimuli (Figure 1.16 G-I) ($p < 0.05$). These data are interpreted as the inhibition of calcineurin causing more SVs to release via a KR mode of exocytosis, which could be due to the increased $[\text{Ca}^{2+}]_i$ level attained during Cys A treatment (Figure 1.16 G-I). The lack of effect upon 4AP5C evoked Glu and FM 2-10 dye, even during an increase in $[\text{Ca}^{2+}]_i$ could suggest calcineurin inhibition only affects the RP, since 4AP5C does not release the RP (Figure 1.7 C, and Figure 1.8), and the RRP is already releasing via KR with both HK5C and ION5C stimuli (Figure 1.11 A).

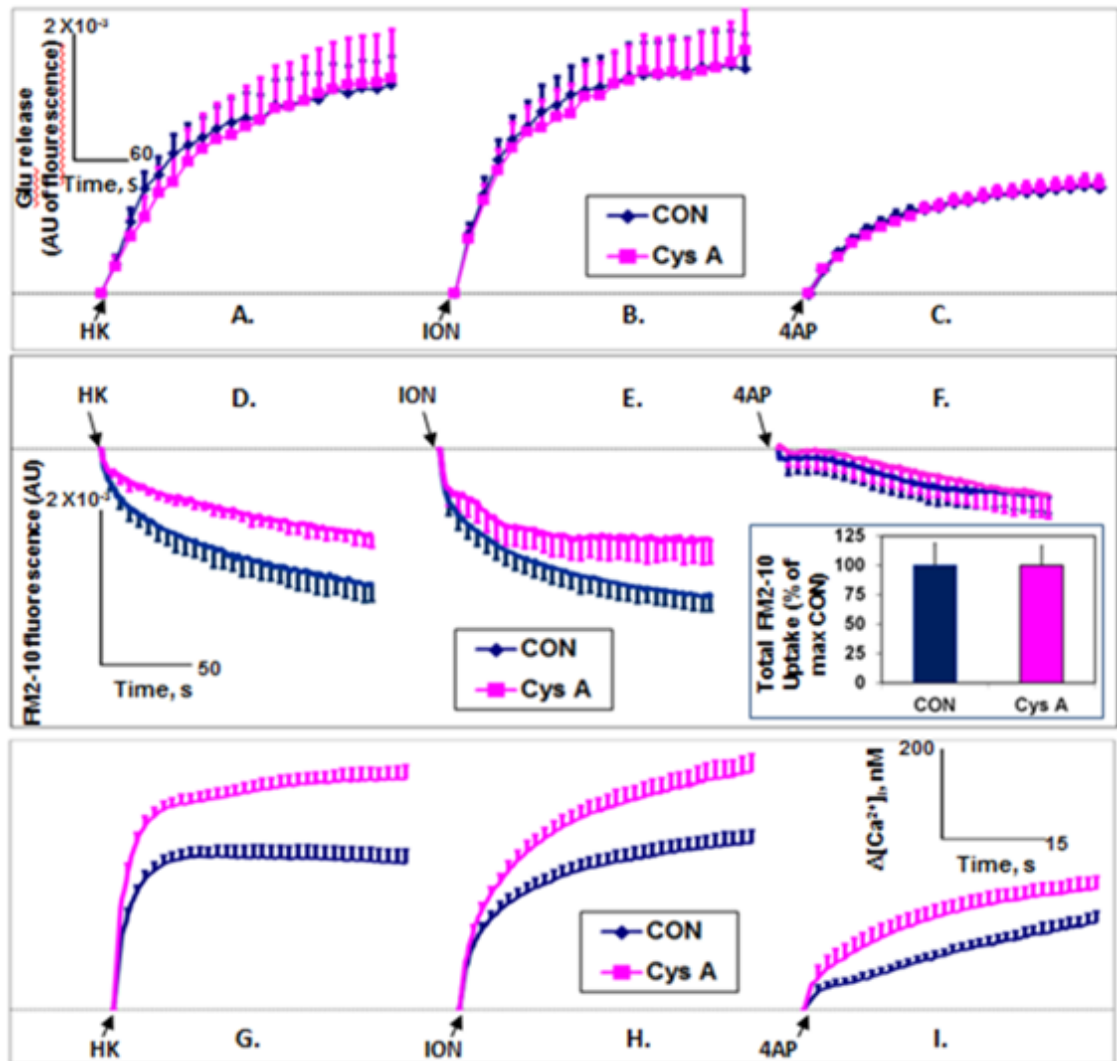


Figure 1.16: Effect of 1 μM Cys A upon Evoked Glu and FM 2-10 Dye Release

1 μM Cys A did not perturb Glu release evoked by HK5C (A), ION5C (B) or 4AP5C (C) ($p > 0.05$ for all). 1 μM Cys A significantly decreased HK5C (D) ($p < 0.025$) and ION5C (E) ($p < 0.023$) evoked FM 2-10 dye release, but had no effect upon 4AP5C (F) ($p = 0.985$) evoked FM 2-10 dye release. 1 μM Cys A significantly increased $[\text{Ca}^{2+}]_i$ levels with HK5C (G) ($p < 0.001$), ION5C (H) ($p < 0.044$) and 4AP5C (I) ($p < 0.049$) stimulation, compared to controls. Values represented are the mean plus S.E.M. from 4 experiments. Figure taken from a manuscript prepared by A. Ashton.

1.9.6 Phosphorylation of Dyn-I Ser-795 *in vivo*

Previous research by Bhuva has proved that synaptosomes treated with 0.8 μ M OA (Figure 1.17 B) or 80 nM of the PKC activator phorbol 12-myristate 13-acetate (PMA) (Figure 1.17 C) exhibit detectable levels of *in vivo* Dyn-I Ser-795 phosphorylation over 2-120 seconds, compared to control synaptosomes where Ser-795 was undetectable (Figure 1.17 A) (Bhuva, 2015, p. 151). The lack of Ser-795 phosphorylation in control samples was explained as Ser-795 either remaining dephosphorylated during this treatment or being dephosphorylated almost immediately after phosphorylation, as pan-Dyn-I (4E67) revealed uniform protein levels in all samples (Figure 1.17 D) (Bhuva, 2015, p. 160). More recent studies have been able to reproducibly demonstrate a basal level of phospho-Ser-795 in drug free terminals (see Chapter 5).

Previous research has also demonstrated that samples stimulated with HK5C or ION5C over 120 sec, show a time-dependent decrease in phosphorylation levels at Ser-774 and Ser-778 during control conditions (Figures 1.18 and 1.19 A), with ION5C stimulation induced a greater decrease in phosphorylation than HK5C (Lanes 11 vs 12). Interestingly, drug treatments can block this dephosphorylation effect, potentially describing roles for these sites in exocytosis (Figures 1.18 and 1.19 B). This decrease in phosphorylation was interpreted as the Ser sites undergoing dephosphorylation after stimulation, as levels of Dyn-I protein did not change in a relative manner (Figures 1.18 and 1.19 C).

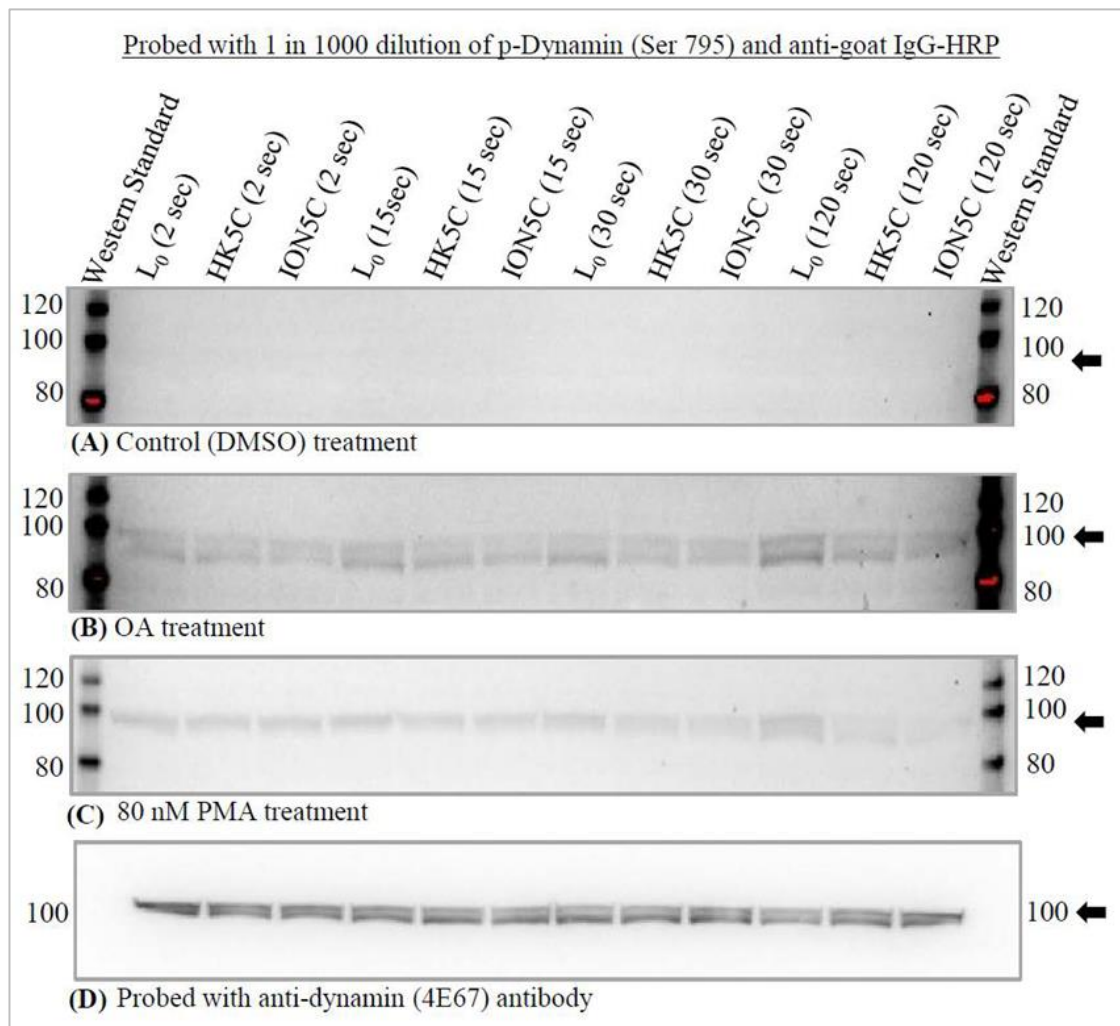


Figure 1.17: Phosphorylation of Dyn-I Ser-795 across a range of Treatments

(A) Ser-795 is not detectable in control conditions. Treatment with 0.8 μ M OA (B) and 80 nM PMA (C) reveal phospho-Ser-795. (D) A representative blot displaying total Dyn-I protein in each sample.

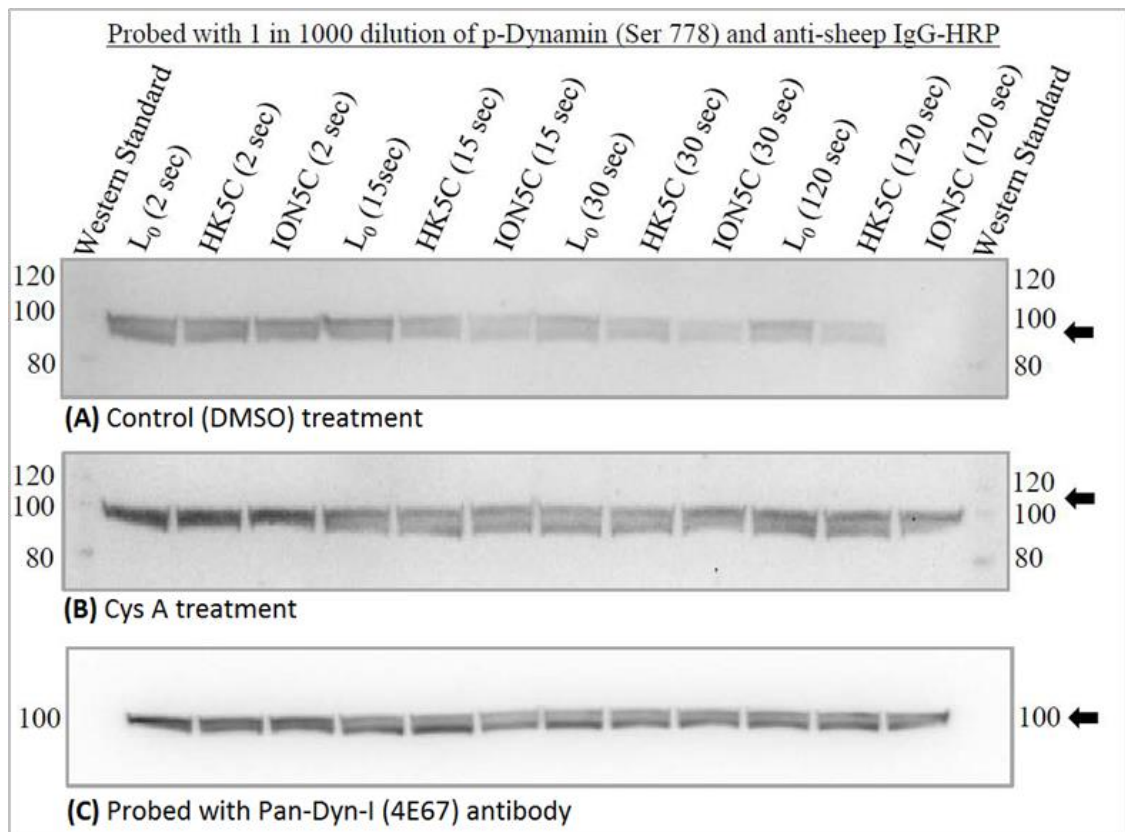


Figure 1.18: Phosphorylation of Dyn-I Ser-778

(A) A time dependent decrease in phosphorylation is noted over 120 sec, with a greater decrease observed with ION5C stimulation. (B) This decrease can be reversed by drug treatments. (C) Uniform levels of protein are present in samples.

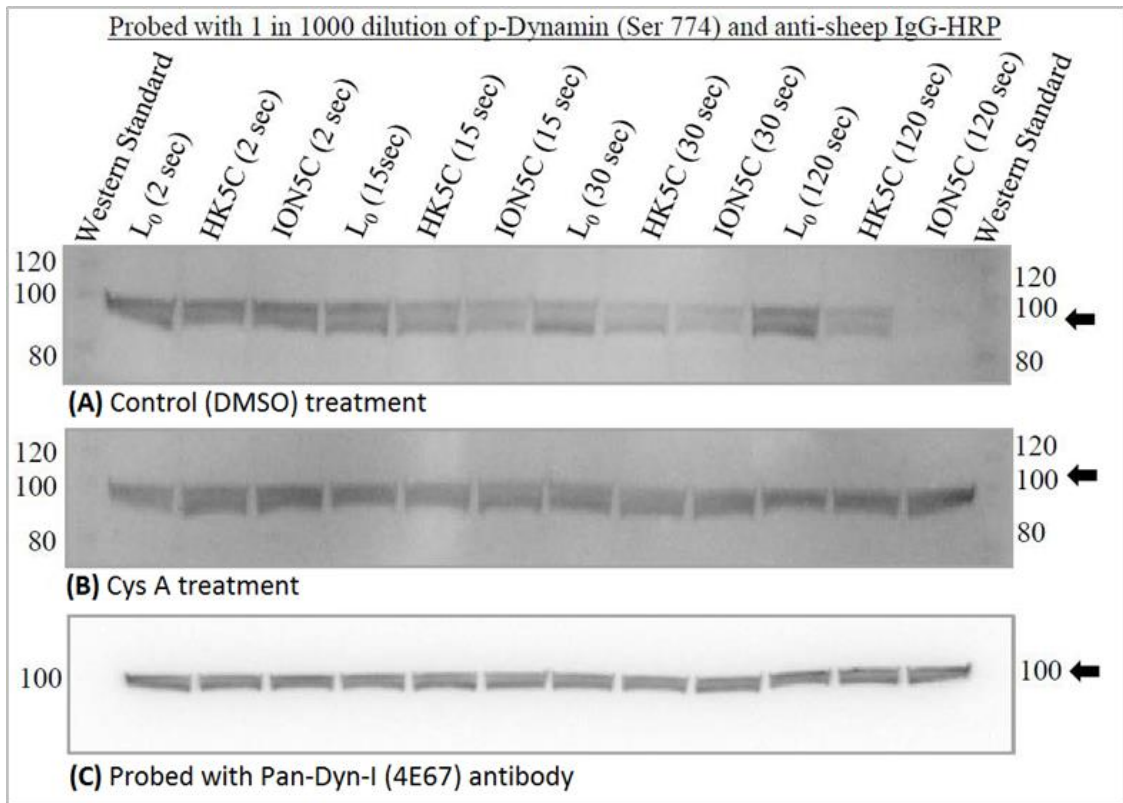


Figure 1.19: Phosphorylation of Dyn-I Ser-774

(A) A time-dependent decrease in phosphorylation over 120 sec, ION5C induces a greater decrease than HK5C. (B) Drug treatment prevents dephosphorylation over 120 sec. (C) Uniform levels of Dyn-I detected in samples.

1.9.7 Conclusion

Collectively these data suggest that stimulation with HK and ION, in the presence of 5 mM $[Ca^{2+}]_e$, can maximally release Glu from the RRP via KR and from the RP by FF in one round of exocytosis. 4AP5C stimulation on the other hand, can only stimulate maximal Glu release of the RRP (half by KR, half via FF) in one round of exocytosis, and the lack of RP release is probably due to the lower average $[Ca^{2+}]_i$ level seen in the terminals with this stimulus, compared to HK5C and ION5C.

Inhibition of Dyn-I increases the FF mode of exocytosis (by blocking FP regulation), but only with stimuli where the increase in $[Ca^{2+}]_i$ is more gradual (ION5C and 4AP5C). It is theorised that the slower increase in $[Ca^{2+}]_i$ activates kinases to drive Dyn-I action (Singh, 2017, p. 99), and when the increase in $[Ca^{2+}]_i$ is more rapid, as with HK5C, Dyn-I may be inactivated by distinct kinases. Interestingly, when the $[Ca^{2+}]_i$ level increases rapidly with HK5C, NM-II can be inhibited with Blebb, suggesting that the high Ca^{2+} may prevent Dyn-I activation, but certain kinases can activate NM-II to be able to regulate the FP (Singh, 2017, p. 98).

1.10 Research Aims

Previous research has indicated that PKC can regulate the mode of exocytosis, but while PKC may induce Dyn-I phosphorylation and switching of the mode of exocytosis, it would appear that other kinases may contribute to the phosphorylation of Ser-795 and the regulation of the FP (Barclay, *et al.*, 2003; Bhuvu, 2015; Singh, 2017). Therefore the aim of this thesis is to establish whether regulating PKA or cAMP levels can control the mode of exocytosis and if such effects could be related to changes in the phosphorylation of Dyn-I Ser-795.

1.10.1 Specific Aims

- (i) Investigate how the activation and inhibition of PKA regulate the release mode of SV pools and what effect Dyn-I inhibition and actin disruption also have on release.
- (ii) Determine how the activation and inhibition of AC affect cAMP levels to regulate the activity of PKA and EPACs, and the impact of such regulation upon the mode of exocytosis.
- (iii) Throughout – Investigate how such pharmacological treatments affect $[Ca^{2+}]_i$ levels during synaptosomal stimulation.
- (iv) Study the phosphorylated profile of Dyn-I during pharmacological treatments to determine any correlation with the mode of exocytosis.

Chapter 2:

Materials and Methods

2.1 Materials

2.1.1 Buffering Reagents

- Basal Physiological buffer (L0): 125 mM NaCl, 5 mM KCl, 1 mM MgCl₂, 20 mM Hepes and 10 mM glucose (pH adjusted to 7.4 with NaOH).
- Isotonic sucrose solution (Homogenisation buffer): 320 mM sucrose and 10 mM Hepes (pH adjusted to 7.4 with NaOH).
- Stock high potassium (HK0) buffer: 130 mM KCl, 20 mM Hepes, 1 mM MgCl₂ and 10 mM glucose (pH adjusted to 7.4 with NaOH).
- Bioenergetics buffer*: (3.5 mM KCl, 120 mM NaCl, 1.3 mM CaCl₂, 0.4 mM KH₂PO₄, 1.2 mM Na₂SO₄, 2 mM MgSO₄, 15 mM glucose, 10 mM pyruvate).

*Note – Bioenergetics buffer has no actual buffering component as this would interfere with the assay measuring proton production.

2.1.2 Stimulation Solutions

Three Ca²⁺ requiring stimuli are used to investigate the mechanisms of NT release; 30 mM K⁺ (high potassium), 5 μM ionomycin or 1 mM 4-aminopyridine, each in the presence of 5 mM [Ca²⁺]_e (HK5C, ION5C and 4AP5C respectively).

High potassium is a clamping stimulus which depolarises the nerve terminal, activating voltage-gated Ca²⁺ channels at the AZ. This creates a large influx of Ca²⁺ immediately at the release site which then diffuses through the terminal, producing a lower Ca²⁺ concentration, allowing release of both the RRP and RP (see Figures 1.7 and 1.8).

Ionomycin is an ionophore which raises $[Ca^{2+}]_i$ levels by transporting Ca^{2+} across the PM. Ionomycin is also able to cross lipid bilayers and due to this can also transport Ca^{2+} out of intracellular stores (Yoshida and Plant, 1992; Kao, Li and Auston, 2010). This creates a uniform increase in $[Ca^{2+}]_i$ across the terminal, releasing both the RRP and RP.

4-aminopyridine is a selective blocker of voltage-gated K^+ channels which induces Ca^{2+} -dependent Glu release through repetitive Na^+ channel firing, leading to random Ca^{2+} channel opening and generation of spontaneous APs (Tibbs, *et al.*, 1989). However 4-aminopyridine may also mobilise Ca^{2+} from intracellular stores to mediate release (Grimaldi, *et al.*, 2001). 4-aminopyridine causes a slower increase in $[Ca^{2+}]_i$ than high potassium or ionomycin, which may be the reason it only releases the RRP of SVs (Tibbs, *et al.*, 1989; Figure 1.8).

These stimuli work through separate mechanisms, and their use highlights similarities and differences in Ca^{2+} -dependent exocytosis (McMahon and Nicholls, 1991; Tibbs, *et al.*, 1989). Previous research by A. Ashton has demonstrated that 5 mM extracellular Ca^{2+} ($[Ca^{2+}]_e$) when utilised with HK and ION produces maximal Glu release from both the RRP and RP, and use with 4AP produces maximal Glu release from just the RRP. This allows study of the Glu released by the RRP and its mode separately from the RP using the assays listed below (see Figure 1.7).

For stimulation with HK5C and 4AP5C, Ca^{2+} free stimulation solutions termed HK0 and 4AP0 were employed for basal conditions in Glu assays. Due to the nature of ionomycin to transport Ca^{2+} across the PM and out of intracellular stores (Yoshida and

Plant, 1992), L0 was used as a basal stimulation solution instead. Through comparison studies (Ashton, *et al.*, unpublished), it was determined that L0 produced indistinguishable results from HK0 and 4AP0 during the FM 2-10 dye release assay, and so L0 was used as the control condition for these experiments.

2.1.3 Drugs and Final Concentrations (Dissolved in DMSO)

- 1-9-dideoxyforskolin (100 μM); Tocris Bioscience; #5034
- 4-Aminopyridine; Sigma-Aldrich; #A78403
- 9-cyclopentyladenine mesylate (9-cp-ade) (100 μM); Sigma-Aldrich; #C4479
- Advasep-7; Sigma-Aldrich; #A3723
- β -Nicotinamide adenine dinucleotide phosphate hydrate (NADP^+); Sigma-Aldrich; #N5775
- Cyclosporine A (Cys A) (10 μM); Tocris Bioscience; #1101
- Dynasore (80-160 μM); Sigma-Aldrich; #D7693
- ESI-09 (10, 33 and 100 μM); Sigma-Aldrich; #SML0814
- FM 2-10 dye; Thermo fisher Scientific; #T7508
- Forskolin (100 μM); Tocris Bioscience; #1099
- Fura-2-AM; Thermo Fisher Scientific; #F1221
- Ionomycin; Tocris Bioscience; #1704
- KT5720 (2 μM); Tocris Bioscience; #1288
- Latrunculin (15 μM); Tocris Bioscience; #3973
- 36 milli-Units (mUnits) of L-Glutamate Dehydrogenase type-II (GDH); Sigma-Aldrich; #MAK099-1KT
- Myristyl trimethyl ammonium bromide (MITMAB) (30 μM); Tocris Bioscience; #4224
- Okadaic acid (OA) (0.8 μM); Tocris Bioscience; #1136
- Pitstop 2TM (15 μM); Abcam Biochemicals; #ab120687
- Sp-5,6-dichloro-cBIMPS (cBIMPS) (50 μM); Santa Cruz Biotechnology; #sc-201566

For the bioenergetics Mito-Stress test:

- Carbonyl cyanide 4-(trifluoromethoxy)phenylhydrazone (FCCP); Sigma-Aldrich; #C2920 (18 μM) (2 μM Final)
- Oligomycin A; Sigma-Aldrich; #75351 (32 μM) (4 μM Final)
- Rotenone; Sigma-Aldrich; #R8875 (5 or 50 μM) (0.5 or 5 μM Final)
- Antimycin A; Sigma-Aldrich; #A8674 (5 or 50 μM) (0.5 or 5 μM Final)

2.1.4 Various Chemicals Employed

- NuPAGE LDS sample buffer (4x Stock); Thermo Fisher Scientific; #NP0008
- NuPAGE MES SDS Running buffer; Thermo Fisher Scientific; #NP000202
- NuPAGE Sample Reducing Agent (10x Stock); Thermo Fisher Scientific; #NP0009
- 15 ml Restore™ PLUS Western Blot Stripping Buffer; Thermo Fisher Scientific; #46430
- StartingBlock T20 Blocking Buffer (TBS); Thermo Fisher Scientific; #37543
- 3 ml SuperSignal™ West Dura Extended Duration Substrate; Thermo Fisher Scientific; #34076
- 3-5 μl Unstained MagicMark™ XP Western Protein Standard; Thermo Fisher Scientific; #LC5602

2.1.5 Equipment

- Avanti® J-25 series centrifuge – Beckman-Coulter
- iBlot Transfer Stack, PVDF, Regular size' Thermo Fisher Scientific; #IB401031
- JA-17 Fixed-Angle Aluminium Rotor – Beckman-Coulter; #369691
- Motor driven, Teflon (pestle)-based homogeniser (Similar to a Potter-Elvehjem tissue homogenizer)
- GENios Pro Infinite 200 multimode microplate reader – Tecan
- NuPAGE 4-12% Bis-Tris Protein Gels, 12-Well; Thermo Fisher Scientific; #NP0322BOX
- NuPAGE Gel Electrophoresis Tanks and pre-cast gel system – Thermo Fisher Scientific
- PowerEase 500 power packs – Thermo Fisher Scientific; #EI8600
- ChemiDoc XRS+ Imaging System – Bio-Rad Laboratories, Inc., with Image Lab software version 3.0.1
- Seahorse Xfp extracellular flux analyser – Seahorse Bioscience, USA

2.1.6 Specific Antibodies Employed

During Western blot analysis, specific commercially available antibodies outlined in Table 2.1 were used to investigate the phosphorylation profile of Dyn-I. All antibodies were sourced from Santa Cruz Biotechnology, Inc., USA.

Primary Antibody	Dilution	Secondary Antibody	Dilution
p-Dyn-I Ser-774			
Sheep Polyclonal (sc-135689)	1:1000	Donkey anti-sheep HRP conjugated (sc-2473)	1:3000
Dyn Ser-778			
Sheep Polyclonal (sc-135690)	1:1000	Donkey anti-sheep HRP conjugated (sc-2473)	1:2000
Dyn Ser-795			
Goat Polyclonal (sc-12937)	1:500	Donkey anti-goat HRP conjugated (sc-2020)	1:2000
Pan-Dyn-I (4E67)			
Mouse Monoclonal (sc-58260)	1:1000	Goat anti-mouse HRP conjugated (sc-2005)	1:5000

Table 2.1: Antibodies for Western Blotting

Catalogue numbers are found beneath each antibody.

2.2 Preparing Synaptosomes

In this study, synaptosomes (pinched-off nerve terminals) prepared from the cerebral cortex of adult male Wistar rat brains were used as the research model. Synaptosomes were prepared according to a method developed by Hebb and Whittaker and modified by Dodd and colleagues (Hebb and Whittaker, 1958; Gray and Whittaker, 1962; Dodd, *et al.*, 1981), with minor alterations. Briefly, one rat was sacrificed by cervical dislocation and the cerebral cortex swiftly removed and put into homogenisation buffer (320 mM sucrose plus 10 mM Hepes pH 7.4) at 4°C. Tissue was then homogenised using a motor driven Teflon homogenizer that was specially designed for preparing synaptosomes. The shearing force provided by the rotating pestle (900 rpm) and the clearance of 150 µm ensured the production of intact and functional synaptosomes. This homogenate was then centrifuged at 1941 × g for 10 min to separate the neuronal cell bodies from the nerve terminals. The resulting pellet (P1) was discarded and the supernatant (S1) was then centrifuged at 21,075 × g for 20 min.

The subsequent pellet (P2), which contained synaptosomes, was then suspended in basal physiological buffer (125 mM NaCl, 5 mM KCl, 1 mM MgCl₂, 20 mM Hepes and 10 mM glucose. pH 7.4) termed 'L0' at 4°C. This suspension was again centrifuged at 21,075 × g for 20 min and the final pellet (P3) was re-suspended in 8 ml of L0, kept at 4°C and gassed with O₂ until required. Synaptosomes prepared by this method represent a good semi-in-vitro model due to the presence of functioning ion channels, receptors, proteins and pathways. They exhibit physiological properties expected of pre-synaptic neurons (Erecińska, Nelson and Silver, 1996). All synaptosomes were used within four hours of preparation, after which viability begins to decrease.

2.3 Glutamate Release Assay

The Glu release assay follows a method developed by Nicholls and colleagues (Nicholls, *et al.*, 1987), and was adapted by Sim and colleagues for use on a fluorescence microtiter plate and plate reader (Sim, *et al.*, 2006). This assay converts the Ca^{2+} -dependent exocytotic release of Glu into a fluorescent signal, which can then be used to calculate which pools of SVs are undergoing release. Minor alterations were made by A. Ashton establishing the measurement parameters and durations set forth here. Figure 2.1 outlines the time course of the Glu assay, the incubation temperatures and relative treatments.

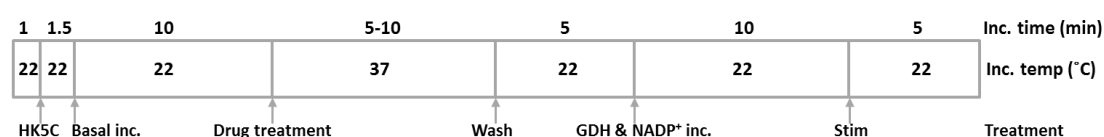


Figure 2.1: Glu Assay Time Course

The time course demonstrates each treatment the synaptosomes underwent during the assay, the duration and the temperature of each treatment. For dual drug treatments a second incubation period of 5-10 min at 37°C follows the first drug treatment. Inc – incubation.

A 2 ml aliquot of synaptosomes, prepared as described, was washed (with L0) and re-suspended in 1 ml of fresh L0. The suspension was stimulated for 90 sec with HK5C, causing all the releasable vesicles in the synaptosomes to undergo exocytosis. The synaptosomes were then spun down at 9589 x g for 45 sec, washed once in L0 spun down again and re-suspended in L0. The suspension was then incubated at room

temperature (RT) for 10 min to allow all the exocytosed SVs to recycle. This stimulation step, though not necessary for the Glu assay directly, allows comparison with the FM 2-10 dye release assay, by treating all samples in a similar manner as the latter assay requires this pre-stimulation.

After this, synaptosomes were incubated with the desired drug or equivalent volume of drug solvent (DMSO for control samples unless otherwise stated) for 5-10 min at 37°C. The samples were washed with L0 then re-suspended in 1.6 ml of fresh L0, plus the corresponding amount of drug or DMSO volume (to prevent the reversibility of the drug action). For dual drug treatments, synaptosomes were again incubated for 5-10 min at 37 °C in a solution containing the second desired drug or drug solvent for control samples.

Aliquots of 121 µl from this preparation were added to wells 1-12 of a row in a Greiner 96 well microtiter plate (black with flat, transparent bottom). In addition 20 µl of L0 was added to each well for a volume of 141 µl. After this 10 µl of 20 mM NADP⁺ and 9 µl of GDH were added to each well (for a final volume of 160 µl and a final concentration of 1 mM NADP⁺ and 36 mUnits GDH) and the resulting mixture was incubated at RT for 10 min.

At this stage, any Glu present outside the synaptosomes is converted to α-ketoglutarate by GDH in the presence of NADP⁺ which itself is converted to NADPH producing background fluorescence, demonstrated in the equation below.



Any increase in fluorescence measured after this point is a result of evoked Glu release from within the synaptosomes, which allows indirect quantification.

After incubation, wells 1-5 were treated with 40 μ l of the desired stimulus (HK5C, 4AP5C or ION5C) and the corresponding stimulus without Ca^{2+} was added to wells 6-12 (e.g. HK0). For samples stimulated with ION5C, LO was added to the basal samples as ionomycin would disrupt the Ca^{2+} gradient and its hydrophobic nature means membrane binding is irreversible (Kao, Li and Auston, 2010).

Fluorescence was then measured from wells 1-9 with the Tecan GENIOS Pro infinite 200 plate reader (at excitation wavelength: 340 nm; emission wavelength: 465 nm; gain: 100; read mode: bottom; and for 21 cycles). This number of cycles reflects an assay time of \sim 5 min to ensure all Glu exocytosed is hydrolysed by GDH. After the measurement, 10 μ l of LO was added to wells 7-9, and 10 μ l of freshly prepared 1 mM stock glutamate (final amount added 10 nmol) was added to wells 10-12. Fluorescence was measured from wells 7-12 using the same setting but at 15 cycles \sim 4 min. These latter settings, allow an internal control to be ran on each drug or control condition and allows for normalisation of all the rows for equivalent sensitivity. Subtracting the background values from the stimulation values provides a true representation of Ca^{2+} dependent vesicular Glu release. Significance values were calculated using two way Student's t-test, with a significance threshold of 0.05.

In some cases, there are large differences in the amount of Glu release observed between ION5C and HK5C and this is because these sets of experiments were done at different times. It could be that there are differences in the total protein between the

different sets of experiments or it could be that the different ages of the rats may have made a difference. This effect has not really been investigated fully and in using rats ranging in size from 250g to 650g, all have displayed the regulation of the modes of exocytosis but it was not observed whether they produced slightly different amounts of release. It should be noted that the comparison between control and drug treatment were always done with the same synaptosomes so that the observed differences and trends are valid. However, it should also be considered that overall in more than 10 years of research, the average ION5C or HK5C evoked control release for Glu and FM dye are comparable (Ashton, unpublished observation). Herein, a comparison has been made for the average maximum release evoked by HK5C and ION5C from 20 independent experiments performed over a period of a year. It can be seen that statistically there is no significant difference between the evoked release of the two stimuli (Figure 2.2).

Throughout this thesis Glu release data is expressed in AU of fluorescence and in order to show equivalence of approach Figure 2.3 demonstrates the conversion of AU to nmol of Glu release per mg of protein. This conversion is done using the average signal for a 10 nmol Glu standard added at the end of each assay, and the average amount of protein (from P2 synaptosomes) calculated per well. This data can also be represented as a percentage of maximum HK5C evoked release (Figure 2.3 C). Figure 2.3 A-C highlights that ION5C and HK5C stimuli evoked similar amounts of Glu release with the different graphs looking similar, so one is able to use AU of fluorescence rather than nmol of Glu per mg of protein.

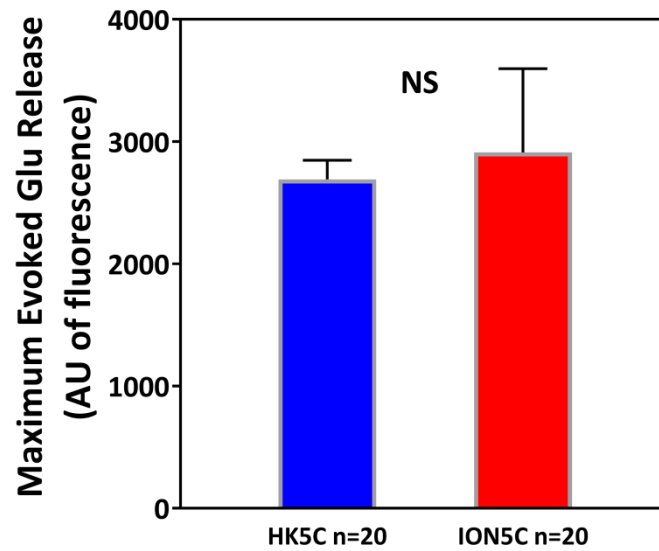


Figure 2.2: Average Size of Maximum Glu Release with HK5C and ION5C Stimulation

Maximum Glu release evoked by HK5C and ION5C from 20 independent experiments, adjusted with 10 nmol Glu standard ($p=0.755$). Values represented are the mean plus S.E.M. from 20 independent experiments. *NS*, not significant.

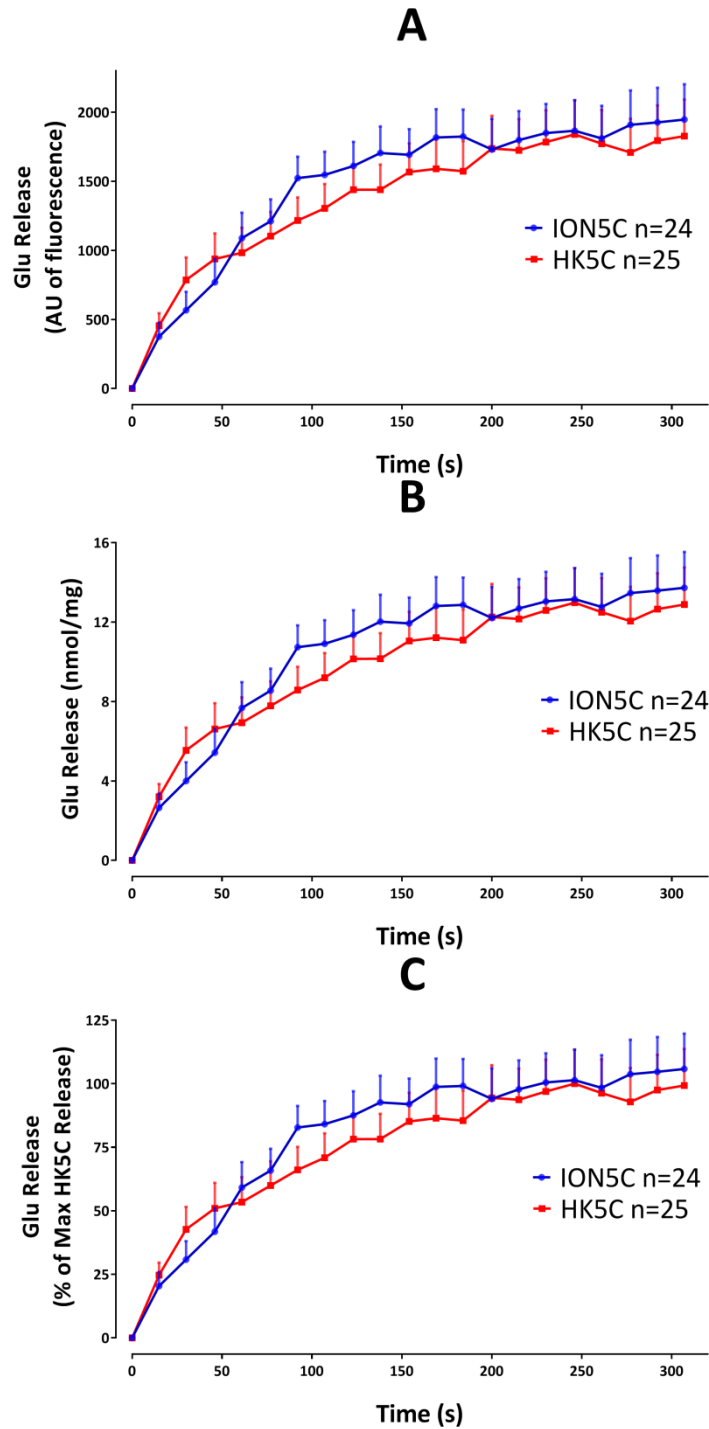


Figure 2.3: Evoked Glu Release Equivalency of Approach

(A) AU of fluorescence of Glu release evoked by ION5C or HK5C, (B) nmol of Glu released per mg of protein evoked by ION5C or HK5C. (C) Glu release represented as a percentage of maximum HK5C evoked Glu release (all $p > 0.05$). Values represented are the mean plus S.E.M. from 5 independent experiments.

2.4 FM 2-10 Styryl Dye Release Assay

2.4.1 Background/Rationale

In order to determine the mode of exocytosis for distinct SV pools, the Styryl dye FM 2-10 was utilised. Styryl dyes are water soluble, non-toxic, lipophilic molecules that can reversibly insert into cell membranes without completely permeating. This is due to a lipophilic hydrocarbon tail that readily dissolves into lipid leaflets and a hydrophilic ammonium head which prevents penetration (Betz, *et al.*, 1992; Iwabuchi, *et al.*, 2014). FM dyes are non-fluorescent in an aqueous environment, but undergo a 100-fold increase in quantum yield (fluorescence) when they associate with lipid membranes (Hoopmann, *et al.*, 2012). Styryl dyes have been used extensively to label lipid membranes in a range of tissue samples and can be internalised by recycling SVs to study the different vesicle pools (Pyle, *et al.*, 2000; Gaffield and Betz, 2006; Iwabuchi, *et al.*, 2014).

Use of FM dyes in CNS nerve terminals demonstrate dye retention during exocytosis, which could be evidence for a fast mode of endocytosis, such as KR (Pyle, *et al.*, 2000; Aravanis, *et al.*, 2003; Richards, *et al.*, 2005). FM 2-10 dye is a good candidate to study KR as it has a faster membrane association time than any other Styryl dye, meaning SVs can be labelled rapidly, and one of the fastest dissociation times due to its shorter lipophilic tail (Wu, *et al.*, 2009; Iwabuchi, *et al.*, 2014). If exocytosis occurs but no FM 2-10 dye is released, this could be good evidence for KR, as the duration of the FP is too short to allow the dye to depart, but fast enough that all NT is released (Stevens and Williams, 2000).

2.4.2 Method

The FM dye release assay follows a method developed by Cousin and Robinson with modification by A. Ashton (Cousin and Robinson, 2000). Previous research has established that FM 2-10 dye can be loaded into all SVs within synaptosomes, and different modes of exocytosis release various amount of dye (Cousin and Robinson, 2000; Rudling, *et al.*, 2018). Therefore studying the amount of FM 2-10 dye released during drug treatments can outline the modes of release for the RRP when synaptosomes are stimulated with 4AP5C and the RP when stimulated with HK5C and ION5C. Figure 2.4 outlines the time course of the FM 2-10 dye assay.

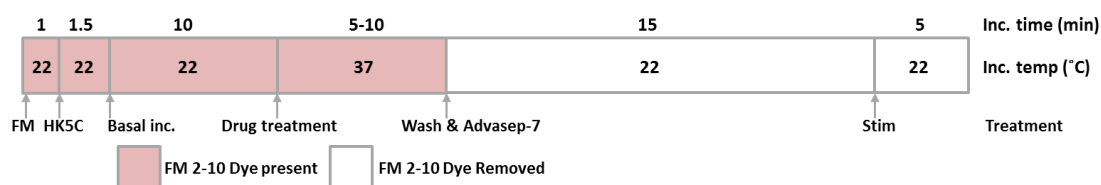


Figure 2.4: FM 2-10 Assay Time Course

The time course demonstrates each treatment the synaptosomes underwent during the assay and the duration and temperature of each treatment. For dual drug treatments a second incubation period of 5-10 min at 37°C follows the first drug treatment. Inc-incubation.

A 1 ml aliquot of synaptosomes, prepared as described, were centrifuged and re-suspended in 1 ml fresh L0. Added to the suspension was 100 µM of FM 2-10 dye and this was incubated for 60 sec at RT. This suspension was then stimulated with HK5C for 90 sec which allows the exocytosis of all releasable SVs, allowing the FM 2-10 dye to bind to the luminal domain of the vesicles. The stimulus was then removed by centrifugation at 9589 x g for 45 sec and the synaptosomes were re-suspended in 1 ml

fresh LO with 100 μ M of FM 2-10 dye, spun down at 9589 x g for 45 sec and re-suspended in FM dye incubated for 10 min at RT. This wash with FM 2-10 dye was to ensure the entire HK5C stimulus had been removed. This allowed all FM-dye labelled SVs to recycle so that they were fluorescently tagged.

Synaptosomes were incubated with the desired drug or equivalent volume of drug solvent (DMSO for control samples) and incubated at 37°C for 5-10 min. A 1 mM aliquot of ADVASEP-7 (final concentration) was then added to the suspension at RT, which removes the FM 2-10 dye from the synaptosomal plasma membrane without removing internalised dye. ADVASEP-7 has a higher affinity for FM dyes than the PM which allows it to remove all non-specifically bound dye from the outer leaflet of the PM, reducing background fluorescence (Kay, *et al.*, 1999). The seven negative charges on ADVASEP-7 make it membrane impermeable, preventing dye removal from the endocytosed SVs (Kay, 2007). Synaptosomes were washed twice (with LO), to help remove all excess FM dye, and re-suspended in 1.5 ml of fresh LO, along with the corresponding concentration of the drug or volume of DMSO (to prevent the reversibility of the drug action).

Aliquots of 160 μ L from this preparation were then added to wells 1-8 in one row of a Greiner 96 well microtiter plate (black with opaque, flat bottom). Fluorescence measurements were performed using Tecan GENIOS Pro infinite 200 plate reader (excitation wavelength: 465 nm; emission wavelength: 555 nm; gain: 40; read mode: top; and for 461 cycles). This number of cycles represents an assay time of \sim 2 min. Just prior to measuring fluorescence, each well was injected with either 40 μ l of the chosen stimulus (HK5C, ION5C or 4AP5C) or 40 μ l of LO for control. For each row 4

wells were stimulated and 4 wells underwent basal (LO) conditions. This procedure was repeated for all the eight rows of the plate, where each row could represent a different drug treatment. Upon subsequent experimental repeats, row order was switched to ensure the age of the synaptosomes did not introduce artefacts with each drug or control condition.

After the experiment, basal data was subtracted from stimulation data for each drug and control condition. This gave a true representation of the Ca^{2+} dependent SV release, expressed in terms of a decrease in fluorescence. All rows were normalised to a constant starting fluorescence. The absolute starting fluorescence measured enabled one to ensure that drug treatments did not perturb loading of FM 2-10 dye into SVs. Significance values were calculated using a two-way Student's t-test with a significance threshold of 0.05.

2.5 Intracellular Ca^{2+} Assay

2.5.1 Background/Rationale

In order to calculate the evoked change in the level of $[\text{Ca}^{2+}]_i$, the Fura-2-acetoxymethyl ester (Fura-2-AM) assay was utilised. Fura-2-AM is a Ca^{2+} insensitive, cell-permeable ester, which when taken up by a cell has its acetoxymethyl (AM) group cleaved off by esterases (Grynkiewicz, *et al.*, 1985; Gulaboski, *et al.*, 2008). This process converts the ester into a Ca^{2+} sensitive, negatively charged acid (Fura-2) which is no longer able to cross lipid membranes, including the PM. When bound to Ca^{2+} Fura-2 fluoresces maximally when excited at a wavelength of 340 nm, but when present in a Ca^{2+} free environment, Fura-2 fluoresces maximally when excited at 380 nm. The

emission wavelength of Fura-2 is constantly 535 nm, regardless of excitation wavelength. Thus the ratio between the recorded 340/380 fluorescence values is proportional to the concentration of cytosolic $[Ca^{2+}]_i$ (nM). This can be calculated using the Grynkiewicz equation (Grynkiewicz, *et al.*, 1985):

$$[Ca^{2+}]_i(nM) = k_d \times \beta \times \frac{(R - R_{min})}{(R_{max} - R)}$$

Where K_d is the constant of Ca^{2+} binding: 224 nM; β is the ratio of average fluorescence at 380 nm under Ca^{2+} free and Ca^{2+} bound conditions; R is the ratio of 340/380; R_{MIN} is 340/380 ratio in Ca^{2+} free environment; R_{MAX} is 340/380 ratio in a Ca^{2+} saturated environment.

2.5.2 Method

The Fura-2 assay follows a method developed by Brent and colleagues (Brent, *et al.*, 1997), with minor modifications (Baldwin, *et al.*, 2003). Briefly, An 8 ml aliquot of synaptosomes, prepared as described, was incubated with 5 μ M Fura-2-acetoxymethyl ester (Fura-2-AM) for 30 min at 37°C, whilst being constantly oxygenated. During this incubation the Fura-2-AM enters the synaptosomes where esterases cleave off the AM group, trapping the dye inside. After this incubation period, synaptosomes were centrifuged using a bench top centrifuge (9589 x g for 45 sec) and re-suspended in fresh, ice cold L0 buffer to remove any remaining extracellular Fura-2-AM. This wash was performed twice, after which synaptosomes were kept oxygenated at 4°C until required. Figure 2.5 outlines the experimental design of the Fura-2 assay.



Figure 2.5: Fura-2 Assay Time Course

The time course demonstrates each treatment the synaptosomes underwent during the course of the assay. Fura-2 was loaded into synaptosomes before being oxygenated on ice until required. Inc – Incubation.

For each test condition, a 1 ml aliquot of synaptosomes was stimulated with 0.25 ml of HK5C (final) for 90 sec. The stimulus was then removed by centrifugation at 9589 x g for 45 sec and the resulting pellet was re-suspended in 1 ml of L0, spun down at 9589 x g for 45 sec and re-suspended in 1 ml L0 and left to incubate for 10 min at RT. These last two steps, though not necessary for the Ca²⁺ assay directly, allow comparison with the Glu and FM 2-10 dye release assays.

After the incubation, synaptosomes had the relevant concentration of drug or an equivalent volume of DMSO (for control conditions) added and were incubated for 5 min at 37°C, or longer depending on the relevant drug treatment. Synaptosomes were then centrifuged at 9589 x g for 45 sec, re-suspended in 1 ml of L0 and centrifuged at 9589 x g for 45 sec again. The final pellet was re-suspended in 1.6 ml of oxygenated L0 which contained the same concentration of drug, or volume of DMSO as used above (to prevent reversibility of drug action). 120 µl aliquots of this final suspension were added to each of the 12 wells in a row of a Greiner 96 well microtiter plate (black, flat bottom). In addition, 40 µl of L0 was added to each well to make a total volume of 160 µl.

Fluorescence was measured from each well individually. The first well was measured for 40 cycles at the excitation wavelength of 340 nm and emission wavelength 535 nm, which is equivalent to ~10 sec, providing an average, baseline-fluorescence value. 40 µl of either a specific stimuli or L0 was injected into the well and the well was read for 160 cycles, ~40 sec, at the same excitation and emission wavelengths. For the second well, a similar procedure is used, with the only change being excitation at 390 nm (this was the nearest filter available to 380 nm, but it had a bandwidth which includes 380 nm).

Use of two excitation wavelengths allows calculation of the 340/390 ratio metric value for these wells. On each row, six wells were injected with 40 µl of a specific stimulus (due to the nature of ionomycin, it could not be injected and thus ionomycin was added to the relevant well just before it was injected with L0 containing 25 mM Ca²⁺ (final concentration 5 mM)), and six wells were injected with 40 µl of L0. The 340/390

ratio calculated for L0 treated wells were subtracted from the 340/390 ratio from stimulated wells in order to estimate the change in $[Ca^{2+}]_i$ evoked by the stimulation alone. Thus each row produces three 340/390 ratio sets for stimulation and control conditions of the drug treatment.

After all 12 wells in a row had been read, aliquots of 2.25 mM Ca^{2+} and 0.3% Triton X-100 (final concentrations) were added to each of the six wells that had been injected with a stimuli, making the final volume 240 μ l. For the six wells which were injected with L0, aliquots of 15 mM EGTA and 0.3% Triton X-100 (final concentrations) were added, making the final volume 240 μ l. After this treatment all 12 wells were measured for 40 cycles, first at the excitation wavelength 340 nm then at excitation wavelength 390 nm. These values were then used to calculate R_{MAX} and R_{MIN} from samples treated with 2.25 mM Ca^{2+} and 15 mM EGTA respectively. A spreadsheet was designed which utilised the Grynkiewicz equation to calculate the concentration of intracellular $[Ca^{2+}]_i$. Significance values were calculated using two way Student's t-test, with a significance threshold of 0.05.

2.6 Western Blotting

2.6.1 Introduction

In order to study the phosphorylated profile of Dyn-I, LDS-PAGE and Western blotting techniques were employed. In Western blotting protein samples are denatured by the addition of anionic detergents such as sodium dodecyl sulfate (SDS) or lithium dodecyl sulfate (LDS). The denatured proteins bind an amount of detergent relative to the molecular mass of the protein, which negatively charges the protein allowing for separation by electrophoresis. In this study LDS was used as the detergent as it required a lower temperature to fully denature the sample compared to SDS. NuPAGE Bis-Tris gels were also utilised due to their more neutral running pH and the preservation of protein integrity for study of post-translational modification (phosphorylation).

2.6.2 Sample Preparation

Synaptosomes prepared as described, were washed in L0, re-suspended in fresh L0 then stimulated for 90 sec with HK5C at RT. The stimulus was then removed by centrifugation as previously described and synaptosomes were re-suspended in fresh L0. Samples were treated with the relevant drug, dissolved in DMSO, or equivalent volume of DMSO for each test condition for 5-10 min at 37°C. Following this treatment and the relevant washes, the appropriate stimulus or basal condition (HK5C, ION5C, 4AP5C or L0) was applied for a range of specific time points (2, 15, 30, 120 sec) before the reaction was terminated by the addition of sample buffer, containing lithium dodecyl sulfate (LDS) and the reducing agent dithiothreitol (DTT) (1x final

concentration). Samples were then vortexed for 5-10 sec, heated at 70°C for 10 min and stored at -20°C until required.

An aliquot of each samples was taken in order to determine the protein concentration of each sample (not containing gel sample buffer), using the Bradford assay. The final protein concentration of samples for blotting was adjusted to 1.5 mg/ml. The Bradford assay measurements were made using the Tecan GENIOS Pro infinite 200 plate reader at an absorbance wavelength of 595 nm.

2.6.3 Electrophoresis and Transfer

Prior to gel electrophoresis, samples were heated for 10 min at 70°C, then into each of the 12 sample wells 45 µl of sample was loaded. Electrophoresis was performed using the NuPAGE gel system with midi protein gels of 4-12% Bis-Tris from Life Technologies and 1x (final concentration) NuPAGE MES running buffer. Western blotting transfer was performed (at 20 V for 7 min) on iBlot or iBlot 2 systems from Thermo Fisher, which transferred the proteins from the protein gel onto a polyvinylidene fluoride (PVDF) membrane. The membrane was then blocked with either 30 ml of blocking buffer (3% dried milk powder, 1% Tween-20 in tris buffered saline (TBS); pH 7.4) or 15 ml of StartingBlock buffer (proprietary protein formulation in Tris-buffered saline at pH 7.5 with 0.05% Tween-20), for 60 min. The blocking buffer was removed and the blots were washed for 10 sec with 1% Tween-20 in TBS.

2.6.4 Probing and Chemiluminescence

The PVDF membrane was then probed for specific phosphorylation sites on proteins of interest with specific primary antibodies suspended in 10-15 ml antibody buffer (1% dried milk powder, 1% Tween-20 in TBS; pH 7.4) for 60-90 min at RT. Antibody solution was then removed from the membrane which was then washed for 6 x 5 min with 25 ml wash buffer (0.5% Tween-20 in TBS; pH 7.4). Wash buffer was then removed and a HRP conjugated secondary antibody, raised against the primary, was then added. The secondary antibody was also suspended in 10-15 ml antibody buffer (1% dried milk powder, 1% Tween-20 in TBS; pH 7.4) and incubated for 60-90 min at RT.

Antibody buffer was again removed, followed by the same washing procedure. Wash buffer was then removed and PVDF membranes were incubated with 3 ml SuperSignal™ West Dura Extended Duration Substrate chemiluminescence agent for 300 sec. Visualisation of the bands was then carried out on the BioRad ChemiDoc XRS+ with Image lab software obtained from Bio-Rad. For re-probing of membranes, the membrane was stripped using 15 ml Restore™ PLUS Western Blot Stripping Buffer for 20 min at RT and re-blocked ready for further antibody probing.

2.6.5 Quantification of Bands from PVDF Membranes

The ChemiDoc XRS+ system in conjunction with Image Lab software detects the chemiluminescence of proteins bands on the membrane, where signal intensity is directly proportional to the amount of protein in the band. Signal intensity is also directly linked to duration of exposure, whereby a longer exposure time could introduce error in band quantification. In order to ensure measured band intensity was in the linear signal range of the sample and antibody, multiple exposures times were

taken for each Western blot and plotted against band intensity. A linear range of band intensity was plotted for each unique antibody used in this thesis (Appendix B), only exposure times which corresponded to a linear range of detection relative to the time point were used to determine sample intensity, minimising overexposure or underexposure of bands which could lead to erroneous and unreproducible results.

The semi-quantification analysis carried out in this thesis was designed to eliminate such variations, by quantifying bands relative to each other. Bands of interest were quantified using the volume calculation tool within the Image Lab software. This tool allows boxes to be drawn around bands of interest after which the software calculates average signal intensity within the box; where more intense bands would give a higher reading in arbitrary units. Furthermore localised errors are reduced as the software accounts for changes in background signal intensity between bands, reducing artefacts potentially introduced by uneven background signal (Bio-Rad). Once all the bands present on a blot were quantified in this manner, they were expressed as a percentage of the unstimulated control sample (in order to get the relative quantities of protein present in the given set of bands). The same blots were also probed with pan-Dyn-I to reveal the total amount of Dyn-I protein in the samples. This allowed the values to be normalised for the phosphorylated bands relative to the amount of protein, reducing errors associated with poor sample loading.

2.7 Bioenergetics Assay

2.7.1 Background/Rationale

Mitochondrial respiration can be measured via oxygen consumption rate (OCR) to assess viability and activity of synaptosomes across both basal and drug treatment conditions (Wallace, 2013; Agilent Technologies, 2019). It is important to ensure incubation periods with pharmacological agents do not perturb the biological integrity of synaptosomes. If this were the case, results observed in other assays may reflect the toxicity of the drug rather than the specific pharmacological treatment. The Xfp analyser from Seahorse (Agilent Technologies) utilises a mitochondrial stress (Mito-Stress) test to measure the OCR of mitochondria in the sample (Agilent Technologies, 2019). Specifically the Mito-Stress test looks at 6 aspects of mitochondrial function to determine the viability of the sample:

- (i) Basal respiration – is calculated over the first 0-15 min while synaptosomes acclimatise to the microtiter plate and represents the amount of oxygen synaptosomes require during baseline conditions.
- (ii) Adenosine triphosphate (ATP) production – represents the portion of basal respiration mitochondria use to produce ATP, meeting the energy demands of the synaptosomes. This is assessed over the next 20 min upon injection of oligomycin, the ATP synthase inhibitor (Agilent Technologies, 2019).
- (iii) Proton leakage – is also calculated over this time period and represents the remaining basal respiration not linked to ATP production.
- (iv) Maximal respiration – is measured over the next 20 min with the addition of the mitochondrial uncoupler FCCP. This treatment collapses the H^+

gradient across the mitochondrial membrane, stimulating the maximal oxygen consumption synaptosomal mitochondrial can achieve.

- (v) Spare respiratory capacity – represents the difference observed between basal and maximal respiration (see above), indicating how well the sample (synaptosomes) can respond to energetic demand. It is calculated at the same time as maximal respiration.
- (vi) Non-mitochondrial respiration – is measured over the final 20 min, where addition of rotenone and antimycin A stop all mitochondrial respiration. Any remaining respiration detected represents oxygen consumption driven by processes outside of mitochondria (Agilent Technologies, 2019).

Specifically designed 8 well (A-H) utility plates along with a sensory cartridge are used by the Xfp analyser. The sensory cartridge fits on the utility plate like a lid, placing 4 channels (known as drug ports; A-D) and a sensory probe into each of the 8 wells in the utility plate. The design of the well bottoms in the utility plate creates a micro-chamber when the sensory cartridge is lowered (by the Xfp analyser). While the micro-chamber is formed, measurements are taken by the probes in close proximity to the synaptosomes. The drug ports hold a small volume of suspended drug which is then added at specific time points during the assay; after which measurements from the wells are taken.

2.7.2 Method

The Mito-Stress assay utilises a kit and procedure developed and supplied by Agilent technologies for the Seahorse bioenergetics analyser. 24 hours before a bioenergetics assay was to take place, the wells of a fresh utility plate were pre-treated with 1:1500 of 50% solution polyethyleneamine (PEA) and incubated at RT. This solutions aids cells (in this case synaptosomes) adhering to the base of the well plate (Vancha, *et al.*, 2004). When performing the assay the PEA solution was removed from the utility plate, and the plate was allowed to dry.

A fresh sensory cartridge was hydrated overnight by filling each well of a fresh utility plate with 200 μ l of calibration buffer (PBS, pH 7.4, supplied by Seahorse Biosciences) and attaching the cartridge so the sensor probes are submerged. This assembly was then incubated at 37°C in a sealed container to prevent buffer evaporation. The utility plate has 4 moat chambers next to the wells which were filled with 400 μ l of calibration buffer, also aiding in evaporation prevention during incubation.

After hydrating for 24 hours, the sensory cartridge was primed with drugs which had been prepared in the basal buffer, and had been carefully adjusted to pH 7.4. 3 of the 4 drug ports (A-C) were loaded with; 25 μ l of 32 μ M oligomycin (port A), 25 μ l of 18 μ M FCCP (port B) and 25 μ l of 0.5 or 5 μ M antimycin A with 0.5 or 5 μ M rotenone (port C). In the Mito-Stress test these drugs work to modulate components of the mitochondrial electron transport chain (ETC). The primed cartridge was then inserted into the Seahorse XFp machine and equilibrated at 37°C for 12 min. This time also serves for the analyser to check the cartridge sensors are working optimally.

0.04 ml aliquot of synaptosomes, prepared as previously described suspended in LO, were centrifuged at 9589 x g for 45 sec. The resulting pellet was suspended in 1.2 ml bioenergetics buffer at 4°C with 4 mg/ml of bovine serum albumin added (adjusted to pH 7.4). 0.175 ml aliquots of the synaptosomal preparation were added to wells B-G of the Seahorse XFp utility plate. While background wells A and H were filled with bioenergetics buffer and BSA only. The plate was then centrifuged in an Eppendorf A-2 MTP swing out rotor at 2000 X g for 20 min at 4°C, to adhere the synaptosomes to the well bottoms, in a uniform layer.

The supernatant from each well was removed and wells B-D were treated with 0.2 ml of bioenergetics buffer with the relevant testing drug concentration at 37°C. Wells E-G were treated with 0.2 ml bioenergetics with an equivalent DMSO volume at 37°C. 0.2 ml of bioenergetics buffer was added to wells A and H, and these represent background conditions which would later be subtracted from the conditions data set. The utility plate was then incubated at 37°C for 5-10 min. After incubation the utility plate was washed two times following drug removal and was inserted into the Xfp analyser and the Mito-Stress test programme was then used to measure:

- (i) 3x3 min measurements of basal OCR and proton production.
- (ii) Injection of 25 µl of 32 µM oligomycin from port A to all wells followed by 3x3 min measurements of OCR and proton production (final concentration of 4 µM).
- (iii) Injection of 25 µl of 18 µM FCCP from port B to all wells followed by 3x3 min measurements of OCR and proton production (final concentration of 2 µM).

- (iv) Injection of 25 μl of 5 or 50 μM of rotenone/actimycin A from port C to all wells followed by 3x3 min measurements of OCR and proton production (final concentration of 0.5 or 5 μM).

Note, earlier experiments conducted in the Mito-Stress test were performed at 37 °C. However, a hardware update allowed the Mito-Stress test to be performed at RT, the temperature at which all release was measured, allowing later experiments to be performed at RT. The machine converts all the data from changes in oxygen consumption or proton production into plots and rates. This resulting data was then analysed with Wave 2 software from Seahorse Bioscience. A later upgrade to the software allowed the data to be directly inserted into Excel. The raw data for each well could then be analysed and such data was amalgamated with repeat experiments to obtain average values amenable to statistical analysis by two-way Student's t-test, with a significance threshold of 0.05.

Chapter 3:

The Role of PKA, Dyn-I and the Actin Cytoskeleton in Regulating the Mode of Exocytosis for SV Pools

3.1 The Effect of Protein Kinase A Regulation on Evoked Glu Release

Dyn-I is a substrate of PKC in both intact synaptosomes and *in vitro* studies (Robinson, 1991; Robinson, 1992). Robinson did not investigate the specific phosphorylation site of Dyn-I however, Powell and colleagues demonstrated that PKC phosphorylation of Dyn-I occurred at Ser-795 *in vitro*, and this prevented Dyn-I interacting with phospholipid membranes (Powell, *et al.*, 2000). Research by Bhuvu has demonstrated Dyn-I Ser-795 can also be phosphorylated *in vivo* (Bhuvu, 2015), however Singh has outlined this may not directly be through PKC action, suggesting another kinase may be responsible (Singh, 2017). Thus, the phosphorylated state of Dyn-I Ser-795 *in vivo* may regulate the ability of Dyn-I to modulate the mode of SV exocytosis.

It is possible that other kinases activated by secondary messengers could be responsible, either directly or indirectly, for phosphorylating Dyn-I Ser-795 during terminal depolarisation. PKA is a viable candidate as it is present in nerve terminals, it phosphorylates serine and threonine residues (Dyn-I is exclusively phosphorylated on serine sites (Graham, *et al.*, 2007)) and it becomes active when cAMP levels increase (Nguyen and Woo, 2003; Seino and Shibasaki, 2005; Park, *et al.*, 2014). PKA has a great number of substrates in the presynaptic terminal, which it can regulate in order to modulate aspects of SV recycling, including exocytosis (Neuberger, *et al.*, 2007; Park, *et al.*, 2014). Therefore, regulation of PKA activity is relevant to a large range of proteins and their pathways. One such PKA substrate is syntaphilin, which regulates the availability of Dyn-I in terminals (Boczan, *et al.*, 2004), and therefore syntaphilin's action by being modulated by PKA activity could subsequently affect the ability of Dyn-I to be phospho-regulated, which would then regulate the mode of exocytosis (Lou, 2018).

PKA activity can enhance presynaptic Ca^{2+} influx (Yoshihara, *et al.*, 2000), and has been implicated in long-term potentiation (LTP) affecting synaptic strength through phosphorylation and modulation of the secretory machinery (Leenders and Sheng, 2005). PKA has also been shown to enhance the release probability of NTs at many types of synapse (Menegon, *et al.*, 2006; Huang, *et al.*, 2010; Wang and Sieburth, 2013). Thus, PKA is a vital kinase to study in synaptic communication, and a viable candidate to modify the mode of exocytosis through the phospho-regulation of Dyn-I. This section investigates the role of PKA activation and inhibition upon regulating the mode of Glu release from the RRP and RP of SVs.

3.1.1 The Effect of PKA Inhibition on Evoked Glu Release

To inhibit PKA enzymatic activity, KT5720 – which blocks PKA action through competitive inhibition of the ATP binding site – was utilised (Kase, *et al.*, 1987). Synaptosomes treated with 2 μM of the PKA inhibitor KT5720 exhibited no significant change in evoked Glu release from the RRP when stimulated with 4AP5C (Figure 3.1 A; Glu release: CON 632.80 ± 129.63 (AU), KT5720 626.35 ± 118.14 ; $p > 0.05$ at 300 sec – bar chart), or from the RRP and RP, when stimulated with HK5C (Figure 3.1 B; CON 1286.40 ± 108.39 (AU), KT5720 1196.81 ± 129.23 ; $p > 0.05$ at 300 sec) or ION5C (Figure 3.1 C; CON 1307.59 ± 296.04 (AU), KT5720 1315.63 ± 390.72 ; $p > 0.05$ at 300 sec), compared to drug free controls. Previous research has already established that 5 mM $[\text{Ca}^{2+}]_e$ evokes maximal release of Glu from the RRP when used with 4AP, and maximal release of Glu from both the RRP and RP when used with HK and ION (Bhuva, 2015) (Figure 1.7). Figure 3.1 demonstrates maximal Glu release from the RRP and RP is still occurring when PKA is inhibited.

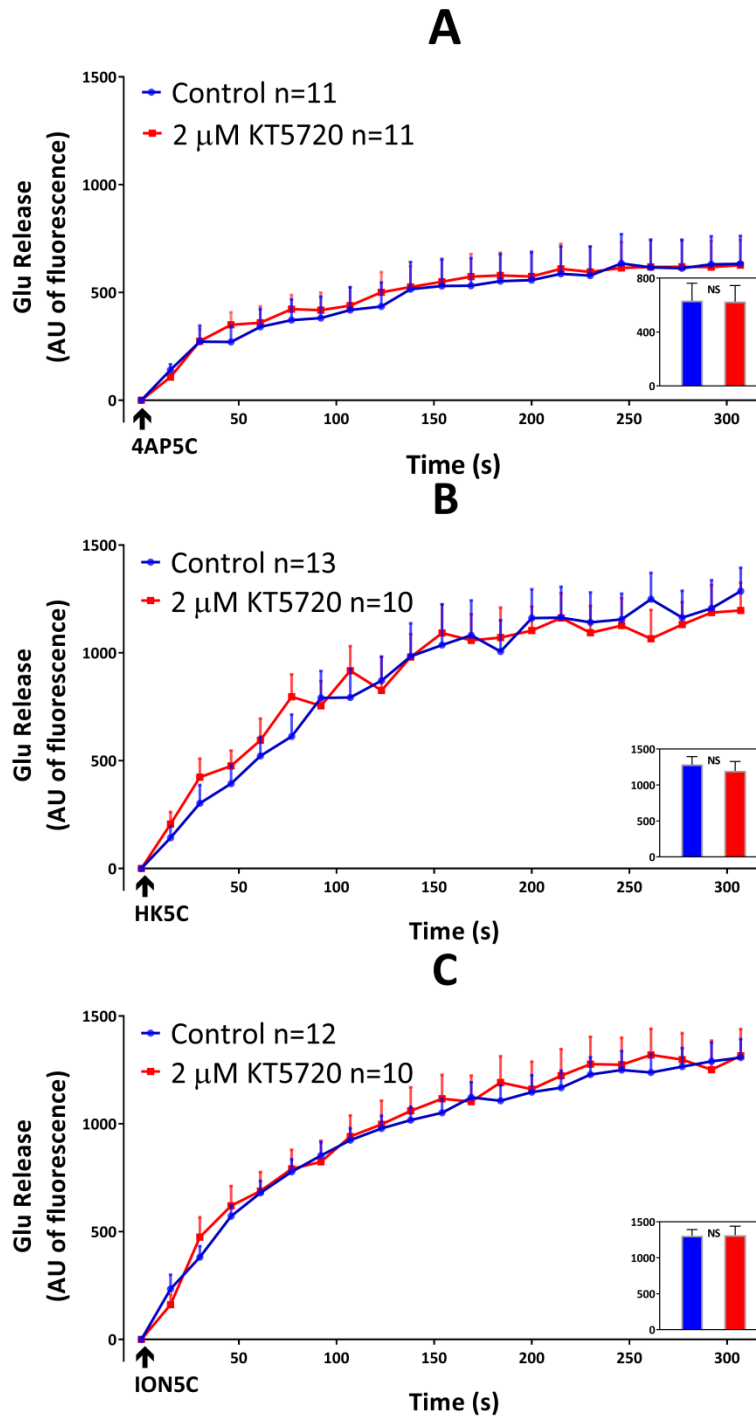


Figure 3.1: Effect of 2 μ M KT5720 vs Control upon Evoked Glu Release

2 μ M KT5720 had no effect upon 4AP5C (A) ($p=0.750$), HK5C (B) ($p=0.934$) or ION5C (C) ($p=0.840$) evoked Glu release, compared to controls. Inserts demonstrate final fluorescence at 300 sec. Values represented are the mean plus S.E.M. from 3 independent experiments. *NS*, not significant.

3.1.2 The Effect of PKA Activation on Evoked Glu Release

As the inhibition of PKA did not perturb evoked Glu release, the effect of PKA activation upon evoked Glu release was investigated. cBIMPS is a cAMP analogue which potently and specifically activates PKA by binding to the A and B sites on the regulatory subunits, exposing the catalytic sites of PKA allowing substrate binding for phosphorylation (Sandberg, *et al.*, 1991). Under basal conditions, PKA has a specific constitutive level of activity and treatment with 50 μ M cBIMPS works to increase this activity to maximal.

A treatment of 50 μ M cBIMPS had no significant effect upon the release of Glu from the RRP evoked by 4AP5C (Figure 3.2 A; Glu release: CON 735.36 \pm 141.62 (AU), cBIMPS 679.01 \pm 115.23, $p > 0.05$ at 300 sec – bar chart), or from the RRP and RP evoked by HK5C (Figure 3.2 B; Glu release: CON 1353.70 \pm 114.06 (AU), cBIMPS 1289.20 \pm 135.11, $p > 0.05$ at 300 sec) or ION5C (Figure 3.2 C; Glu release: CON 1317.38 \pm 124.46 (AU), cBIMPS 1353.73 \pm 126.46, $p > 0.5$ at 300 sec), compared to drug free controls.

Figures 3.1 and 3.2 demonstrate that modulation of PKA activity does not perturb the maximal release of Glu from either the RRP or RP of SVs. Therefore the modes of exocytosis for the SV pools, with KT5720 and cBIMPS treatments, could be investigated using evoked FM 2-10 dye release. As there is no significant change in Glu release, any measured difference in FM 2-10 dye release must be due to changes in the mode of exocytosis and not Glu release.

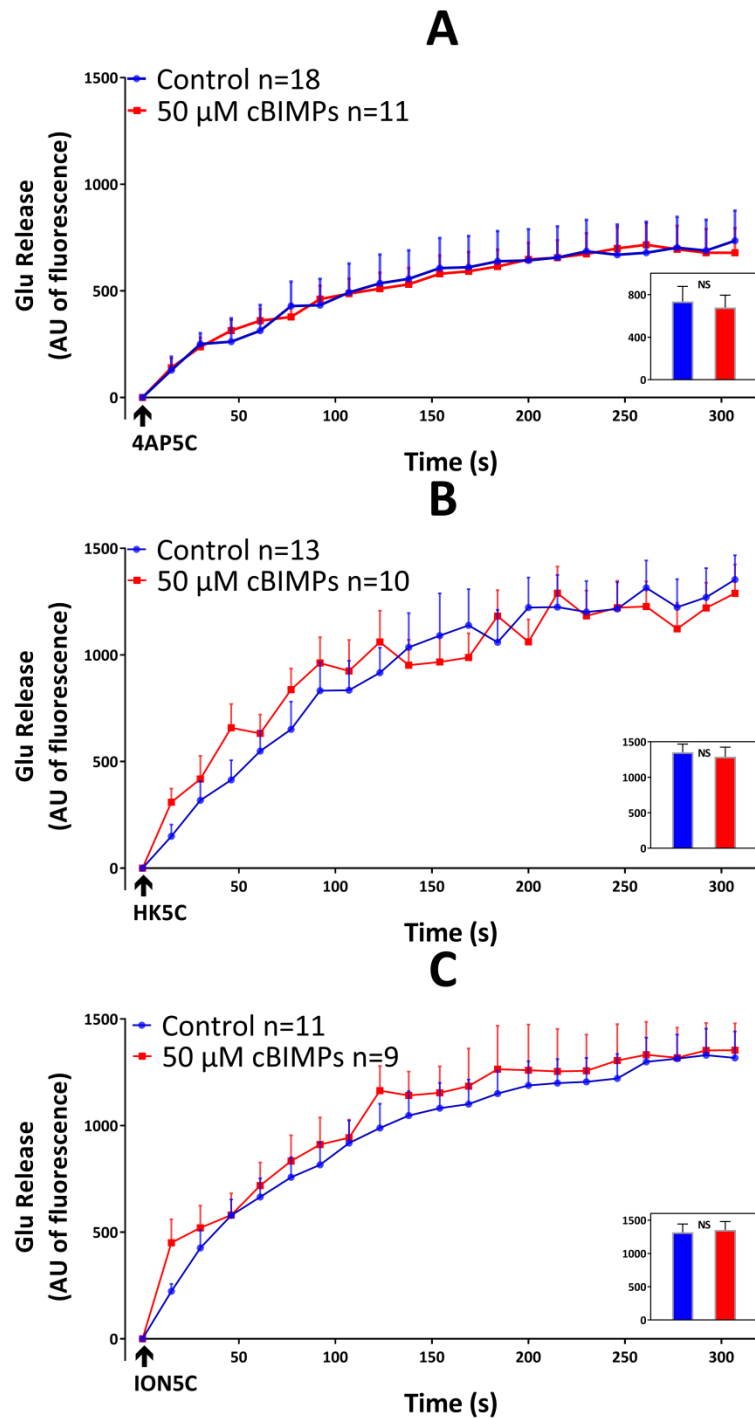


Figure 3.2: Effect of 50 μ M cBIMPS vs Control upon Evoked Glu Release

50 μ M cBIMPS had no effect upon 4AP5C (A) ($p=0.960$), HK5C (B) ($p=0.841$) or ION5C (C) ($p=0.548$) evoked Glu release, when compared to controls. Inserts demonstrate final fluorescence at 300 sec. Values represented are the mean plus S.E.M. from 3 independent experiments. *NS*, not significant.

3.2 The Effect of Dyn-I Inhibition on Evoked Glu Release

Within intact nerve terminals Dyn-I has been shown to reside either in the cytosol (whilst heavily phosphorylated), or upon membranes (whilst dephosphorylated) (Liu, *et al.*, 1994), and can cycle between the two during terminal activity (Damke, *et al.*, 1994; Wu, *et al.*, 2010), in response to phospho-regulation (Robinson, 1994). Dyn-I has been shown to preferentially bind to areas of high membrane curvature, such as clathrin-coated pits and FP necks, and disruption to proteins that generate such membrane curvature prevents Dyn-I recruitment (Sundborger and Hinshaw, 2014). This previous research supports the theory that some Dyn-I is recruited from the cytosol in order to mediate different forms of endocytosis during terminal depolarisation (Lin and Gilman, 1996; Ferguson and De Camilli, 2012), and a sub-pool of Dyn-I, which has been found enriched at the AZ (Wahl, *et al.*, 2013), could be recruited to mediate KR during SV exocytosis, as has been implicated (Fulop, *et al.*, 2008; Chan, *et al.*, 2010; Chang, *et al.*, 2017; Chanaday and Kavalali, 2017).

In order to establish if this was the case synaptosomes were treated with 30 μ M MITMAB, a surface-active small-molecule inhibitor which competitively binds the PH-domain of Dyn-I, preventing it binding to phospholipids present in the PM (Hill, *et al.*, 2004; Quan, *et al.*, 2007). Treatment with 30 μ M MITMAB has previously been shown to inhibit SV endocytosis in synaptosomes, indicating that it prevents cytosolic Dyn-I from being recruited to the PM during multiple forms of endocytosis (Quan, *et al.*, 2007). If cytosolic Dyn-I is being recruited to mediate KR during exocytosis, treatment with MITMAB may affect the mode of release.

To ensure that MITMAB causes changes to the mode of exocytosis without perturbing the release of Glu from either the RRP or RP, the Glu release assay was performed (Figure 3.3). Synaptosomes treated with 30 μ M MITMAB exhibited no significant change in Glu released from the RRP when stimulated with 4AP5C (Figure 3.3 A; Glu release: *CON* 506.92 \pm 141.94 (AU), *MITMAB* 573.03 \pm 70.75, $p > 0.5$ at 300 sec – bar chart) and from the RRP and RP when stimulated with either HK5C (Figure 3.3 B; Glu release: *CON* 689.28 \pm 142.51 (AU), *MITMAB* 588.67 \pm 76.09, $p > 0.5$ at 300 sec) or ION5C (Figure 3.3 C; Glu release: *CON* 914.56 \pm 141.76 (AU), *MITMAB* 890.76 \pm 192.29, $p > 0.5$ at 300 sec). Figure 3.3 demonstrates that inhibition of cytosolic Dyn-I recruitment does not affect Glu release from either the RRP or RP during stimulation. This corresponds well with previous data showing that Dyn-I inhibition with Dynasore does not perturb Glu release (see section 1.9.5; Figure 1.13).

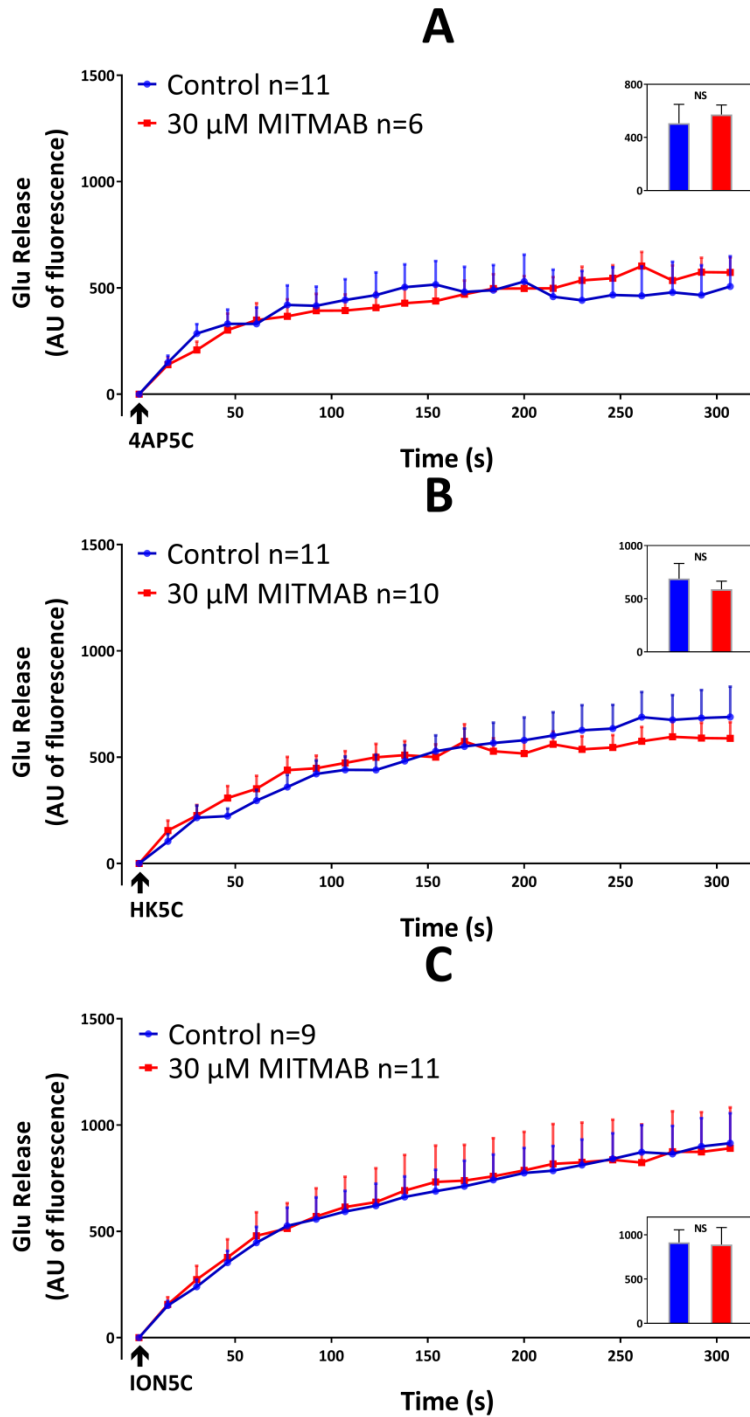


Figure 3.3: Effect of 30 μ M MITMAB vs Control upon Evoked Glu Release

30 μ M MITMAB had no effect upon 4AP5C (A) ($p=0.908$), HK5C (B) ($p=0.810$) or ION5C (C) ($p=0.896$) evoked Glu release, compared to controls. Inserts demonstrate final fluorescence at 300 sec. Values represented are the mean plus S.E.M. from 3 independent experiments. *NS*, not significant.

3.3 The Effect of Actin Disruption on Evoked Glu Release

The actin cytoskeleton is vital to maintain cellular structure, mediate neuronal growth and determine compartmentalisation of organelles (Coles and Bradke, 2015). Theoretically the actin cytoskeleton may be responsible for mediating the mobilisation of SVs during exocytosis, or regulating the mode of exocytosis (Malacombe, *et al.*, 2006; Nightingale, *et al.*, 2012), therefore disrupting the actin cytoskeleton could reveal key roles for actin during SV exocytosis. Latrunculin inhibits actin assembly by binding to actin-monomers, preventing conformational changes required for polymerisation (Morton, *et al.*, 2000). A 15 μ M latrunculin concentration was selected based on prior research (Ashton and Ushkaryov, 2005).

To determine what effect latrunculin had on the release of SVs, the Glu assay was performed. Synaptosomes treated with 15 μ M latrunculin released control levels of Glu from the RRP when stimulated with 4AP5C (Figure 3.4 A; Glu release: *CON* 506.92 ± 141.94 (AU), *latrunculin* 573.03 ± 70.75 , $p > 0.05$ at 300 sec – bar chart). However, a significant decrease in Glu release was seen when treated synaptosomes were stimulated with both HK5C (Figure 3.4 B; Glu release: *CON* 689.28 ± 142.51 (AU), *latrunculin* 362.51 ± 60.11 , $p < 0.05$ at 300 sec) and ION5C (Figure 3.4 C; Glu release: *CON* 914.56 ± 141.76 (AU), *latrunculin* 647.86 ± 78.32 , $p < 0.05$ at 300 sec), when compared to drug free controls. Therefore, Figure 3.4 demonstrates that actin disassembly with 15 μ M latrunculin specifically blocks release of SVs from the RP, as the RRP was able to release maximally with 4AP5C stimulation.

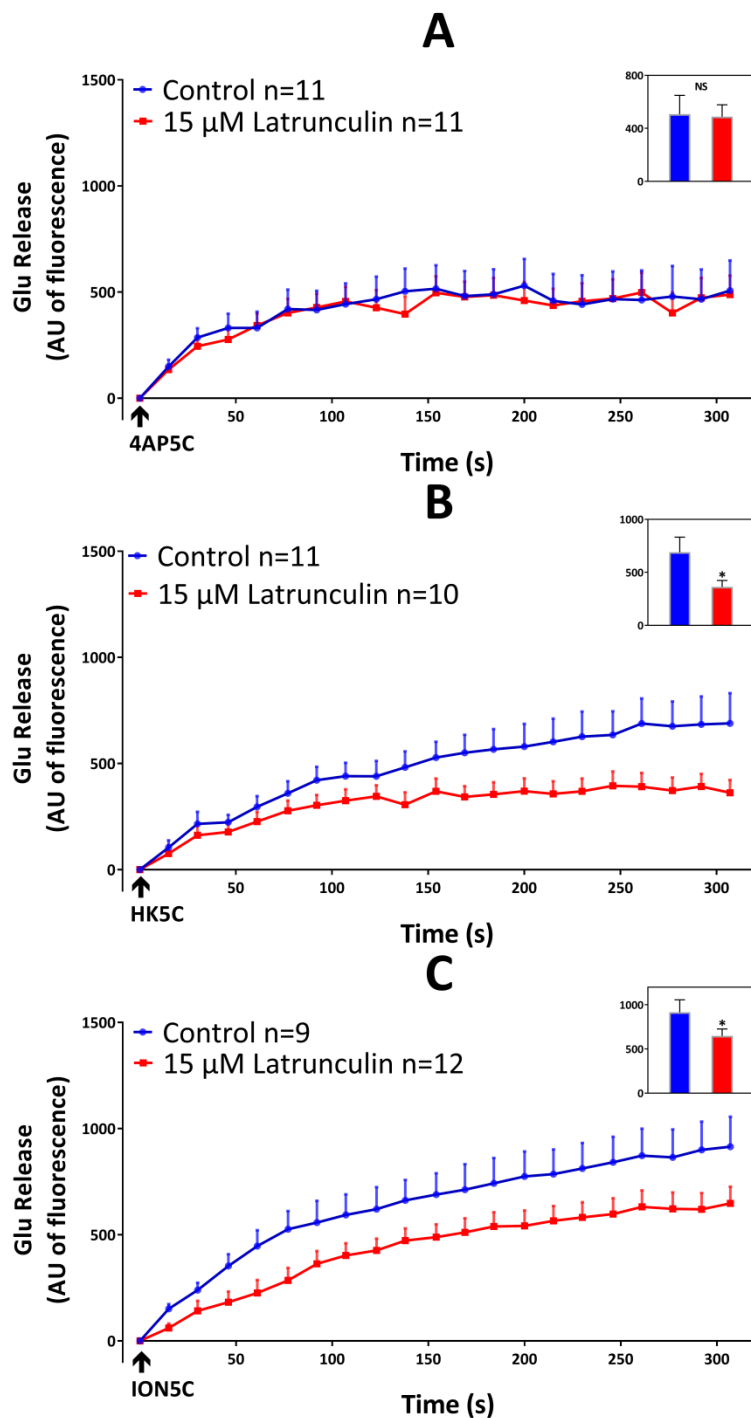


Figure 3.4: Effect of 15 μ M Latrunculin vs Control upon Evoked Glu Release

(A) 15 μ M latrunculin had no effect upon 4AP5C evoked Glu release ($p=0.641$), but did significantly reduce Glu release when stimulated with (B) HK5C ($p=0.002$), and (C) ION5C ($p=0.008$), when compared to controls. Inserts demonstrate final fluorescence at 300 sec. Values represented are the mean plus S.E.M. from 3 independent experiments. *, $p < 0.01$; NS, not significant.

3.4 The Effect of PKA Regulation on Evoked FM 2-10 Dye Release

3.4.1 The Effect of PKA Inhibition on Evoked FM 2-10 Dye Release

Synaptosomes treated with 2 μ M KT5720 released significantly more FM 2-10 dye compared to control conditions, when stimulated with 4AP5C (Figure 3.5 A; FM dye release: *CON* -552.76 ± 329.32 (AU), *KT5720* -1310.21 ± 190.07 , $p < 0.05$ at 120 sec – bar chart) or with ION5C (Figure 3.5 B; FM dye release: *CON* -2526.45 ± 174.74 (AU), *KT5720* -3155.33 ± 198.27 , $p < 0.05$ at 120 sec), whereas stimulation with HK5C produced no significant change in release (Figure 3.5 C; FM dye release: *CON* -1482.03 ± 224.80 (AU), *KT5720* -1342.78 ± 206.45 , $p > 0.05$ at 120 sec).

These results may indicate that SVs from the RRP, which all undergo KR in control conditions with ION5C (Figure 1.11 A), have switched to a FF mode of exocytosis during PKA inhibition when released with this stimuli; whereas with 4AP5C only some RRP SVs undergo KR in control conditions (Figure 1.11 A) but these are switched to FF by KT5720 treatment. Stimulation with HK5C did not switch the mode of exocytosis of any SVs in KT5720 treated terminals and so the RRP SVs were still undergoing KR and the RP SVs were still undergoing FF as seen in control conditions discussed in Section 1.9.4 (Figure 1.11 A).

These data are remarkably similar to previous data collected when Glu and FM 2-10 dye release was studied with the Dyn-I and Dyn-II inhibitor dynasore (Bhuva, 2015), a reversible, non-competitive GTPase activity inhibitor of Dyns (Macia, *et al.*, 2006). Synaptosomes treated with 160 μ M dynasore maximally released Glu from the RP and RRP when stimulated with HK5C (Figure 1.13 A) or ION5C (Figure 1.13 B), and from the RRP when stimulated with 4AP5C (Figure 1.13 C) (see section 1.9.5).

This demonstrates inhibition of Dyns does not perturb the vesicular release of Glu. Furthermore, there was no significant increase in FM 2-10 dye release observed with 160 μ M dynasore treatment when stimulated with HK5C (Figure 1.13 D). However a substantial increase in FM 2-10 dye release was observed when dynasore treated synaptosomes were stimulated with ION5C (Figure 1.13 E) and 4AP5C (Figure 1.13 F).

From these observations of the action of dynasore upon FM 2-10 dye release, it was determined that the ION5C and 4AP5C stimuli have a Dyn-I requirement for closing the FP during exocytosis (Bhuva, 2015, p. 84). These stimuli induce a lower Ca^{2+} concentration at the AZ, which activates local Dyn-I creating a Dyn-dependent KR mode of exocytosis, while HK5C induces a higher Ca^{2+} change at the AZ, inhibiting local Dyn-I creating a Dyn-independent mode of exocytosis. When the GTPase activity of Dyn-I is blocked with dynasore a mode switch to FF is observed, and when PKA is blocked with 2 μ M KT5720, the same mode switch to FF is seen with the same stimuli (4AP5C and ION5C). This could demonstrate that PKA activity plays a role in regulating properties of Dyn-I, allowing it to induce a KR mode of exocytosis at the FP and this could be through changes in the evoked $[Ca^{2+}]_i$ levels or changes in Dyn-I via protein partners or phosphorylation.

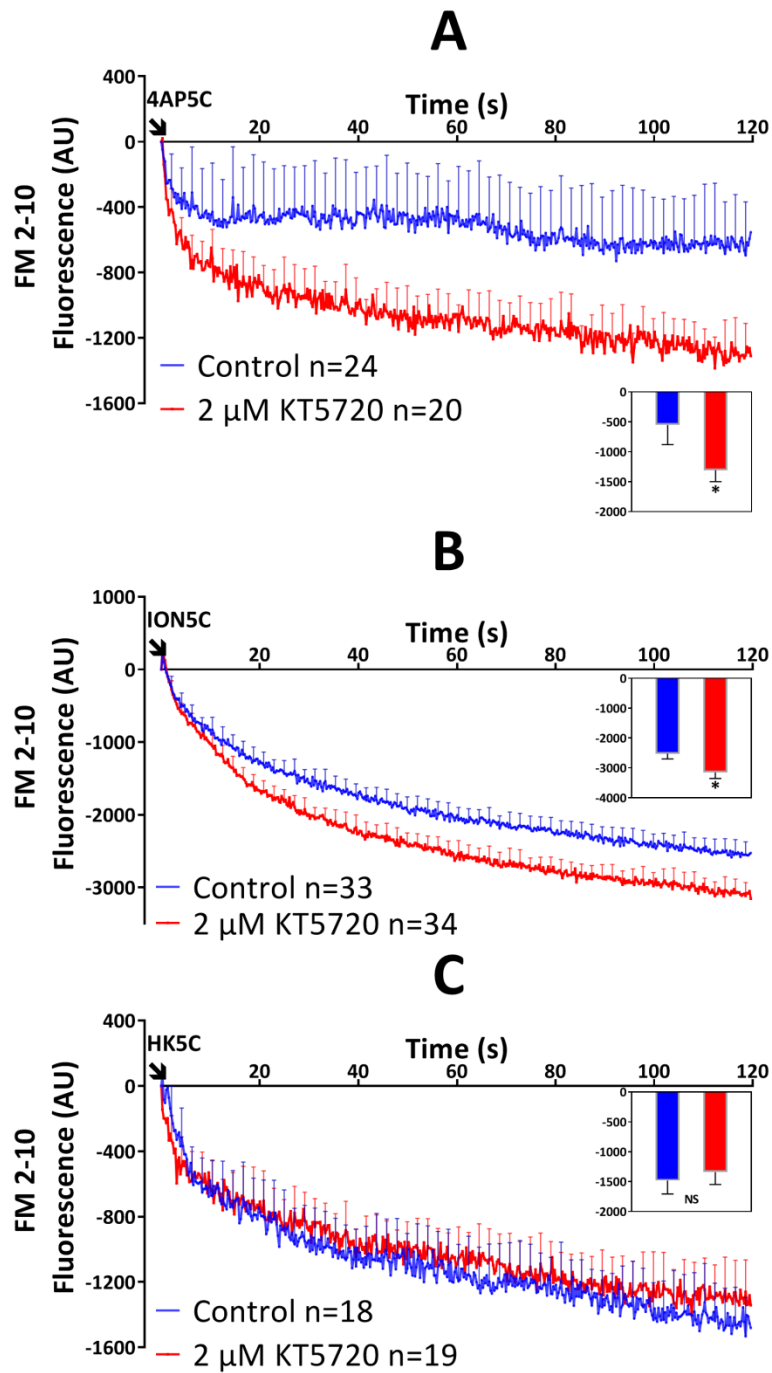


Figure 3.5: Effect of 2 μ M KT5720 vs Control upon Evoked FM 2-10 Dye Release

(A) 2 μ M KT5720 significantly increased 4AP5C ($p < 0.001$) and (B) ION5C ($p < 0.001$) evoked FM 2-10 dye release, but did not affect (C) HK5C evoked FM 2-10 dye release ($p = 0.753$) when compared to drug-free controls. Inserts demonstrate final fluorescence at 120 sec. Values represented are the mean plus S.E.M. from 4 (A, C) and 5 (B) independent experiments. *, $p < 0.001$; NS, not significant.

3.4.2 The Effect of PKA Activation on Evoked FM 2-10 Dye Release

Activation of PKA with 50 μ M cBIMPS made no significant change to the amount of FM 2-10 dye released, compared to controls, when synaptosomes were stimulated with 4AP5C (Figure 3.6 A; FM dye release: *CON* -1108.19 ± 196.61 (AU), *cBIMPS* -1172.19 ± 238.35 , $p > 0.05$ at 120 sec – bar chart). However a significant decrease in FM 2-10 dye release was seen when synaptosomes were stimulated with either HK5C (Figure 3.6 B; FM dye release: *CON* -1482.03 ± 208.56 (AU), *cBIMPS* -942.64 , $p < 0.05$ at 120 sec) or ION5C (Figure 3.6 C; FM dye release: *CON* -2639.23 ± 146.72 (AU), *cBIMPS* -2050.67 ± 184.50 , $p < 0.05$ at 120 sec), compared to non-drug treated controls. This indicates that some SVs in the RP, all of which normally undergo release by FF, have switched to a KR mode of exocytosis. It would appear that with 4AP5C, activation of PKA does not regulate the mode of exocytosis of the RRP, because SVs which normally undergo FF have not been switched (Figure 3.6 A). This highlights that PKA activation has a specific role in regulating the mode of the RP of SVs independently of the RRP.

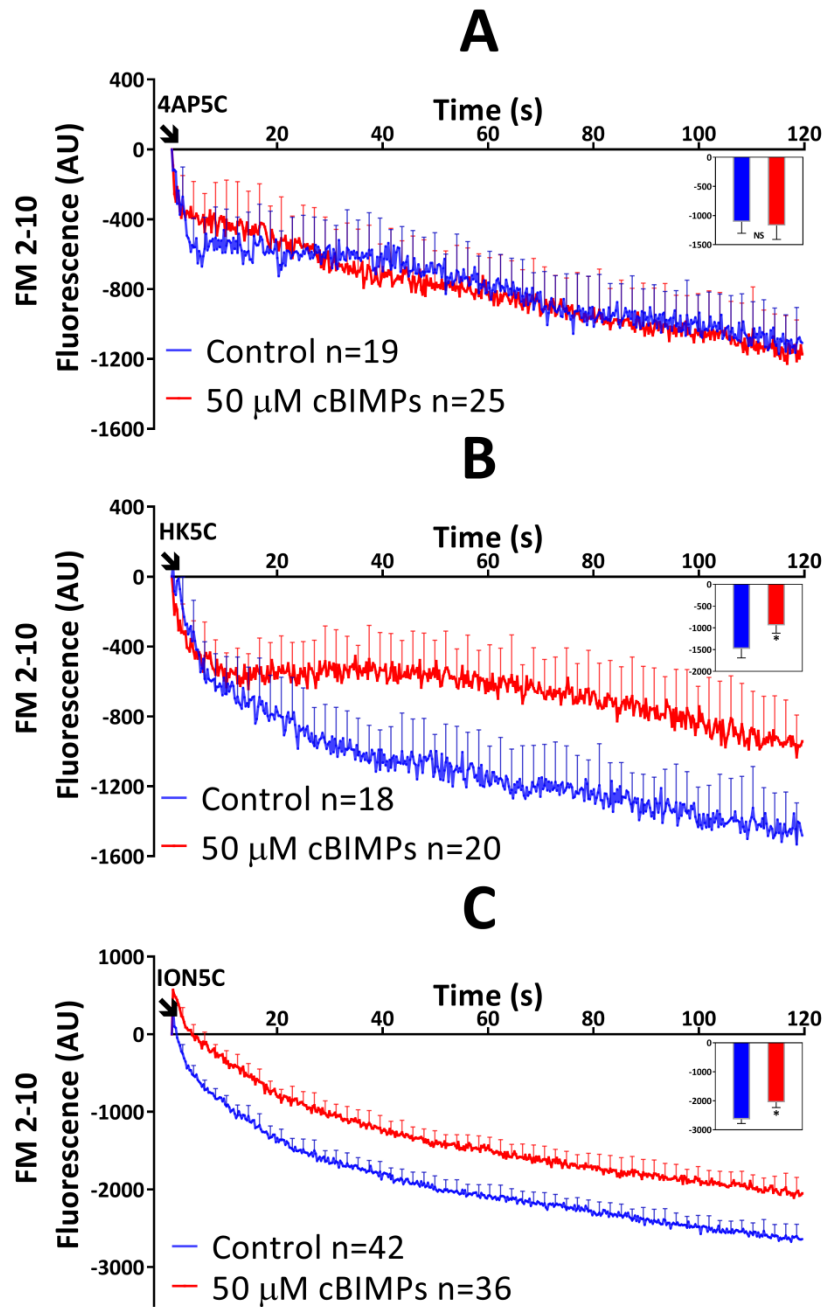


Figure 3.6: Effect of 50 μ M cBIMPS vs Control upon Evoked FM 2-10 Dye Release

(A) 50 μ M cBIMPS had no effect upon 4AP5C evoked FM 2-10 dye release ($p=0.302$), but significantly decreased dye release with (B) HK5C ($p<0.001$) and (C) ION5C ($p<0.001$) stimuli. Inserts demonstrate final fluorescence at 120 sec. Values represented are the mean plus S.E.M. from 3 (A, B) and 6 (C) independent experiments. *, $p < 0.001$; NS, not significant.

This phenotype is similar to previous research results when Glu and FM 2-10 dye release assays were performed in synaptosomes treated with the protein phosphatase 2B (PP2B) inhibitor cyclosporine A (Cys A). A treatment of 1 μ M Cys A did not perturb Glu release from the RP and RRP when stimulated with HK5C (Figure 1.16 A) or ION5C (Figure 1.16 B), or Glu release from the RRP when stimulated with 4AP5C (Figure 1.16 C) (Bhuva, 2015, p. 127). This is different from some studies which show Cys A treatment can increase Glu release (Gaydukov, *et al.*, 2013), but as discussed in section 1.9.5, this indicated maximal Glu release is being observed with this model system under these conditions already (i.e. with 5mM $[Ca^{2+}]_e$) (see Bhuva, 2015, p. 127).

A significant decrease in FM 2-10 dye release was seen when synaptosomes treated with 1 μ M Cys A were stimulated with HK5C (Figure 1.16 D) and ION5C (Figure 1.16 E), while no significant difference was observed when stimulated with 4AP5C (Figure 1.16 F), compared to controls. It is noteworthy that this data may indicate that the PKA substrate that regulates the mode of the RP may be the same substrate that Cys A acts on, PP2B. Moreover, there was no additivity of FM 2-10 dye release when both Cys A and cBIMPS were employed together (data not shown). Treatment with 1 μ M Cys A was accompanied by an increase in $[Ca^{2+}]_i$ levels for HK5C and ION5C stimuli (Figure 1.16 G and H respectively), which is distinct from the effect of cBIMPS (see later).

3.4.3 The Specificity of cBIMPS Action on Evoked FM 2-10 Dye Release

In order to ensure the effect of cBIMPS was specifically due to the activation of PKA, synaptosomes were pre-treated with 2 μ M KT5720 before treatment with 50 μ M cBIMPS. If the action of cBIMPS upon FM dye release were working through PKA, this pre-treatment with KT5720 would block or significantly reduce the number of SVs switching to a KR mode of exocytosis.

Release of FM 2-10 dye from synaptosomes treated with 2 μ M KT5720 and subsequently 50 μ M cBIMPS, was not significantly different to control synaptosomes when stimulated with HK5C (Figure 3.7 A; FM dye release: *CON* -1185.07 ± 208.56 (AU), *KT5720 plus cBIMPS* -1084.62 ± 223.10 , $p > 0.05$ at 120 sec – bar chart) or ION5C (Figure 3.7 B; FM dye release: *CON* -2511.80 (AU), *KT5720 plus cBIMPS* -2717.67 ± 274.45 , $p > 0.05$ at 120 sec). These data highlight the specificity of both cBIMPS and KT5720 for PKA, and reveal pool dependent mode switching for distinct stimuli.

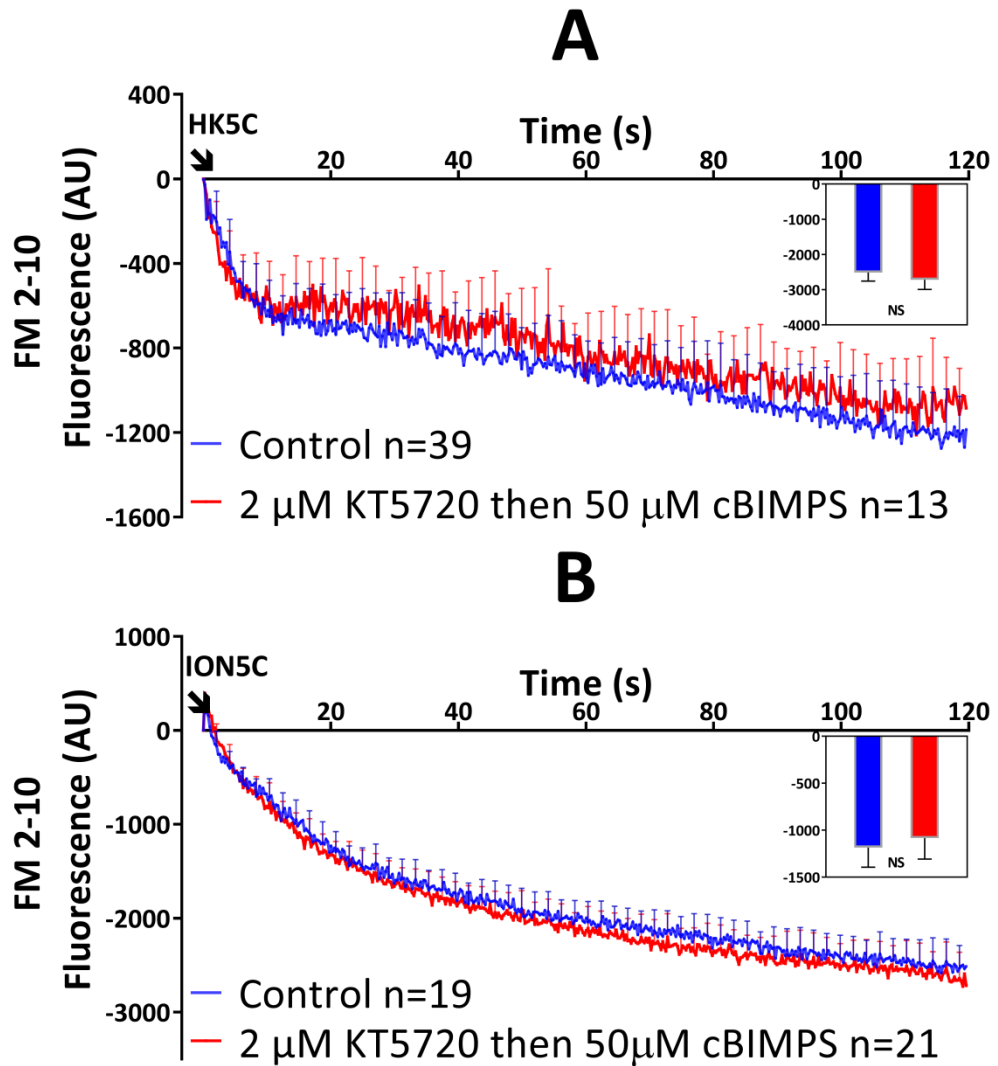


Figure 3.7: Effect of 2 μM KT5720 plus 50 μM cBIMPS Treatment upon Evoked FM 2-10

Dye Release

(A) 2 μM KT5720 plus 50 μM cBIMPS treatment did not perturb FM 2-10 dye release with HK5C ($p=0.461$) or (B) ION5C ($p=0.804$) stimuli. Inserts demonstrate final fluorescence at 120 sec. Values represented are the mean plus S.E.M. from 5 (A) and 3 (B) independent experiments respectively. *NS*, not significant.

3.5 The Effect of Dyn-I Inhibition on Evoked FM 2-10 Dye Release

Though blocking Dyn-I from binding to phospholipids with 30 μ M MITMAB did not perturb the release of Glu (Figure 3.3), it could have an impact upon the mode of exocytosis. Synaptosomes treated with 30 μ M MITMAB did not release significantly more FM 2-10 dye than control synaptosomes when stimulated with HK5C (Figure 3.8 A; FM dye release: *CON* -1743.47 ± 173.16 (AU), *MITMAB* -1601.59 ± 275.92 , $p > 0.05$ at 120 sec – bar chart) or ION5C (Figure 3.8 B; FM dye release: *CON* -1703.83 ± 228.11 (AU), *MITMAB* -1640.11 ± 350.30 , $p > 0.05$ at 120 sec). 30 μ M MITMAB was not tested with 4AP5C as this stimulus only evokes release of the RRP which is mediated by Dyn-I already membrane bound and enriched at the AZ (Wahl, *et al.*, 2013), revealing nothing related to any action of Dyn-I that could be recruited from the cytoplasm (Ferguson and De Camilli, 2012). Figure 3.8 demonstrates that the Dyn-I-dependent KR mode of exocytosis seen for the RRP when stimulated with ION5C is mediated by a sub-pool of Dyn-I which is already bound to the phospholipid membrane, or to SVs directly, and therefore is not able to be inhibited by MITMAB.

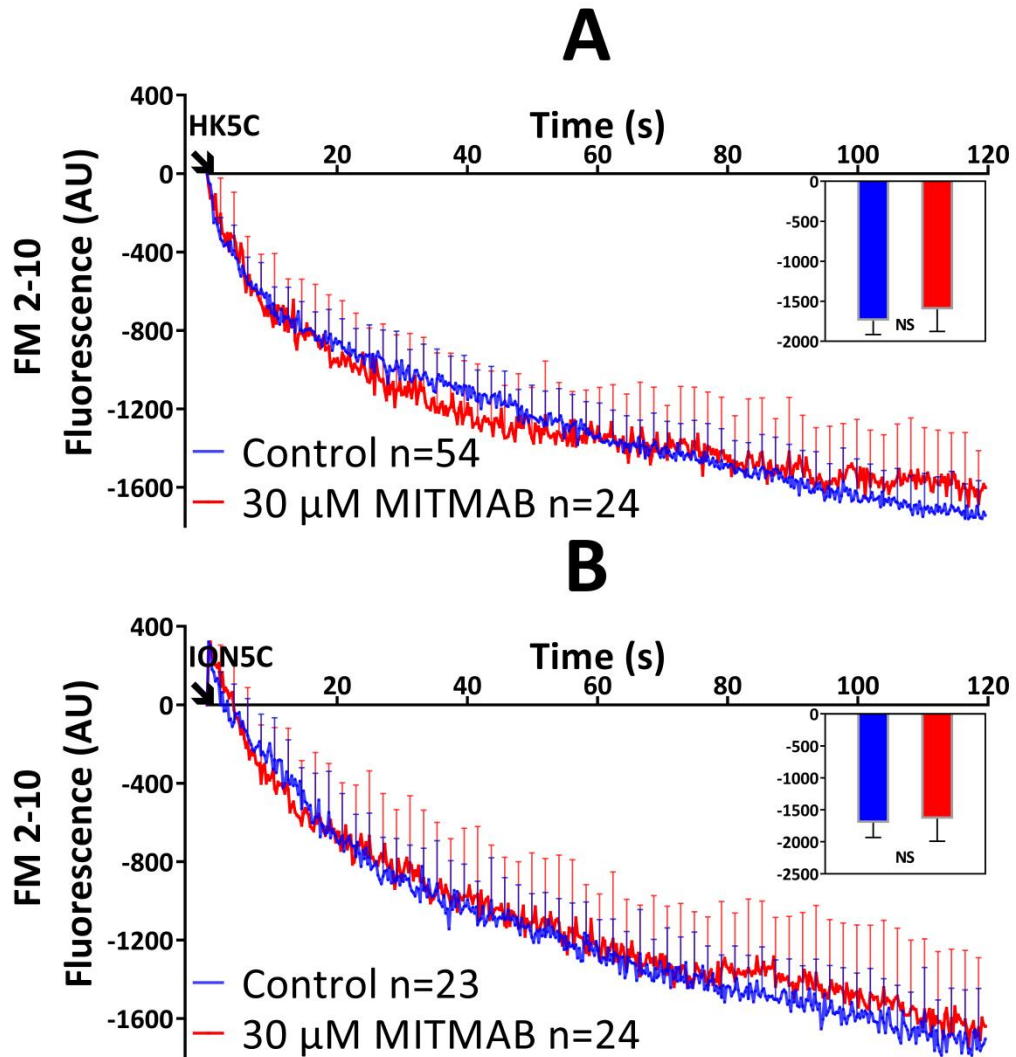


Figure 3.8: Effect of 30 μ M MITMAB vs Control upon Evoked FM 2-10 Dye Release

(A) 30 μ M MITMAB does not significantly affect HK5C evoked ($p=0.342$), (B) or ION5C evoked FM 2-10 dye release ($p=0.114$), when compared to controls. Inserts demonstrate final fluorescence at 120 sec. Values represented are the mean plus S.E.M. from 4 independent experiments. *NS*, not significant.

3.6 The Effect of Actin Disruption on Evoked FM 2-10 Dye Release

Actin may also have a role in regulation of the FP during exocytosis (Nightingale, *et al.*, 2012). Actin may work to either stabilise the releasing SVs in conjunction with Dyn-I during ION5C stimulation, or to work in tandem with NM-II (which actin does frequently in other cell types (Murrell, *et al.*, 2015)) to regulate the FP opening during HK5C stimulation, thus disruption of actin could also affect the mode of release.

No significant change in FM 2-10 dye release was observed from synaptosomes treated with 15 μ M latrunculin and stimulated with either HK5C (Figure 3.9 A; FM dye release: *CON* -1454.28 ± 291.33 (AU), *latrunculin* -1225.63 ± 237.68 , $p > 0.05$ at 120 sec – bar chart) or ION5C (Figure 3.9 B; FM dye release: *CON* -1703.83 ± 228.11 (AU), *latrunculin* -1624.01 ± 221.53 , $p > 0.05$ at 120 sec) when compared to drug free synaptosomes. However, this data is misleading as results in Figure 3.4 already established that Glu released from the RP had been blocked during 15 μ M latrunculin treatment. Therefore, a drop in the amount of FM 2-10 dye released would be expected if the RP was not releasing. One possibility is that the FM dye release is actually from the RP and that the reduction in Glu release is actually due to inhibition of the RRP by latrunculin. However, this is unlikely as the release of the RRP by 4AP5C is not perturbed by this drug and normally it is envisaged that the RP is released only after the RRP is released.

A more feasible explanation is that the FM 2-10 dye seen to be released is coming from the RRP SVs which have switched from a KR mode of exocytosis (which releases no FM 2-10 dye under control conditions) to a FF mode of release, due to the 15 μ M latrunculin treatment.

Thus the KR mode of RRP SVs does appear to have a requirement for intact actin microfilaments, regardless if there is a Dyn-I-dependency as with ION5C, or a NM-II-dependency as with HK5C. It is serendipitous that the FM 2-10 dye curve for RP SVs releasing by FF is similar to the FM 2-10 dye curve for the RRP SVs undergoing FF, but this is expected as in our studies the RRP and RP contain roughly similar numbers of SVs (see Chapter 1).

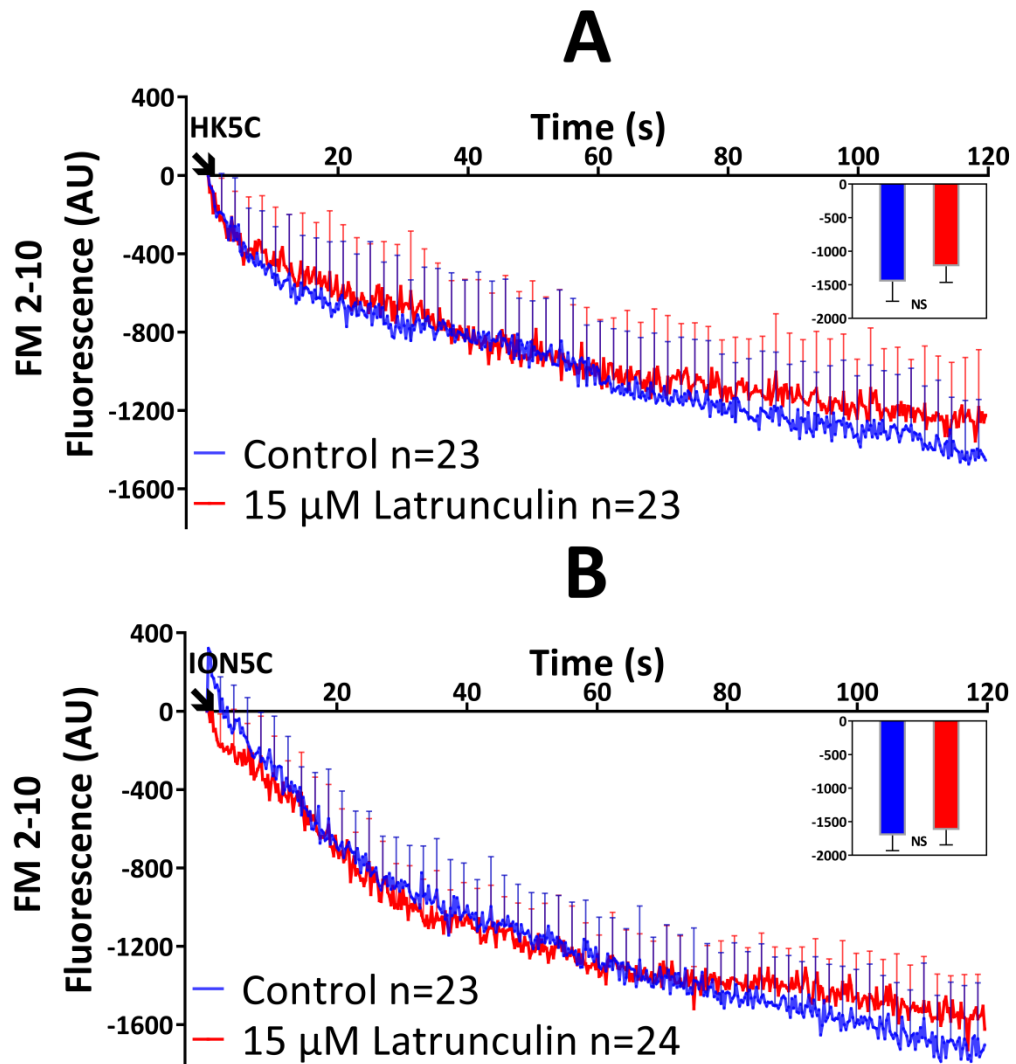


Figure 3.9: Effect of 15 μ M Latrunculin vs Control upon Evoked FM 2-10 Dye Release

(A) 15 μ M latrunculin had no significant effect upon FM 2-10 dye release evoked by either HK5C ($p=0.538$), (B) or ION5C ($p=0.684$), when compared to controls. Inserts demonstrate final fluorescence at 120 sec. Values represented are the mean plus S.E.M. from 4 independent experiments. *NS*, not significant.

In order to determine if treatment with latrunculin was blocking release of all RP SVs, the sum of FM 2-10 dye release data from control synaptosomes and dye release from latrunculin treated synaptosomes was determined and plotted (Figure 3.10). When stimulated with HK5C and ION5C, without drug treatment, SVs in the RRP were releasing via KR and SVs in the RP via FF (see Section 1.9.4) and this is demonstrated by the Control in Figure 3.10 A for HK5C. However latrunculin treatment is suggested to release the RRP only by FF (Figure 3.9), thus an addition of control and latrunculin treatments should present a release curve identical to a condition where all SVs are undergoing FF, e.g. treatment with 0.8 μ M OA. Such OA treatment has been well established to switch the RRP to FF (Figure 1.11; Ashton, *et al.*, 2011), so that all SVs in the terminal are now releasing via FF as exemplified herein for HK5C stimulation (Figure 3.10 A; FM dye release: CON -1412.61 \pm 152.19 (AU), OA -2343.39 \pm 255.28, $p < 0.05$ at 120 sec – bar chart).

Assuming that the FM 2-10 dye released during control treatment (Figure 3.10 A) represents the RP of SVs only (as they undergo FF while the RRP undergoes KR, releasing no dye), then an addition of this data with 15 μ M latrunculin release data (which only releases the RRP by FF) should give a more pronounced FM 2-10 dye release when compared to control conditions, as observed (Figure 3.10 B; FM dye release: CON -14554.28 \pm 377.72 (AU), CON release plus release in presence of latrunculin -2679.91 \pm 395.03, $p < 0.05$ at 120 sec). If this treatment (control + latrunculin) represents all RRP and RP SVs now undergoing FF, it should be comparable (not significantly different) to FM 2-10 dye release seen with 0.8 μ M OA (Figure 3.10 C; FM dye release: OA -2343.39 \pm 255.28 (AU), CON release plus release in presence of latrunculin -2679.91 \pm 395.03, $p > 0.05$ at 120 sec). These data suggest that treatment

with 15 μ M latrunculin only releases the RRP of SVs, as any RP SVs releasing would enhance the release of FM 2-10 dye beyond that observed here.

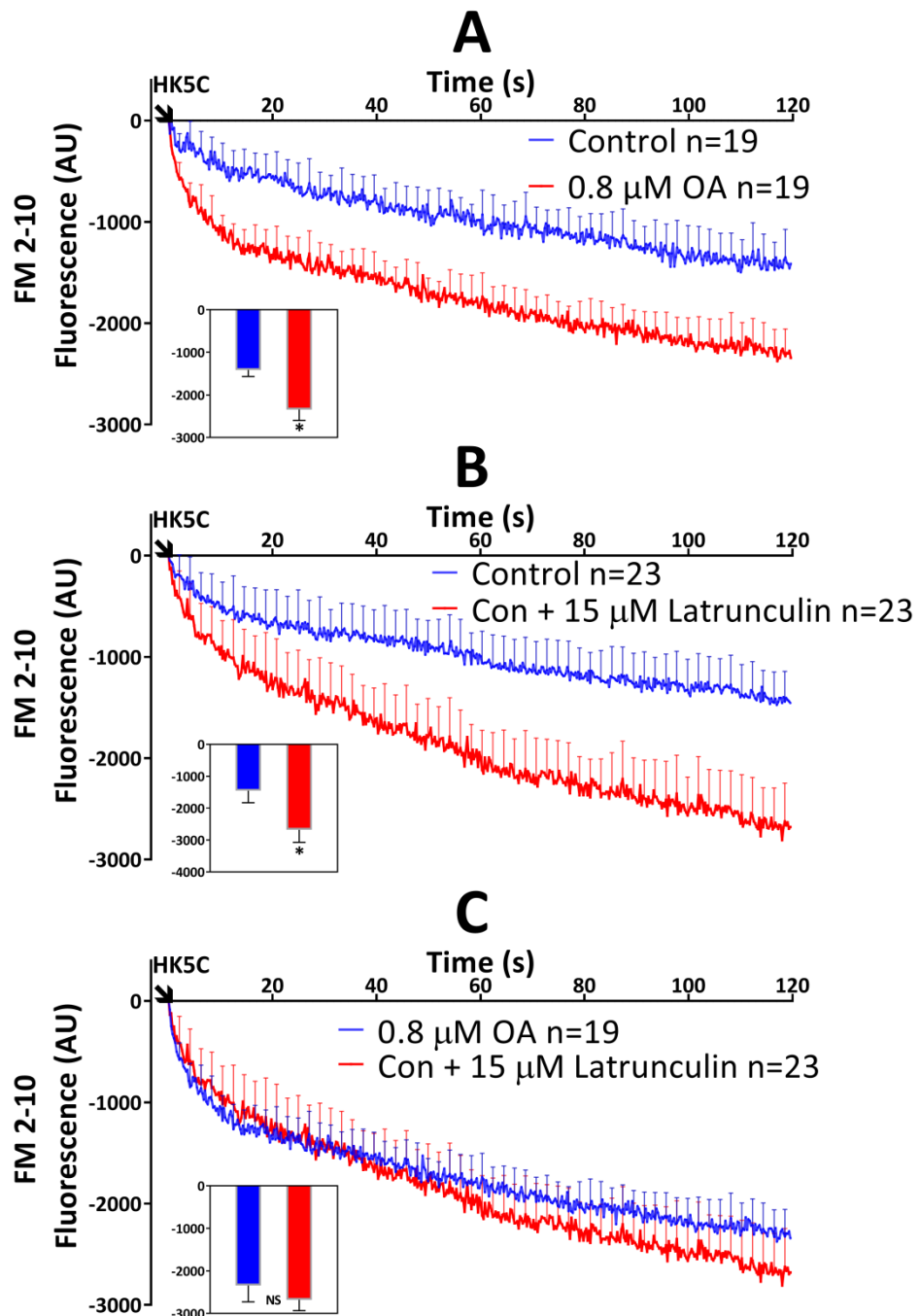


Figure 3.10: Comparison of Latrunculin plus Control upon Evoked FM 2-10 Dye Release

(A) 0.8 μ M OA significantly increased FM 2-10 dye release compared to controls ($p < 0.001$), as did Control plus 15 μ M Latrunculin (B) ($p < 0.001$). (C) There was no significant difference in FM 2-10 dye release when comparing 0.8 μ M OA and Control plus 15 μ M latrunculin ($p = 0.456$). Inserts demonstrate final fluorescence at 120 sec. Values represented are the mean plus S.E.M. from 3 independent experiments.

*, $p < 0.001$; NS, not significant.

3.7 Intracellular Ca^{2+} Levels

High extracellular Ca^{2+} levels have been shown to switch vesicles to a KR mode of exocytosis in chromaffin cells (Alés, *et al.*, 1999), and Richards has demonstrated that changes to $[\text{Ca}^{2+}]_i$ levels can regulate the mode of exocytosis in neurons (Richards, 2010); furthermore Ashton has recently demonstrated that large increases in $[\text{Ca}^{2+}]_i$ can switch some RP SVs to KR (Section 1.9.4). Any perceived changes in mode of exocytosis may then be the result of drug induced changes to $[\text{Ca}^{2+}]_i$ levels upon pools of SVs. Therefore, PKA inhibition with KT5720 and stimulation with 4AP5C and ION5C may be switching the mode of RRP SVs to FF by lowering the level of $[\text{Ca}^{2+}]_i$, whilst PKA activation with cBIMPS and stimulation with HK5C or ION5C may be switching RP SVs to a KR mode of exocytosis through the increase of $[\text{Ca}^{2+}]_i$ levels.

3.7.1 The Effect of PKA Inhibition on Evoked Changes in $[\text{Ca}^{2+}]_i$

Treatment of synaptosomes with 2 μM KT5720 had no significant effect upon $[\text{Ca}^{2+}]_i$ levels evoked by 4AP5C (Figure 3.11 A; $[\text{Ca}^{2+}]_i$: CON 295.82 \pm 23.02 (nM), KT5720 337.38 \pm 28.22, $p > 0.05$, final time point), HK5C (Figure 3.11 B; $[\text{Ca}^{2+}]_i$: CON 369.21 \pm 26.59 (nM), KT5720 402.43 \pm 24.22, $p > 0.05$, final time point) or ION5C (Figure 3.11 C; $[\text{Ca}^{2+}]_i$: CON 1711.59 \pm 147.26 (nM), KT5720 1720.81 \pm 119.86, $p > 0.05$, final time point) compared to non-drug treated controls. This suggests that inhibition of PKA regulates the mode of RRP SVs for 4AP5C and ION5C independently of drug induced changes in the level of $[\text{Ca}^{2+}]_i$.

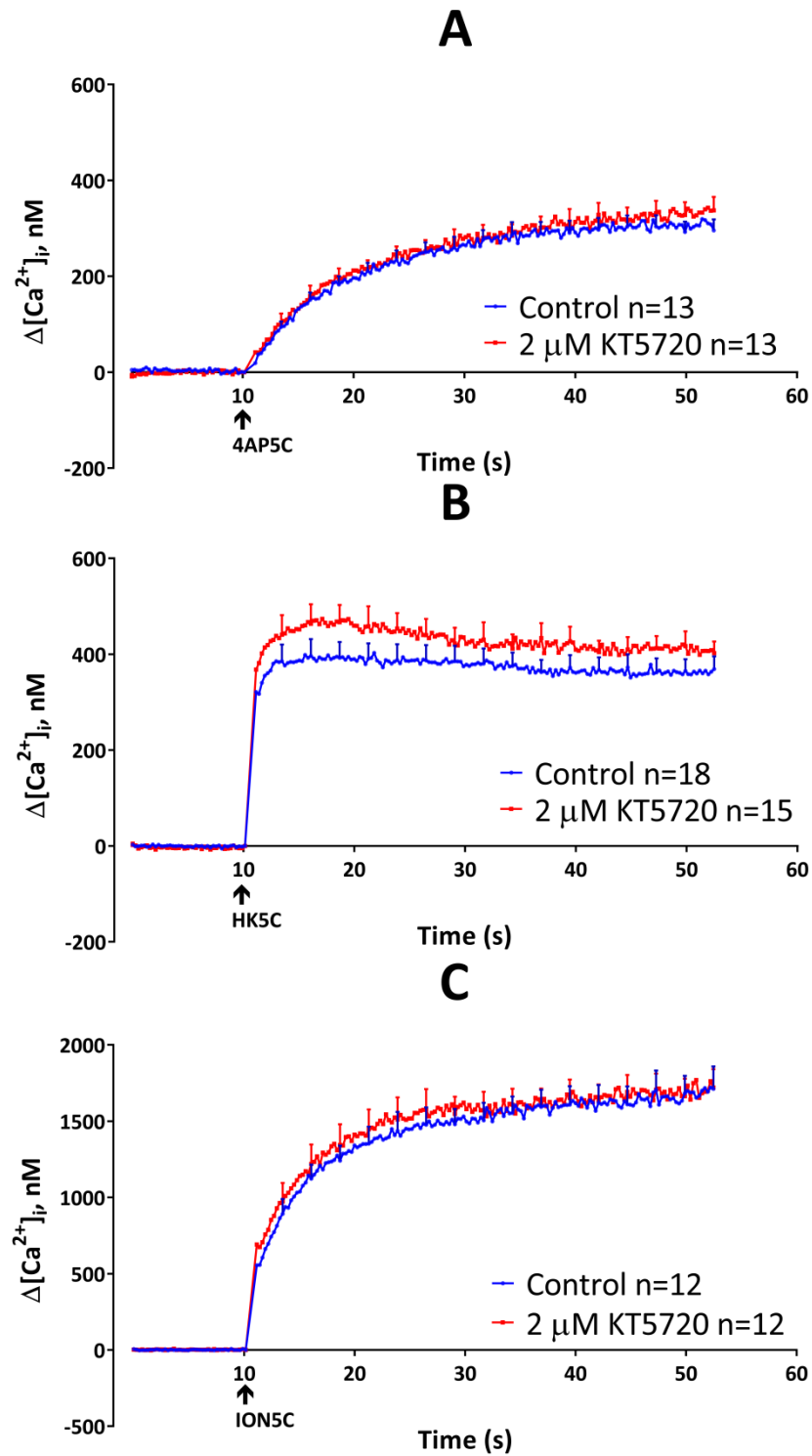


Figure 3.11: Effect of 2 μM KT5720 vs Control upon Evoked $[\text{Ca}^{2+}]_i$ Levels

(A) 2 μM KT5720 did not significantly affect intracellular $[\text{Ca}^{2+}]_i$ levels when stimulated with 4AP5C ($p=0.397$), (B) HK5C ($p=0.425$) or (C) ION5C ($p=0.455$), compared with controls. Values represented are the mean plus S.E.M. from 3 independent experiments.

3.7.2 The Effect of PKA Activation on Evoked Changes in $[Ca^{2+}]_i$

Previous research with Cys A has suggested that an increase in $[Ca^{2+}]_i$ can switch RP SVs to a KR mode of release when stimulated with HK5C (compare Figure 1.16 D and G) or ION5C (compare Figure 1.16 E and H) (Section 1.9.4). Thus, it was possible that a treatment with 50 μ M cBIMPS could also cause an increase in $[Ca^{2+}]_i$ levels when stimulated with HK5C and ION5C, and this may explain why cBIMPS induced more RP SVs to undergo a KR mode of exocytosis.

Treatment with 50 μ M cBIMPS had no significant effect upon $[Ca^{2+}]_i$ levels evoked by 4AP5C (Figure 3.12 A; $[Ca^{2+}]_i$: CON 285.13 ± 37.11 (nM), cBIMPS 283.76 ± 31.38 , $p > 0.05$, final time point) , HK5C (Figure 3.12 B; $[Ca^{2+}]_i$: CON 373.05 ± 25.88 (nM), cBIMPS 403.88 ± 21.76 , $p > 0.05$, final time point) or ION5C (Figure 3.12 C; $[Ca^{2+}]_i$: CON 1711.58 ± 147.26 (nM), cBIMPS 1780.44 ± 101.42 , $p > 0.05$, final time point) stimulation. Activation of PKA therefore, may be acting to switch the mode of RP SVs to KR when stimulated with HK5C or ION5C (Figure 3.6 B and C) without drug induced changes in evoked $[Ca^{2+}]_i$ levels (Figure 3.12). Figures 3.11 and 3.12 show that PKA can switch the mode of exocytosis of distinct SV pools (Figure 3.5 and Figure 3.6) independently of changes to evoked $[Ca^{2+}]_i$ levels, which has previously been shown to affect the mode of release (Chapter 1.9.4; Figure 1.16).

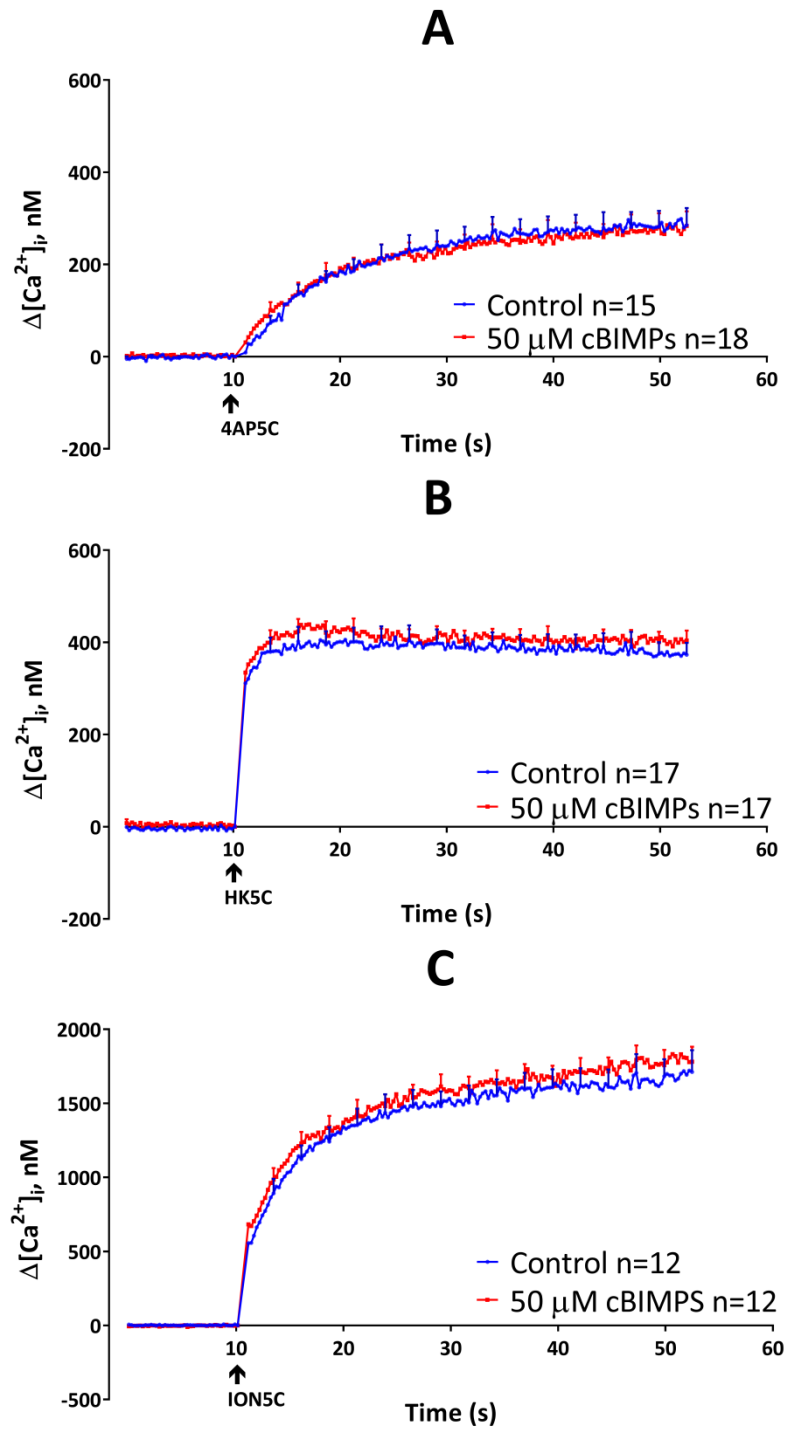


Figure 3.12: Effect of 50 μM cBIMPS vs Control upon Evoked $[\text{Ca}^{2+}]_i$ Levels

(A) 50 μM cBIMPS did not significantly affect $[\text{Ca}^{2+}]_i$ levels evoked by 4AP5C ($p=0.759$)
 (B) HK5C ($p=0.223$) or (C) ION5C ($p=0.301$) stimuli, compared to controls. Values represented are the mean plus S.E.M. from 3 independent experiments.

3.8 Nerve Terminal Bioenergetics

As discussed previously (Chapter 2.7), perceived changes to the mode of release during FM 2-10 dye assays with drug treatments could be the result of respiratory stress in the synaptosomes due to drug treatments perturbing the bioenergetic integrity of the synaptosomes. The results from drug treatments could be due to a decrease in available energy (ATP) stores, or mitochondrial function and not due to a direct effect on Glu release, or on the mode of exocytosis.

In order to account for this, drug treated synaptosomes were subjected to the bioenergetics Mito-Stress test to determine metabolic viability. Drug treatments were investigated without stimulation treatment as the specific action of the drug on their targets are independent of any action due to stimulation (e.g. KT5720 inhibits PKA independent of stimulation action; cBIMPS maximally activates PKA independent of stimulation action, etc.). The Mito-Stress test has a ~90 min duration, therefore treatment with stimuli present would mean synaptosomes are chronically stimulated for a timescale much longer than the maximal 5 min utilised in all assays of this thesis, such a treatment would not correlate with the normal release measurement. Prolonged stimulation might reveal a long-term effect of depolarisation, but this would be done without drug treatment and this cannot be achieved with ionomycin as 20 min treatment has been shown to perturb bioenergetics (Sanchez-Prieto, *et al.*, 1987).

3.8.1 The Effect of PKA Inhibition on Nerve Terminal Bioenergetics

There was no significant difference in the oxygen consumption rate (OCR) of synaptosomes when treated with 2 μ M KT5720, compared to non-drug treated control synaptosomes (Figure 3.13; $p>0.05$). Figure 3.14 outlines the effect of 2 μ M KT5720 upon the 6 aspects of mitochondrial function measured during a Mito-Stress test, as discussed in section 2.7. The values represented in the bar graphs are the average values measured over three time points for each section of the Mito-Stress test; basal (0-15 min), oligomycin treatment (20-35 min), FCCP treatment (40-55 min) and rotenone with antimycin A treatment (60-75 min) (Section 2.7.1). A significant increase in basal mitochondrial respiration over the first 15 min was observed (Figure 3.14 A; $p<0.05$ at 0-15 min), however this change was minimal and had no effect on the other parameters measured.

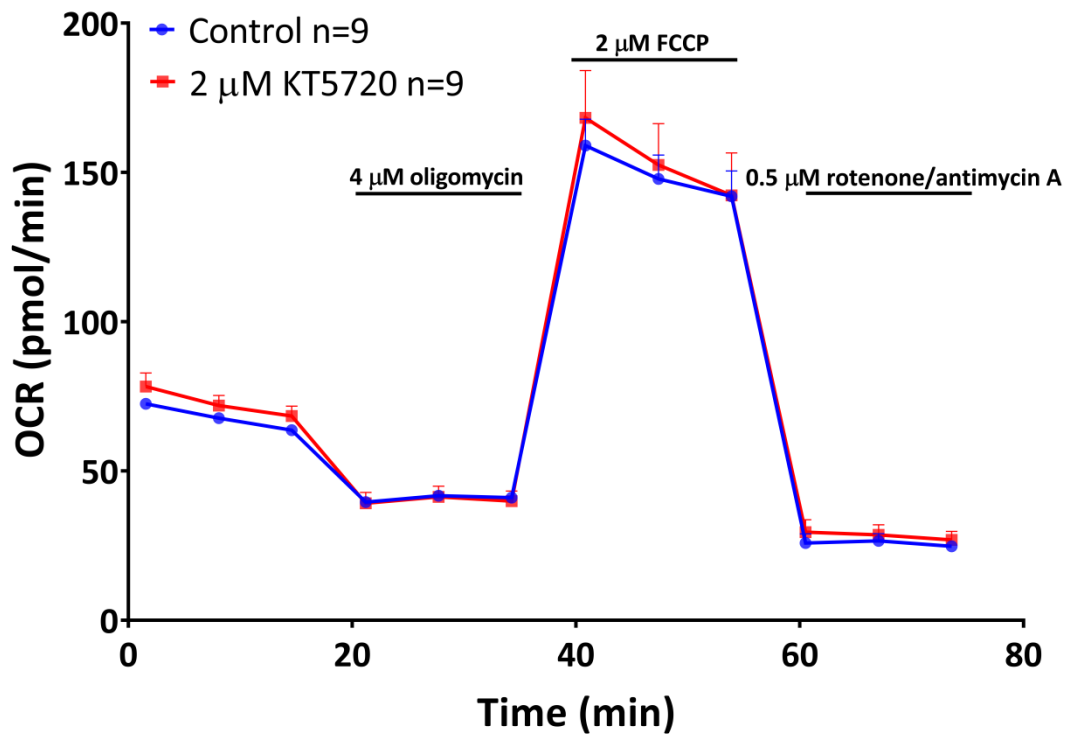


Figure 3.13: Effect of 2 μM KT5720 upon Synaptosomal Bioenergetics

A treatment of 2 μM KT5720 did not significantly affect the bioenergetics of synaptosomes during a Mito-Stress test ($p=0.891$). Values represented are the mean plus S.E.M. from 3 independent experiments. Experiment performed at 37°C in the Seahorse Xfp flux analyser.

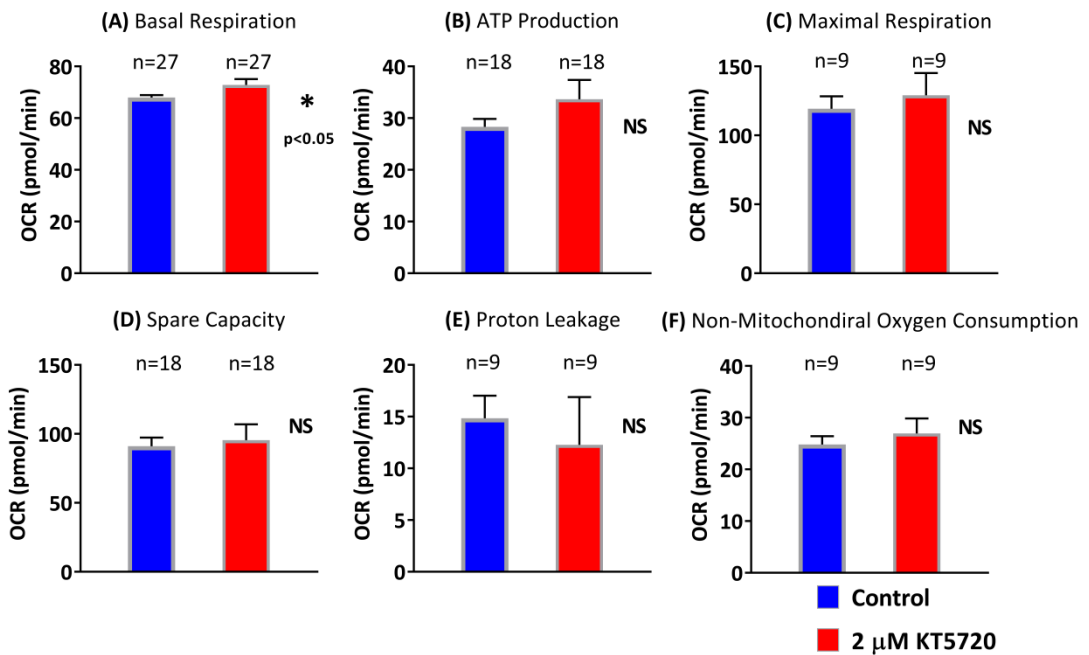


Figure 3.14: Effect of 2 μM KT5720 upon Mitochondrial Function

(A) There was a significant increase in basal respiration over the first 15 min ($p < 0.05$) when synaptosomes were treated with 2 μM KT5720, compared to controls. (B) Synaptosomes treated with 2 μM KT5720 exhibited no significant changes in ATP production at 20-35 min, (C) maximal respiration at 40-55 min, (D) spare capacity at 40-55 min, (E) proton leakage at 20-35 min, (F) or non-mitochondrial respiration at 60-75 min, compared to controls ($p > 0.05$) for all conditions. Values represented are the mean plus S.E.M. from 3 independent experiments. *, $p < 0.05$; NS, not significant.

3.8.2 The Effect of PKA Activation on Nerve Terminal Bioenergetics

Synaptosomes treated with 50 μM cBIMPS were subjected to the bioenergetics Mito-Stress test; no significant difference in OCR was seen when compared to control synaptosomes (Figure 3.15; $p > 0.05$). Figure 3.16 outlines the effect of 50 μM cBIMPS upon the 6 aspects of mitochondrial function, an increase in basal respiration was noted (Figure 3.16 A; $p < 0.05$ at 0-15 min), but again this was minimal and did not affect the other parameters measured.

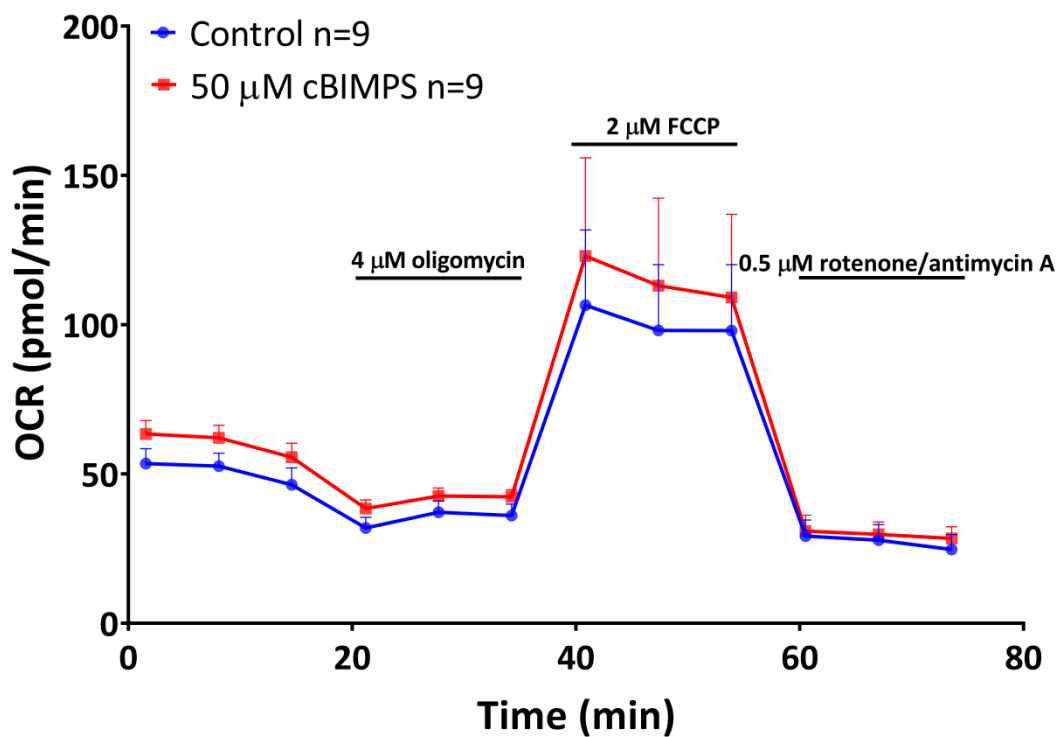


Figure 3.15: Effect of 50 μM cBIMPS upon Synaptosomal Bioenergetics

A treatment of 50 μM cBIMPS did not significantly affect the bioenergetics of synaptosomes during a Mito-Stress test ($p=0.547$). Values represented are the mean plus S.E.M. from 3 independent experiments. Experiment performed at 37°C in the Seahorse Xfp flux analyser.

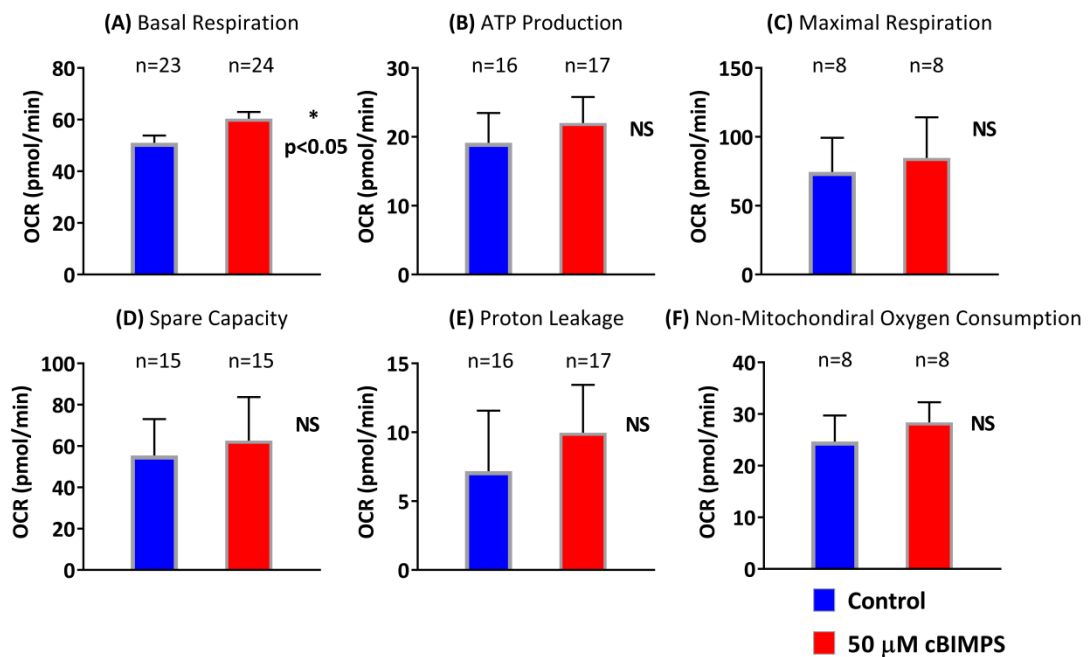


Figure 3.16: Effect of 50 μ M cBIMPS upon Mitochondrial Function

(A) Treatment with 50 μ M cBIMPS led to a significant increase in basal respiration ($p < 0.05$) at 0-15 min, but no significant changes in (B) ATP production at 20-35 min, (C) maximal respiration at 40-55 min, (D) spare capacity at 40-55 min, (E) proton leakage at 20-35 min, (F) or non-mitochondrial respiration compared to controls ($p > 0.05$) for all conditions. Values represented are the mean plus S.E.M. from 3 independent experiments. *, $p < 0.05$; NS, not significant.

These data highlight that exposure to either 2 μM KT5720 (Figure 3.13) or 50 μM cBIMPS (Figure 3.15) for 90-min at 37°C did not perturb the viability of synaptosomes. An acute drug treatment as used in the other assays (≤ 5 -min) would therefore not disrupt the integrity of the synaptosomes and would not be likely to produce non-specific effects upon the measurements taken. Figures 3.14 and 3.16 outline these drug treatments do not have a detrimental impact upon mitochondrial and synaptosomal function, despite an increase in basal respiration (see discussion).

3.8.3 The Effect of Dyn-I Inhibition on Nerve Terminal Bioenergetics

Potentially 30 μ M MITMAB could be perturbing the synaptosomes, so treated nerve terminals were subjected to the bioenergetics Mito-Stress test. No significant difference in OCR was observed between control and 30 μ M MITMAB treated synaptosomes (Figure 3.17; $p>0.05$). Figure 3.18 outlines the effect of 30 μ M MITMAB upon the 6 aspects of mitochondrial function. A significant decrease in non-mitochondrial oxygen consumption was noted (Figure 3.18 F; $p<0.05$ at 60-75 min). Figures 3.17 and 3.18 show that 30 μ M MITMAB does not significantly perturb the bioenergetics of synaptosomes and thus the membrane bound fraction of Dyn-I is sufficient to regulate the release of the RRP via KR and the RP via FF. This one change to non-mitochondrial oxygen consumption seems irrelevant relative to the fact that there was no change in mitochondrial function.

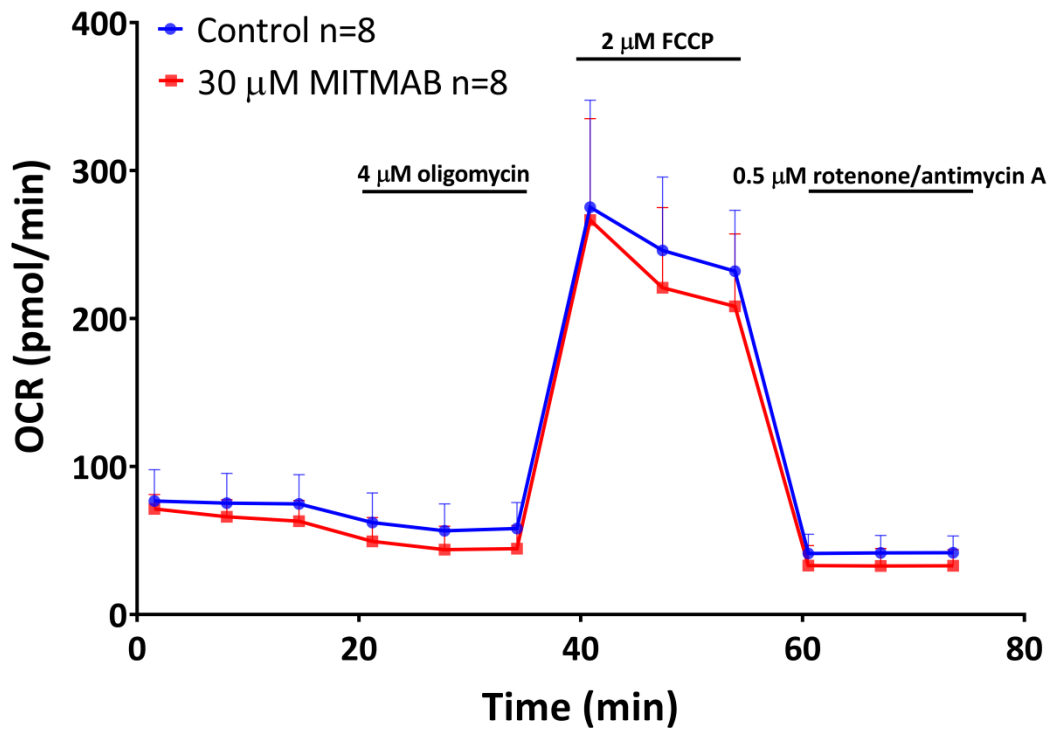


Figure 3.17: Effect of 30 μM MITMAB upon Synaptosomal Bioenergetics

A treatment of 30 μM MITMAB did not significantly affect the OCR of synaptosomes during a Mito-Stress test ($p=0.730$). Values represented are the mean plus S.E.M. from 3 independent experiments. Experiment performed at RT in the Seahorse Xfp flux analyser. Note, the synaptosomes were incubated with the drug or control at 37°C for the normal incubation duration and then washed. The Mito-Stress test was performed at RT.

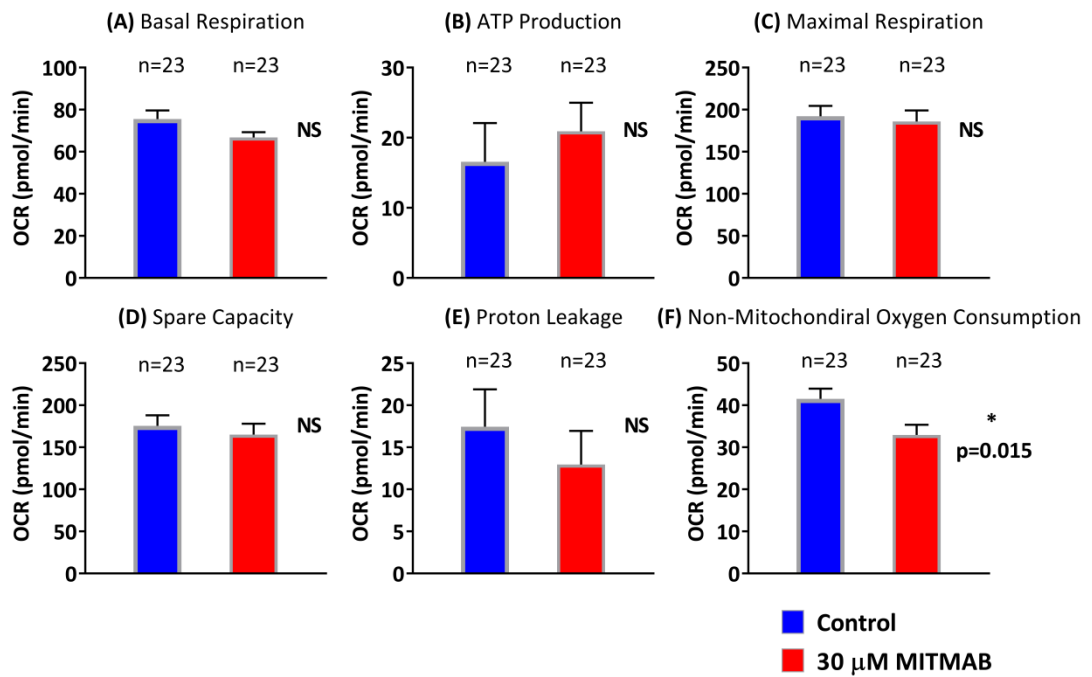


Figure 3.18: Effect of 30 μM MITMAB upon Mitochondrial Function

(A) Treatment with 30 μM MITMAB did not significantly affect basal respiration at 0-15 min, (B) ATP production at 20-35 min, (C) maximal respiration at 40-55 min, (D) spare capacity at 40-55 min, (E) or proton leakage at 20-35 min ($p > 0.05$), (F) but did significantly decrease non-mitochondrial oxygen consumption at 60-75 min compared to drug-free controls ($p = 0.0154$). Values represented are the mean plus S.E.M. from 3 independent experiments. *, $p < 0.05$; NS, not significant.

3.8.4 The Effect of Actin Disruption on Nerve Terminal Bioenergetics

The perturbation of Glu release seen with 15 μM latrunculin may be the result of the drug disrupting the bioenergetics or perturbing the integrity of some of the synaptosomes. In order to determine if this was the case synaptosomes treated with 15 μM latrunculin were subjected to the Mito-Stress test (Figure 3.19; $p>0.05$), no significant difference was observed between control and treated terminals. Figure 3.20 outlines the effect of 15 μM latrunculin upon the 6 aspects of mitochondrial bioenergetics. The disruption of actin with 15 μM latrunculin did not perturb the bioenergetics of the synaptosomes, meaning that the loss of Glu release observed from the RP and the mode switch to FF are specific molecular effects and not simply the nerve terminals being disrupted.

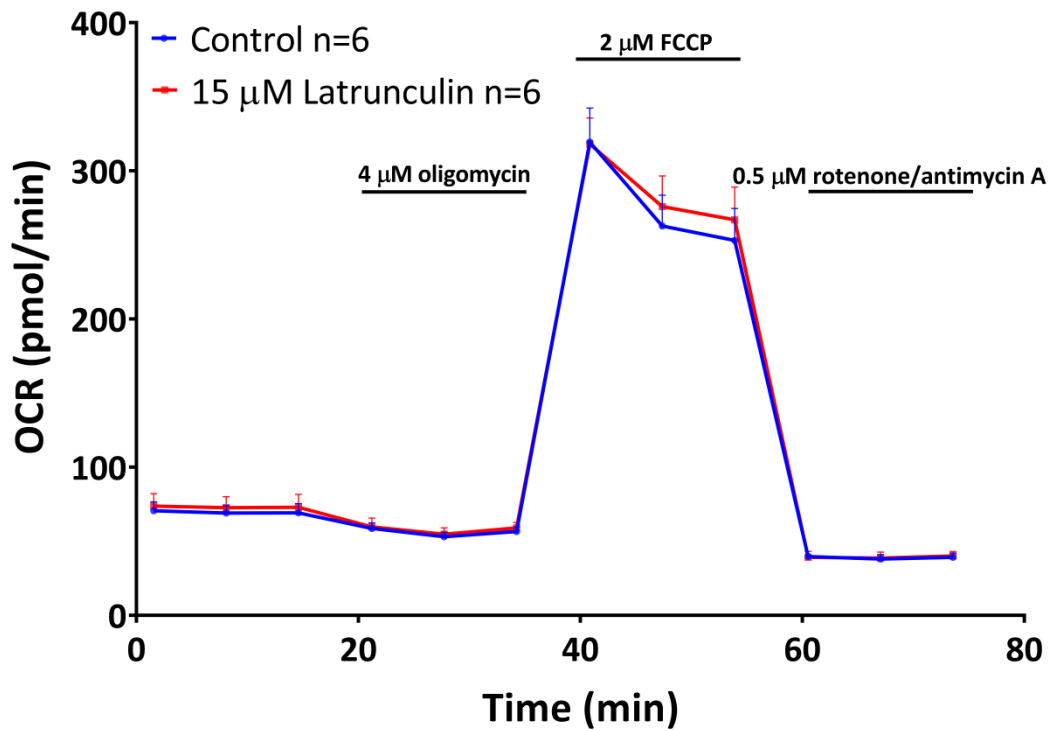


Figure 3.19: Effect of 15 μM Latrunculin upon Synaptosomal Bioenergetics

A treatment of 15 μM latrunculin did not significantly affect the OCR of synaptosomes during a Mito-Stress test ($p=0.934$). Values represented are the mean plus S.E.M. from 3 independent experiments. Experiment performed at RT in the Seahorse Xfp flux analyser. Note, the synaptosomes were incubated with the drug or control at 37°C for the normal incubation duration and then washed. The Mito-Stress test was performed at RT.

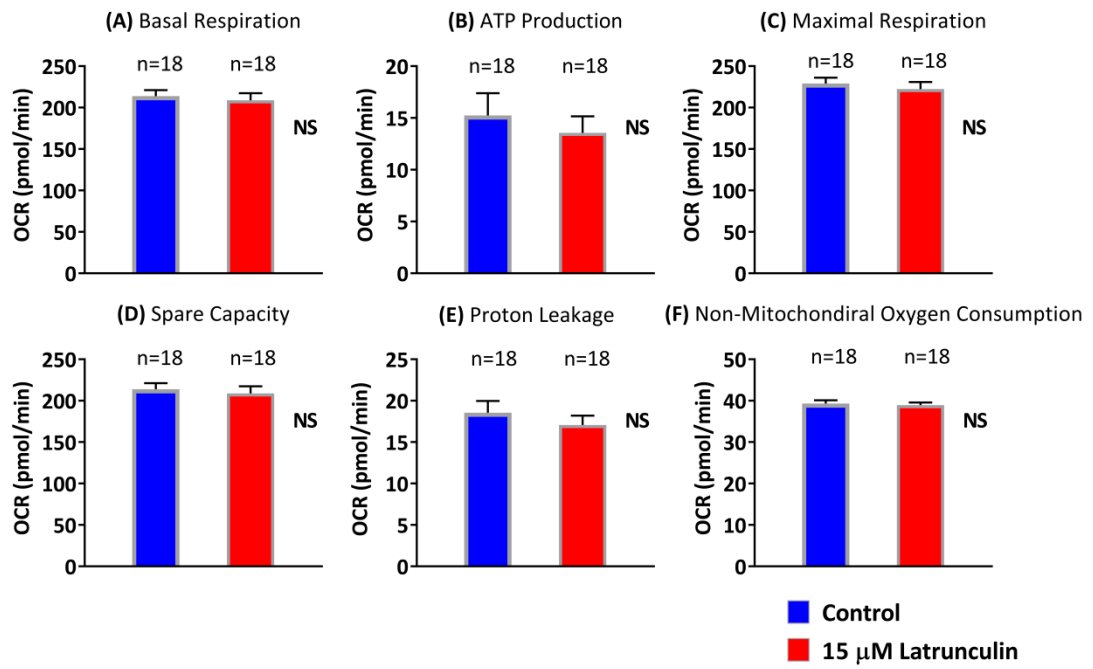


Figure 3.20: Effect of 15 μM Latrunculin upon Mitochondrial Function

(A) Treatment with 15 μM latrunculin did not significantly affect basal respiration at 0-15 min, (B) ATP production at 20-35 min, (C) maximal respiration at 40-55 min, (D) spare capacity at 40-55 min, (E) proton leakage at 20-35 min, (F) or non-mitochondrial oxygen consumption at 60-75 min ($p > 0.05$). Values represented are the mean plus S.E.M. from 3 independent experiments. NS, not significant.

3.9 Discussion

This chapter examined the roles that PKA, Dyn-I and actin might play in the regulation of the mode of NT exocytosis. The effects of PKA inhibition and activation upon Glu release, FM 2-10 dye release, $[Ca^{2+}]_i$ levels and terminal bioenergetics were studied. It was demonstrated that PKA modulation can switch the mode of Glu release in distinct SV pools during stimulation, without affecting the amount of Glu released, the $[Ca^{2+}]_i$ levels and such treatments did not perturb the bioenergetics of nerve terminals. The effects of either inhibiting cytosolic Dyn-I from binding to phospho-lipid membrane, or disassembling the actin cytoskeleton were also investigated upon Glu release, FM 2-10 dye release and terminal bioenergetics. It was shown that blocking cytosolic Dyn-I from binding to lipid membranes does not affect the amount of Glu release, the amount of evoked FM 2-10 dye release and does not perturb the bioenergetics of nerve terminals. Disassembly of actin on the other hand, blocks RP release and switches the RRP mode to FF, but without affecting the bioenergetics of nerve terminals.

Previous research has shown that PKA can enhance NT release probability (Trudeau, *et al.*, 1996), modify synaptic transmission by acting on neurotransmission machinery (Boczan, *et al.*, 2004), and regulate synaptic plasticity and SV priming through phosphorylation of multiple downstream proteins (Nguyen and Woo, 2003; Leenders and Sheng, 2005; Wang and Sieburth, 2013). Considering this, PKA may be able to regulate the phosphorylation, or availability of Dyn-I to regulate the mode of NT release, creating changes in the plasticity of the synapse.

3.9.1 Evoked Glu Release

PKA does not regulate the evoked release of Glu from synaptosomes. Figures 3.1 and 3.2 demonstrate that pre-treatment with 2 μ M KT5720 and 50 μ M cBIMPS respectively, had no effect upon evoked Glu release. As HK5C or ION5C can induce the maximum amount of Glu release from the RRP and RP SVs (as ascertained by $[Ca^{2+}]_e$ dose response curves: Section 1.9.1; Figure 1.7), these data indicate that neither inhibition nor activation of PKA affect the total number of SVs undergoing exocytosis during application of distinct stimuli. This data also concurs with other research groups who find no reduction in Glu release, or the availability of SVs to undergo release, when PKA activity was modulated (Trudeau, *et al.*, 1996; Menegon, *et al.*, 2006).

Any previously observed effects of regulation of release by modifying PKA activity (Chavez-Noriega and Stevens, 1994; Weisskopf, *et al.*, 1994; Tzounopoulos, *et al.*, 1998), may be related to control release being sub-maximal, where these studies do not demonstrate maximal release of NT. Under such conditions PKA may be able to mobilise more SVs to exocytose, enhancing release, but it cannot induce a greater release than the maximum possible, and this has already been achieved with the stimuli used in this study, when in the presence of 5 mM $[Ca^{2+}]_e$, as discussed.

Previous research by A. Ashton's group established that 4AP5C, HK5C and ION5C all evoke SVs to undergo one round of release (Section 1.9.2; Figure 1.9). If SV recycling were occurring, the observed level of evoked Glu would continue to rise over the duration of the assay and not plateau as demonstrated in Figures 3.1 and 3.2; this would be especially true with 4AP5C (which only release the RRP). Similarly, as discussed earlier in Chapter 3, Ashton has shown that 4AP5C maximally releases the

RRP, whilst HK5C and ION5C both maximally release the RRP and the RP; therefore Figures 3.1 and 3.2 cannot reflect PKA activity sub-maximal releasing or recycling any vesicular pool. Note, inhibition of any Dyn or clathrin dependent recycling does not induce any more release, which is further proof that just one round of SV release is occurring (Section 1.9.5).

Blocking cytosolic Dyn-I from binding to membranes does not perturb Glu release for either the RRP or the RP. This agrees well with previous research which indicates a portion of Dyn-I is membrane bound, and this is sufficient to aid exocytosis during evoked release (Robinson, 1991; Wahl, *et al.*, 2013). It could be argued that this result indicates Dyn-I is not present at the AZ, however inhibition of the GTPase activity of Dyn-I has been shown to modulate the mode of exocytosis from glutamatergic synaptosomes, therefore Dyn-I has a role during exocytosis (Figure 1.13; Ashton, manuscript in preparation).

Inhibition of cytoskeletal actin assembly, blocks release of the RP of SVs. Figure 3.4 outlines that treatment with 15 μ M latrunculin has no effect upon RRP SVs released during 4AP5C stimulation, but directly blocks RP release when evoked to release with either HK5C or ION5C. Actin has been well established to play a role in the maintenance of RP SVs in neurons (Doussau and Augustine, 2000; Dillon and Goda, 2005). Furthermore, other research groups have established that high concentrations of latrunculin can reduce release of catecholamines from chromaffin cells (Gasman, *et al.*, 2004) and indeed these results support the theory that actin aids exocytosis during evoked release, rather than being a barrier against vesicular mobilisation (Malacombe, *et al.*, 2006; Lee, *et al.*, 2012; Nightingale, *et al.*, 2012; Glebov, *et al.*, 2017).

3.9.2 Evoked FM 2-10 Dye Release

Though PKA activity does not regulate the release of SV pools, it does have a direct role in regulating the mode of SV exocytosis for distinct pools. Figure 3.5 shows that inhibition of PKA caused synaptosomes to release significantly more FM 2-10 dye than controls, when stimulated with 4AP5C (Figure 3.5 A) and ION5C (Figure 3.5 B). Stimulation with 4AP5C releases only the RRP of SVs, with roughly half being via a KR mechanism and half being through FF during controls (Section 1.9.4).

Stimulation with ION5C and HK5C on the other hand, is theorised to release the RRP exclusively by KR, and the RP exclusively by FF during drug-free conditions (Ashton and Ushkaryov, 2005; Ashton, unpublished observations (see Figure 1.12)). Considering this, Figure 3.5 may indicate that inhibition of PKA causes SVs in the RRP to switch their mode of exocytosis from KR to FF. Interestingly HK5C stimulation does not increase FM 2-10 dye release in a similar manner when PKA was inhibited (Figure 3.5 C), demonstrating that the RRP SVs are still all undergoing KR and not switching to FF, when stimulated with HK5C.

Previously this phenotype was seen when Bhuva inhibited Dyn-I with 160 μ M dynasore (Figure 1.13) (Bhuva, 2015). It was concluded that Dyn-I, which has been shown to have a role at the site of exocytosis, was required to close the FP during KR of the RRP when synaptosomes were stimulated with 4AP5C and ION5C. Ashton previously demonstrated that the 4AP5C and ION5C stimuli induce $[Ca^{2+}]_i$ changes through different kinetics at the AZ, while HK5C is known to induce a higher and faster initial $[Ca^{2+}]_i$ level at the AZ (Figure 1.8). As Dyn-I has been shown to be inhibited by high concentrations of Ca^{2+} (Liu, *et al.*, 1994; Ashton, manuscript in preparation), Dyn-I is

able to mediate KR during 4AP5C and ION5C stimulation, where the $[Ca^{2+}]_i$ level at the AZ is not high enough to inhibit Dyn-I activity; unlike during HK5C stimulation where Dyns are inhibited by this high $[Ca^{2+}]_i$ at the AZ. Even though Dyns are inhibited during HK5C stimulation, RRP SVs are theorised to still be able to release via a KR mode as the higher $[Ca^{2+}]_i$ activates NM-II which is able to close the FP, creating a Dyn-independent KR mode (Figure 1.15).

PKA has not been shown to directly phosphorylate Dyn-I, but it does have a number of phosphorylation targets in the pre-synaptic terminal, such as syntaphilin which regulates the availability of Dyn-I, and such regulation can inhibit Dyn-mediated endocytosis (Das, *et al.*, 2003; Boczan, *et al.*, 2004). Potentially the activity of PKA could regulate syntaphilin to affect the availability of Dyn-I, preventing it from mediating KR during 4AP5C and ION5C stimulation. As non-muscle NM-II is not being inhibited by syntaphilin, NM-II is still free to mediate KR during HK5C stimulation, when Dyn-I is inactive anyway, and this is worth investigating further by assessing the phosphorylated state of syntaphilin following PKA inhibition. Alternatively, PKA could phospho-regulate an unknown phosphatase to dephosphorylate Dyn-I, thus allowing it to mediate KR. Clearly, inhibition of PKA prevents such interactions leading to FF at the AZ, since KR cannot occur.

Results presented in Figure 3.6 demonstrate that PKA activation can also specifically regulate the release mode of RP SVs. Activation of PKA with 50 μ M cBIMPS caused a significant decrease in FM 2-10 dye released from synaptosomes when stimulated with HK5C and ION5C (Figure 3.6 B and C), but not 4AP5C (Figure 3.6 A). As mentioned above both HK5C and ION5C release the RP of SVs via a FF mode of exocytosis during

control conditions (Figure 1.12). When PKA is activated however, at least some SVs in the RP are switched from a FF mode of exocytosis to a KR mode and so less FM 2-10 dye is released. Interestingly, this effect was specific to the RP SVs as no mode switch was seen for the sub-pool of SVs in the RRP, which undergo FF when stimulated with 4AP5C (Figure 3.6 A). Thus, increasing the ability of PKA to phosphorylate substrates leads to a marked increase of RP SVs undergoing KR exocytosis.

This particular phenotype resembles previous research when PP2B (also termed calcineurin) was inhibited with Cys A (Figure 1.16). Calcineurin has been shown to dephosphorylate Dyn-I both *in vitro* and *in vivo*, during terminal depolarisation (Liu, *et al.*, 1994; Marks and McMahon, 1998; Bauerfeind, *et al.*, 1997). As Dyns are dephosphorylated by calcineurin, it was theorised that Dyn-I localised to the RP may require calcineurin mediated dephosphorylation in order to drive FP expansion during FF (Bhuva, 2015). Thus, inhibiting Dyn-I dephosphorylation could prevent some RP SVs switching to a FF mode of exocytosis. However, blocking Dyn-I directly with dynasore does not give the same result (compare Figure 3.6 with Figure 1.13). This demonstrates that though inhibition of calcineurin led to an increase in SVs undergoing KR, it was not directly through regulating Dyn-I activity. Ashton has recently demonstrated that with HK5C stimulation release of the RRP is mediated by NM-II whilst Dyn-I regulates RP release; with ION5C however, both the RRP and RP are released via Dyn-I mechanisms (compare Figures 1.13 and 1.14).

Similarly, some FM 2-10 dye was still lost from the RP SVs when PKA was activated (Figure 3.6 B and C), indicating that not all of this pool of SVs are being switched to KR by PKA activation. This might suggest that there is a sub-pool of SVs within the RP

which are available to switch to a KR mode of exocytosis under the right conditions, however further investigation is needed. Some unpublished results from Ashton suggest that if all the RRP are undergoing KR, it is not possible for all the RP to also undergo KR. This suggests that the site for KR exocytosis may get saturated. If one converts the RRP to FF, it would appear that all RP SVs can undergo KR (Ashton, *et al.*, unpublished).

These data may indicate that PKA and protein phosphatase 2B (calcineurin) share a substrate which regulates the release dynamics of the RP, without regulating the RRP. It is currently unclear what this substrate is, or what role it may play in mode regulation.

3.9.3 Dual Treatments

Recent papers have questioned the specificity of KT5720 for PKA in a range of models, stating KT5720 may potentially inhibit other kinases and alter receptor-binding affinities through non-specific effects when used at lower concentrations than in this study (Olsen, *et al.*, 1998; Davies, *et al.*, 2000; Lazareno, *et al.*, 2000). Though this may seem the case at face value, a few differences in methodology must be highlighted:

- (i) In many models, *in vitro* cells were chronically incubated with KT5720 for longer than 10-min, in some cases hours (Davies, *et al.*, 2000; Lazareno, *et al.*, 2000). In this thesis, all drugs were washed away after a maximum time of 10-min, before being re-added for the duration of the assays <5-min.
- (ii) In some studies cultured cells were kept at 30°C for the duration of the experiments (Davies, *et al.*, 2000), while measurements in this thesis took place at room temperature.

(iii) All models used reflected *in vitro* studies taking place in tissues cultures, bacterial cultures or disrupted cellular membranes (Olsen, *et al.*, 1998; Lazareno, *et al.*, 2000), while synaptosomes used in this study are an *in vivo* model, representing viable nerve terminals.

These differences can lead to fallacious assumptions about the specificity of drugs and their long-term actions during chronic treatments.

To highlight the specificity of both KT5720 and cBIMPS for PKA, a dual treatment was conducted for FM 2-10 dye release. Synaptosomes pre-treated with 2 μ M KT5720 followed by 50 μ M cBIMPS treatment released levels of FM 2-10 dye equivalent to controls when stimulated with HK5C (Figure 3.7 A) and ION5C (Figure 3.7 B). If KT5720 was not inhibiting PKA during such an acute treatment, an increase of evoked FM 2-10 dye would have been seen with ION5C; furthermore, if cBIMPS had not been specifically working on PKA a decrease in evoked FM 2-10 dye would have been noted for this dual treatments with ION5C stimulation.

3.9.4 Effect of Dyn-I and Actin Modulation on Evoked FM Dye Release

MITMAB prevents Dyn-I binding to membranes, but does not disrupt or inhibit Dyn-I that is already associated with the membrane, and synaptosomes treated with 30 μ M MITMAB do not significantly change the amount of Glu released (Figure 3.3) or the amount of FM 2-10 dye released (Figure 3.8). With ION5C stimulation the KR mode of the RRP is Dyn-dependent (as demonstrated with dynasore: Figure 1.13), and this suggests that the sub-pool of Dyn-I that regulates the mode of release is already associated with the membrane. This is a very important discovery, as it suggests that though cytosolic Dyn-I must undergo dephosphorylation in order to become active,

membrane bound Dyn-I is already active, and located at the AZ (Wahl, *et al.*, 2013), and thus can instantly polymerise around forming FPs, without a rate limiting time step. As MITMAB does not perturb the GTPase activity of this membrane bound Dyn-I sub-pool it is still able to regulate the FP during exocytosis, and this may indicate that a sub-pool of Dyn-I is localised to the AZ, or the RRP SVs ready to facilitate KR exocytosis.

Latrunculin disrupts the actin cytoskeleton by preventing polymerisation, and this blocks release of SVs from the RP only (Figure 3.4 B and C). However, when FM 2-10 dye release is investigated there appears to be no switch in the mode of release (Figure 3.9 A and B), as the amount of FM 2-10 dye released is quite similar with or without latrunculin treatment. Interestingly, if the RP (which undergoes FF) is not able to release then no decrease in FM 2-10 dye release should be observed at all (as the RRP releases via KR for both HK5C and ION5C). However, control levels of FM 2-10 dye appear to be released and this indicates that SVs in the RRP are switching to a FF mode of release, as both pools are similar in size (Figure 1.1).

In order to determine if latrunculin was releasing only the RRP, the maximal FM 2-10 dye release of latrunculin was added to control levels of FM 2-10 dye release (Figure 3.10). This presented a result identical to FM 2-10 dye release observed with OA (where all SVs are undergoing FF) (Figure 1.11), suggesting that latrunculin is only releasing the RRP of SVs, and Control FM 2-10 dye traces are showing only the release of RP SVs. Recent studies by Ashton and colleagues (Ashton, unpublished) indicate a dual-treatment of latrunculin and OA gives no extra FM dye release, indicating latrunculin switches all RRP SVs to FF. These data indicate that not only does actin have a direct role in the release of the RP, but it also has a role in the regulation of the FP

during RRP exocytosis. Previous studies have highlighted that actin can coat different types of secretory cells during exocytosis (Miklavc, *et al.*, 2009), and this may work with either Dyn-I or NM-II to stabilise the FP and regulate release (Malacombe, *et al.*, 2006; Nightingale, *et al.*, 2012). Indeed the inhibition of actin prevents any KR taking place which suggests that actin must work to regulate the FP during some stimulation paradigms.

3.9.5 Evoked $[Ca^{2+}]_i$ Levels

Previously changes to $[Ca^{2+}]_i$ levels have been linked to changes in the mode of exocytosis, where an increase leads to a high prevalence of KR (Alés, *et al.*, 1999; Ashton, manuscript in preparation – Figure 1.8).

When PKA was inhibited or activated, distinct changes in the mode of exocytosis were observed for each stimuli, however no significant change in $[Ca^{2+}]_i$ levels occurred. This is good evidence to suggest that PKA activity regulates the mode of exocytosis, independently of $[Ca^{2+}]_i$, through phosphorylation of protein partners, which the neuron could utilise to regulate signalling.

Prevention of PKA from phosphorylating a target protein may inhibit the action of Dyn-I during exocytosis, as this phenotype is similar to Dyn-I inhibition with dynasore (Bhuva, 2015; Figure 1.13), however further studies must be conducted to determine if there is a link between these proteins, and the extent of the protein pathway. During control conditions PKA could be phosphorylating -and thus activating- a phosphatase which dephosphorylates Dyn-I allowing it to mediate KR; the inhibition of PKA may

then prevent the activation of the phosphatase and of Dyn-I, leading to the same phenotype as direct Dyn-I inhibition.

Previously when calcineurin inhibition was shown to give the same phenotype as PKA activation it was assumed to be through changes to protein pathways; however, Bhuva demonstrated that the inhibition of calcineurin with Cyclosporin A significantly raised the $[Ca^{2+}]_i$ level and this is able to switch the mode of RP SVs (Bhuva, 2015). PKA activation however, had no significant effect upon the $[Ca^{2+}]_i$ level, demonstrating the activation of PKA was able to change the mode of RP exocytosis through protein pathways rather than changes to $[Ca^{2+}]_i$. These data concur with other researchers who suggest that PKA activation is able to modulate vesicular exocytosis downstream of changes to $[Ca^{2+}]_i$ levels, potentially describing a regulatory role for PKA in signalling.

3.9.6 Bioenergetics of Synaptosomes

In order to ensure that distinct changes to mode of release were due to targeted drug action and not non-specific perturbation of the synaptosomes by the drugs utilised, drug treated samples were subjected to the bioenergetics Mito-Stress test. The Mito-Stress test measured mitochondrial function and terminal viability by recording the OCR of synaptosomes to determine respiratory stress. If a treatment or condition negatively affects either the energetic demands or the molecular nature of the nerve terminals, this would become apparent through this assay.

Inhibition and activation of PKA did not compromise the viability of synaptosomes over chronic, but more importantly during acute treatments (≤ 5 -min), as used with the Glu, FM 2-10 dye and Fura-2 assays. Drug treatments led to perceived switches in the mode

of exocytosis as discussed above, without non-specific drug action or perturbation of the synaptosomes as the presence of either drug had no effect upon mitochondrial ATP production, maximal respiration, spare capacity, proton leakage, or non-mitochondrial respiration (Figures 3.14 and 3.16 B-F).

However, both drug treatments caused an increase in basal respiration (Figures 3.14 and 3.16 A). Basal respiration reflects the OCR required by the mitochondria of the sample to meet cellular ATP demand during resting conditions. Such an increase in mitochondrial oxygen consumption reflects the cells facing an increased energy demand on the mitochondria (Agilent Technologies, 2019). Potentially some activation or inhibition of PKA pathways may cause some slight increase in respiration, or perhaps synaptosomes were still acclimatising to the microtiter plate. However this effect would need to be studied in more detail in order to determine the significance.

MITMAB prevented cytosolic Dyn-I from binding to the membrane without compromising the viability of the synaptosomes (Figure 3.17). MITMAB does not affect mitochondrial basal respiration, ATP production, maximal respiration, spare capacity or proton leakage (Figure 3.18 A-E), but did decrease non-mitochondrial respiration (Figure 3.218 F). Non-mitochondrial respiration is defined as any oxygen consumption that persists due to a subset of cellular enzymes outside of the mitochondria, which is used to calculate the overall mitochondrial respiration rate; however, as no significant change in any other aspect was noted (Figure 3.18), the implication of this data is not yet fully understood. If MITMAB caused other cellular enzymes to decrease their OCR this could indicate a non-specific effect of the drug during prolonged treatments, however this has not been observed previously.

Synaptosomes treated with latrunculin blocked release of the RP (Figure 3.4 B and C), and potentially switched the mode of release for the RRP from KR to FF (Figure 3.9). However latrunculin did not affect the OCR or the viability of the synaptosomes as no significant change was seen in basal respiration, ATP production, maximal respiration, spare capacity, proton leakage and non-mitochondrial respiration (Figure 3.20 A-F).

3.10 Conclusion

This chapter demonstrates that PKA inhibition potentially reduces the number of SVs undergoing exocytosis via KR by switching these to FF, and this is probably through blocking the action of Dyn-I. Furthermore, PKA activation increases the number of SVs undergoing KR and this could be through Dyn-I or NM-II. KT5720 and cBIMPS specifically work to inhibit and activate PKA respectively, without perturbing the Glu release, the viability of synaptosomes or affecting the $[Ca^{2+}]_i$ level within the terminals.

Significantly, the Dyn-I which is already bound to membranes is sufficient to facilitate KR during SV release, because prevention of further Dyn-I binding to membranes with MITMAB does not impact Glu release, the mode of exocytosis or nerve terminals bioenergetics. Actin is potentially required to mobilise release of the RP, and could also regulate the mode of RRP SVs exocytosis, regardless of which stimuli is used. The role of actin needs to be studied in more detail, since it appears to be important for both Dyn-dependent and NM-II-dependent KR of the RRP.

If PKA is switching the mode of exocytosis through Dyn-I phospho-regulation, this will be revealed using these drug treatments in phosphorylation studies. However, if such a small pool of membrane bound Dyn-I appears to be able to regulate the mode of release, the changes in phosphorylation of this sub-pool of Dyn-I may be very small and beyond the sensitivities of detection of such phosphorylation by Western blotting.

Chapter 4:

The Role of AC in Modulating the Mode of Exocytosis and SV Pool Release via PKA and EPAC Regulation

4.1 Introduction

Chapter 3 of this thesis established that PKA activation can inhibit Dyn-I-dependent RRP KR, PKA inhibition can enhance RP KR without modulating the RRP, cytosolic Dyn-I is not required to regulate the RRP mode of exocytosis, and actin has a role in both the RRP mode, and the mobilisation of the RP. The aim of this chapter is to discover how modulating levels of the secondary messenger cAMP (which activates PKA) affects the mode of release for the RRP and RP. Furthermore, this chapter aims to investigate if cAMP is working through PKA alone to mediate specific changes in mode.

4.2 The Effect of Adenylyl Cyclase Regulation on Evoked Glu Release

PKA is activated by the secondary messenger cAMP (Walsh, *et al.*, 1968; Knighton, *et al.*, 1991). cAMP is synthesised from ATP by the transmembrane enzyme adenylyl cyclase (AC), which has 9 isoforms and is activated by the GTP-bound α -subunit of the stimulatory G-protein (G_{α}) (Sunahara, *et al.*, 1996; Hanoune and Defer, 2001; Sandana and Dessauer, 2009). Changes to intracellular levels of cAMP have been shown to enhance NT release by modifying secretory machinery (Zhong and Wu, 1991; Chen and Regehr, 1997), influence synaptic plasticity including memory and learning (Huang, *et al.*, 1995; Grandoch, *et al.*, 2010), and has been linked to changes in Ca^{2+} sensitivity for fast-releasing SVs during low intensity stimulation (Ster, *et al.*, 2007; Petrov, *et al.*, 2008; Yao and Sakaba, 2010).

For many years these effects were attributed to the action of cAMP upon PKA and certain hyperpolarisation-activated cyclic nucleotide-modulated (HCN) channels (Zambon, *et al.*, 2005; Biel, 2008), but since the discovery of a second family of cAMP activated proteins, exchange proteins directly activated by cAMP (EPACs) (de Rooij, *et*

al., 1998; Kawasaki, *et al.*, 1998), the PKA-independent effects of cAMP have been better explained (Beaumont, *et al.*, 2002; Grandoch, *et al.*, 2010).

As cAMP directly activates PKA, modulation of cAMP levels within the terminals may create similar mode switching conditions to when PKA activity was directly modulated with KT5720 and cBIMPS treatments (see Chapter 3). However, the additional activation of EPACs may also have a direct impact upon release dynamics (Almahariq, *et al.*, 2013; Schmidt, *et al.*, 2013).

Forskolin has long been used to activate AC (Seamon and Daly, 1981; Tang and Hurley, 1998) which raises the level of intracellular cAMP, while 9-cp-ade has been used extensively to inhibit AC (Johnson, *et al.*, 1997). These drugs were utilised in this chapter in order to ascertain what effects the activation and inhibition of AC had upon evoked Glu release, FM 2-10 dye release and the level of $[Ca^{2+}]_i$.

4.2.1 The Effect of AC Inhibition on Evoked Glu Release

AC can be specifically inhibited by 9-cp-ade, a non-competitive inhibitor which targets the P-site of AC to prevent ATP binding and thus cAMP production (Johnson, *et al.*, 1997). No significant change in Glu release was observed from the RRP when synaptosomes were treated with 100 μ M of 9-cp-ade and stimulated with 4AP5C (Figure 4.1 A; Glu release: CON 632.80 ± 129.63 (AU), 9-cp-ade 561.61 ± 110.18 , $p > 0.05$ at 300 sec – bar chart), or from the RRP and RP when stimulated with HK5C (Figure 4.1 B; Glu release: CON 1073.96 ± 105.56 (AU), 9-cp-ade 1093.56 ± 116.78 , $p > 0.05$ at 300 sec) or ION5C (Figure 4.1 C; Glu release: CON 1307.59 ± 85.46 (AU), 9-cp-ade 1356.33 ± 87.78 , $p > 0.05$ at 300 sec).

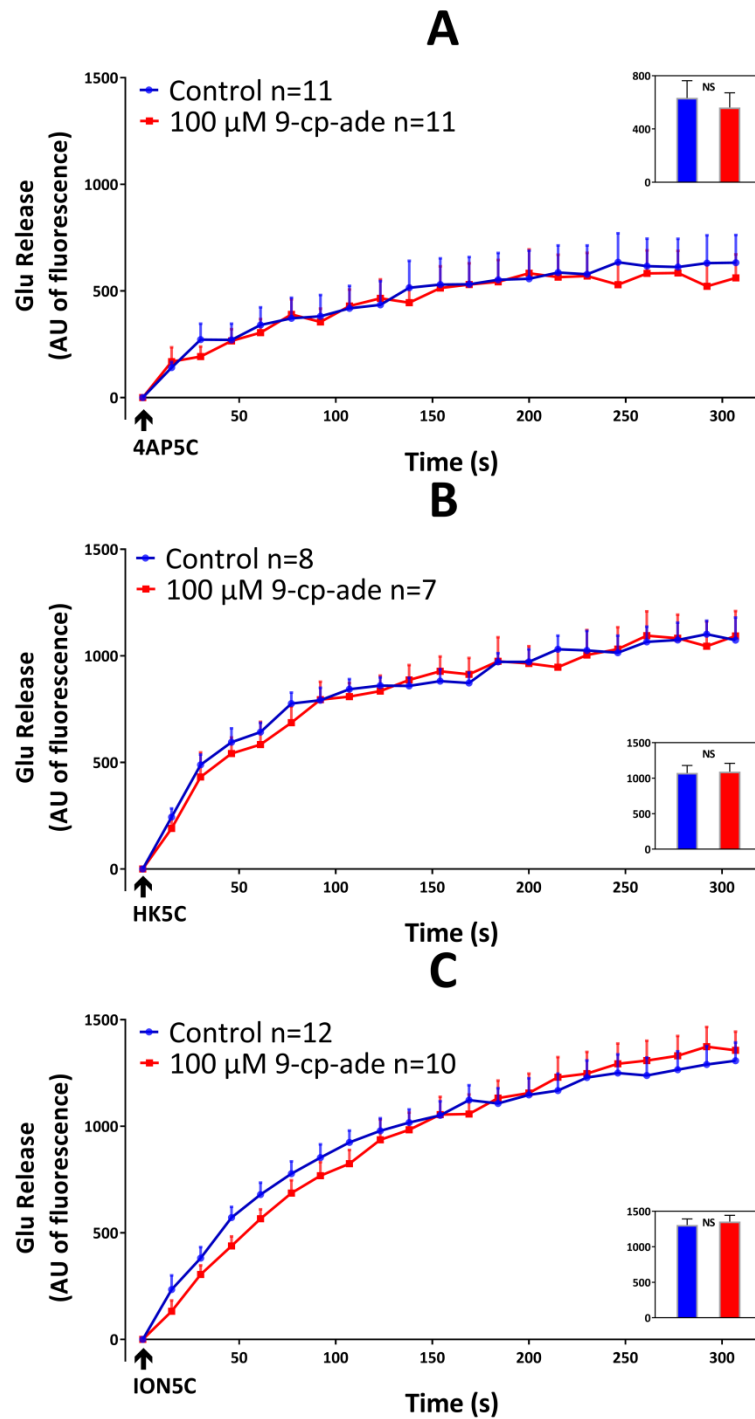


Figure 4.1: Effect of 100 μ M 9-cp-ade vs Control upon Evoked Glu Release

(A) 100 μ M 9-cp-ade had no effect upon 4AP5C ($p=0.655$), (B) HK5C ($p>0.05$) or (C) ION5C ($p=0.872$) evoked Glu release, compared to controls. Inserts demonstrate final fluorescence at 300 sec. Value represented are the mean plus S.E.M. from 3 independent experiments. *NS*, not significant.

4.2.2 The Effect of AC Activation on Evoked Glu Release

As the inhibition of AC with 9-cp-ade did not perturb Glu release, the effect of the selective, reversible AC activator forskolin was investigated upon evoked Glu release. Forskolin increases the binding affinity of two cytoplasmic domains C_1 and C_2 on AC, C_1 is located between two sets of six transmembrane spans, while C_2 is located on the C-terminus. Binding of these two domains promotes a more efficient catalyst to produce cAMP, and significantly increases intracellular cAMP levels (Seamon and Daly, 1981; Dessauer, *et al.*, 1997). Forskolin treatment has been shown to enhance 4AP stimulated Glu release from synaptosomes (but see discussion), and increase $[Ca^{2+}]_i$ levels (Herrero and Sánchez-Prieto, 1996), through the activation of PKA and EPACs (Ferrero, *et al.*, 2013).

Synaptosomes treated with 100 μ M of forskolin exhibited no significant change in Glu released from the RRP when stimulated with 4AP5C compared to drug free controls (Figure 4.2 A; Glu release, *CON* 500.73 ± 148.19 (AU), *forskolin* 490.88 ± 54.78 , $p > 0.05$ at 300 sec – bar chart). Glu released from the RRP and RP was significantly lower in terminals treated with 100 μ M forskolin when evoked by HK5C (Figure 4.2 B; Glu release, *CON* 843.04 ± 73.30 (AU), *forskolin* 492.96 ± 113.39 , $p < 0.05$ at 300 sec) and ION5C (Figure 4.2 C; Glu release: *CON* 1307.59 ± 85.46 (AU), *forskolin* 768.87 ± 70.73 , $p < 0.05$ at 300 sec), compared to untreated controls. Treatment with forskolin perturbed evoked release of SVs from the RP, as release from the RRP (measured using 4AP5C) was not disrupted (Figure 4.2 A).

In order to prove this loss of RP SVs was a specific effect of forskolin, synaptosomes were treated with 100 μ M of the forskolin inactive homologue 1,9-dideoxyforskolin

(Pinto, *et al.*, 2009), and stimulated with HK5C (Figure 4.3 A). This did not change the amount of evoked Glu release compared to controls (Glu release: CON 1073.96 ± 105.56 (AU), 1,9-dideoxyforskolin 914.67 ± 133.35, $p>0.05$ at 300 sec – bar chart), as maximal Glu release was observed from both RRP and RP and this also outlined the specificity of forskolin upon AC.

The specific effect of forskolin upon AC was further confirmed when synaptosomes were pre-treated with 100 µM 9-cp-ade (to inhibit AC) and then subsequently treated with 100 µM forskolin. In these terminals the HK5C evoked Glu release was identical to non-drug treated controls (Figure 4.3 B; Glu release: CON 1073.96 ± 105.56 (AU), 9-cp-ade plus forskolin 901.82 ± 127.44, $p>0.05$ at 300 sec). This pre-treatment condition also had no effect upon Glu release from the RRP evoked by 4AP5C (Figure 4.3 C; Glu release: CON 632.80 ± 129.63 (AU), 9-cp-ade plus forskolin 577.78 ± 82.08, $p>0.5$ at 300 sec). These results indicate that forskolin specifically inhibits release of the RP of SVs evoked by HK5C by activating AC, but if AC is first inhibited forskolin is no longer able to block RP release. This data also demonstrates that 9-cp-ade is actively inhibiting AC.

These are intriguing data, as forskolin raises cAMP levels and cAMP activates PKA, it may be expected that activation of AC by forskolin should share a similar phenotype as when PKA is activated with cBIMPS; however as previously seen cBIMPS had no such effect upon HK5C (Figure 3.2 B) and ION5C (Figure 3.2 C) evoked Glu release from synaptosomes.

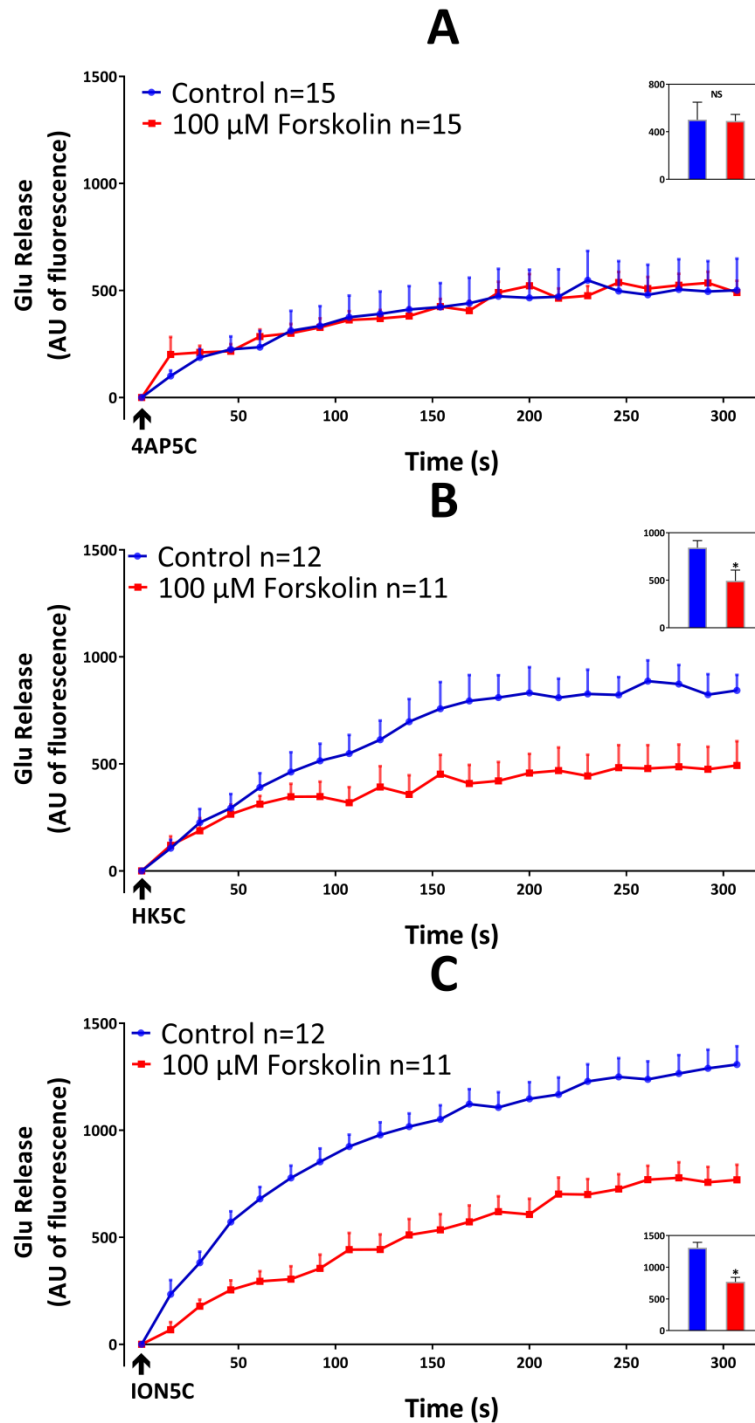


Figure 4.2: Effect of 100 μ M Forskolin vs Control upon Evoked Glu Release

(A) 100 μ M forskolin had no effect upon 4AP5C ($p=0.861$), (B) but perturbed HK5C ($p<0.001$) and (C) ION5C ($p<0.001$) evoked Glu release. Inserts demonstrate final fluorescence at 300 sec. Values represented are the mean plus S.E.M. from 3 (A) and 5 (B, C) independent experiments. *, $p < 0.05$; NS, not significant.

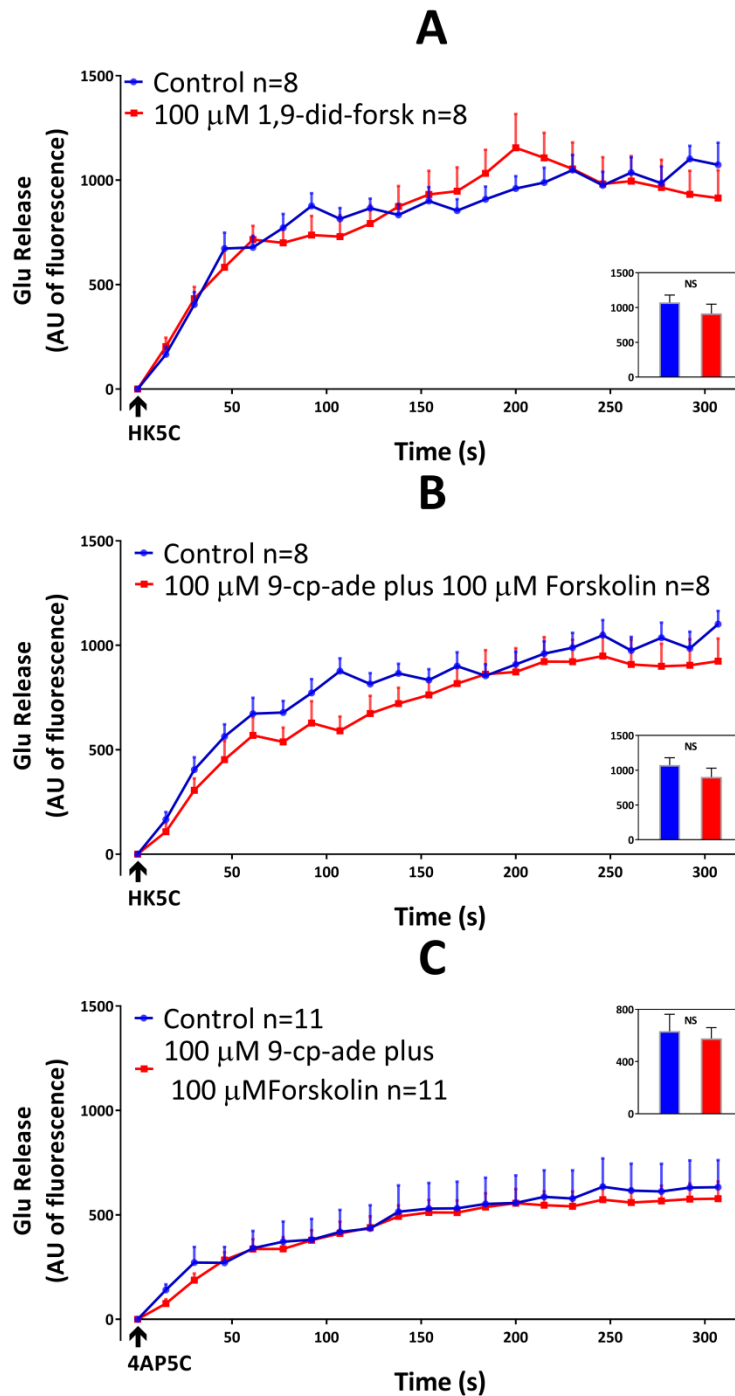


Figure 4.3: Effect of 100 μ M 1,9-dideoxyforskolin and 100 μ M 9-cp-ade plus 100 μ M Forskolin Treatment upon Evoked Glu Release

(A) 100 μ M 1,9-dideoxyforskolin had no effect upon HK5C evoked Glu release ($p=0.991$). (B) Glu release from synaptosomes pre-treated with 100 μ M 9-cp-ade prior to 100 μ M forskolin treatment was equivalent to controls when stimulated with HK5C ($p=0.197$), (C) and when stimulated with 4AP5C ($p=0.587$). Values represented are the mean plus S.E.M. from 3 independent experiments. *NS*, not significant.

4.2.3 The Effect of EPAC Inhibition on Evoked Glu Release

cAMP has two major cellular targets PKA and EPACs. EPAC1 and EPAC2 are proteins which have guanine-nucleotide exchange factor (GEF) activity which is utilised to switch GDP for GTP in the small GTPases Rap1 and Rap2 (de Rooij, *et al.*, 1998; Kawasaki, *et al.*, 1998). EPAC1 has limited expression in the CNS, being enriched in the kidneys and gonads, while EPAC2 is highly expressed in the brain and pancreas (Kawasaki, *et al.*, 1998).

The increase in cAMP within synaptosomes has been shown to activate both EPACs as well as PKA (Dao, *et al.*, 2006). Interestingly the activation of EPACs has been shown to enhance neurotransmitter release from glutamatergic synapses (Grandoch, *et al.*, 2010; Ferrero, *et al.*, 2013) (but see discussion), and has a role in regulation of exocytosis (Fernandes, *et al.*, 2015). If elevation of cAMP levels via treatment with forskolin blocks release of the RP, this could be through the activation of EPACs, as PKA regulation does not affect pool release (Chapter 3). Inhibition of EPACs with the specific inhibitor ESI-09, and a dual treatment with forskolin should reveal if EPACs are regulating RP release.

ESI-09 competitively binds to the cAMP binding domain (CBD) B-site present on the regulatory-domain of both EPAC1 and EPAC2 (Almahariq, *et al.*, 2013). This prevents EPACs undergoing a structural change which exposes the binding site for Rap1 and Rap2 on the catalytic-domain (de Rooij, *et al.*, 2000; Bos, 2006). Treatment with 100 μ M ESI-09 had no effect upon HK5C evoked release of Glu from synaptosomes compared to controls (Figure 4.4 A; Glu release: CON 745.01 \pm 91.02 (AU), ESI-09 770.86 \pm 87.99, $p > 0.05$ at 300 sec – bar chart). A pre-treatment of 100 μ M ESI-09 prior

to the 100 μ M forskolin treatment led to no significant decrease in Glu being released from the RP and RRP, compared to controls (Figure 4.4 B; Glu release: *CON* 715.96 \pm 98.03 (AU), *ESI-09 plus forskolin* 653.24 \pm 170.14, $p > 0.05$ at 300 sec). This indicates that perturbation of Glu release from the RP could be caused by the activation of EPACs due to an increase in cAMP levels, which was mediated by forskolin activating AC. The phenotype induced by forskolin was reversed by blocking EPACs before activating AC.

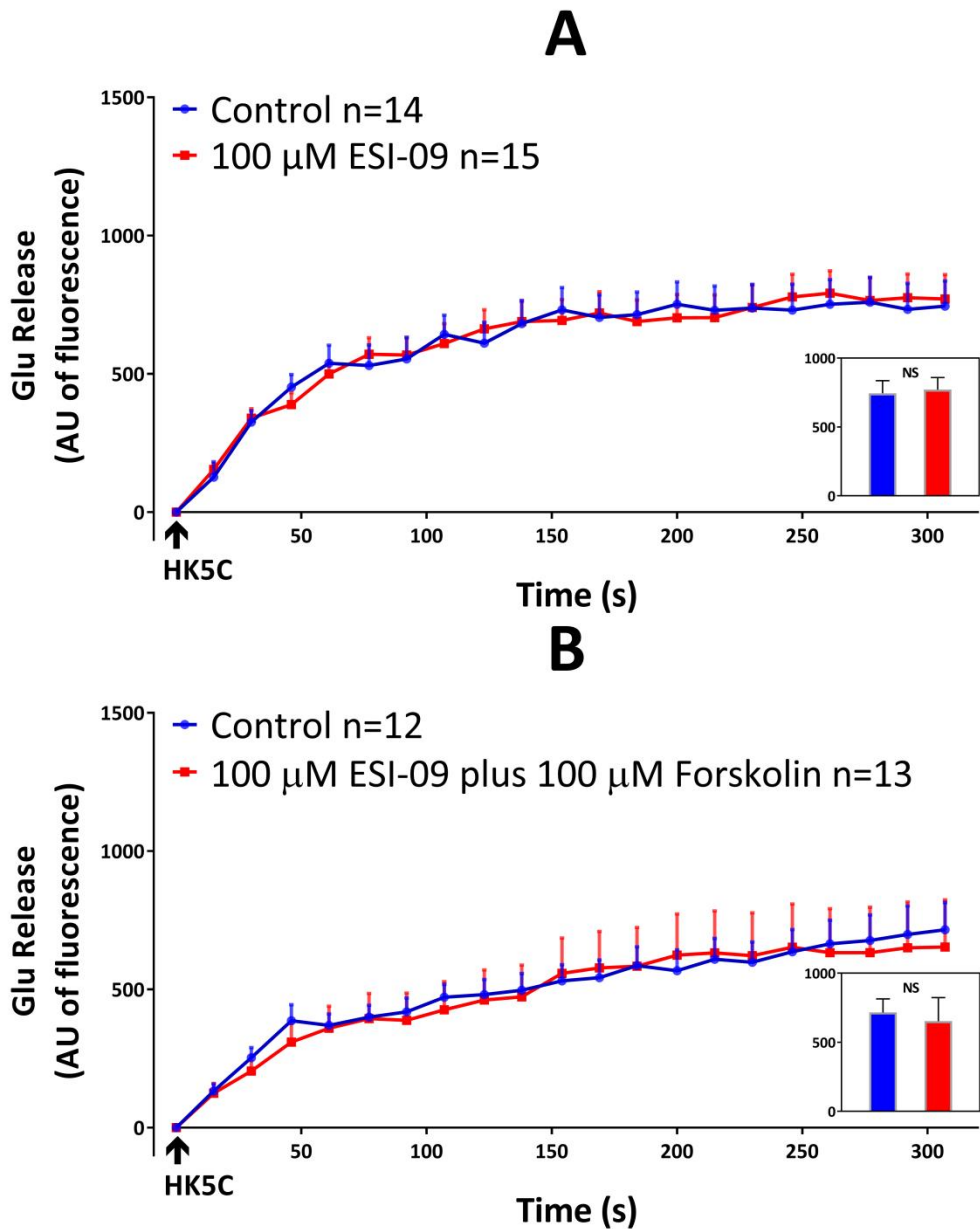


Figure 4.4: Effect of 100 μM ESI-09 and 100 μM ESI-09 plus 100 μM Forskolin upon Evoked Glu Release

(A) 100 μM ESI-09 had no significant effect upon HK5C evoked Glu release ($p=0.964$).

(B) 100 μM ESI-09 plus 100 μM forskolin was not significantly different to control with

HK5C stimulation ($p=0.823$). Inserts demonstrate final fluorescence at 300 sec. Values

represented are the mean plus S.E.M. from 4 independent experiments. *NS*, not

significant.

4.3 The Effect of AC Regulation on Evoked FM 2-10 Dye Release

4.3.1 The Effect of AC Inhibition on Evoked FM 2-10 Dye Release

The effect of 100 μ M 9-cp-ade on FM 2-10 dye release was investigated. Inhibition of AC had no effect upon FM 2-10 dye released from the RRP when stimulated with 4AP5C (Figure 4.5 A; FM dye release: *CON* -626.04 ± 418.25 (AU), *9-cp-ade* -924.86 ± 292.98 , $p > 0.05$ at 120 sec – bar chart), nor did this drug perturb the properties of the dye release from the RP and RRP when stimulated with HK5C (Figure 4.5 B; FM dye release: *CON* -1482.03 ± 224.80 (AU), *9-cp-ade* -1386.21 ± 206.10 , $p > 0.05$ at 120 sec) or ION5C (Figure 4.5 C; FM dye release: *CON* -2750.52 ± 173.69 (AU), *9-cp-ade* -2726.38 ± 211.62 , $p > 0.05$ at 120 sec). Inhibition of AC does not regulate the mode of exocytosis from either the RRP or RP evoked by these stimuli.

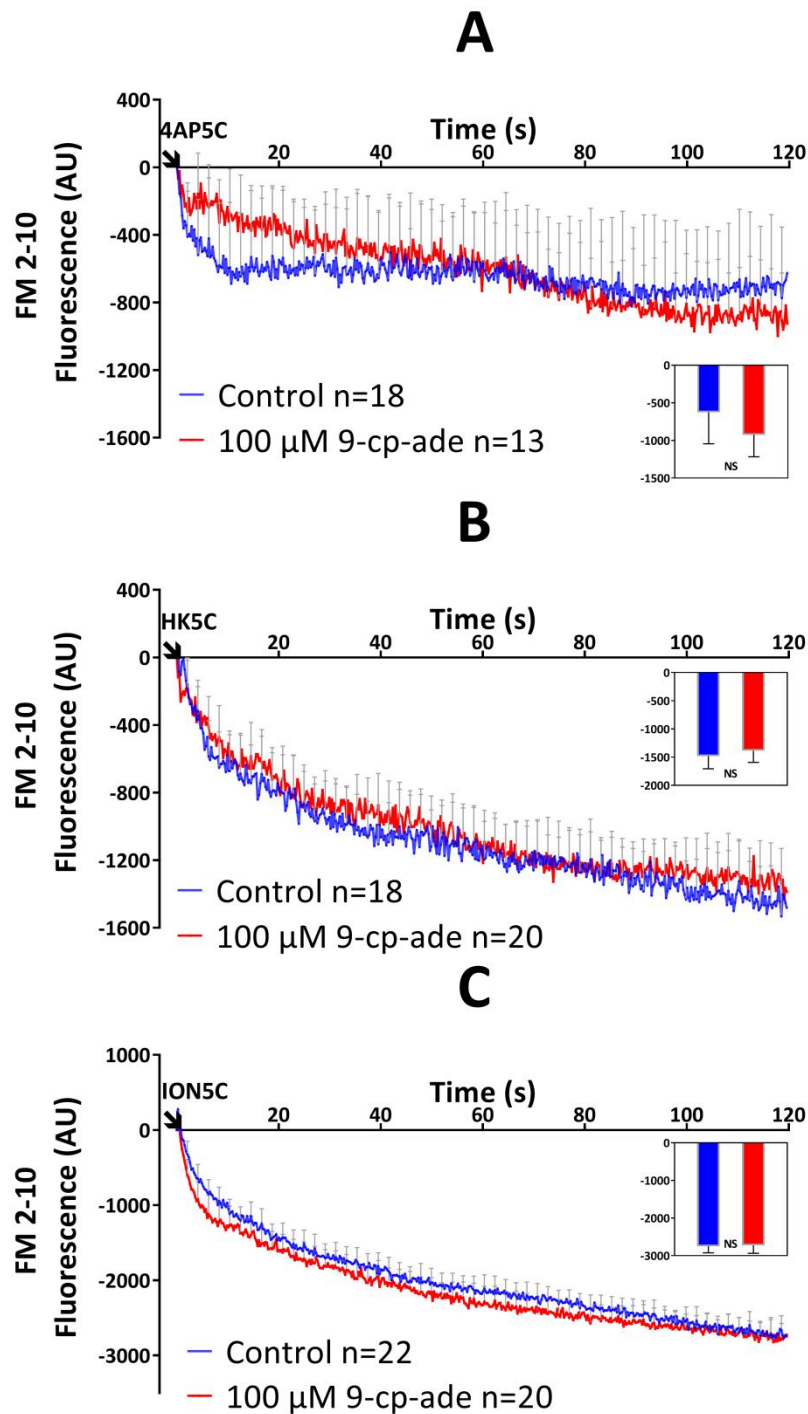


Figure 4.5: Effect of 100 μM 9-cp-ade vs Control upon Evoked FM 2-10 Dye Release

(A) 100 μM 9-cp-ade had no significant effect upon 4AP5C ($p=0.572$), (B) HK5C ($p=0.8064$) or (C) ION5C ($p=0.6343$) evoked FM 2-10 dye release, compared to drug-free controls. Inserts demonstrate final fluorescence at 120 sec. Values represented are the mean plus S.E.M. from 3 independent experiments. *NS*, not significant.

4.3.2 The Effect of AC Activation on Evoked FM 2-10 Dye Release

As forskolin disrupted release of Glu from the RP, only the RRP mode of exocytosis could be studied. Synaptosomes treated with 100 μ M forskolin released significantly less FM 2-10 dye from the RRP with 4AP5C stimulation, compared to non-drug controls (Figure 4.6 A; FM dye release: *CON* -981.65 ± 341.02 (AU), *forskolin* -437.41 ± 278.89 , $p < 0.05$ at 120 sec – bar chart). As about half of the SVs in the RRP undergo 4AP5C evoked exocytosis via FF and half by KR, the results indicate that those SVs which normally undergo a FF mode of exocytosis have been switched to a KR mode.

In order to assess if this forskolin action was specifically working through AC, a pre-treatment with 100 μ M 9-cp-ade was again employed. The amount of 4AP5C evoked FM 2-10 dye release was similar to control levels following 100 μ M 9-cp-ade pre-treatment and subsequent addition of 100 μ M forskolin (Figure 4.6 B; FM dye release: *CON* -1108.19 ± 196.61 (AU), *9-cp-ade plus forskolin* -829.59 ± 193.72 , $p > 0.05$ at 120 sec), indicating that the activation of AC does induce the RRP SVs undergoing FF to switch to KR. It should be noted that forskolin treatment did appear to cause a statistically non-significant reduction in FM dye release following the 9-cp-ade pre-treatment; but this slight decrease may be because a 5-min pre-treatment period with 9-cp-ade may not have completely inhibited all AC in the synaptosomes, so forskolin could still have a minor effect on the AC that were still active.

Though the release of RP SVs is regulated by the activity of EPACs during AC activation, the RRP mode of release may be regulated by the activity of PKA. As shown earlier (Chapter 3), inhibition of PKA with 2 μ M KT5720 causes all 4AP5C evoked SVs to undergo a FF mode of exocytosis, without perturbing Glu release (Figures 3.5 A and 3.1

A respectively). However, no change in 4AP5C evoked FM 2-10 dye is observed when PKA is activated with 50 μ M cBIMPS (Figure 3.6 A), but when PKA is inhibited with 2 μ M KT5720 before being treated with 100 μ M forskolin, control levels of FM 2-10 dye release are observed, with 4AP5C stimulation (Figure 4.7 A; FM dye release: *CON* - 1355.24 ± 258.52 (AU), *KT5720 plus forskolin* - 1656.05 ± 437.07 , $p > 0.05$ at 120 sec – bar chart); which is a significant increase in release when directly compared to FM 2-10 dye release with 100 μ M forskolin (Figure 4.7 B; FM dye release: *forskolin* - 437.41 ± 278.89 (A), *KT5720 plus forskolin* - 1656.05 ± 437.07 , $p < 0.05$ at 120 sec). This may be complicated and whilst the amount of FM 2-10 dye released is similar to control when PKA is activated (Figure 3.6), it could be that this is due to actual switching of those SVs undergoing KR to FF, and those undergoing FF to KR, so that there appears to be no change.

Figure 4.7 indicates that forskolin no longer switches the RRP SVs which undergo FF to KR but the SVs which normally undergo KR, have been switched to FF. This result is consistent with forskolin working on the RRP via activation of PKA, where PKA is inhibited. However, forskolin no longer acts, as KT5720 produces the same phenotype as KT5720 plus forskolin, it could be that the target for KT5720 is downstream of the target for forskolin such that the forskolin action may not involve PKA.

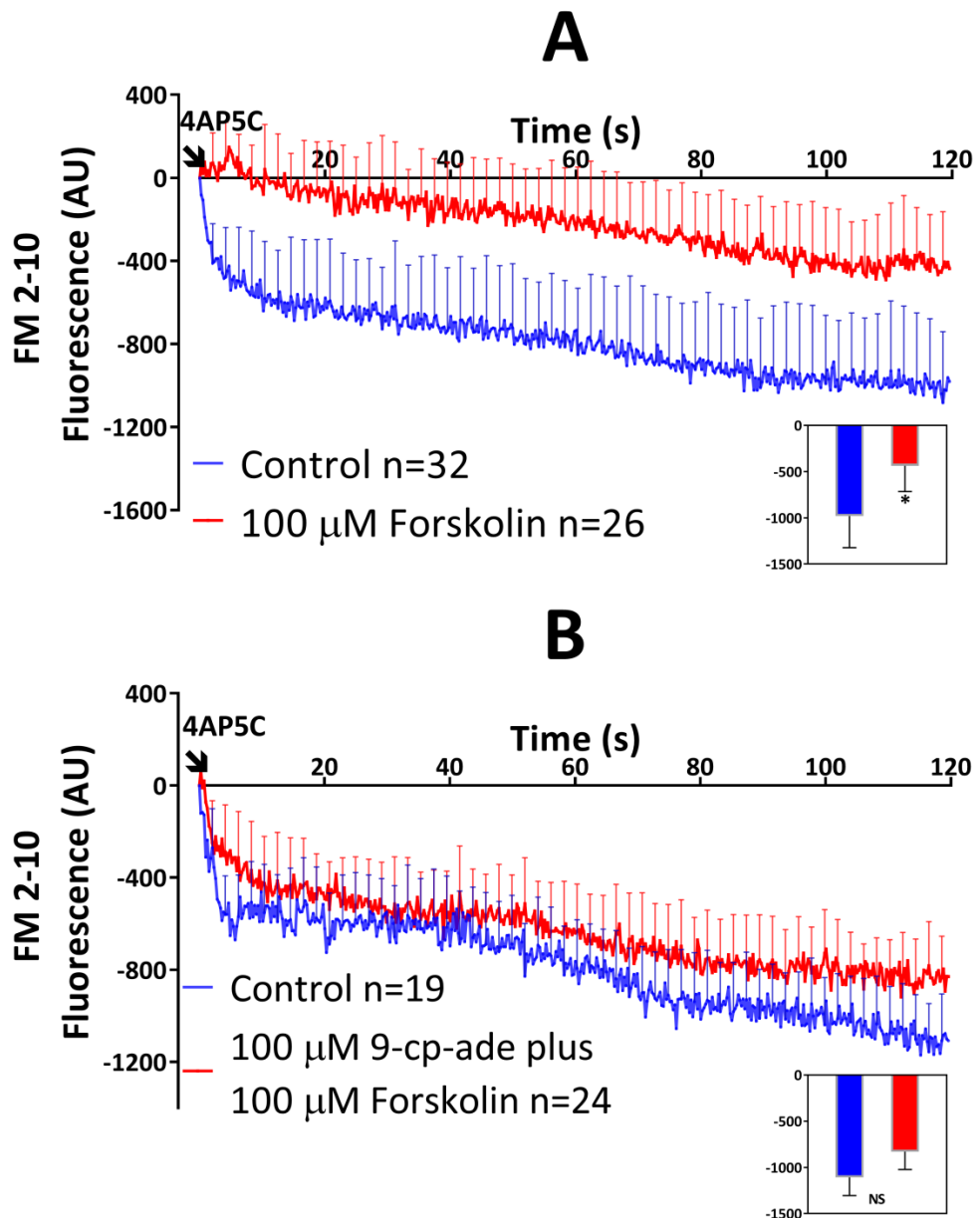


Figure 4.6: Effect of 100 μ M Forskolin; 100 μ M 9-cp-ade plus 100 μ M Forskolin upon 4AP5C Evoked FM 2-10 Dye Release

(A) 100 μ M forskolin significantly reduced the release of FM 2-10 dye from synaptosomes stimulated with 4AP5C ($p < 0.001$). (B) No significant difference in FM 2-10 dye release was observed with 100 μ M 9-cp-ade pre-treatment followed by 100 μ M forskolin, when stimulated with 4AP5C stimulation ($p > 0.145$). Inserts demonstrate final fluorescence at 120 sec. Values represented are the mean plus S.E.M. from 6 (A) and 4 (B) independent experiments. *, $p < 0.001$; NS; not significant.

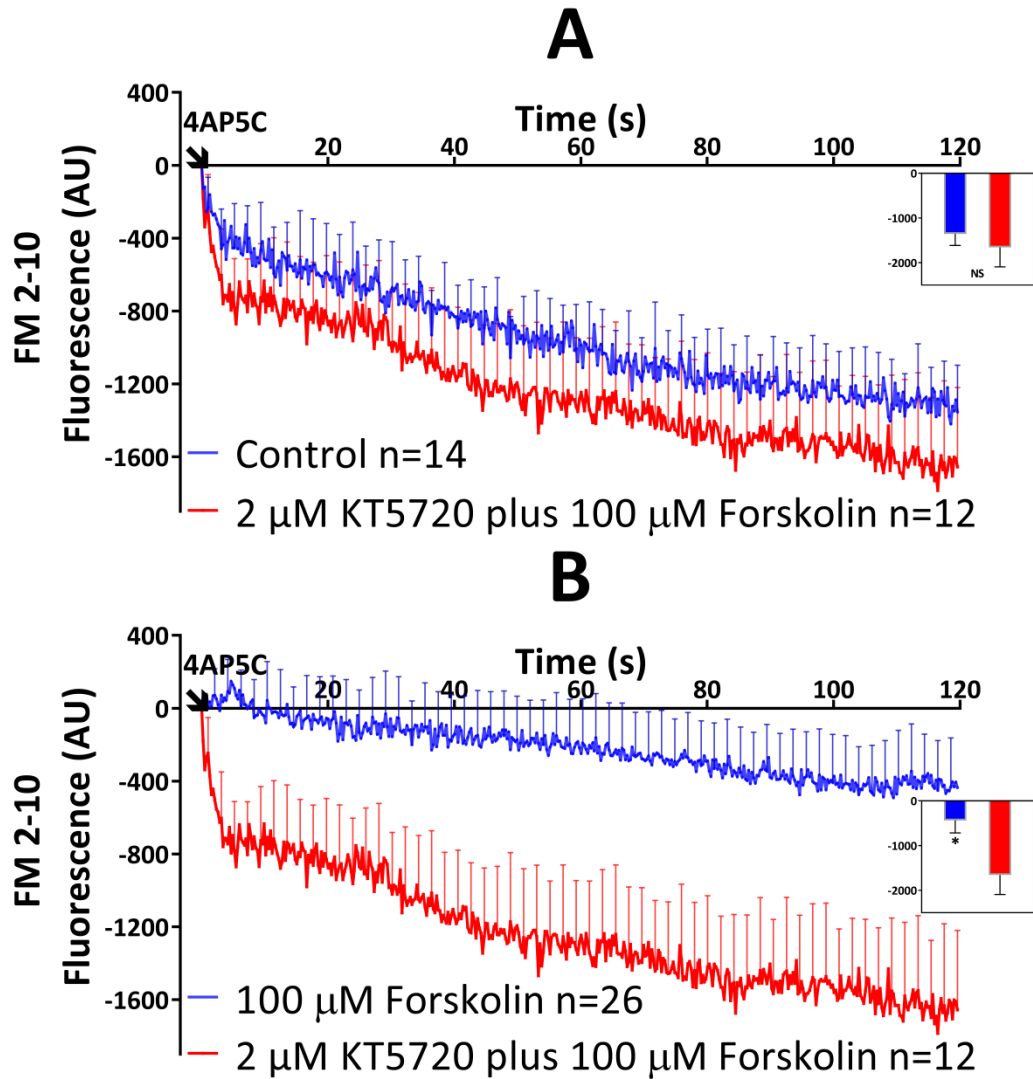


Figure 4.7: Effect of 2 μ M KT5720 Pre-treatment and 100 μ M Forskolin upon 4AP5C

Evoked FM 2-10 Dye Release

(A) Joint pre-treatment with 2 μ M KT5720 and 100 μ M forskolin is not significantly different to control values when stimulated with 4AP5C ($p > 0.05$) (B) but is a significantly increase in release compared to 100 μ M forskolin ($p < 0.001$). Inserts demonstrate final fluorescence at 120 sec. Values represented are the mean plus S.E.M. from 4 independent experiments. *, $p < 0.05$; NS, not significant.

The data with KT5720 plus forskolin, where the RRP switches to a predominantly FF mode of exocytosis resemble previous research results in which FM dye release assays were performed in synaptosomes treated with the protein phosphatase 2A (PP2A) and protein phosphatase 1 (PP1) inhibitor OA. We repeated these experiments herein. 0.8 μ M OA significantly increased FM 2-10 dye release, switching the mode of 4AP5C stimulated RRP SVs so that all undergo FF (Figure 4.8 A; FM dye release: *CON* -1207.59 ± 260.78 (AU), *OA* -1676.45 ± 163.20 , $p < 0.05$ at 120 sec – bar chart) compared to drug-free controls.

Potentially OA may stop the action of forskolin switching the majority of the RRP SVs to a KR mode of exocytosis, just as was found above with KT5720. However, synaptosomes treated with 0.8 μ M OA plus 100 μ M forskolin still released significantly less dye than controls (Figure 4.8 B; FM dye release: *CON* -1207.59 ± 260.78 (AU), *OA plus forskolin* -428.76 ± 234.42 , $p < 0.05$ at 120 sec), and this was similar to forskolin action alone (see Figure 4.6 A). This is clearly different to the KT5720 action, which prevented the effects of forskolin, and this suggests that OA might act on a different substrate to the one that forskolin works on or that forskolin acts downstream of OA.

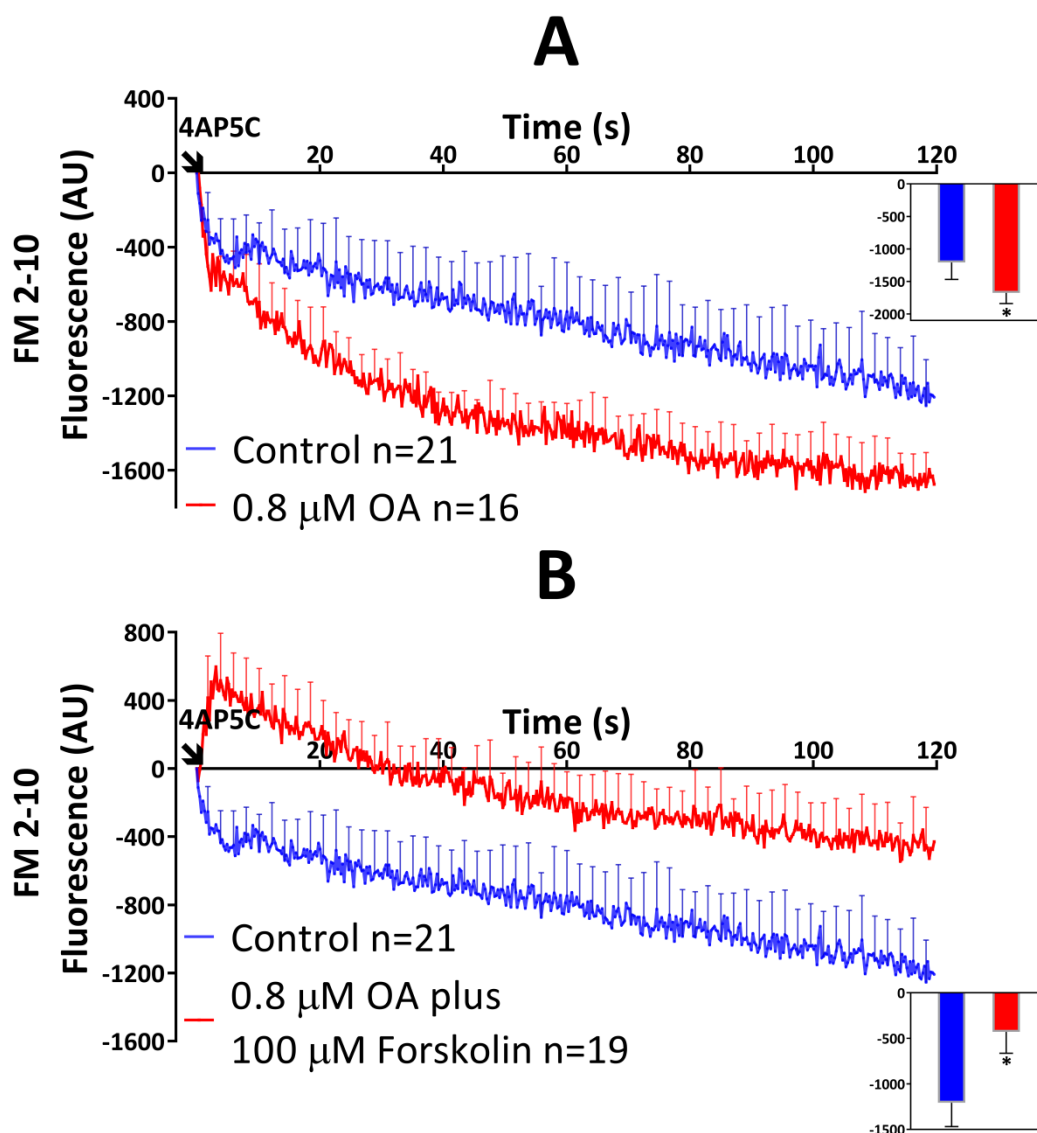


Figure 4.8: Effect of 0.8 μ M OA; 0.8 μ M OA plus 100 μ M Forskolin upon 4AP5C Evoked FM 2-10 Dye Release

(A) 0.8 μ M OA treatment significantly increased 4AP5C evoked FM 2-10 dye release ($p < 0.001$). (B) 0.8 μ M OA pre-treatment with 100 μ M forskolin treatment significantly decreased FM 2-10 dye release when compared to control ($p < 0.001$). Inserts demonstrate final fluorescence at 120 sec. Values represented are the mean plus S.E.M. from 4 independent experiments. *, $p < 0.001$.

4.4 The Effect of AC Regulation on Evoked Changes in $[Ca^{2+}]_i$

4.4.1 The Effect of AC Inhibition on Evoked Changes in $[Ca^{2+}]_i$

Although inhibition of AC with 9-cp-ade did not lead to any significant changes to the maximal release of Glu, or to the mode of exocytosis for either the RRP or RP, it is still possible that such treatments may induce changes to evoked $[Ca^{2+}]_i$ levels within the synaptosomes (as discussed in Chapter 3). This was tested by using Fura-2 to measure evoked changes in $[Ca^{2+}]_i$ following such drug treatment.

Synaptosomes treated with 100 μ M 9-cp-ade exhibited no significant change to $[Ca^{2+}]_i$ levels compared to non-drug treated controls, when stimulated with 4AP5C (Figure 4.9 A; $[Ca^{2+}]_i$: CON 285.13 ± 37.11 (nM), 9-cp-ade 287.96 ± 38.29 , $p > 0.05$, final time point), HK5C (Figure 4.9 B; $[Ca^{2+}]_i$: CON 378.26 ± 28.09 (nM), 9-cp-ade 357.40 ± 24.54 , $p > 0.05$, final time point) or ION5C (Figure 4.9 C; $[Ca^{2+}]_i$: CON 1711.58 ± 147.26 (nM), 9-cp-ade 1780.90 ± 121.30 , $p > 0.05$, final time point). Thus, whilst 9-cp-ade does have an effect upon the terminals as it reversed the action of forskolin (Figures 4.3 B and 4.6 B) and must therefore block AC, it does not cause any changes to the evoked level of $[Ca^{2+}]_i$.

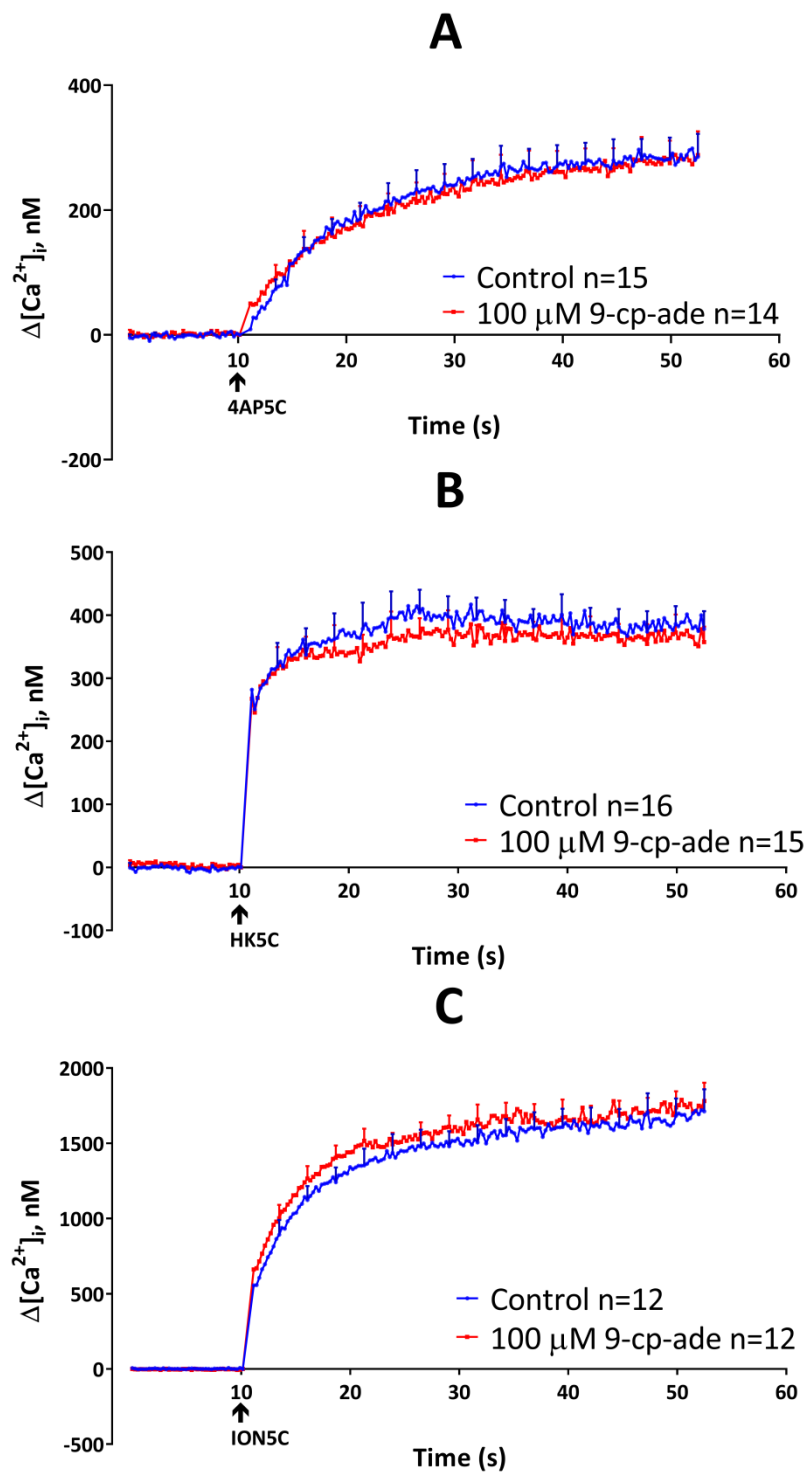


Figure 4.9: Effect of 100 μM 9-cp-ade vs Control upon Evoked $[\text{Ca}^{2+}]_i$ Levels

(A) 100 μM 9-cp-ade did not significantly change $[\text{Ca}^{2+}]_i$ levels when stimulated with 4AP5C ($p=0.649$), (B) HK5C ($p=0.271$) or (C) ION5C ($p=0.289$), compared to drug-free controls. Values represented are the mean plus S.E.M. from 3 independent experiments.

4.4.2 The Effect of AC Activation on Evoked Changes in $[Ca^{2+}]_i$

As the inhibition of AC caused no significant change to $[Ca^{2+}]_i$, the activation of AC with forskolin was investigated. The activation of AC increased the intracellular cAMP level, which blocked release of the RP via activation of EPACs, when stimulated with HK5C or ION5C (Figure 4.2 B and C). Furthermore, the activation of AC caused most RRP SVs stimulated by 4AP5C to exocytosis by a KR mode (Figure 4.6 A). Previous research by A. Ashton's group (Ashton, manuscript in preparation), and others (Alés, *et al.*, 1999), have demonstrated that increases in levels of $[Ca^{2+}]_i$ can switch more SVs to undergo exocytosis via KR (see Section 1.9.4; Figure 1.11). Thus, an investigation was carried out to determine whether the action of forskolin may be due to changes in evoked $[Ca^{2+}]_i$.

Synaptosomes treated with 100 μ M forskolin exhibited a significant increase in 4AP5C evoked $[Ca^{2+}]_i$ levels (Figure 4.10 A; $[Ca^{2+}]_i$: CON 160.07 ± 14.58 (nM), *forskolin* 222.96 ± 21.56 , $p > 0.05$, final time point), whilst HK5C evoked $[Ca^{2+}]_i$ levels decreased significantly (Figure 4.10 B; $[Ca^{2+}]_i$: CON 465.36 ± 34.20 (nM), *forskolin* 368.38 ± 19.83 , $p > 0.05$, final time point). The 4AP5C data would suggest that AC activation and rising cAMP levels increased the level of $[Ca^{2+}]_i$, causing RRP SVs to switch to a KR mode of exocytosis. Research by Ashton and colleagues, has determined that the release of the RP requires a sufficient increase in the average $[Ca^{2+}]_i$ throughout the terminal, and this explains why in control conditions 4AP5C fails to stimulate release of the RP; as it does not produce as significant a $[Ca^{2+}]_i$ increase as HK5C or ION5C (Figure 1.8). The slight increase in the 4AP5C evoked $[Ca^{2+}]_i$ is still not sufficient to induce RP SVs to exocytose; however, forskolin inhibiting release of the RP (Figure 4.6), could be explained by the

average amount of HK5C evoked $[Ca^{2+}]_i$ change within the terminals being insufficient to induce the mobilisation and fusion of the RP, with this drug (Figure 4.10 B).

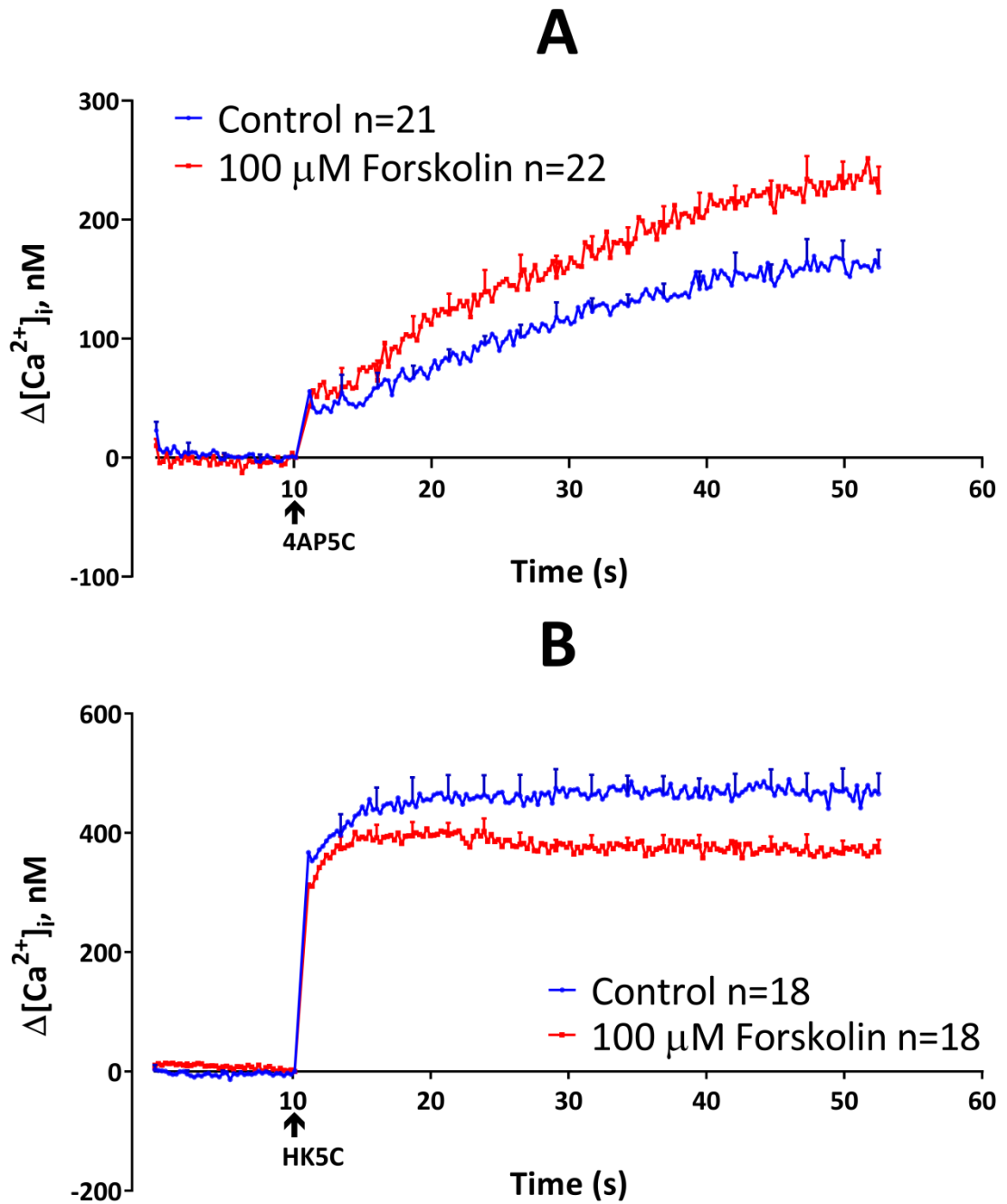


Figure 4.10: Effect of 100 μM Forskolin vs Control upon Evoked $[\text{Ca}^{2+}]_i$ Levels

(A) 100 μM forskolin significantly increased $[\text{Ca}^{2+}]_i$ levels when stimulated with 4AP5C ($p < 0.001$), (B) but significantly decreased $[\text{Ca}^{2+}]_i$ levels when stimulated with HK5C ($P < 0.001$). Values represented are the mean plus S.E.M. from 4 independent experiments.

4.4.3 The Effect of EPAC Inhibition upon Evoked Changes in $[Ca^{2+}]_i$

AC activation with forskolin decreased the HK5C evoked level of $[Ca^{2+}]_i$ within the terminals (Figure 4.10 B), and blocked release of SVs from the RP (Figure 4.2 B). When EPACs were inhibited with ESI-09 and AC was activated with forskolin, RP SV release was restored for HK5C stimulation (Figure 4.4 B). The inhibition of EPACs may restore RP release by increasing the level of $[Ca^{2+}]_i$, thus it is important to establish what effects inhibition of EPACs had upon evoked changes in $[Ca^{2+}]_i$ levels.

Synaptosomes treated with 100 μ M ESI-09 exhibited a significant increase in evoked $[Ca^{2+}]_i$ levels when stimulated with 4AP5C (Figure 4.11 A; $[Ca^{2+}]_i$: CON 209.72 \pm 24.84 (nM), ESI-09 307.70 \pm 31.73, $p < 0.05$, final time point) and HK5C (Figure 4.11 B; $[Ca^{2+}]_i$: CON 378.26 \pm 28.09 (nM), ESI-09 643.52 \pm 47.22, $p < 0.001$, final time point), compared to non-drug treated controls. As the inhibition of EPACs is able to increase in $[Ca^{2+}]_i$ level significantly, this may explain how ESI-09 pre-treatment followed by forskolin is able to restore RP release.

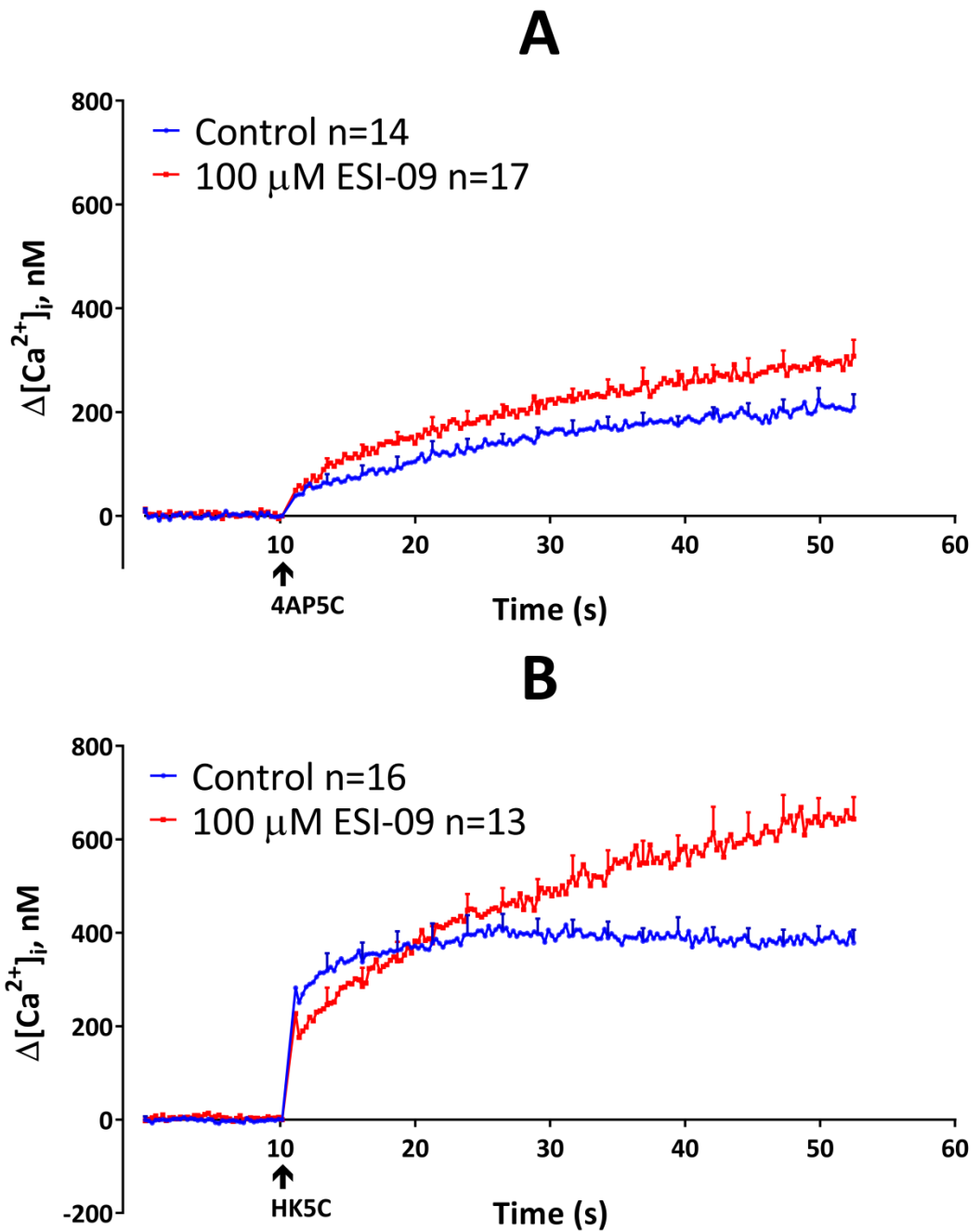


Figure 4.11: Effect of 100 μM ESI-09 vs Control upon Evoked $[\text{Ca}^{2+}]_i$ Levels

(A) 100 μM ESI-09 significantly increased evoked $[\text{Ca}^{2+}]_i$ when stimulated with 4AP5C ($p < 0.001$), and (B) HK5C ($P < 0.001$), when compared to drug-free controls. Values represented are the mean plus S.E.M from 3 independent experiments.

To determine if forskolin was working to decrease HK5C evoked $[Ca^{2+}]_i$ levels through EPACs activation, synaptosomes were pre-treated with 100 μ M ESI-09 (to inhibit EPACs) then 100 μ M forskolin. These treated synaptosomes exhibited a significant increase in the level of 4AP5C evoked $[Ca^{2+}]_i$ (Figure 4.12 A; $[Ca^{2+}]_i$: CON 206.02 ± 22.34 (nM), *ESI-09 plus forskolin* 543.58 ± 37.18 , $p < 0.001$, final time point), and HK5C evoked $[Ca^{2+}]_i$ (Figure 4.12 B; $[Ca^{2+}]_i$: CON 384.97 ± 20.15 (nM), *ESI-09 plus forskolin* 704.22 ± 42.07 , $p < 0.001$, final time point). This demonstrates that inhibition of EPACs reverses the action of forskolin to inhibit the release of the RP by raising the evoked changes in $[Ca^{2+}]_i$ levels within the terminals.

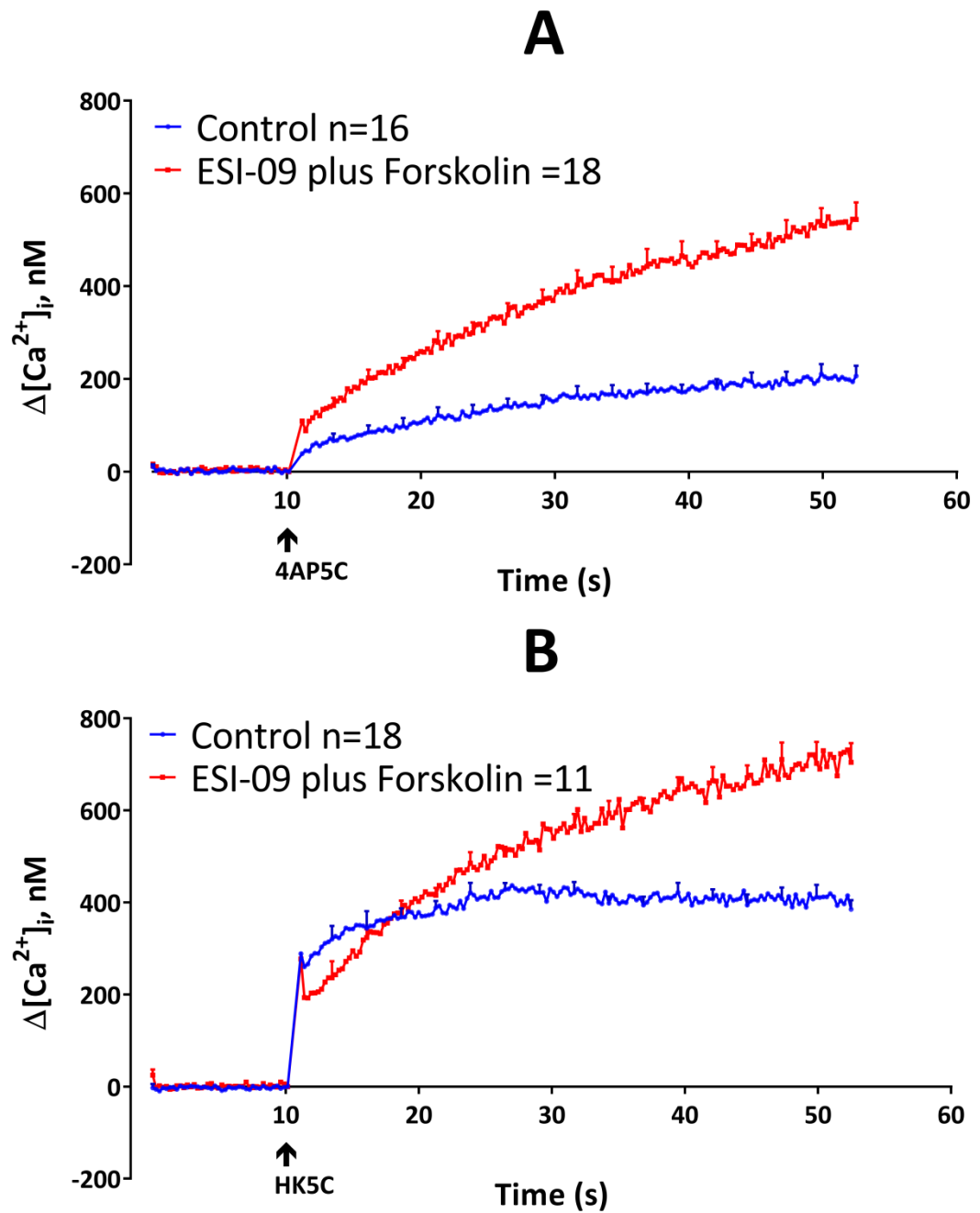


Figure 4.12: Effect of 100 μ M ESI-09 plus 100 μ M Forskolin upon Evoked $[Ca^{2+}]_i$ Levels

(A) 100 μ M ESI-09 plus 100 μ M forskolin significantly increased evoked $[Ca^{2+}]_i$ when stimulated with 4AP5C ($p < 0.001$), (B) and HK5C ($p < 0.001$), compared to controls. Values represented are the mean plus S.E.M from 3 independent experiments.

4.5 The Effect of the Regulation of AC on Nerve Terminal Bioenergetics

4.5.1 The Effect of AC Inhibition on Nerve Terminal Bioenergetics

Potentially changes in Glu release, mode of exocytosis and $[Ca^{2+}]_i$ levels (or the lack of), may be mediated by the synaptosomes being non-specifically perturbed by the drug treatments. Synaptosomes treated with 100 μ M 9-cp-ade were subjected to the bioenergetics Mito-Stress test to determine if they were still metabolically viable after 90-min at 37°C. No significant difference in bioenergetics was observed between terminals treated with 100 μ M 9-cp-ade or controls (Figure 4.13) and furthermore, this treatment did not have any significant effects upon the 6 aspects of mitochondrial function (Figure 4.14 A-F).

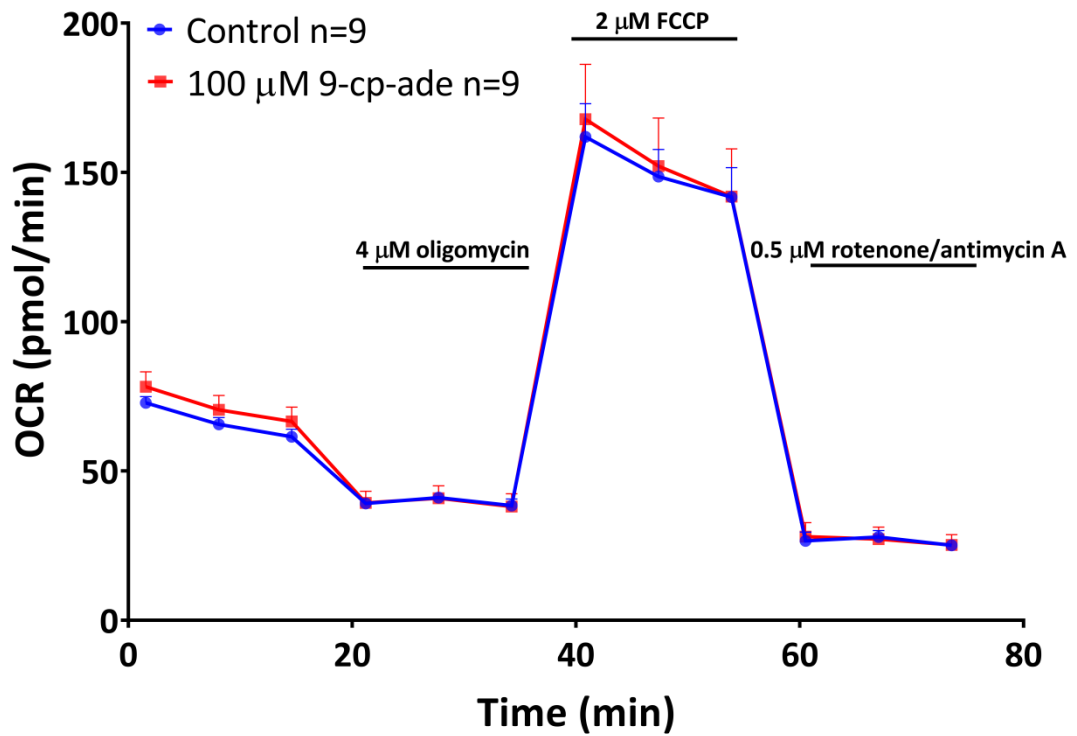


Figure 4.13: Effect of 100 μM 9-cp-ade upon Synaptosomal Bioenergetics

A treatment of 100 μM 9-cp-ade did not significantly affect the bioenergetics of synaptosomes during a Mito-Stress test ($p=0.920$). Values represented are the means plus S.E.M. from 3 independent experiments. Experiment performed at 37°C in the Seahorse Xfp flux analyser.

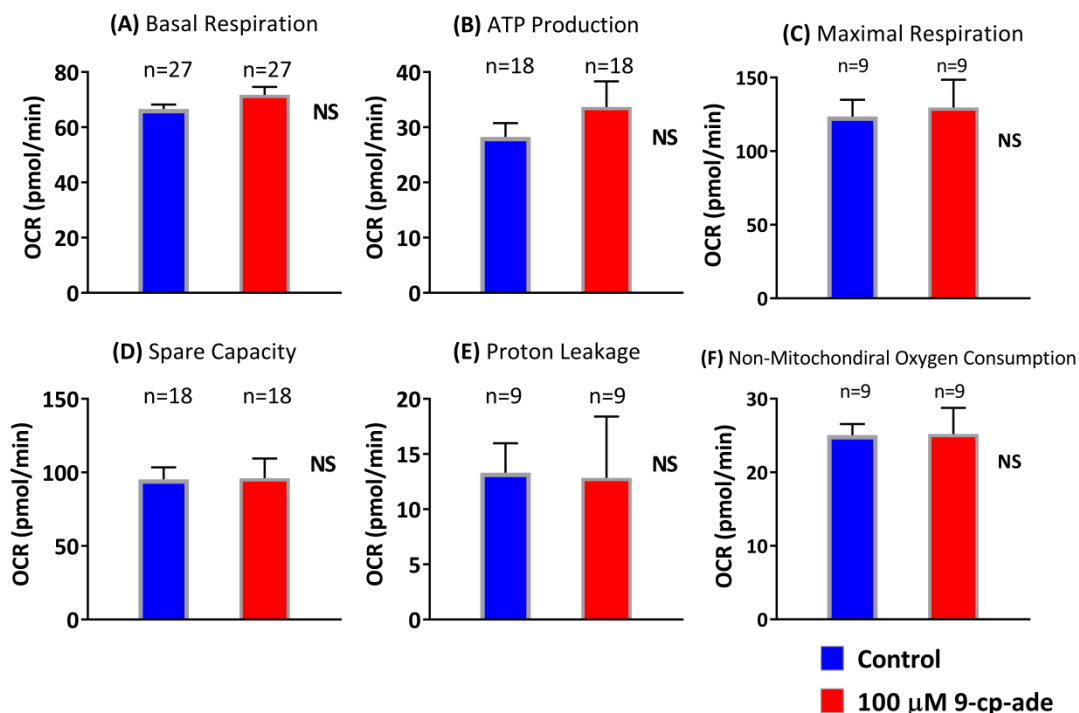


Figure 4.14: Effect of 100 μM 9-cp-ade upon Mitochondrial Function

(A) Synaptosomes treated with 100 μM 9-cp-ade exhibited no significant change in basal respiration over the first 15 min, (B) ATP production at 20-35 min, (C) maximal respiration at 40-55 min, (D) spare capacity at 40-55 min, (E) proton leakage at 20-35 min, (F) or non-mitochondrial oxygen consumption compared to control synaptosomes (all conditions, $p > 0.05$). Values represented are the mean plus S.E.M. from 3 independent experiments. NS, not significant.

4.5.2 The Effect of AC Activation on Nerve Terminal Bioenergetics

Synaptosomes treated with 100 μM forskolin were subjected to the bioenergetics Mito-Stress test, and displayed no significant changes in metabolic viability, when compared with untreated controls (Figure 4.15). Such treatment also did not affect the 6 aspects of mitochondrial function measured during a Mito-Stress test (Figure 4.16 A-F).

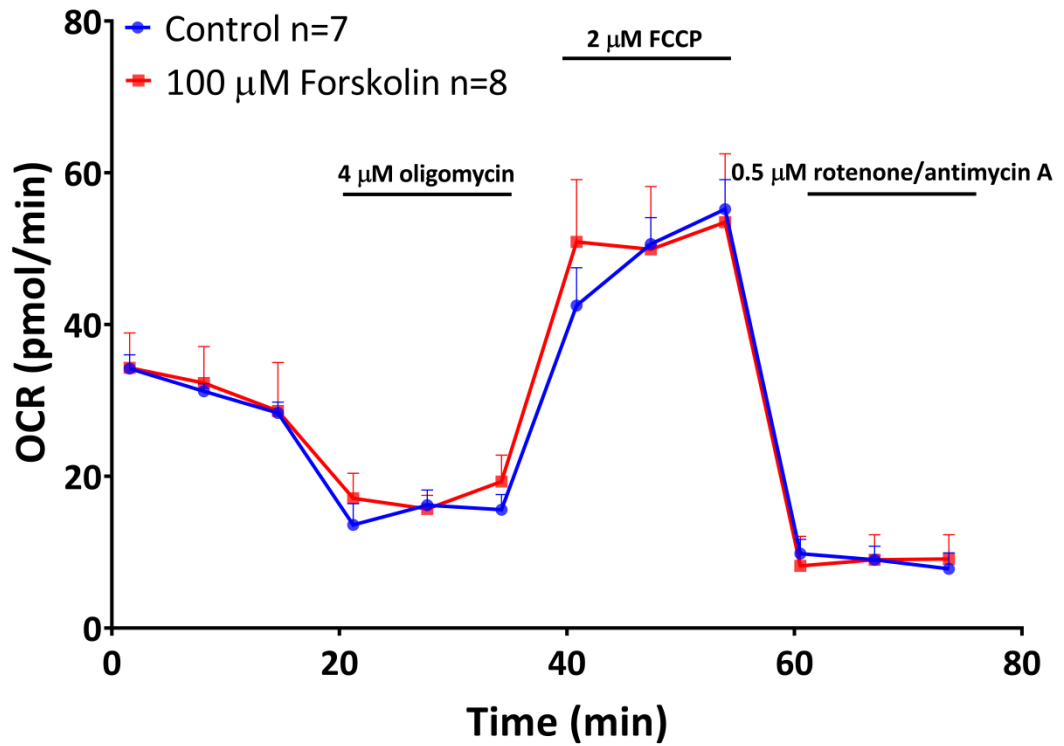


Figure 4.15: Effect of 100 μM Forskolin upon Synaptosomal Bioenergetics

A treatment of 100 μM forskolin did not significantly affect the OCR of synaptosomes during a Mito-Stress test ($p=0.868$). Values represented are the means plus S.E.M. from 3 independent experiments. Experiment performed at 37°C in the Seahorse Xfp flux analyser.

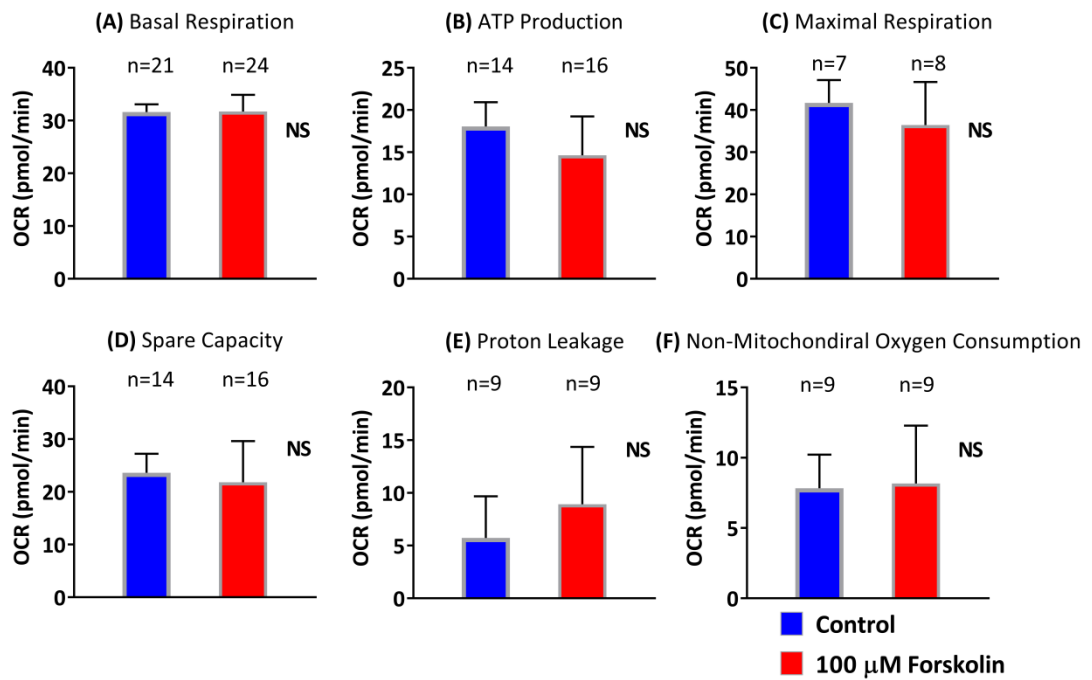


Figure 4.16: Effect of 100 μM Forskolin upon Mitochondrial Function

(A) Synaptosomes treated with 100 μM forskolin exhibited no significant change in basal respiration at 0-15 min, (B) ATP production at 20-35 min, (C) maximal respiration at 40-55 min, (D) spare capacity at 40-55 min, (E) proton leakage at 20-35 min, (F) or non-mitochondrial oxygen consumption at 60-75 min, compared to controls (all conditions, $p > 0.05$). Values represented are the mean plus S.E.M. from 3 independent experiments. *NS*, not significant.

Figure 4.13 and Figure 4.15 demonstrate that the OCR of synaptosomes was not affected by treatment with either 9-cp-ade or forskolin respectively, over 80 min at 37°C. This suggests that the integrity of the synaptosomes would not be perturbed during the acute treatments used in the other assays (≤ 5 -min); any changes to Glu release, FM 2-10 dye release or $[Ca^{2+}]_i$ reflect specific action of the drugs upon their targets and not non-specific action within the synaptosomes. Both Figure 4.14 and Figure 4.16 determine that 9-cp-ade and forskolin respectively have no significant effect upon any aspect of mitochondrial function or responses that were measured and do not impact synaptosomal activity.

4.5.3 The Effect of EPACs Inhibition on Nerve Terminal Bioenergetics

Blocking EPACs with ESI-09 does not perturb Glu release (Figure 4.4 A), but is able to prevent forskolin from blocking the release of RP SVs by increasing the level of $[Ca^{2+}]_i$ (Figure 4.11 B). Treatment with ESI-09 could raise the $[Ca^{2+}]_i$ level through the perturbation of the synaptosomes, thus terminals treated with 100 μ M ESI-09 were subjected to the bioenergetics Mito-Stress test. No significant difference in the viability of synaptosomes was observed when compared to controls (Figure 4.17). Treatment with 100 μ M ESI-09 did not significantly affect several aspect of mitochondrial function (Figure 4.18 A-D and F), but did significantly increase proton leakage (Figure 4.18 E), when compared to controls.

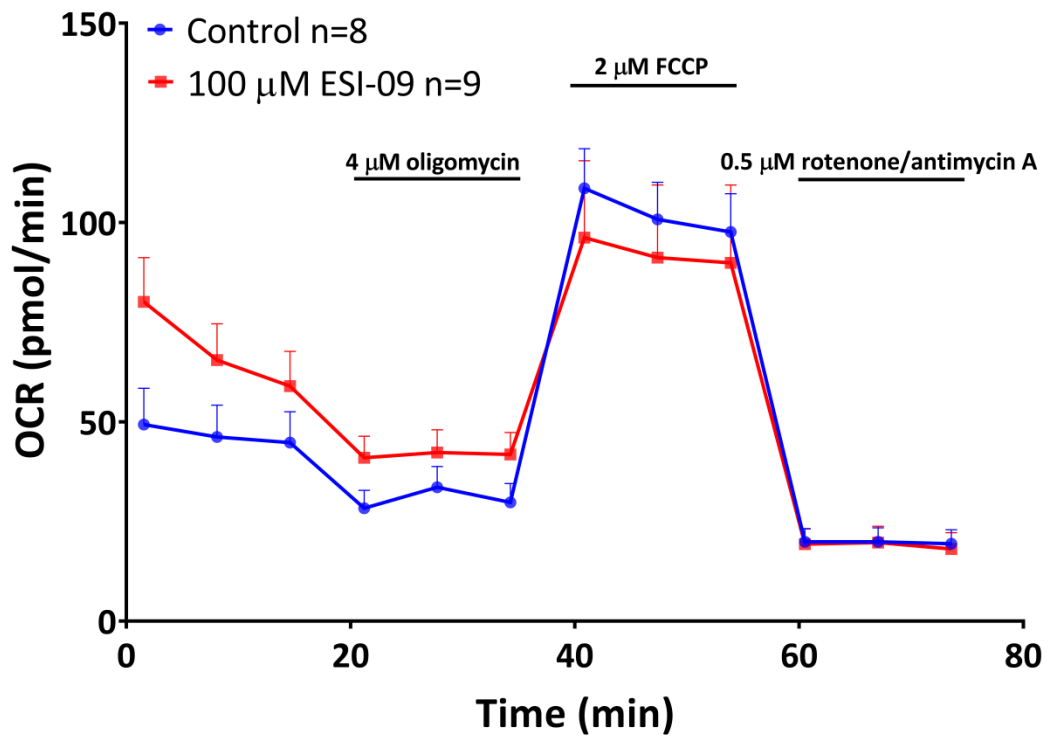


Figure 4.17: Effect of 100 μM ESI-09 upon Synaptosomal Bioenergetics

A treatment of 100 μM ESI-09 had no significant effect upon the OCR of synaptosomes during a Mito-stress test ($p=0.672$). Values represented are the mean plus S.E.M. from 3 independent experiments. Experiment performed at 37°C in the Seahorse Xfp flux analyser.

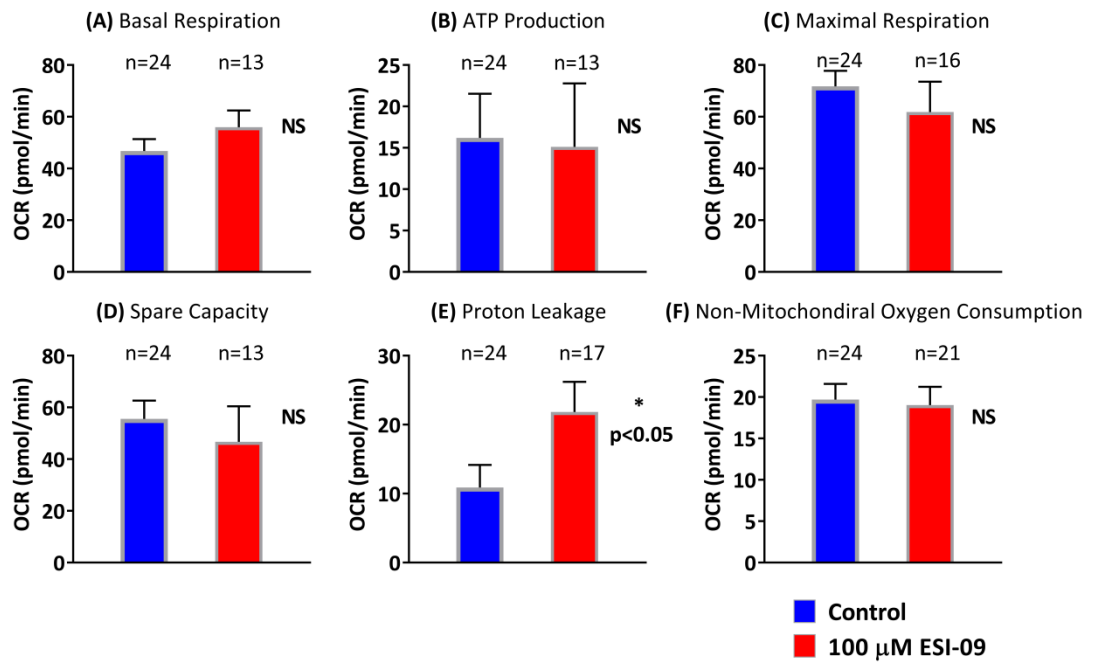


Figure 4.18: Effect of 100 μM ESI-09 upon Mitochondrial Function

(A) 100 μM ESI-09 had no significant effect upon basal respiration over the first 15 min, (B) ATP production at 20-35 min, (C) maximal respiration at 40-55 min, (D) spare capacity at 40-55 min, (F) and non-mitochondrial oxygen consumption at 60-75 min, compared to controls ($p < 0.05$), (E) but did increase proton leakage at 20-35 min ($p > 0.05$). Values represented are the mean plus S.E.M. from 3 independent experiments. *, $p < 0.05$; NS, not significant.

Figure 4.17 demonstrates that EPACs inhibition via 100 μ M ESI-09 had no significant effect upon the bioenergetics of synaptosomes during a Mito-Stress test at 37°C for 90-min, suggesting that an acute drug treatment (\leq 5-min), as used in the other assays, would not disrupt the synaptosomes integrity by producing non-specific affects upon the measurements taken. Figure 4.18 shows the ESI-09 did not perturb any of the 6 aspects of mitochondrial function, over the 90-min assay apart from the proton leakage. The relevance of this is not understood, however, part of the apparent larger proton leakage is due to the higher basal respiration (Figure 4.17), which although is statistically not significant means that following treatment with oligomycin there is higher oxygen consumption in ESI-09 treated terminals. Whilst following rotenone/antimycin A treatment there is similar oxygen consumption, so the difference between these parameters – which is the measure of proton leakage – can explain this.

4.6 Discussion

As discussed in Chapter 3, PKA is able to switch the mode of exocytosis differently for each SV pool, and this could be through the phospho-regulation of Dyn-I activity. PKA is specifically activated by the binding of cAMP which is synthesised by AC (Walsh, *et al.*, 1968). This chapter investigated the role AC and cAMP play in the regulation of the modes of Glu release in synaptosomes.

cAMP is well known to regulate Ca^{2+} -triggered exocytosis, by modifying the molecular machinery (Chen and Regehr, 1997), and in neurons cAMP has been shown to increase NT release and has been implicated in LTP (Huang, *et al.*, 1995; Weisskopf, *et al.*, 1994), which is important for synaptic plasticity. However, this may simply be through the activation of PKA. As discussed in Chapter 3, increases to PKA can enhance NT release, unless NT release is at maximal. Other research on increasing cAMP levels however, has demonstrated a disruption to vesicular mobility (Petrov, *et al.*, 2008), and this could be through the activation of both PKA and EPACs (Dao, *et al.*, 2006; Grandoch, *et al.*, 2010). Since the discovery of EPACs (de Rooij, *et al.*, 1998), many PKA-independent cAMP effects have been shown to be the result of EPACs activation (Beaumont, *et al.*, 2002).

AC was inhibited with 9-cp-ade and activated with forskolin and EPACs were inhibited with ESI-09 to determine how these treatments would affect the release of Glu, the modes of exocytosis for distinct SV pools, and the levels of $[\text{Ca}^{2+}]_i$.

4.6.1 Evoked Glu Release

Inhibition of AC does not regulate the release of Glu from synaptosomes. Glu was released at control levels from the RRP when treated with 9-cp-ade and stimulated with 4AP5C (Figure 4.1 A). Treatment with 9-cp-ade did not disrupt Glu release from the RP when stimulated with HK5C (Figure 4.1 B) or ION5C (Figure 4.1 C). These data demonstrate that the same number of SVs were undergoing release in both drug and non-drug treated synaptosomes during stimulation, as discussed in Chapter 3. As no SVs are recycling and only one round of release is being studied (Section 1.9.2), the inhibition of AC and the decrease in cAMP concentration does not have a role regulating the release of SV pools from synaptosomes, when these are stimulated to evoked maximal release of either pool.

Activation of AC blocks the exocytosis of RP SVs. Glu was released at control levels from the RRP in synaptosomes treated with forskolin and stimulated with 4AP5C (Figure 4.2 A), indicating all RRP SVs were released. However, synaptosomes treated with forskolin exhibited a loss of Glu release when stimulated with HK5C (Figure 4.2 B), or ION5C (Figure 4.2 C). Intriguingly this loss was specifically from the RP as RRP release was not perturbed with 4AP5C stimulation (Figure 4.2 A).

If Forskolin treatment were blocking the release of all SVs when stimulating with HK5C or ION5C no observed Glu release would be seen for these stimuli, which is not the case (Figure 4.2 B and C). As the RRP is not perturbed by forskolin, its action specifically blocks RP SV release by increasing intracellular levels of cAMP.

Petrov and colleagues who utilised cAMP analogues to activate cAMP-dependent proteins reported a similar disruption to SV mobility and NT release (Petrov, *et al.*, 2008). They theorised that activation of cAMP-dependent proteins disrupted the transport of vesicles from a pool termed 'the mobilisation pool' (which is equivalent to the RP discussed in this thesis). Thus, the increase in intracellular cAMP levels activates cAMP-dependent proteins which prevent the release of RP SVs.

Forskolin was specifically working on AC as both 100 μ M of the inactive homologue 1,9-did-forsk, and 100 μ M 9-cp-ade pre-treatment before 100 μ M forskolin, demonstrated Glu release at levels identical to untreated controls (Figure 4.3 A-C). As no loss in Glu release was seen for PKA activation with cBIMPS in Chapter 3 (Figure 3.2), the loss of Glu release from the RP seen when cAMP are raised by AC activation, could be mediated by the activation of EPACs, or a change in $[Ca^{2+}]_i$.

The specific inhibitor of EPACs, ESI-09, did not significantly perturb HK5C evoked Glu release (Figure 4.4 A), and 100 μ M ESI-09 pre-treatment plus 100 μ M forskolin restored Glu release to control levels (Figure 4.4 B). Thus the activation of EPACs, specifically by increasing cAMP levels, is able to block release of the RP of SVs.

Though the inhibition of AC and the presumed lowering of intracellular cAMP levels does not regulate the release dynamics of SV pools, the activation of AC, and the increase in cAMP can block the release of RP SVs specifically through the activation of EPACs. As EPACs have been shown to activate Rap1 and Rap2 (de Rooij, *et al.*, 1998; Kawasaki, *et al.*, 1998), it could be downstream targets of Rap1 and Rap2 play a direct role in the mobilisation of SVs from the RP during stimulation. Indeed Rap proteins

have been implicated in synaptic long-term depression (LTD) (Zhu, *et al.*, 2002), the inhibition of transmission at glutamatergic synapses (Imamura, *et al.*, 2003), at the frog neuromuscular junction (Petrov, *et al.*, 2008), and the indirect disruption of the actin cytoskeleton (Taira, *et al.*, 2004).

Considering cAMP is a vital secondary messenger, the activation of AC may produce a high enough cAMP concentration to saturate PKA (which binds cAMP in the range of 5.0-24.6 nM) and activate EPACs, this may suggest that EPACs have a lower cAMP sensitivity than PKA, allowing for activation either individually or cooperatively (Seino and Shibasaki, 2005; Dao, *et al.*, 2006).

4.6.2 Evoked FM 2-10 Dye Release

AC inhibition does not regulate the mode of SV exocytosis in synaptosomes. FM 2-10 was released at control levels from the RRP when stimulated with 4AP5C (Figure 4.5 A), and from the RRP and RP when stimulated with HK5C (Figure 4.5 B) and ION5C (Figure 4.5 C). These data highlight that lowering the intracellular cAMP level does not play a role in switching the mode of release for SVs from either the RRP or the RP.

AC activation does regulate the mode of SV exocytosis, for the RRP. As the RP did not undergo exocytosis during forskolin treatment (Figure 4.2), only the mode of the RRP could be determined. Treatment with 100 μ M forskolin led to a significant decrease in FM 2-10 dye release when stimulated with 4AP5C (Figure 4.6 A), indicating SVs which release via FF in control conditions had been switched to a KR mode of exocytosis. This mode switch was significantly reduced when synaptosomes were pre-treated with 100 μ M 9-cp-ade (to inhibit AC) before 100 μ M forskolin, which restored FM 2-10 dye

release to control levels (Figure 4.6 B). Thus, forskolin is activating AC and increasing cAMP levels to switch the mode of RRP SVs to KR, and blocking AC can reverse this effect.

However it was not clear if the RRP mode of release was being regulated by EPACs or PKA. As inhibition of PKA with KT5720 produces a majority FF mode of exocytosis when stimulated with 4AP5C (Figure 3.5 A), it was theorised that forskolin may work to switch the RRP mode by activating PKA via increased cAMP levels. Thus, synaptosomes were pre-treated with 2 μ M KT5720 (to inhibit PKA) plus 100 μ M forskolin and FM 2-10 dye release was studied with 4AP5C stimulation (Figure 4.7). A significant increase in FM 2-10 dye release was seen, indicating a switch to a FF mode of exocytosis (Figure 4.7). This highlights that the mode of the RRP is regulated specifically by PKA activity. Interestingly, the activation of PKA with cBIMPS had no effect upon the RRP mode of exocytosis (Figure 3.6). This may reveal that a combination of both PKA and EPACs activation is required in order for the mode of the RRP to be switched to a KR majority. The activation of EPACs was beyond the scope of this research, so how this impacts the modes of release for both SV pools would be an interesting experiment to study in the future.

Treatment with OA is also able to switch RRP SVs to undergo a predominantly FF mode of exocytosis (Figure 4.8 A). OA inhibits PP2A and PP1 to a lesser extent, dramatically increasing the phosphorylated state of numerous proteins (Bialojan and Takai, 1988; Fernández, *et al.*, 2002), which prevents KR mediated exocytosis (Ashton, 2009). In order to see if OA stops the action of forskolin on the RRP, synaptosomes were treated with 0.8 μ M OA plus 100 μ M forskolin. Significantly less FM 2-10 dye release was seen

for this treatment when stimulated with 4AP5C (Figure 4.8 B), which was similar to the action of forskolin alone (Figure 4.6 A), indicating the action of forskolin is still able to switch RRP to KR despite treatment with OA. As KT5720 blocked the effects of forskolin, but OA didn't, this may mean that either forskolin and OA work on different substrates, or forskolin is able to act downstream of the action of OA.

4.6.3 Evoked $[Ca^{2+}]_i$ Levels

It was possible that treatment with 9-cp-ade could be affecting evoked $[Ca^{2+}]_i$ levels, without reaching levels sufficient enough to affect Glu or FM 2-10 dye release; however, treating synaptosomes with 100 μ M 9-cp-ade had no significant effect upon $[Ca^{2+}]_i$ levels evoked by any stimuli (Figure 4.9). This could indicate that the inhibition of AC and the drop in cAMP levels do not play a direct role in regulating evoked $[Ca^{2+}]_i$ levels.

Considering that 9-cp-ade has not had any significant effect upon Glu release, FM 2-10 dye release or evoked $[Ca^{2+}]_i$ levels, it was possible that the drug is not actually inhibiting AC at all (perhaps the drug employed was defective). However, 9-cp-ade treatment is able to restore Glu release to control levels when used as a dual treatment with forskolin (Figure 4.3 B and C), indicating it does indeed inhibit AC.

Activation of AC had a significant impact upon evoked $[Ca^{2+}]_i$ levels. Synaptosomes treated with 100 μ M forskolin and stimulated with 4AP5C released Glu at controls levels from the RRP (Figure 4.2 A), but there was a switch in the mode of exocytosis to KR (Figure 4.6 A) ($p < 0.05$). As previously mentioned a switch to the KR mode of release can be mediated by an increase in evoked $[Ca^{2+}]_i$ levels (Alés, *et al.*, 1999; Ashton,

2009); and in fact there was a significant increase in evoked $[Ca^{2+}]_i$ levels when synaptosomes were treated with 100 μ M forskolin and stimulated with 4AP5C (Figure 4.10). This is good evidence that forskolin may be able to switch the mode of exocytosis of some RRP SVs from FF to KR by inducing an increase in evoked $[Ca^{2+}]_i$. This explains why no similar switch in mode was seen when PKA was activated directly with cBIMPS (Figure 3.6 A), as cBIMPS did not affect $[Ca^{2+}]_i$ levels.

However, activation of AC with forskolin and stimulation with HK5C prevented RP SVs from undergoing exocytosis (Figure 4.2 B). Ashton has previously demonstrated that 4AP5C evokes a lower average $[Ca^{2+}]_i$ level than HK5C in nerve terminals and that is why 4AP5C cannot stimulate the RP to release (Section 1.9.1; Figure 1.8). Therefore it was possible that forskolin may be blocking release of the RP by reducing the $[Ca^{2+}]_i$ level during HK5C stimulation. Synaptosomes treated with 100 μ M forskolin exhibited significantly less evoked $[Ca^{2+}]_i$ when stimulated with HK5C, compared to untreated synaptosomes (Figure 4.10 B). Therefore forskolin may block the release of the RP through the reduction in average $[Ca^{2+}]_i$ levels, note that with HK5C there is an initial large increase in $[Ca^{2+}]_i$ at the AZ which drives the fusion of RRP SVs; but as this Ca^{2+} diffuses within the terminal there is a sufficient build-up of Ca^{2+} away from the AZ to drive fusion and release of RP SVs. If this level of $[Ca^{2+}]_i$ is lowered then RP SVs will not exocytose. Forskolin increases cAMP levels within the terminal which works to reduce the evoked $[Ca^{2+}]_i$ level below a minimum threshold which the RP needs to release. As cAMP has two targets, PKA and cBIMPS, and the stimulation of PKA did not perturb Glu release (Figure 3.2) then cAMP must be activating EPACs to block the release of the RP.

Inhibition of EPACs with 100 μ M ESI-09 did not affect Glu release when stimulated with HK5C (Figure 4.4 A), but did block the action of forskolin (which blocked RP release) when used in a dual treatment, restoring Glu release to controls levels (Figure 4.4 B). As discussed in the last paragraph forskolin blocks RP release by reducing evoked $[Ca^{2+}]_i$ levels through the activation of EPACs. Thus, it is possible that blocking EPACs would lead to an increase in evoked $[Ca^{2+}]_i$ levels, especially if ESI-09 treatment can restore RP Glu release. Synaptosomes treated with 100 μ M ESI-09 exhibited a significant increase in evoked $[Ca^{2+}]_i$ levels when stimulated with both 4AP5C (Figure 4.11 A) and HK5C (Figure 4.11 B). Blocking EPACs does lead to a substantial increase in HK5C evoked $[Ca^{2+}]_i$ which is also observed when synaptosomes are treated with ESI-09 plus forskolin (Figure 4.12). Inhibition of EPACs can prevent forskolin blocking RP release, through an increase in evoked $[Ca^{2+}]_i$, which reaches the sensitivity threshold for the RP SVs.

Together these data highlight how changes in evoked $[Ca^{2+}]_i$ levels can discretely regulate both the mode of SVs release for individual pools, and the availability of whole pools to release.

4.6.4 Bioenergetics of Synaptosomes

To ensure distinct changes to mode of release and regulation of SV pools undergoing exocytosis were due to targeted drug action and not the perturbation of synaptosomes, treated samples were subjected to the bioenergetics Mito-Stress test. As discussed in Chapter 3, the test measures 6 aspects of mitochondrial respiration to determine if drug treatments are causing respiratory or functional stress to mitochondria.

Synaptosomes treated with 100 μ M 9-cp-ade, 100 μ M forskolin or 100 μ M ESI-09 for 90-min at 37°C displayed the same OCR, viability and mitochondrial function as untreated synaptosomes. 9-cp-ade and forskolin were able to regulate AC without significantly affect basal respiration, ATP production, maximal respiration, spare capacity, proton leakage, or non-mitochondrial respiration (Figures 4.14 and 4.16 A-F).

Treatment with ESI-09 also did not affect the majority of mitochondrial functions, but did significantly increase proton leakage. Proton leakage is basal respiration that is not linked to ATP production, and excessive amounts could be a sign of mitochondrial damage (Agilent Technologies, 2019). As no other effect was observed with this treatment, the significance of this is not understood and it may be because of some of the measurement values (see results section). Further repeats with this treatment could aid understanding if this is a result of long-term treatment and what is occurring. These data demonstrate the specific actions observed with these drugs are not non-specific effects or the perturbation of the synaptosomes.

4.7 Conclusion

All this data highlight that increased cAMP levels inhibits the release of the RP of SVs through the activation of EPACs, which reduces the evoked $[Ca^{2+}]_i$ level, without perturbing the bioenergetics of the terminals. Elevation of cAMP levels can also switch the RRP mode of exocytosis to a KR majority through raising $[Ca^{2+}]_i$ via EPACs. Therefore, AC can regulate the RRP and RP independently of one another by modulating Ca^{2+} levels within the terminals. This allows a great deal of plasticity in the synapse.

The inhibition of AC did not have any significant effect upon Glu or FM 2-10 dye release, and neither did it perturb the viability of the synaptosomes or affect the $[Ca^{2+}]_i$ levels. However, inhibition of AC was able to prevent the action of forskolin when used in dual treatments. However, it may be that an incubation time of 5-10-min was not sufficient to inhibit all AC present in the synaptosomes or is unable to block all AC subtypes, allowing a small amount of cAMP to be produced and regulate PKA and EPACs in a reduced way. In concurrence with this, it has been demonstrated that 9-cp-ade does not inhibit AC type II when purified from rat and bovine brains and tested *in vitro* (Johnson, *et al.*, 1997). However, this did not create a significant effect upon FM 2-10 dye release, or play a role in the modulation of mode of exocytosis.

Chapter 5:

Studies of Dyn-I Phosphorylation during Exocytosis

5.1 Introduction

Chapters 3 of this thesis established conditions where PKA inhibition increased SVs undergoing FF (Figure 3.5), and PKA activation enhanced the KR mode of exocytosis (Figure 3.6). These changes in mode were independent from changes to evoked $[Ca^{2+}]_i$ levels, which have previously been shown to regulate the mode of exocytosis (Alés, 1999; Ashton, 2009; Section 1.9.1). Such mode changes could be mediated by a membrane bound fraction of Dyn-I, which the inhibition of has previously been shown to regulate exocytosis (Figure 1.13). Chapter 4 established how cAMP levels regulated PKA activity and mediated blocking of RP release probably via activation of EPACs, whilst a mode switch to KR for the RRP was mediated by an increase in $[Ca^{2+}]_i$.

As discussed in Chapter 1, Dyn-I is well established to mediate certain forms of endocytosis via membrane fission (Herskovits, 1993; van der Bliet, 1993; Artalejo, 1995; Urrutia, 1997), but has also been implicated in FP regulation during vesicular exocytosis (Min, *et al.*, 2007; Fulop, *et al.*, 2008; Chan, *et al.*, 2010), which fits well with an enrichment of Dyn-I found at the AZ (Wahl, *et al.*, 2013). This role in exocytosis has been proven in chromaffin cells where dense-core vesicles are able to undergo KR by rapidly shutting the FP after fusion (Albillos, *et al.*, 1997; Alés, *et al.*, 1999); and active Dyn-I has been found to facilitate the closure of the FP during this form of KR (Chan, *et al.*, 2010; Anantharam, *et al.*, 2011; Samaslip, *et al.*, 2012; Trouillon and Ewing, 2013).

Evidence from FM dye studies has also suggested KR occurs in neurons (Stevens and Williams, 2000). Studies have shown the involvement of Dyn-I in neuronal exocytosis (Zhang, *et al.*, 2007; Alabi and Tsien, 2013; Roman-Vendrell, *et al.*, 2014) and recently Bhuvra demonstrated that Dyn-I can regulate the exocytosing FP in order to mediate KR

in synaptosomes (Bhuva, 2015). All these data suggest a role for Dyn-I in neurons, regulating KR to facilitate sustained and efficient recycling, vital for synaptic plasticity and aspects of learning (Alabi and Tsien, 2013).

Aside from a shorter overall recycling time for SVs (and thus a higher rate of NT release), KR exocytosis may also affect the release dynamics of NT, modifying postsynaptic stimulation. Indeed it has been shown that KR SVs release at the centre of the AZ while vesicles undergoing FF release at the periphery (Park, *et al.*, 2012). This has important postsynaptic implications where the ratio of ionotropic NMDA and AMPA receptors changes between the centre of the post synaptic density (PSD) and the periphery, having a direct impact upon synaptic plasticity (Park, *et al.*, 2012; Scheefhals and MacGillavry, 2018).

If Dyn-I is regulating SV exocytosis at the FP, this may be observed as changes in the phosphorylated profile of Dyn-I during changes to the mode of exocytosis. In order to become active Dyn-I undergoes rapid dephosphorylation upon terminal depolarisation and Ca^{2+} -influx (Robinson, 1991). If a switch in the mode of exocytosis is being observed, a complimentary change in the phosphorylation profile of Dyn-I may also be seen. Previous research has discovered that modification of Dyn-I phosphorylation can play a vital role in regulating properties of endocytosis (for an in-depth review see Smillie and Cousin, 2005), however little research has been done investigating the phosphorylated state of Dyns upon the regulation of exocytosis. The phosphorylation of Ser-774 and Ser-778 are both well known to regulate the activity of Dyn-I during endocytosis (Tan, *et al.*, 2003; Graham, *et al.*, 2007), but no correlation has been discovered between these sites and KR (Bhuva, 2015). The phosphorylation of Dyn-I

Ser-795 has been shown to block the association between Dyn-I and phospholipids *in vitro* (Powell, *et al.*, 2000), and recently Ser-795 has been shown as a genuine *in vivo* site highly phosphorylated during FF (Bhuva, 2015; Singh 2017), making it a prime candidate to study during exocytosis.

It is theorised that in order for Dyn-I to be active at the FP during KR exocytosis, it must be dephosphorylated at Ser-795, while being phosphorylated during a FF mode of exocytosis. Research presented in Chapter 1 has shown that Dyn-I inhibition leads to the mode of exocytosis being switched to FF, for specific stimulation conditions (Figure 1.13 E and F), while PKA inhibition also leads to a FF mode of exocytosis for the same conditions (Figure 3.5).

To determine if PKA and AC are switching the mode of exocytosis through the phospho-regulation of Dyn-I activity, phosphorylation studies were performed for a range of drug treatment conditions used in Chapters 3, while specifically investigating the phosphorylated state of three Dyn-I Ser sites: 774, 778 and 795. Ser-774 and Ser-778 are two well established *in vivo* sites in Dyn-I which have been shown to be dephosphorylated by Ca²⁺-dependent Calcineurin which activated Dyn-I for particular reactions. Whilst such sites are rephosphorylated by cyclin-dependent kinase 5 (Cdk5) and glycogen synthase kinase 3 (Gsk3) and this inactivates these actions of Dyn-I. Ser-795 is a disputed *in vivo* site (Graham, *et al.*, 2007), and this is because under basal conditions this site could not be detected in intact animal tissue. However, as such tissues were not prepared under various stimuli (as in this thesis), and Ser-795 may only normally occur on a sub-pool of Dyn-I (as demonstrated in Chapter 3), the results presented by Graham and colleagues could be explained.

It was established *in vitro* that phospho-Ser-795 prevents Dyn-I binding to phospholipids when phosphorylated by PKC (Powell, *et al.*, 2000), but this has only been studied in a few papers, and PKC has recently appeared not to be the only kinases that may act at this site since OA treatment revealed Ser-795 even when PKCs were inhibited (Bhuva, 2015; Singh, 2017). Herein, it is argued that any significant change in Ser-795 phosphorylation, for conditions where the mode switches, that is not matched by equivalent changes to Ser-774 or Ser-778 are indicative of Ser-795 regulating the activity of Dyn-I on the FP.

5.2 Results

It was not possible to perform Western blots for all drug treatments studied in this thesis. Therefore, results presented in this chapter should be treated as building blocks for future phosphorylation studies. Samples were prepared for Western blotting in three or more experiments, as described in Chapter 2, and PVDF membranes were probed with antibodies specific to Dyn-I Ser-774, Ser-778, Ser-795 or pan-Dyn-I (4E67) which detects all isoforms of Dyn-I present in the sample regardless of phosphorylated state.

All Western blots were subjected to densitometric analysis as described in Chapter 2, and S.E.M. depicting the average changes in phosphorylation relative to the respective LO condition, based on the number of experiments carried out. The effect of 4AP5C stimulation upon Dyn-I phosphorylation was studied for the first time in this thesis. 4AP5C stimulation evokes release of the RRP only, via a mixture of KR and FF (Figure 1.11). As results from Chapter 3 have already demonstrated, Dyn-I is already associated with docked SVs at the AZ, and could have a role in regulating the mode of release. Therefore, it is important to establish how the phosphorylated profile of Dyn-I may change under conditions where the mode of exocytosis is being switched.

5.2.1 Phosphorylation of Dyn-I Ser-795 *in vivo*

Previous research by Bhuva has shown that in control synaptosomes Dyn-I Ser-795 levels are consistently low regardless of stimulation or duration (Section 1.9.6; Figure 1.17 A), but synaptosomes treated with 0.8 μM OA (Figure 1.17 B) or 80 nM of the PKC activator phorbol 12-myristate 13-acetate (PMA) (Figure 1.17 C) exhibit strong bands of *in vivo* Ser-795 phosphorylation over 2-120 seconds (Bhuva, 2015, p. 151). The lack of Ser-795 phosphorylation in control samples was explained as Ser-795 either remaining dephosphorylated during this treatment or being dephosphorylated almost immediately after phosphorylation, as pan-Dyn-I (4E67) revealed uniform levels in all samples (Figure 1.17 D).

It has been speculated that the action of PMA to produce Ser-795 could be due to broken terminals, where PKC and Dyn-I are present in the buffer ready to be phosphorylated (Graham, *et al.*, 2007). To ensure the synaptosomal model utilised in this thesis used intact and functional nerve terminals, 40 nM or 1 μM of PMA was added to synaptosomes in basal buffer (without stimulation) for four time periods equal to the stimulation times studied in Western blot experiments; 2, 15, 30 and 120 sec at RT. Under such conditions PMA would not be able to activate PKC to phosphorylate Ser-795 in intact nerve terminals (as it would need to cross the PM), whilst strong bands of Ser-795 would be observed if the synaptosomes were broken terminals.

When PMA is added to the basal buffer no Dyn-I Ser-795 phosphorylation is visualised at any time point, or any concentration of PMA in 3 different experiments (Figure 5.1 A), but a uniform level of pan Dyn-I protein is detectable within the nerve terminals

(Figure 5.1 B). This gives good reason to assume previous studies revealing Dyn-I Ser-795 (Bhuva, 2015; Singh, 2017), represent *in vivo* phospho-regulation of Dyn-I and not a spurious result produced by PMA acting upon broken synaptosomes.

This data also validates the results obtained from assays in the previous chapters of this thesis. The synaptosomes used with $[Ca^{2+}]_i$ levels, Glu and FM dye release are intact and studying the effect of acute drug treatments in this model represents real effects on synaptosomes.

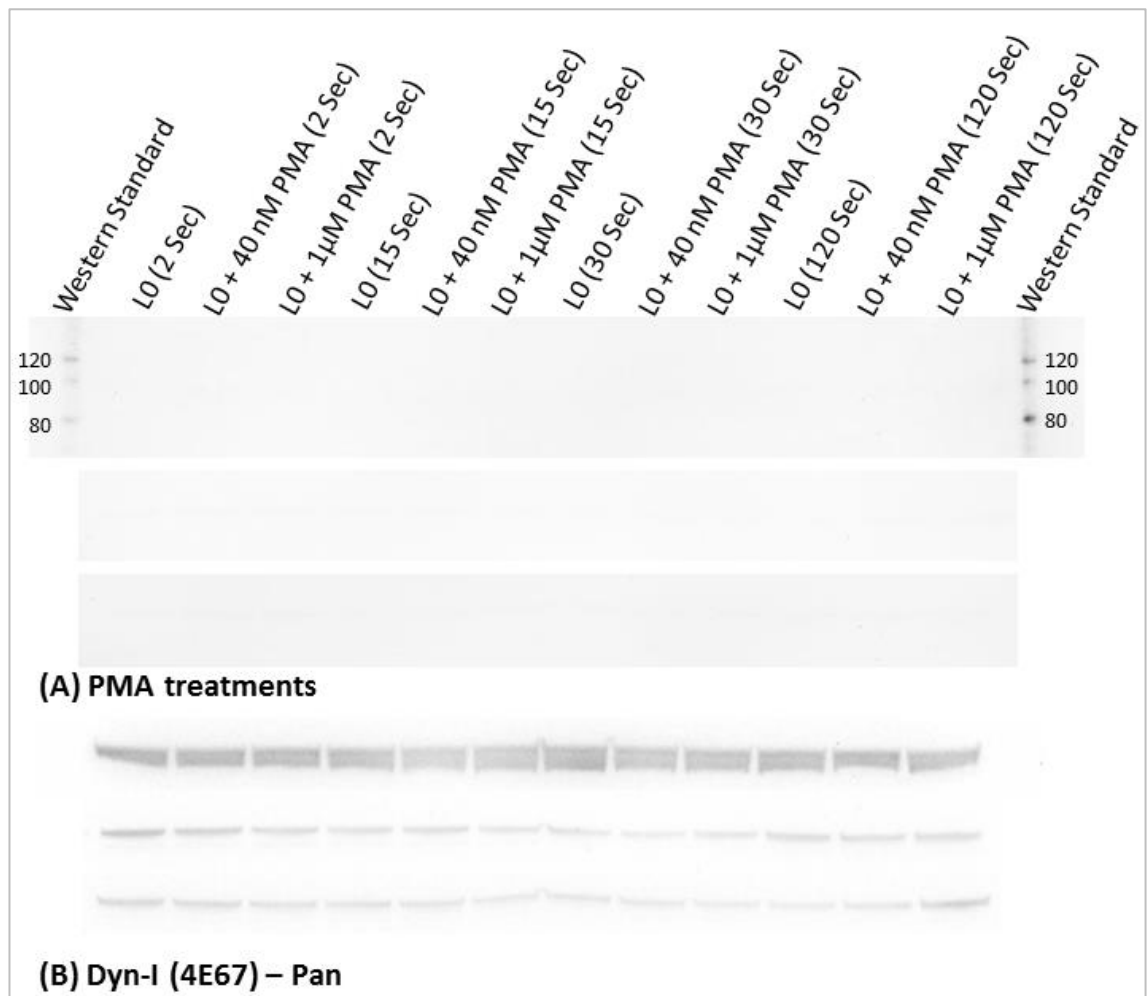


Figure 5.1: Effect of 40 nM or 1 μM PMA upon Dyn-I Ser-795 over 120 sec

(A) Ser-795 is not detectable in synaptosomes which had 40 nM or 1 μM PMA added to the basal buffer (3 experiments). (B) Re-probing blots for pan-Dyn-I revealed uniform levels of Dyn-I protein between samples within each experiment (n=3 experiments).

5.2.2 The Effect of 0.8 μ M OA upon Dyn-I Phosphorylation in the RRP

The RRP of SVs is able to recycle independently of the RP (Ashton and Ushkaryov, 2005) and can release via FF or KR depending upon the stimulation paradigm (see Section 1.9.4). The stimulation 4AP5C used in this thesis is able to reproducibly release only the RRP of SVs from synaptosomes (Figure 1.7 C), and studying how the phosphorylated profiles of proteins changes when subjected to this stimulation may reveal if the RRP has unique regulatory mechanisms separate to those which govern the RP.

The inhibition of protein phosphatase 1 and 2A (PP1 and PP2A) with 0.8 μ M OA has been shown to switch RRP SVs to a FF mode of exocytosis for all stimuli (Section 1.9, Figure 1.11), and as demonstrated in Figure 1.17 OA treatment can increase the level of Ser-795 phosphorylation relative to non-drug treated controls. This may suggest a link between the phosphorylated state of Ser-795 and the mode of exocytosis, where inhibition of PP1 or PP2A is able to regulate the mode of exocytosis by preventing the dephosphorylation of Dyn-I Ser-795.

To investigate the effect of 0.8 μ M OA upon the phosphorylated state of Dyn-I in more detail, samples were treated with 0.8 μ M OA and stimulated with 4AP5C for 2, 15, 30 and 120 seconds. Western blots were probed for all Ser sites of interest (Figure 5.2 and Figure 5.3); all blots are representative of three experiments.

Detectable levels of Ser-795 are visible during control conditions for all time points (Figures 5.2 and 5.3 A, lanes 1-2, 7-8), treatment with 0.8 μ M OA appears to increase Ser-795 levels for all time points (lanes 5-6, 11-12), but slight changes in pan-Dyn-I

levels (Figure 5.2 B) may explain some variation seen with Ser-795. No visible difference is noted in Ser-774 or Ser-778 levels with 0.8 μ M OA treatment (Figures 5.2 and 5.3, C and E), and levels of Dyn-I protein are uniform for these blots (Figures 5.2 and 5.3, D and F).

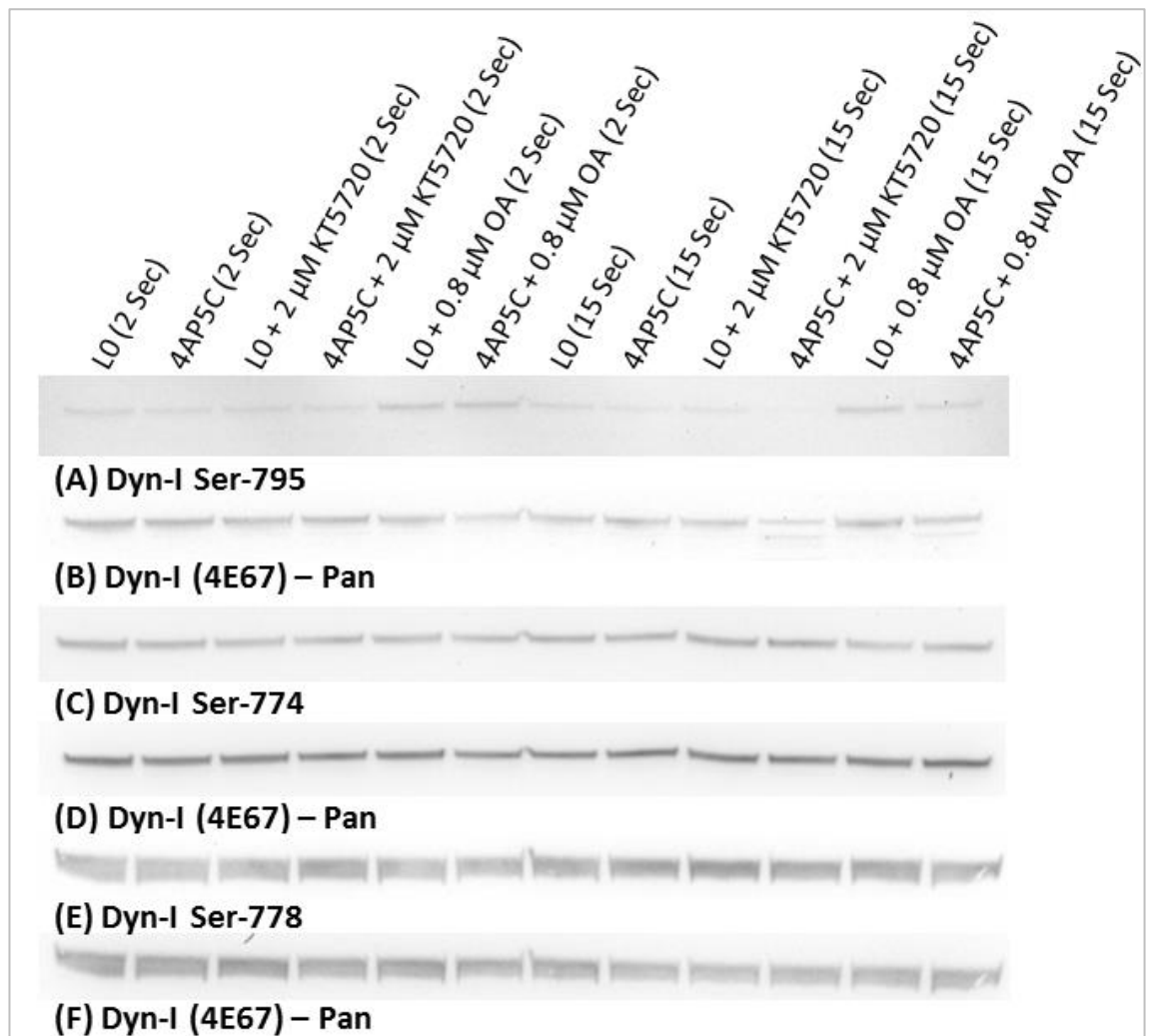


Figure 5.2: Effect of OA or KT5720 upon Dyn-I Ser Sites 2-15 sec

(A) Treatment with 0.8 μM OA increases Ser-795 levels, relative to Con at 2 and 15 sec. Some variations are observed at 15 sec with 2 μM KT5720 treatment, but this could be due to slight variation in levels of Dyn-I protein (B) in sample. (C and E) No change in noted in levels of Ser-774 or Ser-778. (D and F) Uniform levels of Dyn-I are observed between samples (All blots n=3).

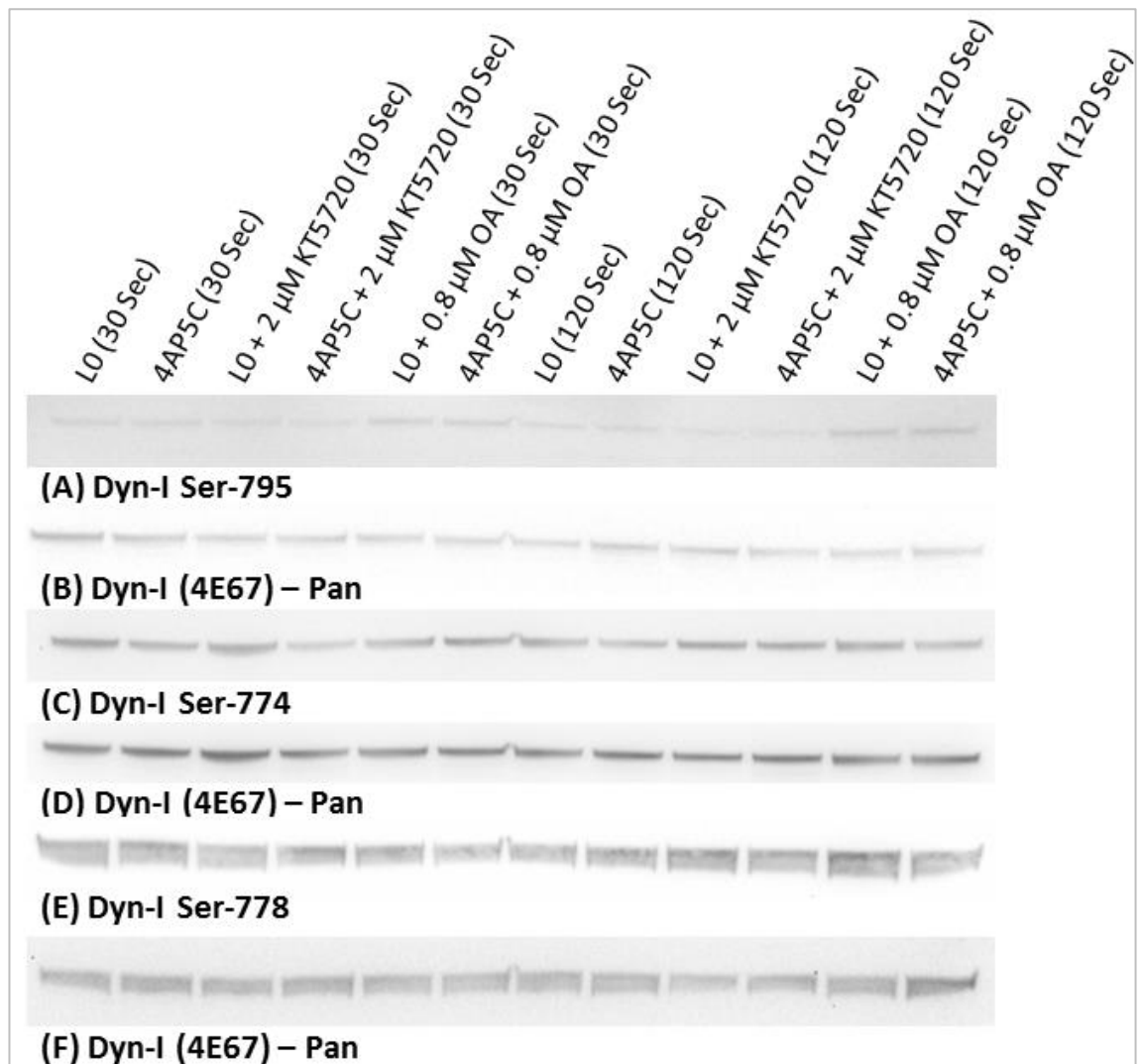


Figure 5.3: Effect of OA or KT5720 upon Dyn-I Ser Sites 30-120 sec

(A) Treatment with 0.8 μM OA increase Ser-795 levels relative to control at 30 and 120 sec. (C) 4AP5C samples see a slight time-dependent decrease in Ser-774 phosphorylation not seen with basal samples. (B and D) Uniform levels of Dyn-I protein are seen in samples. (E) Slight variations in Ser-778 levels may be accounted for by variations in Dyn-I protein levels (F) (All blots $n=3$).

The Western blots in Figures 5.2 and 5.3 were subjected to densitometric analysis and values were normalised based upon the level of pan-Dyn-I present in each sample, as described in Chapter 2.6.4. Figures 5.4-5.6 represent the phosphorylation levels of each Ser site presented as time graphs with S.E.M. error bars.

Stimulation with 4AP5C, without drug, does not affect the phosphorylated state of Ser-795, relative to unstimulated conditions (Figure 5.4, Red and Blue). Treatment with 0.8 μ M OA increased Ser-795 levels significantly, relative to Con L0, regardless if samples were stimulated or not (Green and Purple), suggesting the effect of inhibition of PP1 or PP2A is not stimulation dependent, and phospho-regulation of Dyn-I could occur during this treatment regardless of stimulation.

Samples stimulated with 4AP5C, regardless of drug treatment, saw a decrease in Ser-774 phosphorylation over time (Figure 5.5, Red and Purple), which is a well-established effect (see discussion). Treatment with 0.8 μ M OA did not significantly affect Ser-774 levels relative to their stimulated or unstimulated counterparts, suggesting OA treatment does not regulate Ser-774 with this stimuli.

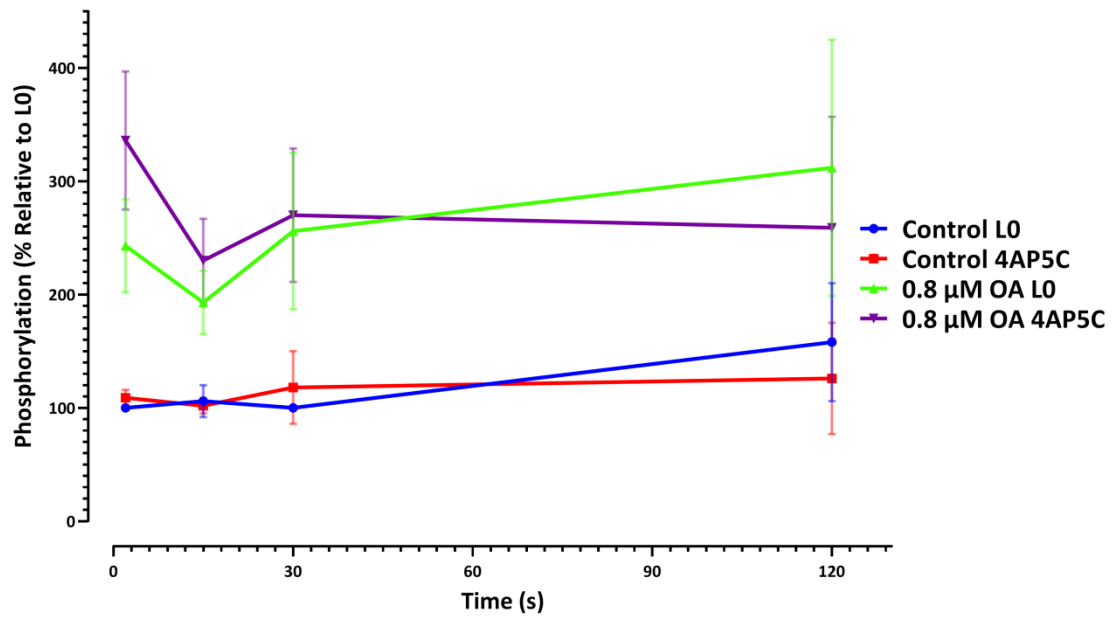


Figure 5.4: Effect of 0.8 μM OA upon Dyn-I Ser-795 over 120 sec

Application of 4AP5C stimulation, without OA treatment (Red), does not significantly increase the phosphorylated state of Ser-795 relative to basal Con (Blue) (All time points $p > 0.05$). OA treatment significantly increases Ser-795 phosphorylation of unstimulated samples (Green) at 2-15 sec relative to Con L0 (Blue) (2 sec $p = 0.025$; 15 sec $p = 0.040$), but not 30-120 ($p > 0.05$); and of stimulated samples (Purple) at 2-30 sec relative to CON L0 (2 sec $p = 0.018$; 15 sec $p = 0.035$; 30 sec $p = 0.045$). Samples treated with OA and stimulated with 4AP5C (Purple) see no significant increase in phosphorylation relative to samples treated with OA and not stimulated (Green) (All time points $p > 0.05$).

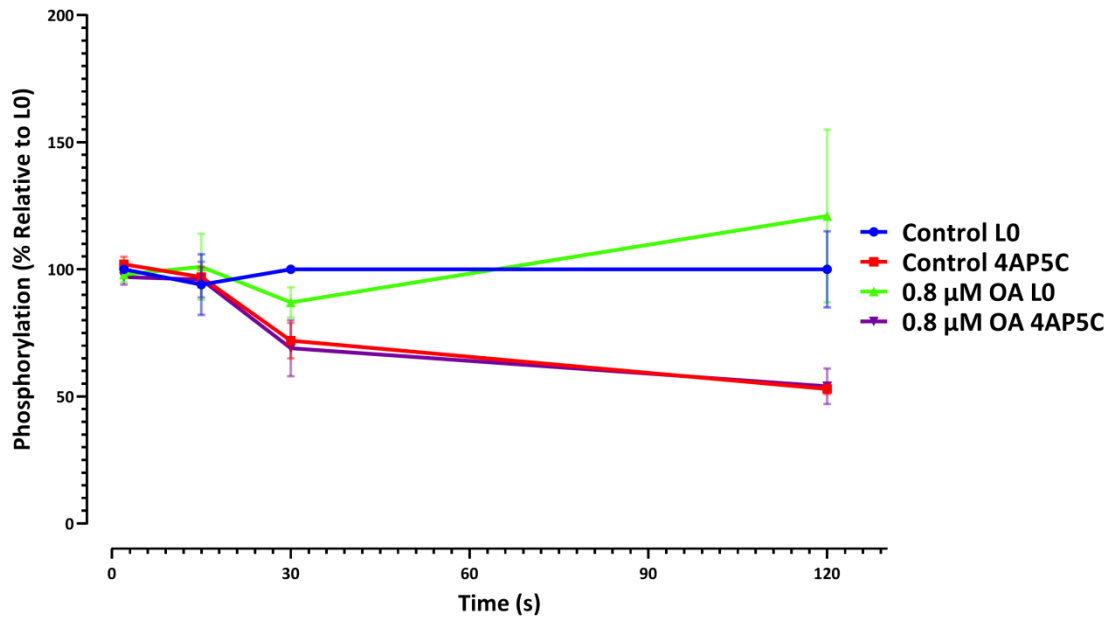


Figure 5.5: Effect of 0.8 μM OA upon Dyn-I Ser-774 over 120 sec

Application of 4AP5C stimulation, without OA treatment (Red), does not significantly affect Ser-774 levels relative to Con L0 (Blue) at 2-15 sec (2 sec- $p=0.524$; 15 sec- $p=0.824$), but sees a significant time-dep decrease in Ser-774 at 30-120 (30 sec- $p=0.016$; 120 sec- $p=0.036$). OA treatment does not affect the Ser-774 level of unstimulated samples (Green) relative to Con L0 (Blue) (all time points $p>0.05$), or relative to CON 4AP (Red) (all time points $p>0.05$). OA treatment does not sig affect Ser-774 levels of 4AP5C stimulated samples (Purple) relative to Con L0 (Blue) at 2-15 sec (time points $p>0.05$), but a significant time-dep decrease is noted at 30-120 sec (30 sec- $p=0.048$; 120 sec- $p=0.049$). No significant difference is seen between 4AP5C stimulated OA treatment (Purple) and Con 4AP5C (RED) (all time points $p>0.05$). Samples treated with OA and stimulated with 4AP5C (Purple) see no significant change in Ser-774, relative to unstimulated OA treatment (Green) (all time points $p>0.05$).

Samples stimulated with 4AP5C display a time-dependent decrease in Ser-778 phosphorylation, regardless of drug treatment (Figure 5.6, Purple and Red). Treatment with 0.8 μ M OA does not significantly affect unstimulated samples compared to controls (Green vs Blue), but OA treatment sees a slight increase in Ser-778 levels at 15 sec when stimulated with 4AP5C, compared to drug free controls (Purple vs Red), however further repeats may reveal this is not a significant effect.

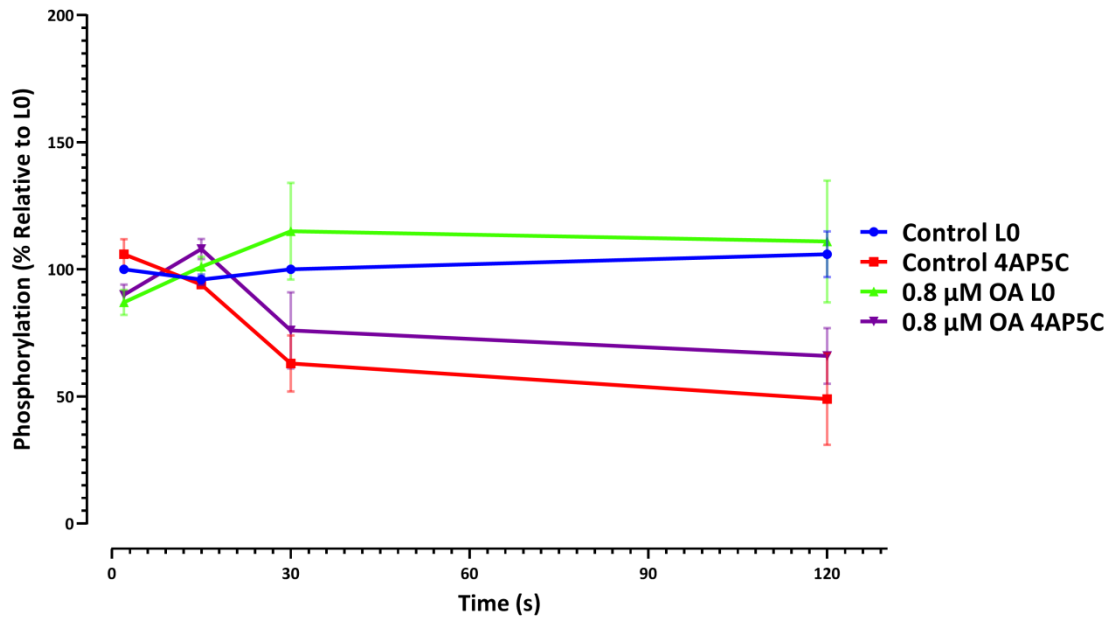


Figure 5.6: Effect of 0.8 μM OA upon Dyn-I Ser-778 over 120 sec

Application of 4AP5C stimulation, without OA treatment (Red), does not significantly affect Ser-778 levels at 2-15 sec relative to Con L0 (Blue) ($p>0.05$), however a significant time-dep decrease was observed at 30-120 sec (30 sec $p=0.028$; 120 sec $p=0.047$). OA treatment of unstimulated samples (Green) does not significantly affect Ser-778 levels relative to Con L0 (Blue) at all time points ($p>0.05$). OA treatment of 4AP5C stimulated samples (Purple) does not significantly affect Ser-778 relative to Con L0 (Blue) at 2-30 sec ($p>0.05$), however a significant difference was observed at 120 sec ($p>0.0481$). No significant difference was observed between OA 4AP5C samples (Purple) and control 4AP5C (Red) at 2, 30 and 120 sec ($p>0.05$), however a significant difference was observed at 15 sec ($p=0.0274$).

5.2.3 The Effect of 2 μ M KT5720 upon Dyn-I Phosphorylation in the RRP

Western blots presented in Figure 5.2 and 5.3 also contain samples treated with the PKA inhibitor KT5720. Treatment with 2 μ M KT5720 switched the mode of exocytosis to FF during stimulation with 4AP5C (Figure 3.5 A), indicating RRP SVs have changed mode from KR to FF (Chapter 3.4.1). Western blots may indicate that samples treated with 2 μ M KT5720 see a change in Ser-795 levels at all time points (Figure 5.2 and 5.3 A, lanes 3-4 and 9-10), with no noticeable changes in Ser-774 or Ser-778 levels (Figure 5.2 and 5.3, C and E). Figures 5.7-5.9 represent the normalised and corrected phosphorylation levels of each Ser site presented as time graphs with S.E.M. error bars.

Treatment with KT5720 did not significantly affect the phosphorylated state of Ser-795 at any time point, regardless of stimulation condition ($p>0.05$) (Figure 5.7). Stimulation with 4AP5C had no significant effect upon Ser-795 levels either ($P>0.05$). These data suggest that inhibition of PKA does not phospho-regulate Ser-795.

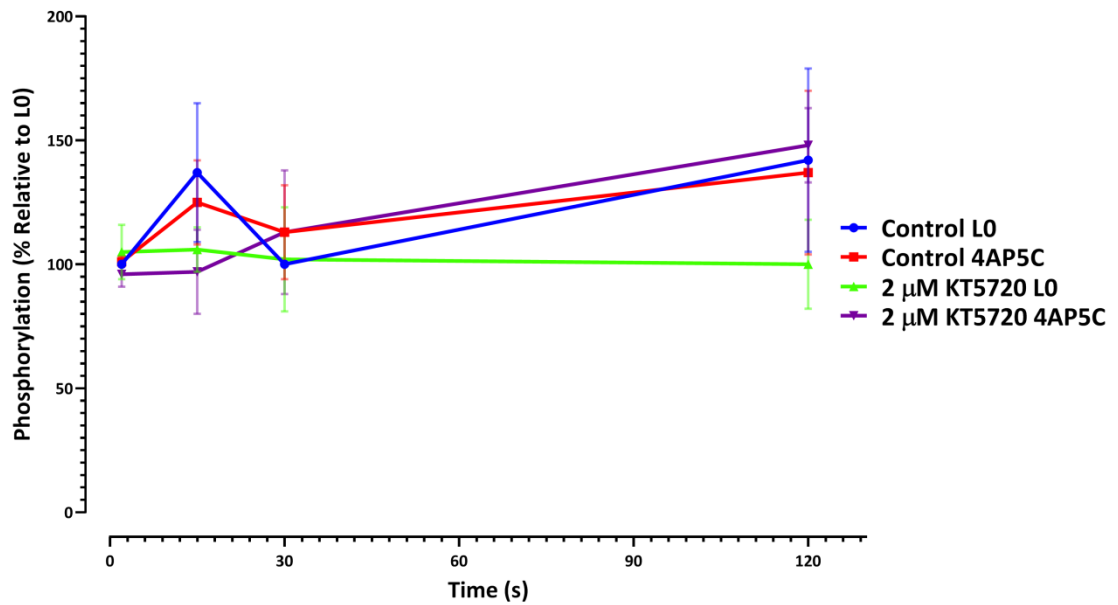


Figure 5.7: Effect of 2 μM KT5720 upon Dyn-I Ser-795 over 120 sec

No significant difference in Ser-795 phosphorylation levels was observed between any condition at any time point ($p>0.05$).

Treatment with 2 μM KT5720 does not significantly affect the phosphorylated state of Dyn-I Ser-774, regardless of stimulation condition ($p>0.05$) (Figure 5.8). Samples stimulated with 4AP5C again see a time dependent decrease in phosphorylation, independent of drug treatment.

Treatment with 2 μM KT5720 does not statistically affect the level of Ser-778 phosphorylation, regardless of stimulation condition ($p>0.05$) (Figure 5.9). A time dependent decrease in Ser-778 is noted over 15-120 sec as described previously.

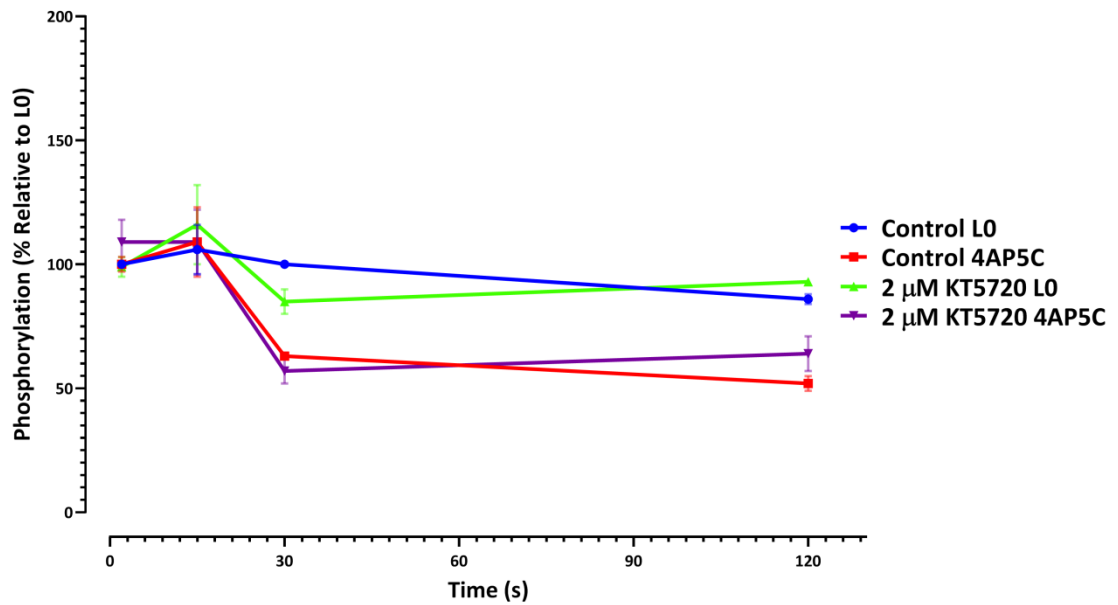


Figure 5.8: Effect of 2 μM KT5720 upon Dyn-I Ser-774 over 120 sec

Application of 4AP5C, without drug (Red), does not significantly affect Ser-774 levels relative to Con L0 (Blue) at 2-15 sec (2 sec $p=0.998$; 15 sec $p=0.870$), but a significant time dependent decrease is noted at 30-120 (30 sec- $p=0.0001$; 120 sec- $p=0.0007$). Treatment with KT5720 does not significantly affect Ser-774 levels of unstimulated samples (Green), relative to Con L0 (Blue) ($p>0.05$). Treatment with KT5720 of 4AP5C stimulated samples (Purple) does not significantly affect Ser-774 levels relative to control 4AP5C (Red) ($p>0.05$), but does significantly decrease Ser-774 relative to Con L0 (Blue) at 30 and 120 sec (30 sec $p=0.001$; 120 sec $p=0.039$).

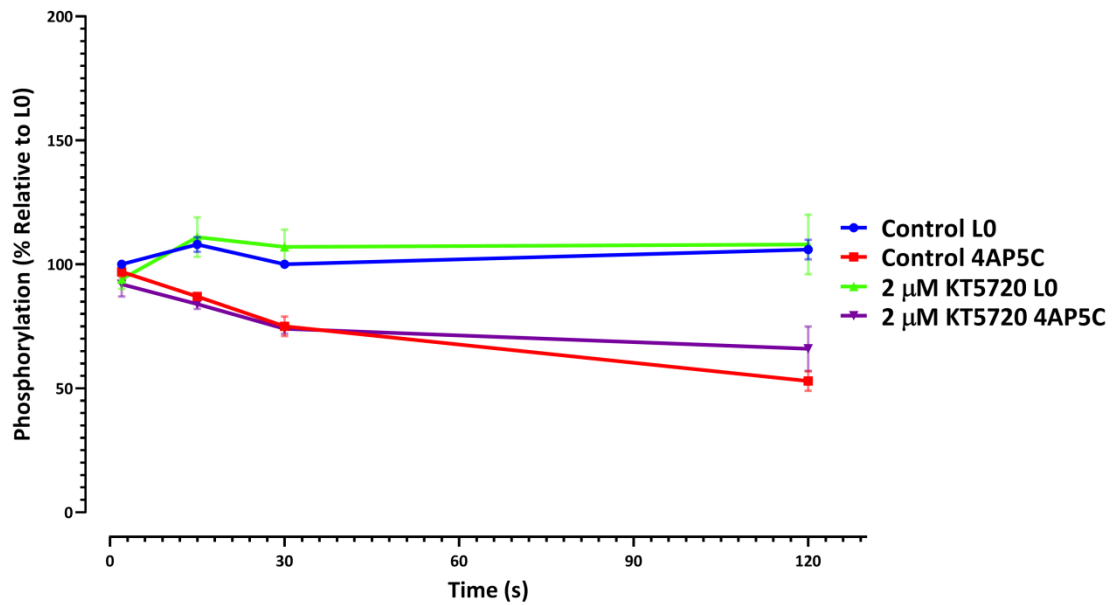


Figure 5.9: Effect of 2 μM KT5720 upon Dyn-I Ser-778 over 120 sec

Application of 4AP5C, without drug (Red), significantly decrease Ser-778 levels at 15-120 sec relative to Con L0 (Blue) (15 sec $p=0.0027$; 30 sec $p=0.0033$; 120 sec $p=0.0007$), but not at 2 sec ($p>0.05$). Treatment with KT5720 does not significantly affect Ser-778 levels of unstimulated samples (Green), relative to Con L0 (Blue) (all time points $p>0.05$). KT5720 treatment does not significantly affect Ser-778 levels of stimulated samples (Purple) relative to Con 4AP5C (Red) (all time points $p>0.05$).

5.2.4 The Effect of 50 μ M cBIMPS upon Dyn-I Phosphorylation

Activation of PKA with 50 μ M cBIMPS has been shown to switch RP SVs to a KR mode of exocytosis with HK5C and ION5C, but not 4AP5C (Figure 3.6), and this could be through the regulation of PP2B, as cBIMPS presents a phenotype similar to PP2B inhibition with Cys A (Figure 1.16). To investigate the effect of PKA activation upon the phosphorylated state of Dyn-I in more detail, samples were treated with 50 μ M cBIMPS and stimulated with HK5C or ION5C for 2 or 15 sec. Western blots were probed for all phospho-Ser sites of interest (Figure 5.10); all blot images are representative of three experiments.

Detectable levels of Ser-795 are visible during control conditions for all time points (Figure 5.10 A, lanes 1-3, 7-9), treatment with 50 μ M cBIMPS may slightly decrease Ser-795 levels for both time points (lanes 4-6, 10-12). No changes in pan-Dyn-I levels (Figure 5.10 B) can be seen. No visible difference is noted in Ser-774 levels with 50 μ M cBIMPS treatment (Figure 5.10 C) or the respective pan-Dyn-I (Figure 5.10 D). A slight decrease in Ser-778 levels in the blot centre (Figure 5.10 E), is explained by a decrease in levels of Dyn-I protein (Figure 5.10 F).

The three repeats of Western blots represented in Figure 5.10 were subjected to densitometric analysis and values were normalised based upon the level of pan-Dyn-I present in each sample, as described in Chapter 2.6.4. Figures 5.11-5.13 represent the phosphorylation levels of each Ser site presented as time graphs with S.E.M. error bars.

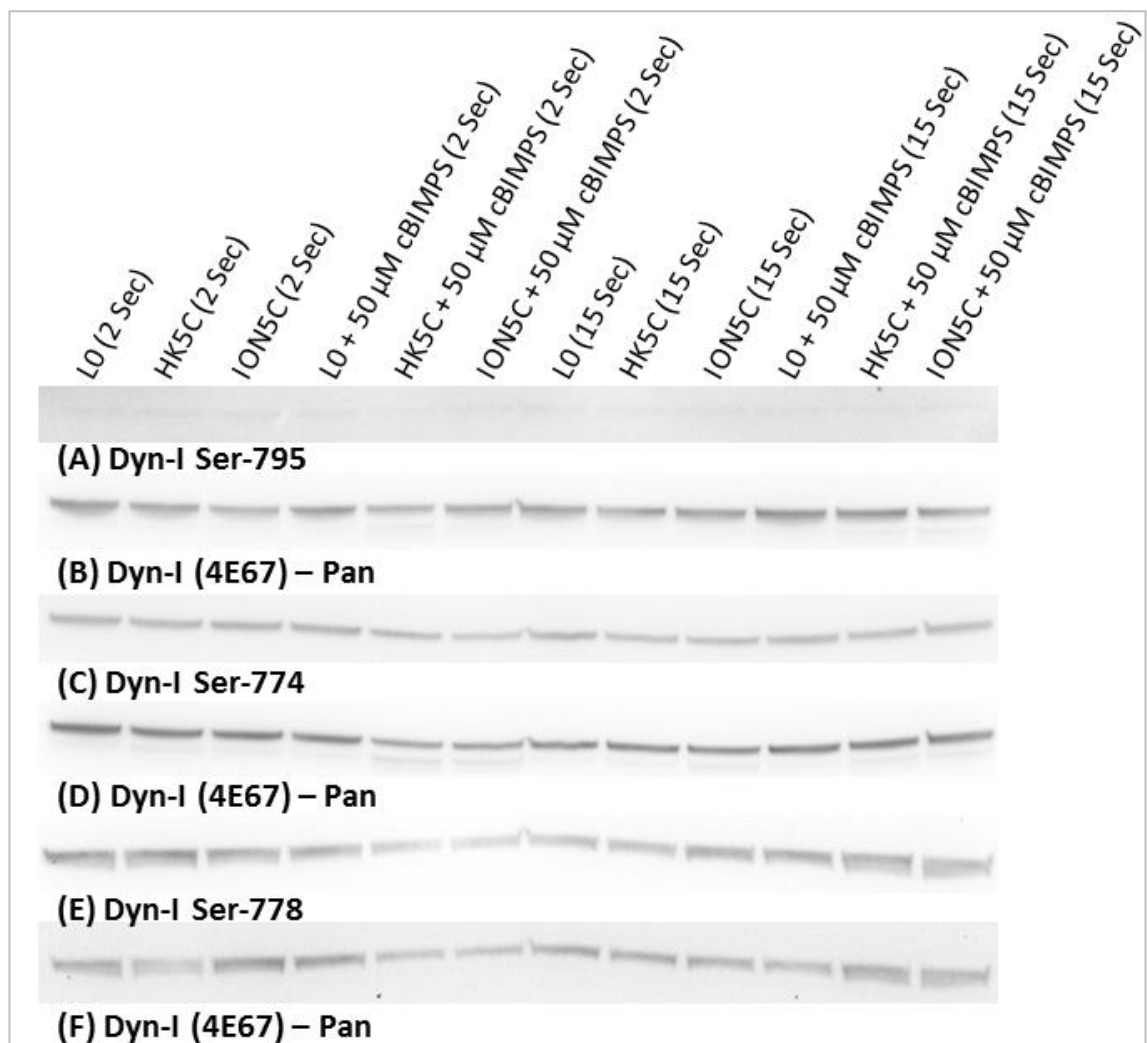


Figure 5.10: Effect of 50 μM cBIMPS upon Dyn-I Ser sites 2-15 sec

(A) Treatment with cBIMPS may decrease Ser-795 levels at both time points, but does not affect Ser-774 levels (C). A slight decrease in Ser-778 levels are observed, but also in the level of Dyn-I protein (F). Uniform levels of Dyn-I protein are seen for Ser-795 and Ser-774 samples (B and D respectively).

Stimulation of drug free samples with HK5C or ION5C did not significantly affect the phosphorylated state of Ser-795 at 2 or 15 sec relative to unstimulated controls (Figure 5.11, Red and Green). Treatment with 50 μ M cBIMPS did not affect the Ser-795 level of unstimulated samples at 2 or 15 sec (Figure 5.11, Purple), but significantly decreased the detectable level of Ser-795 at 2 sec when stimulated with HK5C and ION5C (Figure 5.11, Orange and Light Blue), relative to all control conditions and cBIMPS L0 (Blue). Treatment with 50 μ M cBIMPS significantly decreased the level of Ser-795 at 15 sec when stimulated with HK5C, relative to all control conditions, and stimulation with ION5C was significantly decreased relative to Con L0, Con HK5C and cBIMPS L0, but not Con ION5C.

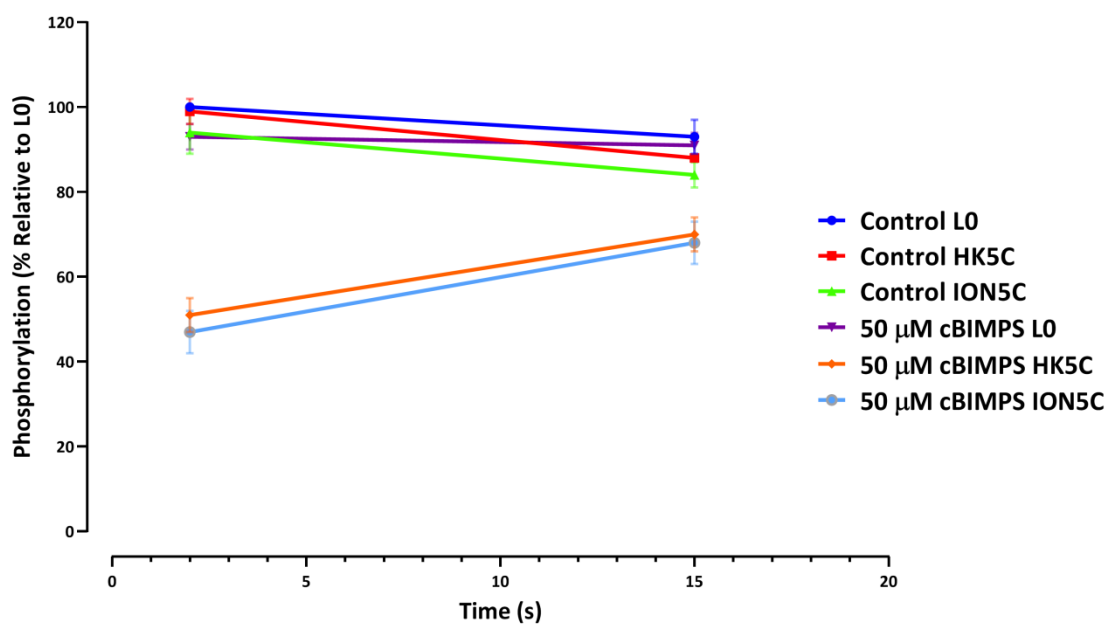


Figure 5.11: Effect of 50 μM cBIMPS upon Dyn-I Ser-795 over 15 sec

Stimulation with HK5C in the presence of 50 μM cBIMPS (Light Blue) significantly decreased levels of Ser-795 at 2 and 15 sec, relative to Con LO, Con HK5C, Con ION5C and cBIMPS LO (all $p < 0.05$). Similarly stimulation with ION5C with 50 μM cBIMPS treatment (Orange), significantly decreased Ser-795 levels at 2 sec, relative to Con LO, Con HK5C, Con ION5C and cBIMPS LO (all $p < 0.05$), and at 15 sec, relative to Con LO, Con HK5C and cBIMPS LO (all $p < 0.05$); but was not significantly different to Con ION5C (Green) at 15 sec ($p = 0.517$). No difference was noted between cBIMPS HK5C (Light Blue) and cBIMPS ION5C (Orange) at 2 sec ($p = 0.5660$), or 15 sec ($p = 0.7704$). Stimulation with HK5C, without drug treatment (Red) or ION5C, without drug (Green) were not significantly different from unstimulated controls (Blue) or each other at 2 or 15 sec (all $p > 0.05$). No significant difference in Ser-795 was observed when samples were treated with 50 μM cBIMPS but not stimulated (LO – Purple) relative to Con LO (Blue), Con HK5C (Red) or Con ION5C (Green), (all conditions $p > 0.05$).

Treatment with 50 μM cBIMPS did not significantly affect the phosphorylation level of Ser-774 at 2 or 15 sec ($p>0.05$) (Figure 5.12), indicating this site has no specific role in the regulation of exocytosis during this drug treatment.

A time dependent decrease in Ser-778 phosphorylation is observed with HK5C and ION5C stimulation, without drug (Figure 5.13), but no significant effect is observed with 50 μM cBIMPS treatment.

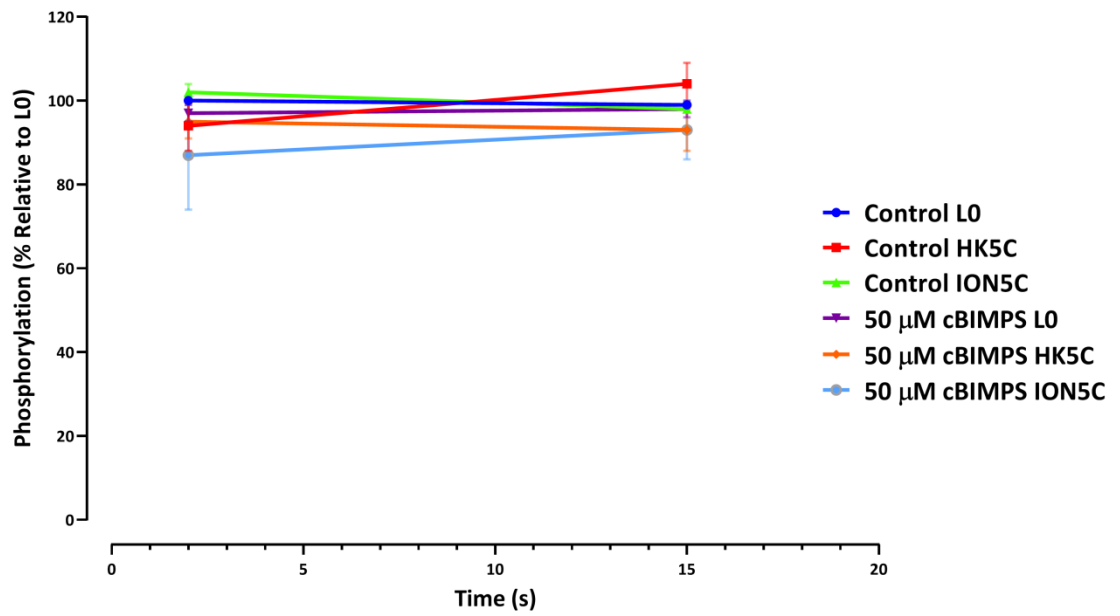


Figure 5.12: Effect of 50 μM cBIMPS upon Dyn-I Ser-774 over 15 sec

Treatment with 50 μM cBIMPS does not significantly affect the phosphorylated state of Ser-774 at 2 or 15 sec. No significant difference was measured between any conditions across either time point (all $p > 0.05$).

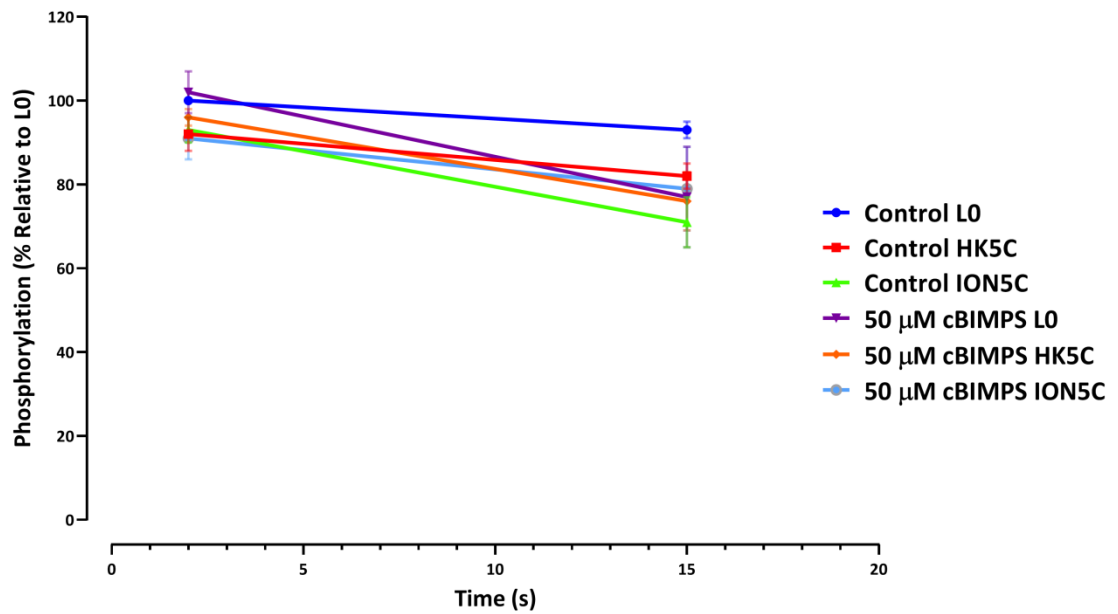


Figure 5.13: Effect of 50 μM cBIMPS upon Dyn-I Ser-778 over 15 sec

Application of either HK5C or ION5C stimuli, without drug treatment (Red or Green respectively), does not significantly affect 778 phosphorylation at 2 sec, relative to Con LO (Blue) ($p>0.05$), but a significant time dependent decrease is observed at 15 sec (HK5C vs LO- $p=0.038$; ION5C vs LO- $p=0.025$). Treatment with 50 μM cBIMPS does not significantly affect the phosphorylated state of Ser-778 at either time point, relative to any condition ($p>0.05$).

5.3 Discussion

This chapter aimed to investigate if perceived changes to the mode of exocytosis induced by certain drug treatments were due to modification of the phosphorylated profile of Dyn-I, in particular Ser-795. As discussed earlier a multitude of evidence points to a regulatory role at the FP for Dyn-I during exocytosis (Fulop, *et al.*, 2008; Chan, *et al.*, 2010). Though as of yet no correlation has been established between the mode of SV exocytosis and the phosphorylated profile of Dyn-I (Singh, 2017).

Dyn-I has a range of *in vivo* phosphorylation sites (Graham, 2007), and these have been shown to be exclusively Ser sites (Robinson, 1991). Ser-778 and Ser-774 are well established as the major phosphorylation sites of Dyn-I *in vivo*, and are responsible for regulating forms of endocytosis (Chapter 1.8) (Tan, *et al.*, 2003; Graham, 2007). However, though Ser-795 is demonstrated as a potent *in vitro* site (Powell, *et al.*, 2000), there is only little evidence to identify it as a truly *in vivo* phosphorylation site (Bhuva, 2015). In order for Dyn-I to be active at the FP during KR, Ser-795 is expected to be dephosphorylated, while during FF it is expected to become more phosphorylated. In this thesis, it is argued that a change seen in the phosphorylated state of Ser-795 without an equivalent change in either Ser-778 or Ser-774, during a mode switch is indicative of Ser-795 regulating the mode of exocytosis.

This thesis describes a correlation between the phosphorylated state of Ser-795 and a distinct switch in mode, for two stimuli which could be how the synaptosomes regulate exocytosis.

5.3.1 Phosphorylation of Dyn-I Ser-795 *in vivo*

The inhibition of PP1 and PP2A with 0.8 μ M OA, and the activation of PKCs with 80 nM PMA have previously been shown to increase the level of phosphorylation at Ser-795, relative to controls (Figure 1.17). It was possible however, that such an increase in phosphorylation at Ser-795 could be a result of PMA acting upon broken terminals. In such a situation Dyn-I Ser-795 would be immediately available for phosphorylation much as seen *in vitro* (Powell, *et al.*, 2000); unlike with intact terminals, where the PMA must first cross the PM in order to access Dyn-I.

In order to establish if the changes to Ser-795 were strictly *in vivo*, 40 nM PMA was added to the basal buffer around the synaptosomes without any stimulation (Figure 5.1). Even after 120 seconds no detectable level of Ser-795 was present (Lanes 10-12), unlike Figure 1.17 where 40 nM PMA (pre-incubation) increases the phosphorylation of Ser-795 at 15 seconds, before darkening at 120 seconds (Figure 1.17; lanes 10-11). Therefore, the synaptosomes contain very few lysed terminals as no PMA induced phosphorylation of Ser-795 was observed, and a pre-stimulation is required for the PMA to be taken up by the intact terminals to interact with the intracellular PKCs.

PMA is able to specifically increase the phosphorylated profile of Dyn-I Ser-795 *in vivo* through the activation of PKCs only when it has entered the terminals. This demonstrates that Ser-795 is a viable *in vivo* phosphorylation target for PKCs, and requires specific conditions for it to be detectable (Bhuva, 2015). However, PKCs may not regulate the mode of exocytosis via Ser-795 as high level of Ser-795 has still been observed even when PKCs were first inhibited before treatment (Singh, 2017).

5.3.2 The Effect of 0.8 μM OA upon Dyn-I during 4AP5C Stimulation

The phosphorylated profile of Dyn-I has never before been investigated during terminal stimulation with 4AP5C, so these data present completely novel results where only the RRP on SVs are undergoing release (see Section 1.9.1). During 4AP5C stimulation a lower, more gradual increase in $[\text{Ca}^{2+}]_i$ is observed (Figure 1.8) which is theorised to activate Dyn-I at the FP to mediate the mode of release (see Section 1.9.5).

Inhibition of PP1 and PP2A with 0.8 μM OA during basal or 4AP5C stimulation increases *in vivo* Ser-795 phosphorylation relative to untreated synaptosomes, and no similar phenotype is observed for either Ser-774 or Ser-778. Data presented earlier in this thesis also demonstrates OA treatment increases the number of RRP SVs undergoing FF with all stimuli (Figure 1.11), and this could indicate OA mediates a switch in the mode of exocytosis from KR to FF by preventing the dephosphorylation of Dyn-I.

Potentially the inhibition of PP1, PP2A or both, prevents the dephosphorylation of Dyn-I Ser-795, suggesting one (if not both) could be specific phosphatases for Ser-795. However, due to the well-established, long reaching effects of PP1 and PP2A (Zolnierowicz, 2000; Cohen, 2002), it is difficult to accurately say through what means their inhibition increases Ser-795 phosphorylation, potentially several proteins and their interaction partners could be mediating this change, but it is important to note no changes are seen at Ser-774/778 demonstrating some specificity at Ser-795.

During control conditions a time-dependent decrease in Ser-774 and Ser-778 phosphorylation is observed with 4AP5C stimulation, which is not seen with unstimulated samples (L0) (Figure 5.5 and 5.6). This occurs during a prolonged stimulation process, but one after 15 sec, indicating a Ca^{2+} -dependent mechanism. Such an observation has previously been described for both HK5C and ION5C stimulated samples (Bhuva, 2015, p. 155), however this is the first time 4AP5C stimulation has been investigated in this paradigm, and the similarity could indicate how a relative increase in $[\text{Ca}^{2+}]_i$ is able to mediate dephosphorylation of a portion of Dyn-I Ser sites. Further research should be conducted into the effect of prolonged stimulation (≤ 5 min) upon dephosphorylation of specific sites.

As treatment with OA does not significantly affect this trend seen between stimulated and unstimulated samples for Ser-774 and Ser-778 (Figure 5.5 and 5.6), this suggests that PP1 and PP2A are probably not phosphatases for these two sites. Further, these sites have no correlation between OA treatment and changes to levels of phosphorylation, unlike what is seen with Ser-795, again suggesting these sites have no regulatory effect upon the mode.

5.3.3 The Effect of PKA Inhibition upon Dyn-I during 4AP5C Stimulation

The inhibition of PKA with 2 μM KT5720 significantly increased the number of RRP SVs undergoing FF with 4AP5C (Figure 3.5), presenting a similar phenotype to OA treatment. From this it was expected a similar increase in Ser-795 phosphorylation could be observed during KT5720 treatment, however the inhibition of PKA does not

significantly affect the *in vivo* phosphorylation of Ser-795 when releasing the RRP with 4AP5C.

The inhibition of PKA also does not affect the phosphorylated state of Dyn-I Ser-774 or Ser-778 over 120 sec (Figure 5.8 and 5.9). Again a time-dependent decrease in phosphorylation is noted for both these Ser sites when stimulated with 4AP5C, compared to L0, and this is not measurably altered by KT5720 treatment. This could indicate that the time-dependent decrease in phosphorylation is a trend in response to the stimulation and represents the effect of prolonged elevated $[Ca^{2+}]_i$.

As inhibition of PKA does regulate the mode of exocytosis, specifically switching KR SVs to FF with 4AP5C stimulation, this may suggest PKA inhibition is able to mediate this RRP mode switch independently of changes to Ser-795, Ser-774 or Ser-778. This could indicate that Dyn-I does not have a role in regulating the RRP FP during this paradigm and another protein recruited at the FP is involved, or that another Ser site on Dyn-I is being regulated to mediate this form of KR. Investigation of the Dyn-I phosphorylation profile via mass-spectrometry could reveal more information with this drug treatment.

Inhibition of PKA also caused an increase in FF with ION5C stimulation, but not HK5C stimulation. Preliminary Western blots revealed no significant changes in Ser-795, Ser-774 or Ser-778 phosphorylation between these stimuli during PKA inhibition, suggesting PKA activity regulates the mode of exocytosis in other ways.

5.3.4 The Effect of PKA Activation upon Dyn-I Phosphorylation

The activation of PKA with 50 μ M cBIMPS has been shown to switch RP SVs to KR with both HK5C and ION5C (Figure 3.6), without affecting RRP SVs. Potentially cBIMPS may increase the occurrence of KR by decreasing the phosphorylated state of Ser-795. Treatment with cBIMPS did significantly decrease Ser-795 phosphorylation during HK5C stimulation at 2 and 15 sec, and during ION5C stimulation at 2 sec (Figure 5.11). Samples treated with cBIMPS and unstimulated (LO), saw no significant change in Ser-795 phosphorylation levels across either time point, suggesting an effect linked to stimulation.

The activation of PKA with cBIMPS had no significant effect upon the phosphorylated state of Dyn-I Ser-774 and Ser-778 over the same time points (Figures 5.12 and 5.13). These data may suggest that the action of cBIMPS to increase KR of the RP is working through Dyn-I Ser-795, partly due to the specificity, though sites not studied here should be investigated further. As treatment with OA and PMA have been shown to increase Ser-795 (Figure 1.17) and switch RRP SVs to FF (Figure 1.11 B), it could be the Dyn-I associated with these vesicles has become phosphorylated thus the RP undergoes FF too. However, when cBIMPS activates PKA the RP Dyn-I Ser-795 becomes dephosphorylated allowing the RP to undergo KR exocytosis.

5.4 Conclusion

Dyn-I Ser-795 is an *in vivo* phosphorylation site that may undergo changes in phosphorylation during stimulation. Ser-795 becomes dephosphorylated when RP SVs release via KR during PKA activation, and an increase in Ser-795 phosphorylation is observed when PP1 and PP2A are inhibited, increasing the number of SVs undergoing

FF. Both of these results suggest the mechanism to switch the mode of exocytosis can sometimes be linked to the phosphorylated state of Ser-795. Both Dyn-I Ser-774 and Ser-778 display a time-dependent dephosphorylation when stimulated with 4AP5C, independent of drug treatments, and this could be a general effect of prolonged increased $[Ca^{2+}]_i$ levels, as it is similar to what has been observed with HK5C and ION5C.

Chapter 6:

General Discussion

6.1 Results

The KR mode of exocytosis has been a controversial topic in neuronal communication since its inception over 40 years ago (Heuser and Reese, 1973; Ceccarelli, *et al.*, 1973). Since these seemingly opposing discoveries FF has been well established as a predominant mode of exocytosis in neurons, and while there is consensus that multiple modes of recycling exist (CME, ADBE, UE) with new modes being theorised (Soykan, *et al.*, 2017), there is still conflict surrounding KR in neurons (Chanaday and Kavalali, 2017).

KR has been well studied in non-neuronal secretory cells, such as chromaffin cells where exocytosis is both larger and slower (Elhamdani, *et al.*, 2006; Chan, *et al.*, 2010; Guček, *et al.*, 2016), but such a presence in neurons is more debatable due to the difficulty of visualising KR, in part owed to the speed at which it occurs and the small FP size (for in-depth reviews see: Rizzoli and Jahn, 2007; He and Wu, 2007; Chanaday and Kavalali, 2017).

Recently work by Ashton and colleagues has determined that SVs in rat cerebral cortical synaptosomes can release via KR during certain stimulation paradigms (Figure 1.11), and that the mode of release can be determined using a combination of maximal Glu release (determined using Ca^{2+} dose response curves – Figure 1.7) and FM 2-10 dye release assays. Ashton and colleagues have also outlined a major role for $[\text{Ca}^{2+}]_i$ in the regulation of the mode of exocytosis, specifically, increases in $[\text{Ca}^{2+}]_i$ can switch SVs which undergo FF to KR (Ashton, manuscript in preparation; Figures 1.8 and 1.16).

The aim of this thesis was to establish whether regulating the activity of PKA, or the level of cAMP in nerve terminals, via AC activity, could affect the mode of exocytosis, and if such effects could be related to changes in the phosphorylated state of Dyn-I. The results presented here further support the existence of KR as a common mode of exocytosis in neurons and have identified PKA and cAMP levels as regulators of the mode of release, and EPACs as regulators of the release of the RP of SVs. Results presented in Chapter 5 also demonstrate that Dyn-I Ser-795 is an *in vivo* phosphorylation site that retains a low level of phosphorylation during rest, seeing an increase in phosphorylation upon terminal stimulation. Ser-795 has also been shown to undergo specific changes in phosphorylation which correlate with expected changes in the mode of exocytosis.

6.1.1 The Roles of PKA, Dyn-I and Actin in Neurotransmission

This thesis has established that changes to the activity of PKA can switch the mode of exocytosis for both SV pools, independently of changes to $[Ca^{2+}]_i$, and without compromising the bioenergetics of nerve terminals. Inhibition of PKA can specifically switch RRP SVs to release via FF in a similar manner to the inhibition of Dyn-I with Dynasore can switch the mode. This could implicate Dyn-I in the regulation of RRP release, however, further research needs to be conducted to determine if PKA regulates a phosphatase that dephosphorylates Dyn-I or perhaps a binding partner (e.g. syntaphilin) which can bind and inhibit Dyn-I directly.

Activation of PKA can increase the number of RP SVs releasing via KR, and this could be through the activation of Dyn-I, though as Dyn-I requires dephosphorylation to become active PKA cannot be working directly upon Dyn-I. Clearly an intermediate

phosphatase (such as calcineurin) which is activated by PKA is a viable option to dephosphorylate Dyn-I. These data reveal a major role for Dyn-I in regulating release dynamics, though potentially not all Dyn-I within the terminal is required to regulate the mode of release.

Preventing cytosolic Dyn-I from binding to phospholipid membranes (SVs, PM, etc.), did not perturb Glu release or FM 2-10 dye release with either HK5C or ION5C stimuli. Therefore, only a sub-pool of Dyn-I is required to regulate the mode of release during exocytosis, but further research needs to be performed to determine if this Dyn-I is bound to the PM or to SVs as this may have an important implication in the characterisation of specific SV pools, or the structure of the AZ. Though if both the RRP and RP are capable of releasing via either KR or FF, this may indicate that distinct SV pools do not have different proteins present for regulating their mode, but rather non-vesicular components can do this.

Actin plays a vital role in the mobilisation of RP SVs, as destabilising the actin cytoskeleton with latrunculin specifically prevented release of all RP SVs without affecting the RRP. Though actin has previously been described as creating a barrier that SVs cannot cross until terminal depolarisation (Papadopulos, 2017), this is good evidence to prove actin may also have a role in the transport of SVs to the PM for release (Meunier and Gutiérrez, 2016). Actin may also have a role in regulating the mode of the RRP SVs, as perturbation of actin microfilaments affected FM dye release in a way that suggests more SVs releasing via FF.

Actin has been shown to be regulated by, and bind directly to Dyns, and this interaction is enhanced when Dyns can also bind lipids (e.g. at the AZ) (Gu, *et al.*, 2010), which may suggest a role during KR. It has also been suggested that Dyn-I may regulate actin nucleation during endocytosis to aid membrane scission (Lee and De Camilli, 2002), and this could also happen at the FP. Furthermore, actin interacts with intracellular membranes, and research groups have demonstrated that actin can form rings around releasing secretory granules to regulate exocytosis (Nightingale, *et al.*, 2012). As inhibition of actin switches the RRP to FF, it is suggested that actin in conjunction with Dyn-I could regulate the FP of RRP SVs with ION5C stimulation, and that NM-II and actin are regulating the FP of RRP SVs with HK5C stimulation (as HK5C inhibits Dyn-I via PKCs and activates NM-II, while with ION5C Dyn-I is active).

Clearly more research in this area is required to establish what effects actin stabilisation such as with Jasplakinolide (Holzinger, 2009), has upon the release of distinct SV pools and their modes of exocytosis, and utilisation of other research models could aid in this.

6.1.2 The Roles of cAMP and EPACs in Neurotransmission

PKA is regulated by cAMP which is produced by AC, and investigations into the activity of AC determined it can regulate the RRP and RP independently most probably through the regulation of the $[Ca^{2+}]_i$ level via EPACs and PKA activity. The activation of AC blocks release of RP SVs through the activation of EPACs which works to lower the average $[Ca^{2+}]_i$ level within the terminals. Though Ca^{2+} -dependent exocytosis is well established, this is the first evidence to demonstrate that specific changes to $[Ca^{2+}]_i$ levels can regulate the release of distinct SV pools when protein phosphorylation

pathways are modulated. However the link between a decrease in $[Ca^{2+}]_i$ and the loss of RP exocytosis does correlate well with previous work by Ashton and colleagues which demonstrate stimulation with 4AP5C releases only the RRP (Figure 1.7), and induces a lower and more gradual average $[Ca^{2+}]_i$ level (Figure 1.8). Further work to investigate this link between $[Ca^{2+}]_i$ and pools undergoing release could identify a role for Ca^{2+} to regulate aspects of release.

When stimulating with 4AP5C and releasing only the RRP, the activation of AC (with forskolin) appears to switch RRP SVs to a KR mode of exocytosis through the activation of PKA and EPACs. Again this could be due to increases in $[Ca^{2+}]_i$ levels and should also be investigated further.

Interestingly the direct activation of PKA, did not show change, when release was stimulated with 4AP5C, but when PKA is inhibited (with KT5720) before AC is activated, the RRP switches to a FF mode of exocytosis. This may imply that both PKA and EPACs are required to regulate the RRP mode, but clearly further research must be performed with the EPACs inhibitor ESI-09. Alternatively, the lack of a change in the RRP mode when PKA is activated (with cBIMPS) may be due to the RRP SVs that are undergoing FF switching to KR, and the SVs that are undergoing KR switching to FF showing no overall mode switch. Investigating the specific activation of EPACs may reveal more details surrounding the regulation of RP release and the role of Rap1 and Rap2.

Collectively these results demonstrate that PKA can regulate the mode of release distinctly for each SV pool and AC can regulate the release of the RP through activation

of EPACs which reduce the level of $[Ca^{2+}]_i$ and the mode of the RRP potentially through the activation of PKA and EPACs, where the $[Ca^{2+}]_i$ level decreases. These data present many situations where the change in mode could be mediated by a change in the phosphorylated profile of Dyn-I.

6.1.3 The Role of Dyn-I Ser-795 in Mode Regulation

As only a sub-pool of Dyn-I has been shown to be required to regulate the mode of release, changes to the phosphorylated profile of Dyn-I were less easy to determine as the antibodies, though Ser-specific, show all Dyn-I in the terminal not just that which is actually regulating the mode of release. This thesis confirms that Dyn-I Ser-795 is an *in vivo* phosphorylation site, as the presence of PMA only during the final stimulation period (when PMA would be expected to activate PKCs in lysed samples and phosphorylate substrates that may not be available for phosphorylation in the intact tissues) displayed no phospho-Ser-795, but when synaptosomes were pre-treated with PMA before stimulation, intense bands were observed for phosphorylated Ser-795, indicating the PMA was able to cross the PM to activate PKCs to phosphorylate Dyn-I. This demonstrates that the nerve terminals are intact, and that PMA acts by crossing the PM to activate PKCs within the terminal. Research with OA also demonstrates that Ser-795 is a target of either PP1 or PP2A, as an increase in phosphorylation is observed with this treatment, and these changes are independent of changes to other Dyn-I phospho-Ser-sites of interest.

PKA inhibition does not modulate the phosphorylated state of any Dyn-I Ser-site over 5 min when stimulated with 4AP5C, though this treatment has been shown to switch the RRP to FF. A time-dependent decrease in phosphorylation was observed for Ser-778

and Ser-774 with control samples, but PKA inhibition did not disrupt this. Furthermore, no difference in the phosphorylated state of Ser-795 was observed with either HK5C or ION5C stimuli during preliminary research, even though a difference in phosphorylation phenotype was expected, as ION5C switches the mode to FF with PKA inhibition, but HK5C does not. This potentially means that PKA inhibition may not regulate the mode of exocytosis through Dyn-I. Collectively these data suggest that though PKA inhibition is able to switch the specific mode of the RRP, it is not through Ser-795, Ser-778 or Ser-774.

This is the first time a time-dependent decrease in phosphorylation has been observed during 4AP5C stimulation; however a similar observation has been made with HK5C and ION5C stimulation previously (Bhuva, 2015). This is probably the effect of prolonged increased $[Ca^{2+}]_i$ levels as described previously, however further studies could establish the extent of this effect.

The activation of PKA decreased the detectable level of Ser-795 during stimulation with both HK5C and ION5C. As the activation of PKA has been shown to switch only the RP to KR, these data could suggest that Dyn-I Ser-795 must be dephosphorylated in order for RP SVs to release by KR, and a certain threshold of phosphorylation is required for this pool to release via FF. Though this could just be a correlation, it is the first time a significant decrease in Ser-795 phosphorylation has been report during KR (where Dyn-I is theorised to undergo dephosphorylation in order to mediate this mode). As the inhibition of PP1 and PP2A with OA treatment has been shown to increase both the number of SVs undergoing FF, and the phosphorylated state of Ser-795, these data could indicate a reduction of Ser-795 is required to mediate KR.

In order to establish if there is a causal relationship between the level of Ser-795 phosphorylation and the mode of exocytosis, further Western blotting studies of conditions which induce KR should be investigated. The AC activator, forskolin, used in this thesis, did display an increase in KR with 4AP5C stimulation, however this was attributed to a noticeable increase in $[Ca^{2+}]_i$ during the same period, which may indicate Ser-795 is not involved. Similarly inhibition of calcineurin with Cys A has displayed an increase in KR with HK5C and ION5C (Figure 1.16 D-E) which could be studied, however $[Ca^{2+}]_i$ levels also increased with these stimulations (Figure 1.16 G-H). Previous Western blot research has not established any change in the phosphorylated state of Ser-795 during Cys A treatment (Bhuva, 2015; Singh, 2017), over a range of stimulation conditions.

Future studies should look at alternative means to analyse the phosphorylated profile of Dyn-I under mode switching conditions, such as using phosphoproteomics in mass spectrometry. This could reveal if there is a causal link between Dyn-I Ser-795 and the mode of exocytosis, or if other Dyn-I Ser sites are involved.

6.2 Future Studies

This thesis contributes new knowledge to the understanding of how the distinct pools of SVs are released, how the activity of PKA and AC (via cAMP) pathways can regulate the mode of exocytosis, and how the phosphorylated profile of Dyn-I can regulate the modes of exocytosis. However, further research must be undertaken in order to establish what other factors can regulate the mode of SV exocytosis, what the specific differences between the SVs pools are during release, and to further reveal the relationship between the mode of release and the phosphorylated state of Dyn-I. Some of the experiments suggested in this section may aid current knowledge and expand the understanding surrounding SV exocytosis in neurons.

- Chapter 3 of this thesis presents the investigation of the activity of PKA through the use of cBIMPS and KT5720. A dual-treatment to study FM 2-10 dye release was performed with both these drugs, but a Glu release assay was not. For completeness it would be useful to perform the Glu release assay for the dual-drug treatment of KT5720 and cBIMPS, even though individually these drugs do not perturb Glu release.
- MITMAB and latrunculin have shown very interesting specific effects and it is important to perform the Fura-2 $[Ca^{2+}]_i$ assay with both MITMAB and latrunculin to determine if they affect the level of $[Ca^{2+}]_i$, as this could help explain the phenotype produced by latrunculin.
- Though the mode of release during inhibition of EPACs with ESI-09 was not studied in this thesis, this is clearly an important experiment to determine how EPACs may affect the mode of exocytosis, particularly for the action of forskolin upon 4AP5C evoked exocytosis.

- Though 9-cp-ade had no effect on any assays utilised in this thesis (though the drug itself was working by preventing the action of forskolin), it is important to perform further research with 9-cp-ade focusing on longer drug incubation times (e.g. 20 min at 37°C), to determine any specifics that may be time-dependent.
- Western blotting may not provide the whole story of the phosphorylated profile of Dyn-I, as there are many other Ser sites that could be undergoing changes during exocytosis. Therefore, preparing synaptosomal samples treated with various drug conditions to induce specific modes of exocytosis, then immunopurifying the Dyn-I for analysis by mass spectrometry may reveal more details surrounding the phosphorylation sites which could aid in finding a link between the mode of release and the phosphorylated profile of Dyn-I.
- In order to determine if the modes of exocytosis are detectable in other experimental models primary cultures of rat cerebrocortical neurons could be prepared and the FM 2-10 dye assay could be modified to be used with a fluorescent microscope to be able to visualise KR and FF events. This will be important in order to do the transfection experiments, highlighted below.
- If analysis by mass spectrometry highlights a number of key Ser-sites developing phosphomimetic Dyn-I constructs where Ser sites of interest (Ser-795, Ser-778 and Ser-774) are either continually phosphorylated or dephosphorylated and transfecting them into neurons could permanently switch the mode of exocytosis, establishing these sites are mode regulators. A longer term aim of this project would be to make transgenic animals by CRISPR/Cas9 technology (Cong, *et al.*, 2013), to replace the Ser-795 residue with either alanine to prevent phosphorylation, or replace the Ser with aspartic

acid to mimic constant phosphorylation. This could be used with our assays to confirm this site and how it can have a role in the regulation of the mode. Further, such animals may present a specific phenotype which may reveal the importance of phospho-Ser-795 on Dyn-I in higher order processes involving synaptic plasticity such as memory and behaviour.

- As the disassembly of actin perturbs release of the RP, it is important to investigate how the stabilisation of actin with jasplakinolide affects the release of SV pools and influences the mode of exocytosis. This would create a better picture for the role of actin in neurons, beyond that of a simple cytoskeletal element.
- Over the long-term it would be important to utilise super-resolution fluorescence microscopy alongside fluorescent monoclonal antibodies to detect the phospho-Ser-795 site, during stimulation. As we believe this site only occurs in a sub-pool of Dyn-I, specific changes in sub-cellular compartments may be observed (e.g. on the SVs or at the AZ).

Chapter 7:

References and Appendix

- Agilent Technologies, Inc. (2019). Agilent Seahorse XF Cell Mito Stress Test Kit: User Guide: 103016-400. Wilmington, DE: Author.
- Alabi, A. A. and Tsien, R. W. (2012). Synaptic Vesicle Pools and Dynamics. *Cold Spring Harb. Perspect. Biol.*, **4**:a013680.
- Alabi, A. A. and Tsien, R. W. (2013). Perspectives on kiss-and-run: role in exocytosis, endocytosis, and neurotransmission. *Annu. Rev. Physiol.*, **75**, 393-422.
- Albillos, A., Dernick, G., Horstmann, H., Almers, W., Alvarez de Toledo, G. and Lindau, M. (1997). The exocytotic event in chromaffin cells revealed by patch amperometry. *Nature.*, **389**, 509-512.
- Alés, E., Tabares, L., Poyato, J. M., Valero, V., Lindau, M. and Alvarez de Toledo, G. (1999). High calcium concentrations shift the mode of exocytosis to the kiss-and-run mechanism. *Nat. Cell. Biol.*, **1**, 40-44.
- Almahariq, M., Tsalkova, T., Mei, F. C., Chen, H., Zhou, J., sastry, S. K., schwede, F. and Cheng, X. (2013). A novel EPAC-specific inhibitor suppresses pancreatic cancer cell migration and invasion. *Mol. Pharmacol.*, **83**, 122-128.
- Anantharam, A., Bittner, M. A., Aikman, R. L., Stuenkel, E. L., Schmid, S. L., Axelrod, D. and Holz, R. W. (2011). A new role for the dynamin GTPase in the regulation of fusion pore expansion. *Mol. Biol. Cell.*, **22**, 1907-1918.

- Anantharam, A., Axelrod, D. and Holz, R. W. (2012). Real-time imaging of plasma membrane deformations reveals pre-fusion membrane curvature changes and a role for dynamin in the regulation of fusion pore expansion. *J. Neurochem.*, **122**, 661-671.
- Anggono, V. and Robinson, P. J. (2009). Dynamin. *Encyclopedia of Neuroscience*. Edited by Larry R. Squire. Amsterdam , The Netherlands: Elseiver.725-735.
- Antony, B., Burd, C., De Camilli, P., Chen, E., Daumke, O., Faelber, K., Ford, M., Frolov, V. A., Frost, A., Hinshaw, J. E., Kirchhausen, T., Kozlov, M. M., Lenz, M., Low, H. H., McMahon, H., Merrifield, C., Pollard, D., Robinson, P. J., Roux, A. and Schmid, S. (2016). Membrane fission by dynamin: what we know and what we need to know. *EMBO. J.*, **35**, 2270–2284.
- Aravanis, A. M., Pyle, J. L., Harata, N. C. and Tsien, R. W. (2003). Imaging single synaptic vesicles undergoing repeated fusion events: kissing, running, and kissing again. *Neuropharmacol.*, **45**, 797-813.
- Armbruster, M. and Ryan, T. A. (2011). Synaptic vesicle retrieval time is a cell-wide not an individual synapse property. *Nat. Neurosci.*, **14**, 824-826.

- Armbruster, M., Messa, M., Ferguson, S. M., De Camilli, P. and Ryan, T. A. (2013). Dynamin phosphorylation controls optimization of endocytosis for brief action potential bursts. *eLife.*, **2**, e00845. doi:10.7554/eLife.00845.
- Artalejo, C. R., Henley, J.R., McNiven, M. A. and Palfrey, H. C. (1995). Rapid endocytosis coupled to exocytosis in adrenal chromaffin cells involves Ca²⁺, GTP, and dynamin but not clathrin. *PNAS.*, **92**, 8328-8332.
- Artalejo, C. R., Elhamdani, A. and Palfrey, H. C. (2002). Sustained stimulation shifts the mechanism of endocytosis from dynamin-1-dependent rapid endocytosis to clathrin- and dynamin-2-mediated slow endocytosis in chromaffin cells. *PNAS.* **99**, 6358-6363.
- Ashton, A. C. and Ushkaryov, Y. A. (2005). Properties of Synaptic Vesicle Pools in Mature Central Nerve Terminals. *J. Biol. Chem.*, **280**, 37278-37288.
- Ashton, A. C., Patel, M. H. and Sihra, T. S. (2009). Changes in protein phosphorylation and calcium regulate switching between distinct modes of synaptic vesicle exocytosis. *Soc. Neurosci.*
- Ashton, A. C., Sihra, T. S., Babar, P., Patel, M. H., Bhuva, D. A., Singh, D. and Green, J. (Manuscript in preparation for submission). Switching between distinct modes of synaptic vesicle exocytosis depends upon changes in protein phosphorylation and calcium: the contribution of dynamins and myosin 2.

- Bähring, R. and Covarrubias, M. (2011). Mechanisms of closed-state inactivation in voltage-gated ion channels. *J. Physiol.*, **589**, 461-479.
- Balaji, J. and Ryan, T. A. (2007). Single-vesicle imaging reveals that synaptic vesicle exocytosis and endocytosis are coupled by a single stochastic mode. *PNAS.*, **104**, 20576-20581.
- Baldwin, M. L., Rostas, J. A. P. and Sim, A. T. R. (2003). Two modes of exocytosis from synaptosomes are differentially regulated by protein phosphatase types 2A and 2B. *J. Neurochem.*, **85**, 1190-1199.
- Bao, H., Das, D., Courtney, N. A., Jiang, Y., Briguglio, J. S., Lou, X., Roston, D., Cui, Q., Chanda, B. and Chapman, E. R. (2018). Trans-SNARE complex dynamics and number determine nascent fusion pore properties. *Nature.*, **554**, 260-263.
- Barclay, J. W., Craig, T. J., Fisher, R. J., Ciuffo, L. F., Evans, G. J., Morgan, A. and Burgoyne, R. D. (2003). Phosphorylation of Munc18 by protein kinase C regulates the kinetics of exocytosis. *J. Biol. Chem.*, **278**, 10538-10545.
- Barclay, J. W., Morgan, A. and Burgoyne, R. D. (2005). Calcium-dependent regulation of exocytosis. *Cell Calcium.*, **38**, 343-353.

- Bauerfeind, R., Takei, K. and De Camilli, P. (1997). Amphiphysin I is associated with coated endocytic intermediates and undergoes stimulation-dependent dephosphorylation in nerve terminals. *J. Biol. Chem.*, **272**, 30984-30992.
- Beaumont, V., Zhong, N., Fromke, R. C., Ball, R. W. and Zucker, R. S. (2002). Temporal synaptic tagging by I(h) activation and actin: involvement in long-term facilitation and cAMP-induced synaptic enhancement. *Neuron.*, **33**, 601-613.
- Berberian, K., Torres, A. J., Fang, Q., Kisler, K. and Lindau, M. (2009). F-actin and myosin II accelerate catecholamine release from chromaffin granules. *J. Neurosci.*, **29**, 863-870.
- Betz, W. J., Mao, F. and Bewick, G. S. (1992). Activity-dependent Fluorescent Staining and Destaining of Living Vertebrate Motor Nerve Terminals. *J. Neurosci.*, **12**, 363-375.
- Bhuva, D. (2015). Dynamins and myosin-II regulate the distinct modes of synaptic vesicle exocytosis in mature cerebrocortical nerve terminals and this involves calcium dependent phosphorylations. Doctoral thesis, UCLan, Preston.
- Bialojan, C. and Takai, A. (1988). Inhibitory effect of a marine-sponge toxin, okadaic acid, on protein phosphatases. Specificity and kinetics. *Biochem. J.*, **256**, 283-290.

- Biel, M. (2008). Cyclic Nucleotide-regulated Cation Channels. *J. Biol. Chem.*, **284**, 9017-9021.
- Bittner, G. D. and Kennedy, D. (1970). Quantitative aspects of transmitter release. *J. Cell. Biol.*, **47**, 585-592.
- Boczan, J., Leenders, A. G. M. and Sheng, Z. H. (2004). Phosphorylation of Syntaphilin by cAMP-dependent Protein Kinase Modulates Its Interaction with Syntaxin-1 and Annuls Its Inhibitory Effect on Vesicle Exocytosis. *J. Biol. Chem.*, **279**, 18911-18919.
- Bos, J. L. (2006). Epac proteins: multi-purpose cAMP targets. *Trends. Biochem. Sci.*, **31**, 680-686.
- Brent, P. J., Herd, L., Saunders, H., Sim, A. T. R. and Dunkley, P. R. (1997). Protein Phosphorylation and Calcium Uptake into Rat Forebrain Synaptosomes: Modulation by the σ Ligand, 1,3-Ditolyguanidine. *J. Neurochem.*, **68**, 2201-2211.
- Byczkowicz, N., Ritzau-Jost, A., Delvendahl, I. And Hallermann, S. (2017). How to maintain active zone integrity during high-frequency transmission. *Neurosci. Res.* **127**, 61-69.

- Cano, R. and Tabares, L. (2016). The Active and Periaxial Zone Organization and the Functional Properties of Small and Large Synapses. *Front. Synaptic Neurosci.*, **8**, doi: 10.3389/fnsyn.2016.00012.
- Cao, H., Garcia, F. and McNiven, M. A. (1998). Differential distribution of dynamin isoforms in mammalian cells. *Mol. Biol. Cell.* **9**, 2595-2609.
- Del Castillo, J. and Katz, B. (1954). Quantal components of the end-plate potential. *J. Physiol.*, **124**, 560-573.
- Cazares, V. A., Njus, M. M., Manly, A. Saldate, J. J., Subramani, A., Ben-Simon, Y., Sutton, M. A., Ashery, U. and Stuenkel, E. L. (2016). Dynamic Partitioning of Synaptic Vesicle Pools by the SNARE-Binding Protein Tomosyn. *J. Neurosci.*, **36**, 11208–11222.
- Cesca, F., Baldelli, P., Valtorta, F. and Benfenati, F. (2010). The synapsins: Key actors of synapse function and plasticity. *Prog. Neurobiol.*, **91**, 312-348.
- Chamberland, S. and Tóth, K. (2016). Functionally heterogeneous synaptic vesicle pools support diverse synaptic signalling. *J. Physiol.*, **594**, 825–835.
- Chan, S., Doreian, B. and Smith, C. (2010). Dynamin and Myosin Regulate Differential Exocytosis from Mouse Adrenal Chromaffin Cells. *Cell Mol. Neurobiol.*, **30**, 1351-1357.

- Chanaday, N. L. and Kavalali, E. T. (2017). How do you recognize and reconstitute a synaptic vesicle after fusion? *F1000Research.*, **6**, doi:10.12688/f1000research.12072.1
- Chang, C. Y., Jiang, X., Moulder, K. L. and Mennerick, S. (2010). Rapid Activation of Dormant Presynaptic Terminals by Phorbol Esters. *J. Neurosci.*, **30**, 10048-10060.
- Chang, C. W., Chiang, C. W. and Jackson, M. B. (2017). Fusion pores and their control of neurotransmitter and hormone release. *J. Gen. Physiol.*, **149**, 301-322.
- Chavez-Noriega, L. E. and Stevens, C. F. (1994). Increased transmitter release at excitatory synapses produced by direct activation of adenylate cyclase in rat hippocampal slices. *J. Neurochem.*, **14**, 310-317.
- Chen, C. and Regehr, W. G. (1997). The mechanism of cAMP-mediated enhancement at a cerebellar synapse. *J. Neurosci.*, **17**, 8687-8694.
- Cheung, G., Jupp, O. J. and Cousin, M. A. (2010). Activity-dependent bulk endocytosis and clathrin-dependent endocytosis replenish specific synaptic vesicle pools in central nerve terminals. *J. Neurosci.*, **30**, 8151-8161.

- Chung, C., Barlyko, B., Leitz, J., Liu, X. and Kavalali, E. T. (2010). Acute dynamin inhibition dissects synaptic vesicle recycling pathways that drive spontaneous and evoked neurotransmission. *J. Neurosci.*, **30**, 1363-1376.
- Cingolani, L. A. and Goda, Y. (2008). Actin in action: the interplay between the actin cytoskeleton and synaptic efficacy. *Nat. Rev. Neurosci.*, **9**, 344-356.
- Clayton, E. L., Evans, G. J. O. and Cousin, M. A. (2007). Activity-dependent control of bulk endocytosis by protein dephosphorylation in central nerve terminals. *J. Physiol.*, **585**, 687-691.
- Clayton, E. L., and Cousin, M. A. (2008). Differential labelling of bulk endocytosis in nerve terminals by FM dyes. *Neurochem. Int.*, **53**, 51-55.
- Clayton, E. L. and Cousin, M. A. (2009). The molecular physiology of activity-dependent bulk endocytosis of synaptic vesicles. *J. Neurochem.*, **111**, 901-914.#
- Clayton, E. L., Anggono, V., Smillie, K. J., Chau, N., Robinson, P. J. and Cousin, M. A. (2009). The Phospho-Dependent Dynamin-Syndapin Interaction Triggers Activity-Dependent Bulk Endocytosis of Synaptic Vesicles. *J. Neurosci.*, **29**, 7706-7717.
- Clayton, E. L., Sue, N., Smillie, K. J., O'Leary, T., Bache, N., Cheung, G., Cole, A. R., Wyllie, D. J., Sutherland, C., Robinson, P. J. and Cousin, M. A. (2010).

Dynamin I phosphorylation by GSK3 controls activity-dependent bulk endocytosis of synaptic vesicles. *Nat. Neurosci.*, **13**, 845-851.

- Cocucci, E., Gaudin, R. and Kirchhausen, T. (2014). Dynamin recruitment and membrane scission at the neck of a clathrin-coated pit. *Mol. Biol. Cell.*, **25**, 3595-3609.
- Cohen, P. T. W. (2002). Protein phosphatase 1 – targeted in many directions. *J. Cell. Sci.*, **115**, 241-256.
- Coles, C. H. and Bradke, F. (2015). Coordinating neuronal actin-microtubule dynamics. *Curr. Biol.*, **25**, 677-691.
- Cong, L., Ran, F. A., Cox, D., Lin, S., Barretto, R., Habib, N., Hsu, P. D., Wu, X., Jiang, W., Marraffini, L. A. and Zhang, F. (2013). Multiplex genome engineering using CRISPR/Cas systems. *Sci.*, **339**, 819-823.
- Cook, T. A., Urrutia, R. and McNiven, M. A. (1994). Identification of dynamin 2, an isoform ubiquitously expressed in rat tissues. *PNAS.*, **91**, 644-648.
- Cook, T. A., Messa, K. and Urrutia, R. (1996). Three dynamin-encoding genes are differentially expressed in developing rat brain. *J. Neurochem.*, **67**, 927-931.

- Cortès-Saladelafont, E., Lipstein, N. and garcía-cazorla. (2018). Presynaptic disorders: a clinical and pathophysiological approach focused on the synaptic vesicle. *J. Inherit. Metab. Dis.*, **41**, 1131-1145.
- Cotter, K., Stransky, L., McGuire, C. and Forgac, M. (2015). Recent Insights into the Structure, Regulation and Function of the V-ATPases. *Trends. Biochem. Sci.*, **40**, 611-622.
- Cousin, M. A. and Robinson, P. J. (2000). Two Mechanisms of Synaptic Vesicle Recycling in Rat Brain Nerve Terminals. *J. Neurochem.*, **75**, 1645–1653.
- Cousin, M. A. and Robinson, P. J. (2001). The dephosphins: dephosphorylation by calcineurin triggers synaptic vesicle endocytosis. *Trends Neurosci.*, **24**, 659-665.
- Cousin, M. A. (2017). A (free) radical approach reveals the physiological function of different synaptic vesicle pools. *J. Physiol.*, **595**, 1005-1006.
- Damke, H., Baba, T., Warnock, D. E. and Schmid, S. L. (1994). Induction of mutant dynamin specifically blocks endocytic coated vesicle formation. *J. Cell. Biol.*, **127**, 915-934.
- Dao, K. K., Teigen, K., Kopperud, R., Hodneland, E., schwede, F., Christine, A. E., Martinez, A. and Døskeland, S. O. (2006). Epac1 and cAMP-dependent protein kinase holoenzyme have similar cAMP affinity, but their cAMP domains have

distinct structural features and cyclic nucleotide recognition. *J. Biol. Chem.*, **281**, 21500-21511.

- Das, S., Gerwin, C. and Sheng, Z. H. (2003). Syntaphilin binds to dynamin-1 and inhibits dynamin-dependent endocytosis. *J. Biol. Chem.*, **278**, 41221-41226.
- Davies, S. P., Reddy, H., Caivano, M. and Cohen, P. (2000). Specificity and mechanism of action of some commonly used protein kinase inhibitors. *Biochem. J.*, **351**, 95-105.
- Denker, A. and Rizzoli, S. O. (2010). Synaptic vesicle pools: an update. *Front Synaptic Neurosci.*, **2**, doi: 10.3389/fnsyn.2010.00135.
- Denker, A., Kröhnert, K., Bückers, J., Neher, E. and Rizzoli, S. O. (2011). The reserve pool of synaptic vesicles acts as a buffer for proteins involved in synaptic vesicle recycling. *Proc. Natl. Acad. Sci. USA.*, **108**, 17183-17188.
- Dessauer, C. W., Scully, T. T. and Gilman, A. G. (1997). Interactions of Forskolin and ATP with the Cytosolic Domains of Mammalian Adenylyl Cyclase. *J. Biol. Chem.*, **272**, 22272–22277.
- Dillon, C. and Goda, Y. (2005). The actin cytoskeleton: integrating form and function at the synapse. *Annu. Rev. Neurosci.*, **28**, 25-55.

- Dodd, P. R., Hardy, J. A., Oakley, A. E., Edwardson, J. A., Perry, E. K. and Delaunoy, J. P. (1981). A rapid method for preparing synaptosomes: comparison, with alternative procedures. *Brain. Res.*, **226**, 107-118.
- Doreian, B. W., Fulop, T. G. and Smith, C. B. (2008). Myosin II activation and actin reorganization regulate the mode of quantal exocytosis in mouse adrenal chromaffin cells. *J. Neurosci.*, **28**, 4470-4478.
- Doussau, F. and Augustine, G. J. (2000). The actin cytoskeleton and neurotransmitter release: an overview. *Biochimie.*, **82**, 353-363.
- Doussau, F., Schmidt, H., Dorgans, K., Valera, A. M., Poulain, B. and Isope, P. (2017). Frequency-dependent mobilization of heterogeneous pools of synaptic vesicles shapes presynaptic plasticity. *eLife* 2017;6:e28935.
- Douthitt, H. L., Luo, F., McCann, S. D. and meriney, S. D. (2011). Dynasore, an inhibitor of dynamin, increases the probability of transmitter release. *Neuroscience.*, **172**, 187-195.
- Dunaevsky, A. and Connor, E. A. (2000). F-Actin Is Concentrated in Nonrelease Domains at Frog Neuromuscular Junctions. *J. Neurosci.*, **20**, 6007-6012.
- Elhamdani, A., Azizi, F. and Artalejo, C. R. (2006). Double patch clamp reveals that transient fusion (kiss-and-run) is a major mechanism of secretion in calf

adrenal chromaffin cells: high calcium shifts the mechanism from kiss-and-run to complete fusion. *J. Neurosci.*, **26**, 3030-3036.

- Erecińska, M., Nelson, D. and Silver, I. A. (1996). Metabolic and energetic properties of isolated nerve ending particles (synaptosomes). *Biochim. Biophys. Acta.*, **1277**, 13-34.
- Esposito, G., Ana Clara, F. and Verstreken, P. (2012). Synaptic vesicle trafficking and Parkinson's disease. *Dev. Neurobiol.*, **72**, 134-144.
- Evans, G. J. O. (2015). The Synaptosome as a Model System for Studying Synaptic Physiology. *Cold. Spring. Harb. Protoc.*, **5**, 421-424.
- Fà, M., Staniszewski, A., Saeed, F., Francis, Y. I. and Arancio, O. (2014). Dynamin 1 Is Required for Memory Formation. *PLoS ONE.*, **9**(3), doi:10.1371/journal.pone.0091954.
- Faelber, K., Posor, Y., Gao, S., Held, M., Roske, Y., Schulze, D., Haucke, V., Noé, F. and Daumke, O. (2011). Crystal structure of nucleotide-free dynamin. *Nature.*, **477**, 556-560.
- Fatt, P. and Katz, B. (1952). Spontaneous subthreshold activity at motor nerve endings. *J. Physiol.*, **117**, 109-128.

- Ferguson, S. M., Brasnjo, G., hayashi, M., Wölfel, M., Collesi, C., Giovedi, S., Raimondi, A., Gong, L. W., Ariel, P., Paradise, S., O'Toole, E., Flavell, R., Cremona, O., Miesenböck, G., Ryan T. A. and De Camilli, P. (2007). A selective activity-dependent requirement for dynamin 1 in synaptic vesicle endocytosis. *Science.*, **316**, 570-574.
- Ferguson, S. M., Raimondi, A., Paradise, S., Shen, H., Mesaki, K., Ferguson, A., Destaing, O., Ko, G., Takasaki, J., Cremona, O., O' Toole, E. and De Camilli, P. (2009). Coordinated Actions of Actin and BAR Proteins Upstream of Dynamin at Endocytic Clathrin-Coated Pits. *Dev. Cell.*, **17**, 811-822.
- Ferguson, S. M. and De Camilli, P. (2012). Dynamin, a membrane-remodelling GTPase. *Nat. Rev. Mol. Cell Biol.*, **13**, 75-88.
- Fernandes, H. B., Riordan, S., Nomura, T., Remmers, C. L., Kraniotis, S., Marshall, J. J., Kukreja, L., Vassar, R. and Contractor, A. (2015). Epac2 Mediates cAMP-Dependent Potentiation of Neurotransmission in the Hippocampus. *J. Neurosci.*, **35**, 6544-6553.
- Fernández, J. J., Cadenas, M. L., Souto, M. L., Trujillo, M. M. and Norte, M. (2002). Okadaic acid, useful tool for studying cellular processes. *Curr. Med. Chem.*, **9**, 229-262.
- Ferrero, J. J., Alvarez, A. M., Ramirez-Franco, J., Godino, M. C., Bartolome-Martin, D., Aguado, C., Torres, M., Lujan, R., Ciruela, F. and Sanchez-Prieto, J.

(2013). β -adrenergic receptors activate Epac, translocate Munc13-1 and enhance the Rab3A-Rim1 α interaction to potentiate glutamate release at cerebrocortical nerve terminals. *J. Biol. Chem.*, **288**, 31370-31385.

- Fesce, R., Grohovaz, F., Valtorta, F. and Meldolesi, J. (1994). Neurotransmitter release: fusion or 'kiss-and-run'? *Trends Cell Biol.*, **4**, 1-4.
- Ford, M. G. J., Jenni, S. and Nunnari, J. (2011). The crystal structure of dynamin. *Nature.*, **477**, 561-566.
- Fowler, M, W. and Staras, K. (2015). Synaptic vesicle pools: Principles, properties and limitations. *Exp. Cell. Res.*, **335**, 150-156.
- Fulop, T., Doreian, B. and Smith C. (2008). Dynamin I plays dual roles in the activity-dependent shift in exocytic mode in mouse adrenal chromaffin cells. *Arch. Biochem. Biophys.*, **477**, 146-154.
- Gaffield, M. A., and Betz, W. J. (2006). Imaging synaptic vesicle exocytosis and endocytosis with FM dyes. *Nat. Protoc.*, **1**, 2916–2921.
- Gan, Q. and Watanabe, S. (2018). Synaptic Vesicle Endocytosis in Different Model Systems. *Front. Cell. Neurosci.*, **28**, 171, doi:10.3389/fncel.2018.00171.
- Gao, J., Hirata, M., Mizokami, A., Zhao, J., Takahashi, I., Takeuchi, H. and Hirata, M. (2016). Differential role of SNAP-25 phosphorylation by protein kinases A

and C in the regulation of SNARE complex formation and exocytosis in PC12 cells. *Cell. Sig.*, **28**, 425-437.

- Gasman, S., Chasserot-Golaz. S., Malacombe, M., Way, M. and Bader, M. F. (2004). Regulated Exocytosis in Neuroendocrine Cells: A Role for Subplasmalemmal Cdc42/N-WASP-induced Actin Filaments. *Mol. Biol. Cell.*, **15**, 520-531.
- Gaydukov, A. E., Tarasova, E. O. and Balezina, O. P. (2013). Calcium-dependent phosphatase calcineurin downregulates evoked neurotransmitter release in neuromuscular junctions of mice. *Neurochem. J.*, **7:29**, 29-33.
- Glebov, O. O., Jackson, R. E., Winterflood, C. M., Doherty, P., Ewers, H. and Burrone, J. (2017). Nanoscale Structural Plasticity of the Active Zone Matrix Modulates Presynaptic Function. *Cell. Rep.*, **18**, 2715-2728.
- Graham, M. E., O'Callaghan, D. W., McMahon, H. T. and Burgoyne, R. D. (2002). Dynamin-dependent and dynamin-independent processes contribute to the regulation of single vesicle release kinetics and quantal size. *PNAS.*, **99**, 7124-7129.
- Graham, M. E., Anggono, V., bache, N., Larsen, M. R., Craft, G. E. and Robinson, P.J. (2007). The in vivo phosphorylation sites of rat brain dynamin I. *J. Biol. Chem.*, **282**, 14695-14707.

- Grandoch, M., Roscioni, S. S. and Schmidt, M. (2010). The role of Epac proteins, novel cAMP mediators, in the regulation of immune, lung and neuronal function. *Br. J. Pharmacol.*, **159**, 265-284.
- Granseth, B., Odermatt, B., Royle, S. J. and Lagnado, L. (2006). Clathrin-mediated endocytosis is the dominant mechanism of vesicle retrieval at hippocampal synapses. *Neuron.*, **51**, 773-786.
- Granseth, B., Odermatt, B., Royle, S. J. and Lagnado, L. (2007). Clathrin-mediated endocytosis: the physiological mechanism of vesicle retrieval at hippocampal synapses. *J. Physiol.*, **585**, 681-686.
- Gray, E. G. and Whittaker V. P. (1962). The isolation of nerve endings from brain: an electron-microscopic study of cell fragments derived by homogenization and centrifugation. *J. Anat.*, **96**, 79-88.
- Grimaldi, M., Atzori, M., Ray, P. and Alkon, D. L. (2001). Mobilization of Calcium from Intracellular Stores, Potentiation of Neurotransmitter-Induced Calcium Transients, and Capacitative Calcium Entry by 4-Aminopyridine. *J. Neurosci.*, **21**, 3135-3143.
- Grynkiewicz, G., Poenie, M. and Tsien, R. Y. (1985). A new generation of Ca²⁺ indicators with greatly improved fluorescence properties. *J. Biol. Chem.* **260**, 3440-3450.

- Gu, C., Yaddanapudi, S., Weins, A., Osborn, T., Reiser, J., Pollak, M., Hartwig, J. and Sever, S. (2010). Direct dynamin-actin interactions regulate the actin cytoskeleton. *EMBO J.*, **29**, 3593-3606.
- Guarnieri, F. C. (2017). How Do Synaptic Vesicles “Know” Which Pool They Belong to? *J. Neurosci.*, **37**, 2276-2278.
- Guček, A., Jorgačevski, J., Singh, P., Geisler, C., Lisjak, M., Vardjan, N., Kreft, M., Egner, A. and Zorec, R. (2016). Dominant negative SNARE peptides stabilize the fusion pore in a narrow, release-unproductive state. *Cell. Mol. Life. Sci.*, **73**, 3719-3731.
- Gulaboski, R., Pereira, C. M., Cordeiro, M. N., Silva, A. F., Hoth, M. and Bogeski, I. (2008). Redox properties of the calcium chelator Fura-2 in mimetic biomembranes. *Cell. Calcium.*, **43**, 615-621.
- Gutiérrez, L. M. and Villanueva, J. (2018). The role of F-actin in the transport and secretion of chromaffin granules: an historic perspective. *Pflugers Arch.*, **470**, 181-186.
- Hanoune, J. and Defer, N. (2001). Regulation and role of adenylyl cyclase isoforms. *Annu. Rev. Pharmacol. Toxicol.*, **41**, 145-174.
- Harata, N., Pyle, J. L., Aravanis, A. M., Mozhayeva, M., Kavalali, E. T. and Tsien, R. W. (2001). Limited numbers of recycling vesicles in small CNS nerve

terminals: implications for neural signaling and vesicular cycling. *Trends. Neurosci.*, **24**, 637-643.

- Harata, N. C., Aravanis, A. M. and Tsien, R. W. (2006). Kiss-and-run and full-collapse fusion as modes of exo-endocytosis in neurosecretion. *J. Neurochem.*, **97**, 1546-1570.
- He, L., Wu, X. S., Mohan R. and Wu, L. G. (2006). Two modes of fusion pore opening revealed by cell-attached recordings at a synapse. *Nature.*, **444**, 102-105.
- He, L. and Wu, L. G. (2007). The debate on the kiss-and-run fusion at synapses. *Trends Neurosci.*, **30**, 447-455.
- Hebb, C. O. and Whittaker, V. P. (1958). Intracellular distributions of acetylcholine and choline acetylase. *J. Physiol.*, **142**, 187-196.
- Henkel, A. W., Kang, G. and Kornhuber, J. (2001). A common molecular machinery for exocytosis and the 'kiss-and-run' mechanism in chromaffin cells is controlled by phosphorylation. *J. Cell. Sci.*, **114**, 4613-4620.
- Herrero, I. and Sánchez-Prieto, J. (1996). cAMP-dependent Facilitation of Glutamate Release by β -Adrenergic Receptors in Cerebrocortical Nerve Terminals. *J. Biol. Chem.*, **271**, 30554–30560.

- Herskovits, J. S., Burgess, C. C., Obar, R. A. and Vallee, R. B. (1993). Effect of mutant rat dynamin on endocytosis. *J. Cell. Biol.*, **122**, 565-578.
- Heuser, J. E. and Reese, T. S. (1973). Evidence for recycling of synaptic vesicle membrane during transmitter release at the frog neuromuscular junction. *J. Cell. Biol.*, **57**, 315-344.
- Heuser, J. E., Reese, T. S., Dennis, M. J., Jan, Y., Jan, L. and Evans, L. (1979). Synaptic vesicle exocytosis captured by quick freezing and correlated with quantal transmitter release. *J. Cell. Biol.*, **81**, 275-300.
- Heymann, J. A. and Hinshaw, J. (2009). Dynamins at a glance. *J. Cell. Sci.*, **122**, 3427-3431.
- Hilfiker, S., Czernik, A. J., Greengard, P. and Augustine, G. J. (2001). Tonicly active protein kinase A regulates neurotransmitter release at the squid giant synapse. *J. Physiol.*, **531**, 141-146.
- Hill, T. A., Odell, L. R., Quan, A., Abagyan, R., Ferguson, G., Robinson, P. J. and McCluskey, A. (2004). Long chain amines and long chain ammonium salts as novel inhibitors of dynamin GTPase activity. *Bioorg. Med. Chem. Lett.*, **14**, 3275-3278.
- Hinshaw, J. E. (2000). Dynamin and its role in membrane fission. *Annu. Rev. Cell. Dev. Biol.*, **16**, 483-519.

- Holroyd, P., Lang, T., Wenzel, D., De Camilli, P. and Jahn, P. (2002). Imaging direct, dynamin-dependent recapture of fusing secretory granules on plasma membrane lawns from PC12 cells. *PNAS*, **99**, 16806-16811.
- Hosoi, N., Holt, M. and Sakaba, T. (2009). Calcium dependence of exo- and endocytotic coupling at a glutamatergic synapse. *Neuron*, **63**, 216-229.
- Huang, K. P. (1989). The mechanism of protein kinase C activation. *Trends. Neurosci.*, **12**, 425-432.
- Huang, Y. Y., Kandel, E. R., Varshavsky, L., Brandon, E. P., Qi, M., Idzerda, R. L., McKnight, G. S. and Bourtschouladze, R. (1995). A genetic test of the effects of mutations in PKA on mossy fiber LTP and its relation to spatial and contextual learning. *Cell*, **83**, 1211-1222.
- Huang, Y., Chen-Hwang, M. C., Dolios, G., Murakami, N., Padovan, J. C., Wang, R. and Hwang, Y. W. (2004). Mnb/Dyrk1A phosphorylation regulates the interaction of dynamin 1 with SH3 domain-containing proteins. *Biochemistry*, **43**, 10173-10185.
- Huang, T. N., Chang, H. P. and Hsueh, Y. P. (2010). CASK phosphorylation by PKA regulates the protein-protein interactions of CASK and expression of the NMDAR2b gene. *J. Neurochem.*, **112**, 1562-1573.

- Ikeda, K. and Bekkers, J. M. (2009). Counting the number of releasable synaptic vesicles in a presynaptic terminal. *PNAS.*, **106**, 2945-2950.
- Imamura, Y., Matsumoto, N., Kondo, S., Kitayama, H. and Noda, M. (2003). Possible involvement of Rap1 and Ras in glutamatergic synaptic transmission. *Neuroreport.*, **14**, 1203-1207.
- Iwabuchi, S., Kakazu, Y., Koh, J. Y., Goodman, K. M., Harata, N. C. (2014). Examination of Synaptic Vesicle Recycling Using FM Dyes During Evoked, Spontaneous, and Miniature Synaptic Activities. *J. Vis. Exp.*, **85**, 50557. doi: 10.3791/50557.
- Jackman, S. L., Turecek, J., Belinsky, J. E. and Regehr, W. G. (2016). The calcium sensor synaptotagmin 7 is required for synaptic facilitation. *Nature.*, **529**, 88-91.
- Jackson, M. B. and Chapman, E. R. (2006). Fusion pores and fusion machines in Ca^{2+} -triggered exocytosis. *Annu. Rev. Biophys. Biomol. Struct.*, **35**, 135-160.
- Johnson, R. A., Desaubry, L., Bianchi, G., Shoshani, I., Lyons, E., Taussig, R., Watson, P. A., Cali, J. J., Krupinski, J., Pieroni, J. P. and Iyengar, R. (1997). Isozyme-dependent Sensitivity of Adenylyl Cyclases to P-site-mediated Inhibition by Adenine Nucleosides and Nucleoside 3'-Polyphosphates. *J. Biol. Chem.*, **272**, 8962-8966.

- Jung, J. H., Szule, J. A., Stouder, K., Marshall, R. M. and McMahan, U. J. (2018). Active Zone Material-Directed Orientation, Docking, and Fusion of Dense Core Vesicles Alongside Synaptic Vesicles at Neuromuscular Junctions. *Front. Neuroanat.*, **12**:72. doi: 10.3389/fnana.2018.00072.
- Kaeser, P. S. and Regehr, W. G. (2017). The readily releasable pool of synaptic vesicles. *Curr. Opin. Neurobiol.*, **43**, 63-70.
- Kao, J., Li, G. and Auston, D. (2010). Calcium in Living Cells. *Method Cell Biol.* **99**, 113-152.
- Kase, H., Iwahashi, K., Nakanishi, S., Matsuda, Y., Yamada, K., Takkahashi, M., Murakata, C., Sato, A. and Kaneko, M. (1987). K-252 compounds, novel and potent inhibitors of protein kinase C and cyclic nucleotide-dependent protein kinases. *Biochem. Biophys. Res. Commun.*, **142**, 436-440.
- Katz, B. (1969). The release of neural transmitter substances. Charles C. Thomas. Springfield, IL, USA.
- Kavalali, E. T. (2007). Multiple vesicle recycling pathways in central synapses and their impact on neurotransmission. *J. Physiol.*, **585**, 669-679.
- Kavalali, E. T. (2015). The mechanisms and functions of spontaneous neurotransmitter release. *Nat. Rev. Neurosci.*, **16**, 5–16.

- Kawasaki, H., Springett, G. M., Mochizuki, N., Toki, S., Nakaya, M., Matsuda, M., Housman, D. E. and Graybiel, A. M. (1998). A family of cAMP-binding proteins that directly activate Rap1. *Science.*, **282**, 2275-2279.
- Kay, A. R., Alfonso, A., Alford, S., Cline, H. T., Holgado, A. M., Sakmann, B., Snitsarev, V. A., Stricker, T. P., Takahashi, M. and Wu, L. (1999). Imaging Synaptic Activity in Intact Brain Slices with FM1-43 in *C. elegans*, Lamprey, and Rat. *Neuron.*, **24**, 809-817.
- Kay, A. R. (2007). Imaging FM Dyes in Brain Slices. *CHS Protoc.*, **1**, doi:10.1101/pdb.prot4853.
- Von Kleist, L., Stahlschmidt, W., Bulut, H., Gromova, K., Puchkov, D., Robertson, M. J., MacGregor, K. A., Tomilin, N., Pechstein, A., Chau, N., Chircop, M., Sakoff, J., von Kries, J. P., Saenger, W., Kräusslich, H. G., Shupliakov, O., Robinson, P. J., McCluskey, A. and Haucke, V. (2011). Role of the clathrin terminal domain in regulating coated pit dynamics revealed by small molecule inhibition. *Cell.*, **146**, 471-484.
- Knighton, D. R., Zheng, J. H., Ten Eyck, L. F., Xuong, N. H., Taylor, S. S. and Sowadski, J. M. (1991). Structure of a peptide inhibitor bound to the catalytic subunit of cyclic adenosine monophosphate-dependent protein kinase. *Science.*, **253**, 414-420.

- Kokotos, A. C. and Low, D. W. (2015). Myosin II and Dynamin Control Actin Rings to Mediate Fission during Activity-Dependent Bulk Endocytosis. *J. Neurosci.*, **35**, 8687-8688.
- Köles, L., Kató, E., Hanuska, A., Zádori, Z. S., Al-Khrasani, M., Zelles, T., Rubini, P. and Illes, P. (2016). Modulation of excitatory neurotransmission by neuronal/glia! signalling molecules: interplay between purinergic and glutamatergic systems. *Purinergic signalling*, **12**, 1–24.
- Kononenko, N. L., Pechstein, A. and Haucke, V. (2013). The tortoise and the hare revisited. *elife* 2013;**2**:e01233.
- Kovacs, M., Tóth, J., Hetényi, C., Málnási-Csizmadia, A. and Sellers, J. R. (2004). Mechanism of blebbistatin inhibition of myosin II. *J. Biol. Chem.*, **279**, 35557-35563.
- Larsen, M. R., Graham, M. E., Robinson, P. J. and Roepstorff, P. (2004). Improved detection of hydrophilic phosphopeptides using graphite powder microcolumns and mass spectrometry: evidence for *in vivo* doubly phosphorylated dynamin I and dynamin III. *Mol. Cell. Proteomics.*, **3**, 456-465.
- Lasič, E., Stenovec, M., Kreft, M., Robinson, P. J. and Zorec, R. (2017). Dynamin regulates the fusion pore of endo- and exocytotic vesicles as revealed by membrane capacitance measurements. *BBA – Gen. Subj.*, **1861**, 2293-2303.

- Laurent, P., Ch'ng, Q. L., Jospin, M., Chen, C., Lorenzo, R. and de Bono, M. (2018). Genetic dissection of neuropeptide cell biology at high and low activity in a defined sensory neuron. *PNAS.*, **115**, E6890–E6899.
- Lazareno, S., Popham, A. and Birdsall, N. J. (2000). Allosteric interactions of staurosporine and other indolocarbazoles with N-[methyl-(3)H]scopolamine and acetylcholine at muscarinic receptor subtypes: identification of a second allosteric site. *Mol. Pharmacol.*, **58**, 194-207.
- Lee, E. and De Camilli, P. (2002). Dynamin at actin tails. *PNAS.*, **99**, 161-166.
- Lee, J. S., Ho, W. K. and Lee, S. H. (2012). Actin-dependent rapid recruitment of reluctant synaptic vesicles into a fast-releasing vesicle pool. *PNAS*, **109**, E765-774.
- Leenders, A. G. M. and Sheng, Z. H. (2005). Modulation of neurotransmitter release by the second messenger-activated protein kinases: Implications for presynaptic plasticity. *Pharmacol. Ther.*, **105**, 69-84.
- Li, Y. C. and Kavalali, E. T. (2017). Synaptic Vesicle-Recycling Machinery Components as Potential Therapeutic Targets. *Pharmacol. Rev.*, **69**, 141-160.
- Lin, H. C. and Gilman, A. G. (1996). Regulation of Dynamin I GTPase Activity by G Protein $\beta\gamma$ Subunits and Phosphatidylinositol 4,5-Bisphosphate. *J. Biol. Chem.*, **271**, 27979-27982.

- Lindau, M. and Alvarez de Toledo, G. (2003). The fusion pore. *Biochem. Biophys. Acta.* **1641**, 167-173.
- Liu, J. P., Sim, A. T. and Robinson, P. J. (1994). Calcineurin inhibition of dynamin I GTPase activity coupled to nerve terminal depolarization. *Science.*, **265**, 970-973.
- Liu, Y. W., Surka, M. C., Schroeter, T., Lukiyanchuk, V. and Schmid, S. L. (2008). Isoform and splice-variant specific functions of dynamin-2 revealed by analysis of conditional knock-out cells. *Mol. Biol. Cell.*, **19(12)**, 5347-5359.
- Liu, Y. W., Neumann, S., Ramachandran, R., Ferguson, S. M., Pucadyil, T. J. and Schmid, S. L. (2011). Differential curvature sensing and generating activities of dynamin isoforms provide opportunities for tissue-specific regulation. *PNAS*, **108**, 234-242.
- Lou, X. (2018). Sensing Endocytosis and Triggering Endocytosis at the Synapses: Synaptic Vesicle Exocytosis-Endocytosis Coupling. *Front. Cell. Neurosci.*, **12(66)**, doi: 10.3389/fncel.2018.00066.
- Macia, E., Ehrlich, M., Massol, R., Boucrot, E., Brunner, C. and Kirchhausen, T. (2006). Dynasore, a cell-permeable inhibitor of dynamin. *Dev. Cell.*, **10**, 839-850.

- Maeno-Hikichi, Y., Polo-Parada, L., Kastanenka, K. and Landmesser, L. T. (2011). Frequency dependent modes of synaptic vesicle endocytosis and exocytosis at adult mouse neuromuscular junctions. *J. Neurosci.*, **31**, 1093-1105.
- Malacombe, M., Bader, M. F. and Gasman, S. (2006). Exocytosis in neuroendocrine cells: new tasks for actin. *Biochim. Biophys. Acta.*, **1763**, 1175-1183.
- Maritzen, T. and Haucke, V. (2018). Coupling of exocytosis and endocytosis at the presynaptic active zone. *Neurosci. Res.*, **127**, 45-52.
- Marks, B. and McMahon, H.T. (1998). Calcium triggers calcineurin-dependent synaptic vesicle recycling in mammalian nerve terminals. *Curr. Biol.* **8**, 740-749.
- Martinsen, A., Schakman, O., Yerna, X., Dessy, C. and Morel, N. (2014). Myosin light chain kinase controls voltage-dependent calcium channels in vascular smooth muscle. *Pflugers Arch.*, **466**(7), 1377-1389.
- Matteoli, M., Haimann, C., Torri-Tarelli, F., Polak, J. M., Ceccarelli, B. and De Camilli, P. (1988). Differential effect of ci-latrotoxin on exocytosis from small synaptic vesicles and from large dense-core vesicles containing calcitonin gene-related peptide at the frog neuromuscular junction. *PNAS.*, **85**, 7366-7370.
- McMahon, H. T. and Nicholls, D. G. (1991). The bioenergetics of neurotransmitter release. *Biochim, Biophys, Acta.*, **1059**, 243-264.

- Meinecke, M., Boucrot, E., Camdere, G., Hon, W. C., Mittal, R. and McMahon, H. T. (2013). Cooperative Recruitment of Dynamin and BIN/Amphiphysin/Rvs (BAR) Domain-containing Proteins Leads to GTP-dependent Membrane Scission. *J. Biol. Chem.*, **288**, 6651-6661.
- Mellander, L. J., Trouillon, R., Svensson, M. I. and Ewing, A. G. (2012). Amperometric post spike feet reveal most exocytosis is via extended kiss-and-run fusion. *Sci. Rep.*, **2**, doi: 10.1038/srep00907.
- Menegon, A., Bonanomi, D., Albertinazzi, C., Lotti, F., Ferrari, G., Kao, H. T., Benfenati, F., Baldelli, P. and Valtorta, F. (2006). Protein kinase A-mediated synapsin I phosphorylation is a central modulator of Ca²⁺-dependent synaptic activity. *J. Neurosci.*, **26**, 11670-11681.
- Mettlen, M., Pucadyil, T., Ramachandran, R. and Schmid, S. L. (2009). Dissecting dynamin's role in clathrin-mediated endocytosis. *Biochem. Soc. Trends.*, **37**, 1022-1026.
- Michel, K., Müller, J. A., Opreşoreanu, A. and Schoch, S. (2015). The presynaptic active zone: A dynamic scaffold that regulates synaptic efficacy. *Exp. Cell Res.*, **335**, 157-164.
- Miki, T., Malagon, G., Pulido, C., Llano, I., Neher, E. and Marty, A. (2016). Actin- and Myosin-Dependent Vesicle Loading of Presynaptic Docking Sites Prior to Exocytosis. *Neuron.*, **91**, 808-823.

- Miklavc, P., Wittekindt, O. H., Felder, E. and Dietl, P. (2009). Ca²⁺-Dependent Actin Coating of Lamellar Bodies after Exocytotic Fusion: A Prerequisite for Content Release or Kiss-and-Run. *Annals. New. York. Accad. Sci.*, **1152**, 43-52.
- Milosevic, I. (2018). Revisiting the Role of Clathrin-Mediated Endocytosis in Synaptic Vesicle Recycling. *Front. Cell. Neurosci.*, **12**, 27. doi: 10.3389/fncel.2018.00027.
- Min, L., Leungm Y. M., Tomas, A., Watson, R. T., Gaisano, H. Y., Halban, P. A., Pessin, J. E. and Hou, J. C. (2007). Dynamin is functionally coupled to insulin granule exocytosis. *J. Biol. Chem.*, **282**, 33530-33536.
- Moghadam, P. K. and Jackson, M. B. (2013). The functional significance of synaptotagmin diversity in neuroendocrine secretion. *Front. Endocrinol.*, **4**, doi:10.3389/fendo.2013.00124.
- Morton, A., Marland, J. R. and Cousin, M. A. (2015). Synaptic vesicle exocytosis and increased cytosolic calcium are both necessary but not sufficient for activity-dependent bulk endocytosis. *J. Neurochem.*, **134**, 405-415.
- Morton, W. M., Ayscough, K. R. and McLaughlin, P. J. (2000). Latrunculin alters the actin-monomer subunit interface to prevent polymerization. *Nat. Cell. Biol.*, **2**, 376-378.

- Murrell, M., Oakes, P. W., Lenz, M. and Gardel, M. L. (2015). Forcing cells into shape: the mechanics of actomyosin contractility. *Nat. Rev. Mol. Cell. Biol.* **16**, 486-498.
- Neco, P., Fernández-Peruchena, C., Navas, S., Gutiérrez, L. M., Alvarez de Toledo, G. and Alés, E. (2008). Myosin II Contributes to Fusion Pore Expansion during Exocytosis. *J. Biol. Chem.*, **283**, 10949-10957.
- Neher, E. (2015). Merits and Limitations of Vesicle Pool Models in View of Heterogeneous Populations of Synaptic Vesicles. *Neuron.*, **87**, 1131-1142.
- Neuberger, G., Schneider, G. and Eisenhaber, F. (2007). pkaPS: prediction of protein kinase A phosphorylation sites with the simplified kinase-substrate binding model. *Biol. Direct.*, **2**, 1. doi:10.1186/1745-6150-2-1.
- Nguyen, P. V. and Woo, N. H. (2003). Regulation of hippocampal synaptic plasticity by cyclic AMP-dependent protein kinases. *Prog. Neurobiol.* **71**, 401-437.
- Nicholls, D. G., Sihra, T. S. and Sanchez-Prieto, J. (1987). Calcium-Dependent and-Independent Release of Glutamate from Synaptosomes Monitored by Continuous Fluorometry. *J. Neurochem.*, **49**, 50-57.

- Nicholson-Fish, J. C., Kokotos, A. C., Gillingwater, T. H., Smillie, K. J. and Cousin, M. A. (2015). VAMP4 Is an Essential Cargo Molecule for Activity-Dependent Bulk Endocytosis. *Neuron.*, **88**, 973-984.
- Niemann, H. H., Knetsch, M. L. W., Scherer, A., Manstein, D. J. and Kull, F. J. (2001). Crystal structure of a dynamin GTPase domain in both nucleotide-free and GDP-bound forms. *EMBO. J.*, **20**, 5813-5821.
- Nightingale, T. D., Cutler, D. F. and Cramer, L. P. (2012). Actin coats and rings promote regulated exocytosis. *Trends. Cell. Biol.*, **22**, 329-337.
- Olsen, M. K., Reszka, A. A. and Abraham, I. (1998). KT5720 and U-98017 inhibit MAPK and alter the cytoskeleton and cell morphology. *J. Cell. Physiol.*, **176**, 525-536.
- Papadopulos, A., Tomatis, V. M., Kasula, R. and Meunier, F. A. (2013). The Cortical Acto-Myosin Network: From Diffusion Barrier to Functional Gateway in the Transport of Neurosecretory Vesicles to the Plasma Membrane. *Front. Endocrinol.*, **4**, 153. doi:10.3389/fendo.2013.00153.
- Papadopulos, A. (2017). Membrane shaping by actin and myosin during regulated exocytosis. *Mol. Cell. Neurosci.*, **84**, 93-99.

- Park, H., Li, Y. and Tsien, R. W. (2012). Influence of Synaptic Vesicle Position on Release Probability and Exocytotic Fusion Mode. *Science.*, **335**, 1362-1366.
- Park, R. J., Shen, H., Liu, L., Liu, X., Ferguson, S. M. and De Camilli, P. (2013). Dynamin triple knockout cells reveal off target effects of commonly used dynamin inhibitors. *J. Cell. Sci.*, **126**, 5305-5312.
- Park, A. J., Havekes, R., Choi, J. H., Luczak, V., Nie, T., Huang, T. and Abel, T. (2014). A presynaptic role for PKA in synaptic tagging and memory. *Neurobiol. Learn. Mem.*, **114**, 101-112.
- Palade, G. E. and Palay, S. L. (1954). Electron microscope observations of interneuronal and neuromuscular synapses. *Anat. Rec.*, **118**, 335-336.
- Palay, S. L. (1956). Synapses in the central nervous system. *J Biophys. Biochem. Cytol.* **2**, 193-202.
- Persoon, C. M., Moro, A., Nassal, J. P., Farina, M., Broeke, J. H., Arora, S., Dominguez, N., van Weering, J. R. T., Toonen, R. F. and Verhage, M. (2018). Pool size estimations for dense-core vesicles in mammalian CNS neurons. *EMBO. J.*, **37**, e99672. doi:10.15252/emboj.201899672.
- Petrov, A. M., Giniatullin, A. R. and Zefirov, A. L. (2008). Role of the cAMP cascade in the turnover of synaptic vesicles of the frog motor nerve terminal. *Neurochem. J.*, **2**, 175-182.

- Petrov, A. M., Zakyranova, G. F., Yakovleva, A. A. and Zefirov, A. L. (2015). Inhibition of protein kinase C affects on mode of synaptic vesicle exocytosis due to cholesterol depletion. *Biochem. Biophys. Res. Commun.*, **456**, 145-150.
- Pinto, C., Hübner, M., Gille, A., Richter, M., Mou, T. C., Sprang, S. R., Seifert, R. (2010). Differential Interactions of the Catalytic Subunits of Adenylyl Cyclase with Forskolin Analogs. *Biochem. Pharmacol.*, **78**, 62-69.
- Powell, K. A., Valova, V. A., Malladi, C. S., Jensen, O. N., Larsen, M. R. and Robinson, P. J. (2000). Phosphorylation of dynamin I on Ser-795 by protein kinase C blocks its association with phospholipids. *J. Biol. Chem.*, **275**, 11610–11617.
- Pyle, J. L., Kavalali, E. T., Piedras-Rentería, E. S. and Tsien, R. W. (2000). Rapid Reuse of Readily Releasable Pool Vesicles at Hippocampal Synapses. *Neuron.*, **28**, 221-231.
- Quan, A., McGeachie, A. B., Keating, D. J., van Dam, E. M., Rusak, J., Chau, N., Malladi, C. S., Chen, C., McCluskey, A., Cousin, M. A. and Robinson, P. J. (2007). Myristyl trimethyl ammonium bromide and octadecyl trimethyl ammonium bromide are surface-active small molecule dynamin inhibitors that block endocytosis mediated by dynamin I or dynamin II. *Mol. Pharmacol.*, **72**, 1425-1439.

- Raimondi, A., Ferguson, S. M., Lou, X., Armbruster, M., Paradise, S., Giovedi, S., Messa, M., Kono, N., Takaski, J., Cappello, V., O'Toole, E., Ryan, T. A. and De Camilli, P. (2011). Overlapping role of dynamin isoforms in synaptic vesicle endocytosis. *Neuron.*, **70**, 1100-1114.
- Reubold, T. F., Faelber, K., Plattner, N., Posor, Y., Ketel, K., Curth, U., Schlegel, J., Anand, R., Manstein, D. J., Noé, V., Haucke, V., Daumke, O. and Eschenburg, S. (2015). Crystal structure of the dynamin tetramer. *Nature.*, **525**, 404-408.
- Richards, D. A., Bai, J. and Chapman, E. R. (2005). Two modes of exocytosis at hippocampal synapses revealed by rate of FM1-43 efflux from individual vesicles. *J. Cell. Biol.*, **168**, 929-939.
- Richards, D. A. (2010). Regulation of exocytic mode in hippocampal neurons by intra-bouton calcium concentration. *J. Physiol.*, **588**, 4927-4936.
- Ritter, B., Murphy, S., Dokainish, H., Girard, M., Gudheti, M. V., Kozlov, G., Halin, M., Philie, J., Jorgensen, E. M., Gehring, K. and McPherson, P. S. (2013). NECAP 1 Regulates AP-2 Interactions to Control Vesicle Size, Number, and Cargo During Clathrin-Mediated Endocytosis. *PLoS. Biol.*, **11**, e1001670. doi:10.1371/journal.pbio.1001670.

- Rizo, J. and Rosenmund, C. (2008). Synaptic vesicle fusion. *Nat. Struct. Mol. Biol.* **15**, 665-674.
- Rizzoli, S. O. and Betz, W. J. (2003). Neurobiology: All change at the synapse. *Nature.*, **423**, 591-592.
- Rizzoli, S. O. and Betz, W. J. (2004). The structural organization of the readily releasable pool of synaptic vesicles. *Science.*, **303**, 2037-2039.
- Rizzoli, S. O. and Betz, W. J. (2005). Synaptic vesicle pools. *Nat. Rev. Neurosci.*, **6**, 57-69.
- Rizzoli, S. O. and Jahn, R. (2007). Kiss-and-run, collapse and 'readily retrievable' vesicles. *Traffic.*, **8**, 1137-1144.
- Rizzoli, S. O. (2014). Synaptic vesicle recycling: steps and principles. *EMBO J.*, **33**, 788-822.
- De Robertis, E. D. P. and Bennett, H. S. (1955). Submicroscopic vesicular component in the synapse. *Fed. Proc.* **13**, 35.
- Robinson, P. J. (1991). Dephosphin, a 96,000 Da substrate of protein kinase C in synaptosomal cytosol, is phosphorylated in intact synaptosomes. *FEBS Lett.*, **282**, 388-392.

- Robinson, P. J. (1992). Differential Stimulation of Protein Kinase C Activity by Phorbol Ester or Calcium/Phosphatidylserine in Vitro and in Intact Synaptosomes. *J. Biol. Chem.* **267**, 21637-21644.
- Robinson, P. J., Liu, K.A., Powell, K. A., Fyske, E. M. and Südhof, T.C. (1994). Phosphorylation of dynamin I and synaptic-vesicle recycling. *Trends Neurosci.*, **17**, 348-353.
- Roman-Vendrell, C., Chevalier, M., Acevedo-Canabal, A. M., Delgado-Peraza, F., Flores-Otero, J. and Yudowski, G. A. (2014). Imaging of kiss-and-run exocytosis of surface receptors in neuronal cultures. *Front. Cell. Neurosci.*, **8**, 363. doi:10.3389/fncel.2014.00363.
- de Rooij, J., Zwartkuis, F. J., Verheijen, M. H., Col, R. H., Nijman, S. M., Wittinghofre, A. and Bos, J. L. (1998). Epac is a Rap1 guanine-nucleotide-exchange factor directly activated by cyclic AMP. *Nature.*, **396**, 474-477.
- de Rooij, J., Rehmann, H., van Triest, M., Cool, R. H., Wittinghofer, A. and Bos, J. L. (2000). Mechanism of regulation of the Epac family of cAMP-dependent RapGEFs. *J. Biol. Chem.*, **275**, 20829-20836.
- Rudling, J. E., Drever, B. D., Reid, B. and Bewick, G. S. (2018). Importance of Full-Collapse Vesicle Exocytosis for Synaptic Fatigue-Resistance at Rat Fast and Slow Muscle Neuromuscular Junctions. *Int. J. Mol. Sci.*, **19**, doi:10.3390/ijms19071936.

- Saheki, Y. and De Camilli, P. (2012). Synaptic Vesicle Endocytosis. *Cold Spring Harb Perspect Biol.*, 4:a005645.
- Samaslip, P., Chan, S. A. and Smith, C. (2012). Activity-Dependent Fusion Pore Expansion Regulated by Calcineurin-Dependent Dynamin-Syndapin Pathway in Mouse Adrenal Chromaffin cells. *J. Neurosci.*, **32**, 10438-10447.
- Sanchez-Prieto, J., Sihra, T. S., Evans, D., Ashton, A., Dolly, J. O. and Nichols, D. G. (1987). Botulinum toxin A blocks glutamate exocytosis from guinea-pig cerebral cortical synaptosomes. *Eur. J. Biochem.*, **165**, 675-681.
- Sandberg, M., Butt, E., Nolte, C., Fischer, L., Halbrügge, M., Beltman, J., Jahnsen, T., Genieser, H. G., Jastorff, B. and Walter, U. (1991). Characterization of Sp-5,6-dichloro-1-beta-D-ribofuranosylbenzimidazole-3',5'-monophosphorothioate (Sp-5,6-DCl-cBiMPS) as a potent and specific activator of cyclic-AMP-dependent protein kinase in cell extracts and intact cells. *Biochem. J.*, **279**, 521-527.
- Sandana, R. and Dessauer, C. W. (2009). Physiological roles for G protein-regulated adenylyl cyclase isoforms: insights from knockout and overexpression studies. *Neurosignals.*, **17**, 5-22.
- Scheefhals, N. and MacGillavry, H. D. (2018). Functional organization of postsynaptic glutamate receptors. *Mol. Cell. Neurosci.*, **91**, 82-94.

- Schikorski, T. and Stevens C. F. (1997). Quantitative Ultrastructural Analysis of Hippocampal Excitatory Synapses. *J. Neurosci.*, **17**, 5858-5867.
- Schikorski, T. (2014). Readily releasable vesicles recycle at the active zone of hippocampal synapses. *PNAS.*, **111**, 5415-5420.
- Schmidt, M., Dekker, F. J. and Maarsingh, H. (2013). Exchange Protein Directly Activated by cAMP (epac): A Multidomain cAMP Mediator in the Regulation of Diverse Biological Functions. *Pharmacol. Rev.*, **65**, 670-709.
- Schweizer, F. E. and Ryan, T. A. (2006). The synaptic vesicle: cycle of exocytosis and endocytosis. *Curr. Opin. Neurobiol.*, **16**, 298-304.
- Seamon, K. B. and Daly, J. W. (1981). Forskolin: a unique diterpene activator of cyclic AMP-generating systems. *J. Cyclic. Nucleotides. Res.*, **7**, 201-224.
- Seino, S. and Shibasaki, T. (2005). PKA-dependent and PKA-independent pathways for cAMP-regulated exocytosis. *Physiol. Rev.* **85**, 1303-1342.
- Sharma, S. and Lindau, M. (2018). Molecular mechanism of fusion pore formation driven by the neuronal SNARE complex. *PNAS.*, **115**, 12751-12756.
- Shi, L., Shen, Q. T., Kiel, A., Wang, J., Wang, H. W., Melia, T. J., Rothman, J. E. and Pincet, F. (2012). SNARE proteins: one to fuse and three to keep the nascent fusion pore open. *Science.*, **335**, 1355-1359.

- Shu, S., Liu, X. and Korn, E. D. (2005). Blebbistatin and blebbistatin-inactivated myosin II inhibit myosin II-independent processes in Dictyostelium. *PNAS.*, **102**, 1472-1477.
- Siksou, L., Rostaing, P., Lechaire, J. P., Boudier, T., Ohtsuka, T., Fejtová, A., Kao, H. T., Greengard, P., Gundelfinger, E. D., Triller, A. and Marty, S. (2007). Three-Dimensional Architecture of Presynaptic Terminal Cytomatrix. *J. Neurosci.*, **27**, 6868-6877.
- Sim, A. T. R., Herd, L., Proctor, D. T., Baldwin, M. L., Meunier, F. A. and Rostas, J. A. P. (2006). High throughput analysis of endogenous glutamate release using a fluorescence plate reader. *J. Neurosci. Methods.* **153**, 43-47.
- Singh, D. (2017). Phosphorylation sites on specific neuronal protein can control the mode of synaptic vesicle exocytosis and thereby regulate synaptic transmission. Doctoral thesis, UCLan, Preston.
- Smillie, K. J. and Cousin, M. A. (2005). Dynamin I Phosphorylation and the Control of Synaptic Vesicle Endocytosis. *Biochem Soc Symp.*, **72**, 87-97.
- Sone, M., Suzuki, E., Hoshino, M., Hou, D., Kuromi, H., Fukata, M., Kuroda, S., Kaibuchi, K., Nabeshima, Y. and Hama, C. (2000). Synaptic development is controlled in the periaxonal zones of Drosophila synapses. *Development.*, **127**, 4157-4168.

- Sontag, J., Fyske, E. M., Ushkaryov, Y., Liu, J., Robinson, P. J. and Südhof, T. C. (1994). Differential Expression and Regulation of Multiple Dynamins. *J. Biol. Chem.*, **269**, 4547-4554.
- Soykan, T., Maritzen, T. and Haucke, V. (2016). Modes and mechanisms of synaptic vesicle recycling. *Curr. Opin. Neurobiol.*, **39**, 17-23.
- Soykan, T., Kaempf, N., Sakaba, T., Vollweiler, D., Goerdeler, F., Puchkov, D., Kononenko, N. L. and Haucke, V. (2017). Synaptic Vesicle Endocytosis Occurs on Multiple Timescales and Is Mediated by Formin-Dependent Actin Assembly. *Neuron.*, **93**, 854-866.
- Srinivasan, S., Burckhardt, C. J., Bhawe, M., Chen, Z., Chen, P. H., Wang, X., Danuser, G. and Schmid, S. L. (2018). A noncanonical role for dynamin-1 in regulating early stages of clathrin-mediated endocytosis in non-neuronal cells. *PLoS. Biol.*, **16**(4). e2005377. doi: 10.1371/journal.pbio.2005377.
- Ster, J., Bock, F. D., Guerineau, N. C., Janossy, A., Barrere-Lemaire, S., Bos, J. L., Bockaert, J. and Fagni, L. (2007). Exchange protein activated by cAMP (Epac) mediates cAMP activation of p38 MAPK and modulation of Ca²⁺-dependent K⁺ channels in cerebellar neurons. *PNAS.*, **104**, 2519-2524.
- Stevens, C. F. and Williams, J. H. (2000). "Kiss and run" exocytosis at hippocampal synapses. *PNAS.*, **97**, 12828-12833.

- Stowell, M. H., Marks, B., Wigge, P. and McMahon, H.T. (1999). Nucleotide-dependent conformational changes in dynamin: evidence for a mechanochemical molecular spring. *Nat. Cell. Biol.*, **1**, 27-32.
- Südhof, T. C. (2004). The Synaptic Vesicle Cycle. *Annu. Rev. Neurosci.*, **27**, 509–47.
- Südhof, T. C. (2013). Neurotransmitter release: the last millisecond in the life of a synaptic vesicle. *Neuron.*, **80**, 675-690.
- Sun, M. K. and Alkon, D. L. (2012). Activation of protein kinase C isozymes for the treatment of dementias. *Adv. Pharmacol.*, **64**, 273-302.
- Sunahara, R. K., Dessauer, C. W. and Gilman, A. G. (1996). Complexity and diversity of mammalian adenylyl cyclases. *Annu. Rev. Pharmacol. Toxicol.*, **36**, 461-480.
- Sundborger, A. C. and Hinshaw, J. E. (2014). Regulating dynamin dynamics during endocytosis. *F1000prime reports*, **6**, 85. doi:10.12703/P6-85.
- Taira, K., Umikawa, M., Takei, K., Myagmar, B. E., Shinzato, M., Machida, N., Uezato, H., Nonaka, S. and Kariya, K. (2004). The Traf2- and Nck-interacting kinase as a putative effector of Rap2 to regulate actin cytoskeleton. *J. Biol. Chem.*, **279**, 49488-49496.

- Takamori, S., Holt, M., Stenius, K., Lemke, E. A., Grønborg, M., Riedel, D., Urlaub, H., Schenck, S., Brügger, B., Ringler, P., *et al.*, (2006). Molecular anatomy of a trafficking organelle. *Cell.*, **127**, 831–846.
- Tan, T. C., Valova, V. A., Malladi, C. S., Graham, M. E., Berven L. A., Jupp O. J., Hansra G., McClure S. J., Sarcevic B., Boadle R. A., *et al.*, (2003). Cdk5 is essential for synaptic vesicle endocytosis. *Nat. Cell Biol.* **5**, 701-710.
- Tang, W. J. and Hurley, J. H. (1998). Catalytic mechanism and regulation of mammalian adenylyl cyclases. *Mol. Pharmacol.*, **54**, 231-240.
- Tibbs, G. R., Barrie, A. P., Mieghem, F. J. E., McMahon, H. T. and Nicholls, D. G. (1989). Repetitive Action Potentials in Isolated Nerve Terminals in the Presence of 4-Aminopyridine: Effects on Cytosolic Free Ca²⁺ and Glutamate Release. *J. Neurochem.*, **53**, 1693-1699.
- Trouillon, R. and Ewing, A. G. (2013). Amperometric measurements at cells support a role for dynamin in the dilation of the fusion pore during exocytosis. *Chemphyschem.*, **14**, 2295-2301.
- Trudeau, L. E., Emery, D. G., Haydon, P. G. (1996). Direct Modulation of the Secretory Machinery Underlies PKA-Dependent Synaptic Facilitation in Hippocampal Neurons. *Neuron.*, **17**, 789-797.

- Tzounopoulos, T., Janz, R., Südhof, T. C., Nicoll, R. A. and Malenka, R. C. (1998). A role for cAMP in long-term depression at hippocampal mossy fiber synapses. *Neuron.*, **21**, 837-845.
- Urrutia, R., Henley, J. R., Cook, T. and McNiven, M. A. (1997). The dynamins: Redundant or distinct function for an expanding family of related GTPases? *PNAS.*, **94**, 377-384.
- van der Blik, A. M., Redelmeier, T. E., Damke, H., Tisdale, E. J., Meyerowitz, E. M. and Schmid, S. L. (1993). Mutations in human dynamin block an intermediate stage in coated vesicle formation. *J. Cell. Biol.*, **122**, 553-563.
- van den Pol A. N. (2012). Neuropeptide transmission in brain circuits. *Neuron.*, **76**, 98–115.
- Vancha, A. R., Govindaraju, S., Parsa, K. V. L., Jasti, M., González-García, M. and Ballesteros, R. P. (2004). Use of polyethyleneimine polymer in cell culture as attachment factor and lipofection enhancer. *BMC. biotechnol.*, **4**, (23). doi:10.1186/1472-6750-4-23.
- Wahl, S., Katiyar, R. and Schmitz, F. (2013). A Local, Periaxonal Zone Endocytic Machinery at Photoreceptor Synapses in Close Vicinity to Synaptic Ribbons. *J. Neurosci.*, **33**, 10278-10300.

- Waites, C. L. and Garner, C. C. (2011). Presynaptic function in health and disease. *Trends. Neurosci.*, **34**, 326-337.
- Wallace, D. C. (2013). A mitochondrial bioenergetic etiology of disease. *J. Clin. Invest.*, **123**, 1405-1412.
- Walsh, D. A., Perkins, J. P. and Krebs, E. G. (1968). An adenosine 3',5'-monophosphate-dependant protein kinase from rabbit skeletal muscle. *J. Biol. Chem.*, **243**, 3763-3765.
- Wang, H. and Sieburth, D. (2013). PKA Controls Calcium Influx into Motor Neurons during a Rhythmic Behavior. *PLoS. Genet.*, **9(9)**:e1003831.
- Watanabe, S., Rost, B. R., Camacho-Pérez, M., Davis, M. W., Söhl-Kielczynski, B., Rosenmund, C. and Jorgenson, E. M. (2013). Ultrafast endocytosis at mouse hippocampal synapses. *Nature.*, **504**, 242-247.
- Watanabe, S., Trimbuch, T., Camacho-Pérez, M., Rost, B. R., Brokowski, B., Söhl-Kielczynski, B., Felies, A., Davis, M. W., Rosenmund, C. and Jorgenson, E. M. (2014). Clathrin regenerates synaptic vesicles from endosomes. *Nature.*, **515**, 228-233.
- Weiskopf, M. G., Castillo, P. E., Zalutsky, R. A. and Nicoll, R. A. (1994). Mediation of hippocampal mossy fiber long-term potentiation by cyclic AMP. *Science.*, **265**, 1878-1882.

- Whittaker, V. P. (1959). The isolation and characterization of acetylcholine containing particles from brain. *Biochem. J.*, **72**, 694-706.
- Whittaker, V. P., Michaelson, I. A. and Kirkland, R. J. A. (1964). The separation of synaptic vesicles from nerve-ending particles ('Synaptosomes'). *Biochem. J.*, **90**, 293-303.
- Wu, W. and Wu, L. G. (2007). Rapid bulk endocytosis and its kinetics of fission pore closure at a central synapse. *PNAS.*, **104**, 10234–10239.
- Wu, Y., Yeh, F. L., Mao, F. and Chapman, E. R. (2009). Biophysical Characterization of Styryl Dye-Membrane Interactions. *Biophys. J.*, **97**, 101-109.
- Wu, M., Huang, B., Graham, M., Raimondi, A., Heuser, J. E., Zhuang, X. and Camilli, P. (2010). Coupling between clathrin-dependent endocytic budding and F-BAR-dependent tubulation in a cell-free system. *Nat. Cell. Biol.*, **12**, 902-908.
- Wu, Y., O'Toole, E. T., Girard, M., Ritter, B., Messa, M., Liu, X., McPherson, P. S., Ferguson, S. M. and De Camilli, P. (2014). A dynamin 1-, dynamin 3- and clathrin-independent pathway of synaptic vesicle recycling mediated by bulk endocytosis. *ELife.*, **3**, e01621. doi:10.7554/eLife.01621.
- Wu, X. S., Lee, S., Sheng, J., Zhang, Z., Zhao, W., Wang, D., Jin, Y., Charnay, P., Ervasti, J. M. and Wu, L. G. (2016). Actin is crucial for all kinetically distinguishable forms of endocytosis at synapses. *Neuron.*, **92**, 1020-1035.

- Xie, W., Adayev, T., Zhu, H., Wegiel, J., Wieraszko, A. and Hwang, Y. W. (2012). Activity-dependent phosphorylation of dynamin 1 at serine 857. *Biochemistry.*, **51**, 6786-6796.
- Xue, J., Graham, M. E., Novelle, A. E., Sue, N., Gray, N., McNiven, M. A., Smillie, K. J., Cousin, M. A. and Robinson, P. J. (2011). Calcineurin Selectively Docks with the Dynamin I α Splice Variant to Regulate Activity-dependent Bulk Endocytosis. *J. Biol. Chem.*, **286**, 30295-30303.
- Yamashita, T., Hige, T. and Takahashi, T. (2005). Vesicle endocytosis requires dynamin-dependent GTP hydrolysis at a fast CNS synapse. *Science.*, **307**, 124-127.
- Yao, L. and Sakaba, T. (2012). Activity-dependent modulation of endocytosis by calmodulin at a large central synapse. *PNAS.*, **109**, 291-296.
- Yoshida, S. and Plant, S. (1992). Mechanism of release of ca²⁺ from intracellular stores in response to ionomycin in oocytes of the frog *xenopus laevis*. *J. Physiol.*, **458**, 307-318.
- Yoshihara, M., Suzuki, K. and Kidokoro, Y. (2000). Two Independent Pathways Mediated by cAMP and Protein Kinase A Enhance Spontaneous Transmitter Release at *Drosophila* Neuromuscular Junctions. *J. Neurosci.*, **20**, 8315-8322.

- Zambon, A. C., Zhang, L., Minovitsky, S., Kanter, J. R., Prabhakar, S., Salomonis, N., Vranizan, K., Dubchak, I., Conklin, B. R. and Insel, P. A. (2005). Gene expression patterns define key transcriptional events in cell-cycle regulation by cAMP and protein kinase A. *PNAS.*, **102**, 8561-8566.
- Zhang, Q., Cao, Y. and Tsien, R. W. (2007). Quantum dots provide an optical signal specific to full collapse fusion of synaptic vesicles. *PNAS*, **104**, 17843-17848.
- Zhang, Q., Li, Y. and Tsien, R. W. (2009). The dynamic control of kiss-and-run and vesicular reuse probed with single nanoparticles. *Science.*, **323**, 1448-1453.
- Zhang, Q., Huang, H., Zhang, L., Wu, R., Chung, C. L., Zhang, S. Q., Torra, J., Schepis, A., Coughlin, S. R., Kornberg, T. B. and Shu, X. (2018). Visualizing Dynamics of Cell Signaling In Vivo with a Phase Separation-Based Kinase Reporter. *Mol. Cell.*, **69**, 334-346.
- Zhao, W. D., Hamid, E., Shin, W., Wen, P. J., Krystofiak, E. S., Villarreal, S. A., Chiang, H. C., Kachar, B. and Wu, L. G. (2016). Hemi-fused structure mediates and controls fusion and fission in live cells. *Nature.*, **23**, 548-552.
- Zhong, Y. and Wu, C. F. (1991). Altered synaptic plasticity in *Drosophila* memory mutants with a defective cyclic AMP cascade. *Science.*, **251**, 198-201.

- Zhou, Q., Lai, Y., Bacaj, T., Zhao, M., Lyubimov, A. Y., Uervirojnangkoorn, M., Zeldin, O. B., Brewster, A. S., Sauter, N. K., Cohen, A. E., *et al.*, (2015). Architecture of the synaptotagmin–SNARE machinery for neuronal exocytosis. *Nature.*, **525**, 62-67.
- Zhu, J. J., Qin, Y., Zhao, M., Van Aelst, L. and Malinow, R. (2002). Ras and Rap control AMPA receptor trafficking during synaptic plasticity. *Cell.*, **110**, 443-455.
- Zhu, Y., Xu, J. and Heinemann, S. F. (2009). Synaptic vesicle exocytosis-endocytosis at central synapses: Fine-tuning at differential patterns of neuronal activity. *Commun. Integr. Biol.*, **2**, 418-419.
- Zolnierowicz, S. (2000). Type 2A Protein Phosphatase, the Complex Regulator of Numerous Signaling Pathways. *Biochem. Pharmacol.*, **60**, 1225-1235.
- Zupanc, G. K. (1996). Peptidergic transmission: from morphological correlates to functional implications. *Micron.*, **27**, 35-91.

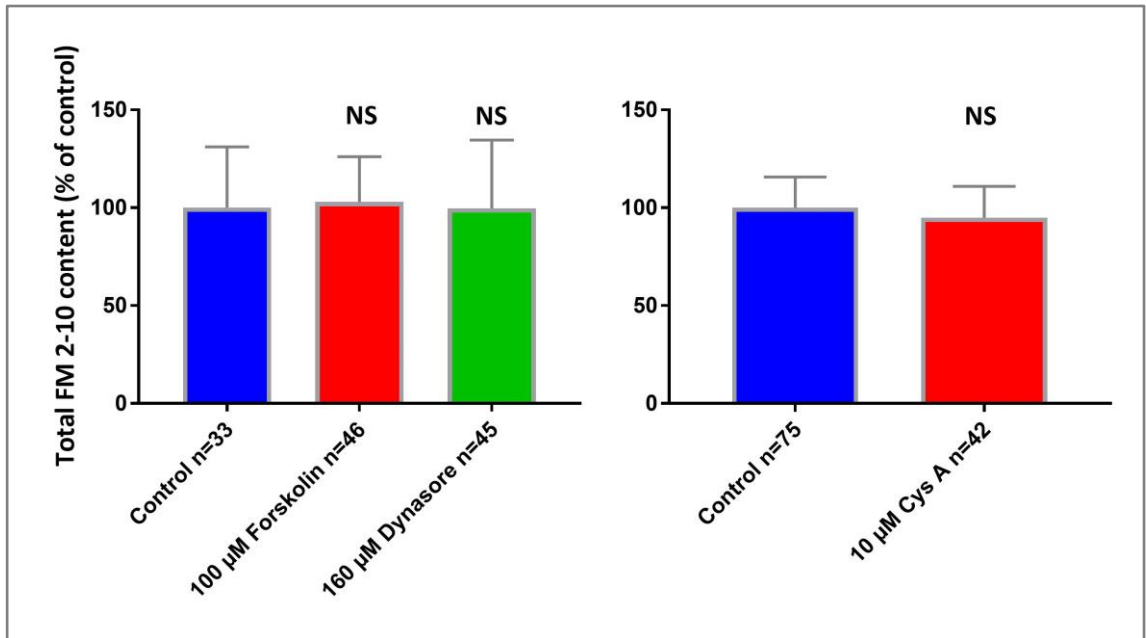
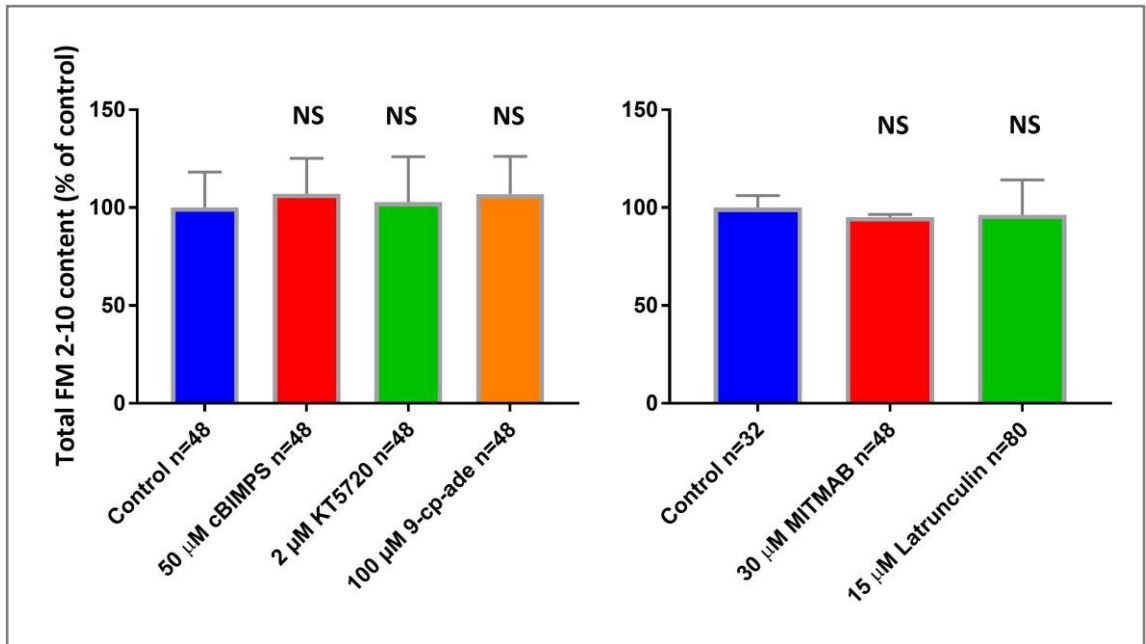
Appendix A

Total FM 2-10 Dye Content at the beginning of Measurements

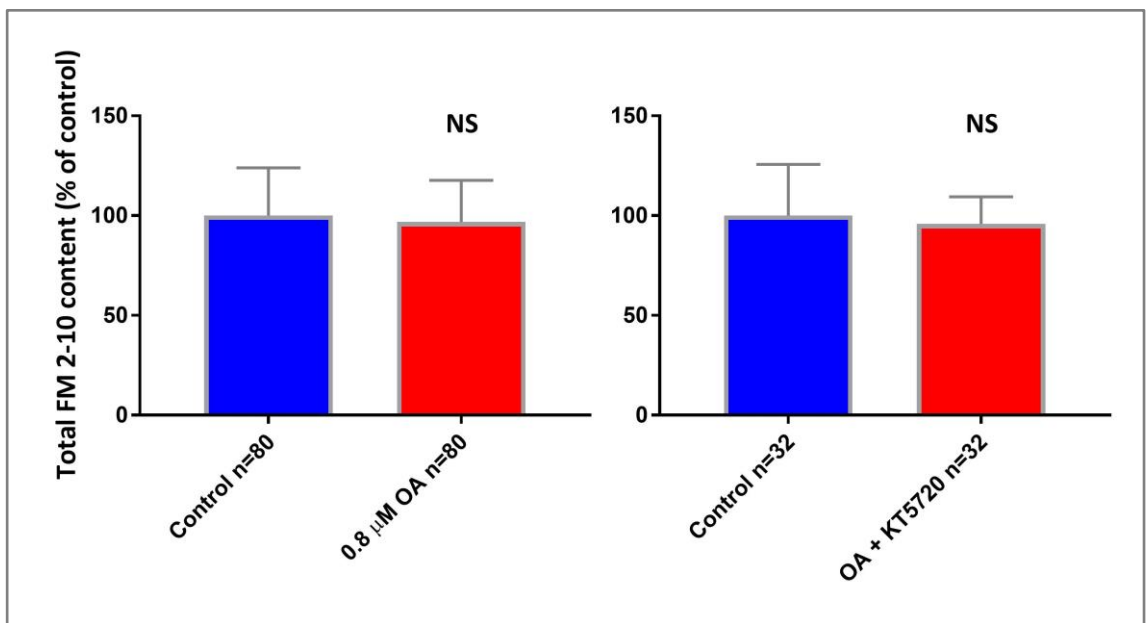
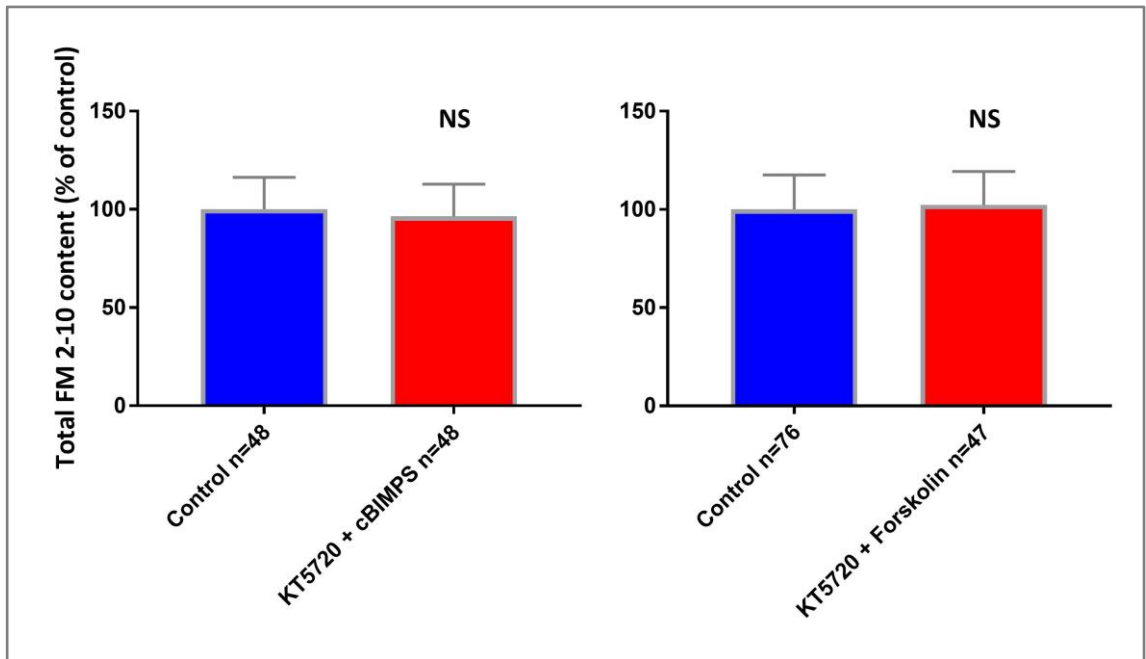
It is vital to establish if any of the drug treatments perturb the amount of FM 2-10 dye being loaded into the nerve terminals in order for key interpretations drawn in this thesis to be accurate. Otherwise, comparisons between the FM 2-10 dye release and Glu assays would lead to fallacious assumptions. The fluorescence of the FM 2-10 dye was measured prior to stimulation (time zero) and compared with the control used in each assay. None of the drugs utilised in this thesis have had a significant impact upon the total FM 2-10 dye uptake ($p>0.05$).

Below are bar charts displaying the average nerve terminal fluorescence before stimulation began, error bars are plus S.E.M.

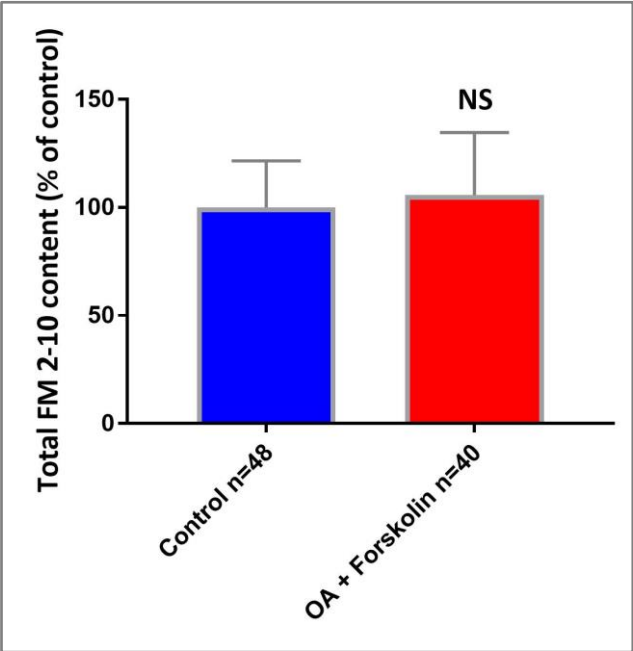
Appendix A (Continued)



Appendix A (Continued)



Appendix A (Continued)



Appendix B

